Complexation of Trivalent Lanthanides by Three Diphosphonate Ligands in Blood Plasma

By

Jan Rijn Zeevaart

A dissertation submitted in fulfillment
of the requirements for the degree of

Master of Science

University of Cape Town

March 1997

Contents

8. Appendixes 159

Acknowledgements

The author wishes to acknowledge the following:

Dr. N. V. Jarvis for his supervision and co-promotorship of this dissertation and the splendid introduction to potentiometry and blood plasma modelling.

Dr. I. Cukrowski of the University of the Witwatersrand for all the help with polarography and introducing me to this valuable technique, also used to derive formation constants.

Prof. G.E. Jackson for his supervision of this dissertation and advice.

Dr. L. Carlton of the University of the Witwatersrand for the use of the NMR apparatus and assistance with interpreting NMR spectra.

The Atomic Energy Corporation of South Africa Ltd., my employer, for assistance and permission to use this work for a dissertation.

AEC management especially Dr. Mingay and Dr. Van Zyl de Villiers for encouragement.

My colleagues in the division of Radiochemistry especially Dr. W.K.A. Louw for advice and a cheerful working environment.

My parents for their care and the tremendous background I received from them.

God for letting me realise that for now, the world is our home, where we have an assignment which includes science.

Summary

It has been shown that ^{153}Sm complexed with the bone seeking ligand ethylene-diaminetetramethylene phosphonate (EDTMP) is effective in pain palliation therapy of bone cancer. Blood plasma models for this ligand with Sm(III) and Ho(III) have been successfully constructed explaining the differences between ^{153}SmEDTMP and ^{166}HoEDTMP. The latter isotope is preferred because of its more energetic β particle, thought to improve the therapeutic effect of the radiopharmaceutical. However, ^{166}HoEDTMP is not an effective pain palliation agent and consequently the search for a more effective bone cancer therapeutic radiopharmaceutical involving ^{166}Ho continues. A ligand is being sought which complexes Ho(III) with a formation constant high enough to survive competition from blood plasma ligands but not so high to prevent ^{166}Ho from being accessible to metastases. EDTMP is unsuitable as such a ligand because of its inability to compete with citrate for complexation of Ho(III).

For this study three diphosphonate ligands applied in radiation imaging of bone or non-radiative treatment of osteoporosis were chosen. They are APD (1-hydroxy-3-amino-propylidene-diphosphonic acid), MDP (methylenediphosphonic acid) and HEDP (1-hydroxy-ethylene-diphosphonic acid). Formation constants for the complexation of Ca(II), Mg(II), Zn(II), Sm(III) and Ho(III) with all of these ligands were measured using potentiometry and polarography. The latter was used to complement potentiometry in systems where precipitates formed. The complexation of Cd(II) by HEDP was used to compare the two techniques and to show that the values found by either technique are comparable. NMR studies were attempted on some complexes in solution to investigate the role the of the hydroxy-group (APD and HEDP) in complexation. The program ECCLES was used together with the formation constants measured in this study to predict the speciation of Ho(III) and Sm(III) with these three ligands in blood plasma. The results gathered for Ho(III) and APD were used as an indication and in an application to an ethical committee before animal testing. A baboon test was carried out using ^{166}HoAPD, the most promising system.

ethical committee before animal testing. A baboon test was carried out using ^{166}HoAPD, the most promising system.

The resulting bone-uptake and side-effects found in the animal study confirmed the predictions made by ECCLES. It proved that ^{166}HoAPD would be ineffective as a therapeutic agent due to high liver uptake. Valuable information on how a future radiopharmaceutical should be designed was obtained in this study.

General Abbreviations

EDTMP	- Ethylenediaminetetramethylene phosphonate
APD	- 1-Hydroxy-3-amino-propylidene-diphosphonic acid
MDP	- Methylenediphosphonic acid
HEDP	- 1-Hydroxy-ethylene-diphosphonic acid
AEC	- Atomic Energy Corporation of South Africa Ltd.
ECCLES	- Evaluation of Constituent Concentration in Large Equilibrium Systems
ESTA	- Equilibrium Simulation for Titration Analysis; a library of computer programs
ESTA2A	- Optimisation module of ESTA
ESTA1	- Simulation module of ESTA
Qbar / $\overline{Q}$	- deprotonation function, the average number of protons released as a result of complexation per metal ion.
Zbar / $\overline{Z}$	- formation function, the average number of protons bound per metal ion
$\overline{Z}_H$	- formation protonation function, the average number of protons bound per metal ion
$\overline{n}$	- average number of protons per ligand in the absence of metal ion
K_w	- water dissociation constant
K_x where x = 1,2,3...	- Formation constant
β	- Overall formation constant
pH / pL	- negative logarithm of the free acid concentration
pA	- negative logarithm of the free deprotonated ligand concentration
pK_a	- negative logarithm of the acid dissociation constant
E_0	- electrode constant
NMR	- Nuclear Magnetic Resonance
M	- $mol.dm^{-3}$ of metal ion
L	- ligand

1. Introduction

Bone-seeking radiopharmaceuticals are receiving considerable attention for therapeutic treatment of bone metastases (commonly known as bone cancer). In this regard satisfactory results were achieved using ^{153}SmEDTMP [1], in the pain palliation therapy of patients suffering from this form of cancer by a multi-disciplinary task group, from which the AEC of SA is a member.

1.1 Bone cancer and pain palliative therapy

Although direct tumour invasion of bone can occur, the most common pathway for the spread of malignancies is from the bone marrow, which is affected first, to the firm bone matrix [2]. Secondary bone metastases occur commonly in advanced cancer of the bone, a feature of i.a. breast, lung and prostate cancer patients [2,3]. (Metastatic sites are commonly found in the axial skeleton rather than the appendicular skeleton.) This follows an increased rate of bone resorption mediated largely by the osteoclasts. Osteoclasts are responsible for bone resorption in normal remodelling of bone. On the other hand, osteoblasts handle bone deposition as the other half of the remodelling of bone, a process undergone throughout life [2]. The disruption of the structural integrity of bone is what causes so much pain to the patient. A good quality of life can be maintained by an effective pain palliation therapy. There are a few therapeutic options available. Chemotherapy, hormone manipulation agents to inhibit bone resorption and radiation therapy using radiopharmaceuticals. The research described herein and already used by the AEC is related to the latter

The mechanisms by which pain relief is thought to occur is still speculative. One theory on how radiopharmaceuticals work in pain palliation treatment is that the radioactive isotope chemisorbs to areas of increased osteoblastic activity due to the bone seeking ligand. Radiation will then cause death in a percentage of cells within β-range (3 mm for Sm-153 and 8 mm for Ho-166). The resulting decrease in intraosseous mass and pressure bringing relief to the patient. However, it is found that the reduction in pain levels occur within a few days, i.e. before the tumour cell mass shrinks. The mechanism is therefore more complex. One of the most radiation-sensitive cell types is the lymphocyte, which secretes a

variety of cytokineses that have been associated with pain modulation. Perhaps lymphocyte cell death at the tumour site is responsible for this rapid pain reduction [4].

^{153}SmEDTMP as a radiopharmaceutical is a very successful pain palliation agent for patients suffering from bone metastases. It consists of ^{153}Sm complexed to a phosphonate viz. ethylenediaminetetramethylphosphonate (EDTMP) and has been studied extensively by our department [5].

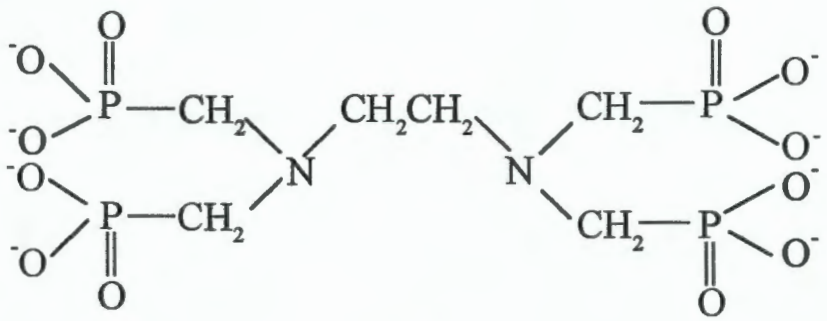

EDTMP

Photo 1. Skeletal image of a patient injected with ^{153}SmEDTMP taken by a γ-camera.

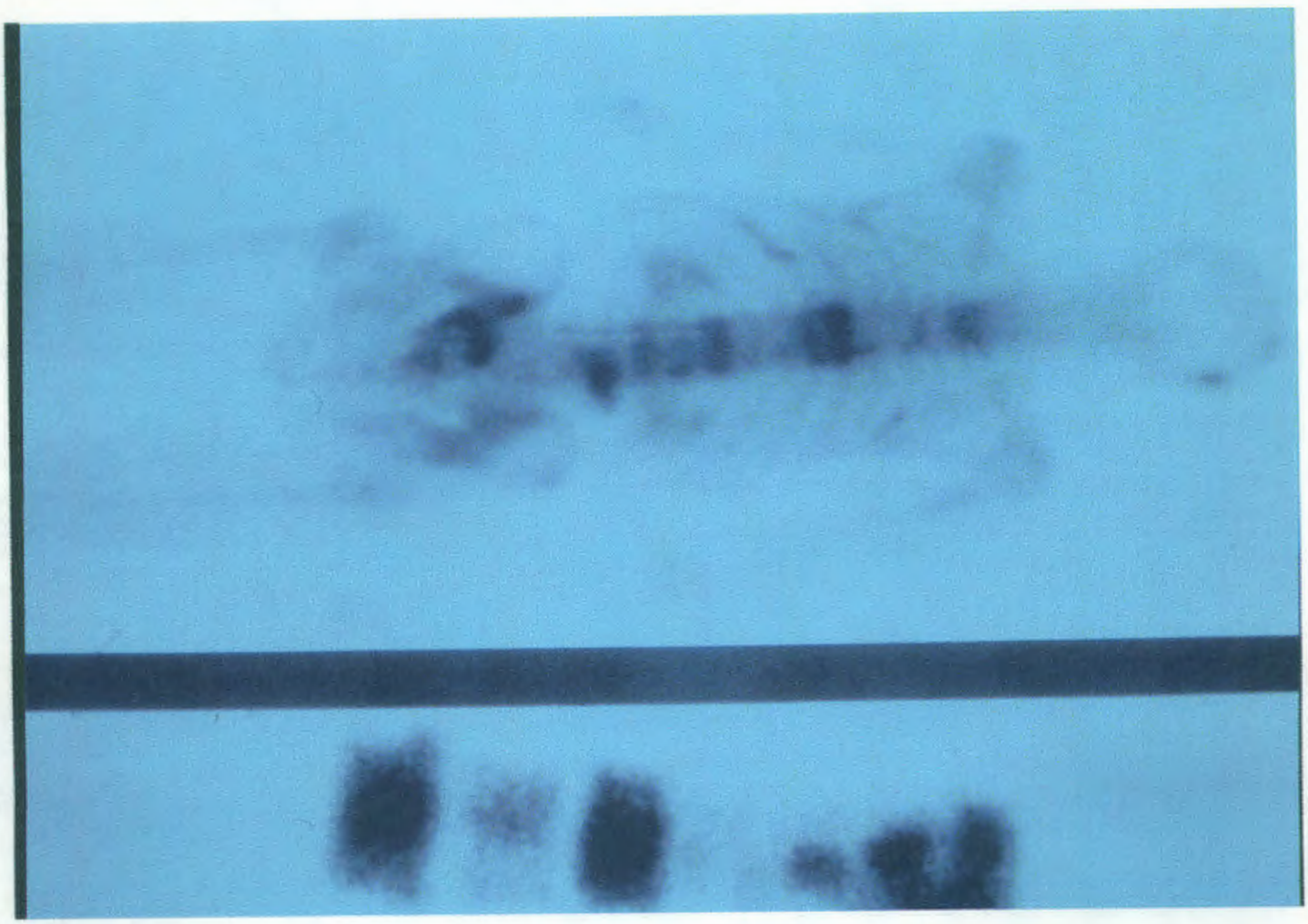

Photo 2. Comparison between a visible and γ-ray image of a patient's spinal cord. Note that the lighter areas on the visible image indicate cancer tissue which correspond to the darker areas on the γ-image indicating higher uptake of ^{153}SmEDTMP. The round spot on the third vertebra from the right is a good example of ^{153}SmEDTMP's selective uptake.

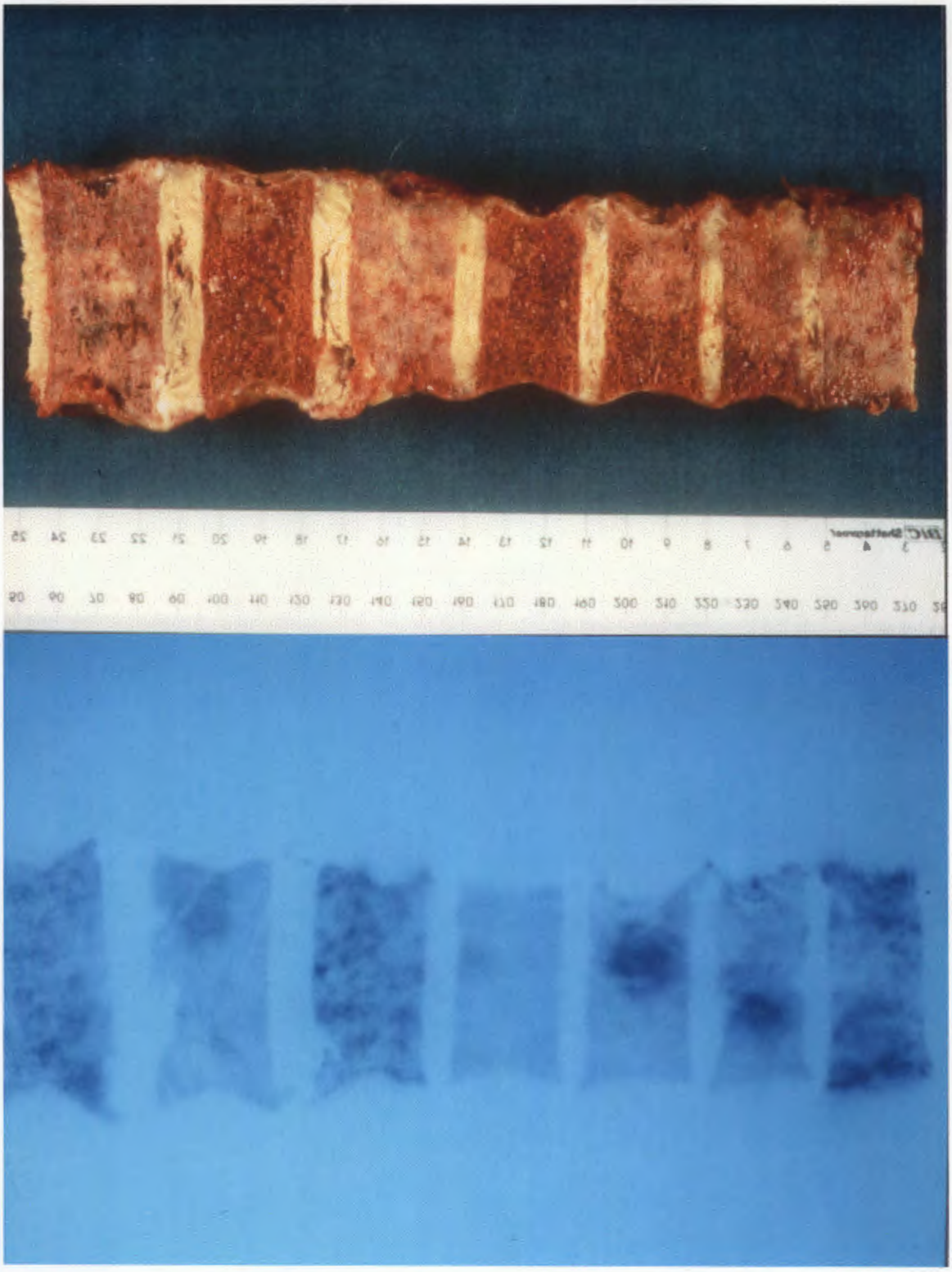

^{153}Sm has a half-life of 46.7 hours, emits β^--rays with energies 805[21%]; 702[44%] and 632[34%]keV and a γ-ray with energy 103[28%]keV with a max. soft tissue penetration of ~0.3 cm [6]. This illustrates that ^{153}Sm is a mild treatment and after 9 weeks further treatment is necessary once radiation levels have declined and the pain palliation subsides [7]. The corresponding figures for ^{166}Ho are t½ = 26.9 hr; β^- 1776[48%]keV and 1840[51%]keV; γ (81 keV [6.2%] and 1380 [1%]keV); max. soft tissue penetration 0.84 cm [6]. This suggests that ^{166}Ho might be a better therapeutic radionuclide especially for large lytic type tumours, broadening the scope from palliative purposes to use in curative therapy [7,8]. Together with the high natural abundance of ^{165}Ho (100%), from which ^{166}Ho is produced by neutron activation, and a neutron capture cross-section = 64 barns, the cost of production is much lower. (^{152}Sm enriched Sm is used to produce ^{153}Sm). This is why Mumper *et. al.* chose Ho-166 as their radioactive isotope for the internal radiation therapy of hepatic tumours [9].

To get a better understanding of this phenomenon a skeletal image taken using a γ-camera is presented (Photo 1). The image (taken 3 hrs after injection) is of a patient who was injected with ^{153}SmEDTMP on a Thursday and died over the week-end. The photograph shows the selectivity of this pharmaceutical for bone tissue alone. The darker areas show higher ^{153}Sm absorption and correspond to the bone areas mostly affected by the cancer. Because of the patient's death an autopsy could be performed and a closer look could be taken at the vertebral column. Photo 2 shows the remarkable selectivity of ^{153}SmEDTMP. The two photos compare the cross sectional cut of the spinal cord in visible light and as a γ-image. On the visible picture the cancer affected areas of the spinal marrow show as lighter areas; light brown to milky white. The brown-red segment, second from the left is unaffected tissue. The thin horizontal bands represent the cushions between the dorsal vertebra. On the γ-image the darker areas show more absorption of ^{153}Sm and correspond to the lighter areas on the visible image viz. the cancer cells. Thus ^{153}SmEDTMP is not only selective for bone tissue but also prefers the cancer cells above normal tissue.

Although the chemistry of Ho and Sm is similar (both are lanthanides), the skeletal localisation of ^{166}HoEDTMP proved to be inferior to ^{153}SmEDTMP [1]. From a medical viewpoint, the spread of radioactivity throughout the body should be avoided because of the ineffective dose reaching the tumour cells and the side effects of radiation throughout the body.

Photo 3. A computer enhanched image of ^{153}Sm uptake in various parts of the body. The white areas show the highest levels of radiation being emitted and thus the highest uptake.

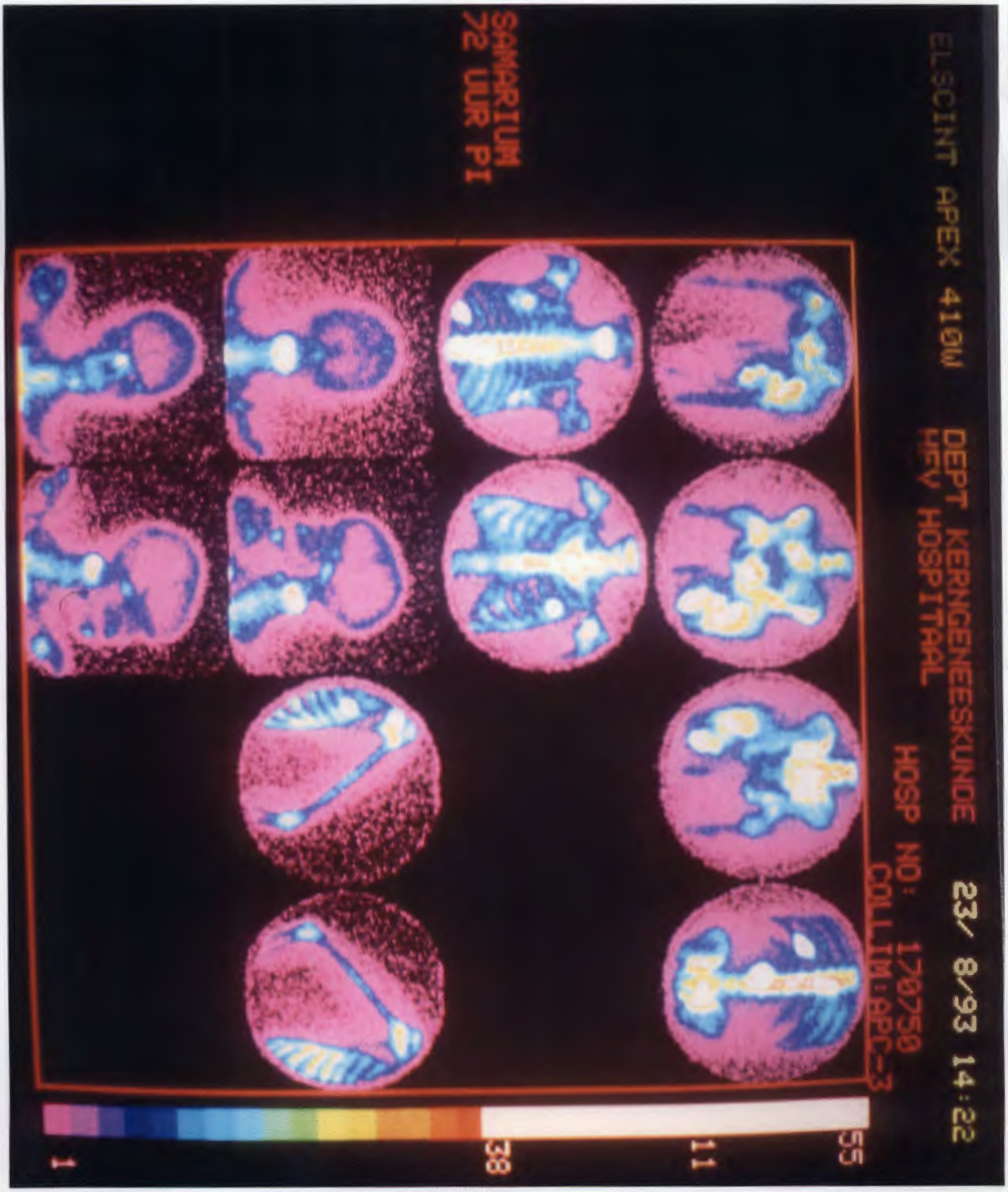

Photo 4. Comparative γ-images for ^{99m}TcMDP, ^{153}SmEDTMP and ^{166}HoEDTMP (from top to bottom). No clear skeletal picture is produced by ^{166}HoEDTMP (bottom).

This is just what Photo 3 shows. In Photo 3 the bone uptake of ^{153}Sm in various parts of the body is displayed. This is a computer enhanced image in which the reddish to blue to white areas correspond to the higher levels of radiation being emitted and therefore the higher uptake. The maximum bone accumulation of ^{153}SmEDTMP in a baboon (used as a model for humans) has been reported to be 53% 4 hrs after intravenous injection [6]. The bone to background (cardiac pool) uptake for ^{153}SmEDTMP was 91% in comparison to 95% for ^{99m}TcMDP (a bone imaging agent). The figures for ^{166}HoEDTMP are 45% and 69% respectively. The 45% total accumulation is not worrying because it only leads to a higher urine excretion of ^{166}Ho. The bone to blood ratio of 69% is the concern. This can be seen quite clearly on Photo 4 which shows comparative γ-images of ^{153}SmEDTMP and ^{166}HoEDTMP 4 hours after administration. The bottom side shows the ^{166}Ho uptake. No clear skeletal picture is produced. The bone uptake of ^{166}HoEDTMP from blood plasma seems to be insufficient [6].

^{153}SmEDTMP will shortly be marketed as a pain palliation therapy for bone cancer. Pre-clinical and clinical trails tests were successful. The search for better radiopharmaceuticals to treat bone cancer has not stopped here but continues.

1.2 Ligands tested as possible bone cancer remedies.

This dissertation has focused on three diphosphonate ligands viz. APD = 1-Hydroxy-3-amino-propilydenediphosphonicacid, MDP = Methylenediphosphonicacid and HEDP = 1-Hydroxy-ethylenediphosphonicacid.

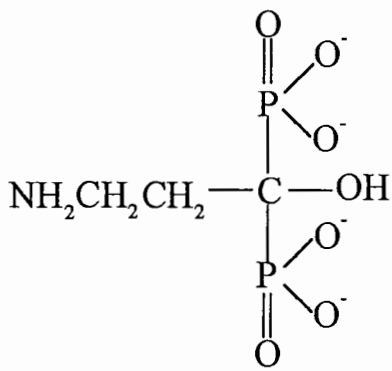

APD

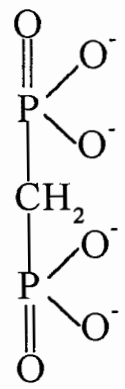

MDP

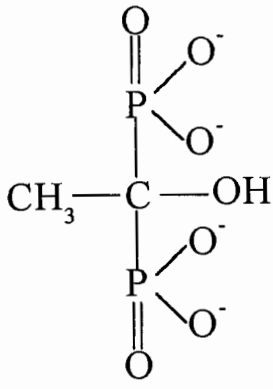

HEDP

All three of them are currently used as bone-seeking ligands.

1.2.1. APD

Since 1994, APD has been commercially produced by Ciba, Switzerland, and marketed under the trade names Pamidronate or Aredia (disodium pamidronate). It is used to suppress osteolytic bone metastases by inhibiting both bone resorption and osteolytic activation. Both these are features of bone cancer and cause increased 'bone turnover'. APD as well as the other diphosphonates have the ability to sorb strongly to hydroxyapatite and thus inhibit bone resorption [10]. According to Ciba, APD functions by binding to the bone surface thereby inhibiting resorption, the functioning of osteoclasts and interferes with the maturation of osteoclast precursors [3]. A further aspect is that APD mobilises Ca(II) and Mg(II) in blood plasma to such an extent that an increased amount of these two metal ions is available for deposition on the bone, thus assisting in regenerating bone tissue [11]. In short this remedy is used to stop the "eating away" of the bone by the cancer cells. It does not destroy the cancer cells but repairs the damage they do to the bone. The resorption of bone causes pain and therefore APD is marketed as a pain palliation therapy for osteolytic bone cancer patients. A study of this ligand would be interesting as it already has palliative effects on its own and if it could deliver a radioactive metal-ion to the bone, it may be a highly effective therapeutic agent.

1.2.2. MDP

MDP (also known as Medronate) is commercially applied in the radionuclide bone imaging agent ^{99m}Tc(Sn)-MDP. Because of the soft γ-ray it emits, ^{99m}Tc is widely used as an imaging agent [12]. Different ligands deliver Tc-99m to different organs. The presence of Sn(II) in the above skeletal imaging agent helps to reduce pertechnetate. To what oxidation state the Tc is being reduced is still one of the unknown aspects of the chemical composition of ^{99m}Tc-radiopharmaceuticals [13]. HMDP (hydroxymethane diphosphonate) is sometimes used to replace MDP in targeting the bone. Studies showed that the cancerous/compact bone uptake is greater for HMDP than MDP [14]. Another ligand used is HEDP. The bone uptake of ^{99m}Tc HEDP is lower than that of MDP but gives a greater contrast between regions of higher and lower calcification rates. However Tc-99m MDP has a faster rate of blood clearance [15]. Both HEDP and HMDP have an hydroxy-group which MDP lacks. It was therefore decided to choose MDP and HEDP for further studies as possible pain palliative radiopharmaceuticals.

Degrossi, Oliveri and Garcia del Rio *et. al.* compared ^{99m}Tc-MDP with ^{99m}Tc-APD as bone scanning agents [16]. They were able to show that APD appears to be an adequate agent for bone scintigraphy. The whole body retention after 24-hrs was 17.6% ± 4.6 for ^{99m}Tc-APD as compared to 28.6% ± 3.9 for ^{99m}Tc-MDP. The blood clearance time was similar for both compounds and the lesion/normal bone ratio was found to be 4.6 in studies using APD and 4.8 using MDP.

1.2.3. HEDP

HEDP (also known as Etidronate) is sometimes used as ^{99m}Tc(Sn)-HEDP because of its higher specific bone uptake than MDP [15]. As the areas with higher rates of calcification should be the target of a possible palliative radiopharmaceutical HEDP seems to be a promising candidate. HEDP has also a unique relationship with rapid growing hydroxyapatite which gives it the potential in controlling abnormal high rates of bone growth as occurs in Paget's disease [17]. In the above pharmaceutical application the diphosphonate is the bone seeker and it localises the ^{99m}Tc at the bone to give the skeletal image wanted. ^{99m}Tc is not a β-emitter, has a half-life of 6.0 hours and emits only γ-rays and therefore has no therapeutic effect. Research is being done on replacing Tc by Re (an

element with similar chemistry to Tc) which is a strong β-emitter. Studies on the use of ^{188}Re (half-life of 16.0 hours) complexes of MDP and HEDP as bone therapeuticals is currently underway [18,19]. ^{188}Re-HEDP may also be used therapeutically in the future. The high bone uptake of HEDP makes it worth investigating complexes of this ligand with the lanthanide's ^{153}Sm and ^{166}Ho.

1.2.4. Theories on the hydroxy-group function in bone uptake

In the literature various theories on the purpose of the hydroxy-group in diphosphonate ligands have been suggested. In this study, only MDP lacks this group. The most popular postulate is that the hydroxy-group binds to the hydroxyapatite of the bone and so increases the ligand's selectivity for bone. This postulate is supported by a comparison of MDP and HEDP. HEDP has a higher bone uptake than MDP and co-ordinates much faster to hydroxyapatite than MDP[15]. This leads one to believe that the hydroxy group plays an important role in adsorption on hydroxyapatite. However, the hydroxy group may paradoxically also be involved in complexing the metal ion. For ^{153}SmEDTMP adsorption on hydroxyapatite, Chirby *et al* [20] have found that ^{153}Sm is adsorbed as part of the ^{153}SmEDTMP complex and not as free ^{153}Sm(III) which would follow the dissociation of the complex just before adsorption. There is however some evidence to support the idea that dissociation takes place first [21].

1.3 Chemical speciation

To elucidate the performance of these chosen ligands in treating bone cancer the reactions between metal-ions and ligands needs to be understood [22]. When looking at bonding between a ligand and a metal-ion one way to describe this phenomenon is to consider the thermodynamic equilibria occurring. The formation constant, β for the equilibrium of complex formation is defined as follow:

$\beta_{pqr} = [M_pL_qH_r] / [M]^p[L]^q[H]^r$ for the reaction $pM + qL + rH \rightarrow M_pL_qH_r$

(M = metal-ion, L = ligand and H = hydrogen ions bonded to the complex)

Where p = 0 the protonation constants are used to describe the protonation of bases.

For a particular ligand and metal-ion several complexes may form at different pH values e.g. ML, MLH, M_2L, ML_2 and MLOH. The distribution between these different species is

called the speciation of that ligand. Duffield and Williams [23] have defined speciation as follows: Speciation defines the oxidation state, concentration and composition of each of the species present in a chemical sample. Better computing and analytical methods in recent years have led to an increased understanding of the speciation underlying many chemical reactions, with interesting conclusions in medicine, industry and the environment [23]. An example of this are broad-breasted bronze turkey chicks who failed to grow despite having a balanced diet which contained Soya meal and the required metal ions like zinc. It was shown that that the zinc firmly complexed with the Soya protein and were therefore unavailable to the animal. The solution to this problem was the introduction of a complexing ligand which removed the zinc from the protein, making it bioavailable. Prolinate was such a ligand which did not complex too strongly to zinc so that the body would be stripped of zinc [24,25].

Findlow *et. al.* [26] were able to show with chemical speciation that the link between high levels of aluminium in the blood and Altzheimer's disease is rather tenuous. Only a small percentage of dietary aluminium exists in neutral lipid soluble fractions which can migrate across intestinal mucosal cells into blood plasma.

On the same note it was shown that only 2-3 % of cadmium metal in crabmeat is available from the gastrointestinal tract [27]. This observation saved the crabmeat industry from closing down when the levels of cadmium in this meat exceeded the limits set by the UK ministry of Agriculture and Fisheries and Food. This gave the food a safety factor of one or two orders of magnitude. In this context Jones *et. al.* [28] also used speciation to assess the ability of various pharmaceutical agents to remove Cd(II) from humans.

Huang *et. al.* [29] were able to show that Razoxane, a drug used in cancer treatment, may influence cancer cell growth as follows: Firstly being lipophilic in blood plasma it is able to enter cells. Once inside the cell, the molecule's ring opens and forms a chelating ligand which seeks out essential metal ions and so stops cell growth.

With the help of speciation, Williams [30], shed some light on the working of thalidomide.

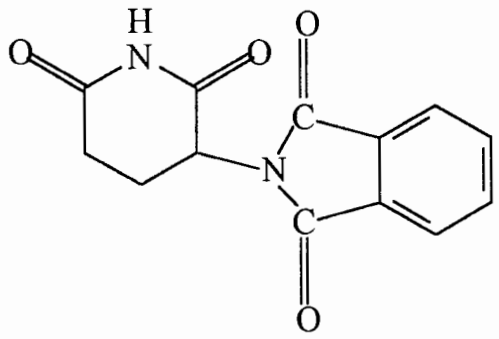

Thalidomide

If the molecule is subjected to peptide hydrolysis by enzymes which are ubiquitous in humans, the 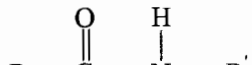 bonds are cleaved giving the parent RCOOH and NH_2R' agents. If two of the four possible sites in thalidomide are cleaved, an agent similar to EDTA may result. This is capable of sequestering calcium ions near to the limb buds in the developing foetus, with the risk of deformation. By using speciation data one could optimise the desirable reactions and suppress threatening reactions.

Hurford *et. al.* [31] described the benefits of zinc's addition to toothpaste. Because of its bacteriostatic effect upon oral flora, zinc hinders calcium deposition on plaque and is responsible for the anti-swelling effect in dental calculus. Speciation showed how the toothpaste must be formulated. The zinc species must be lipophilic to be bioavailable to the bacteria, have the correct speciation to poison calcium plaque bonding and penetrate the tissue to ease gum inflammation.

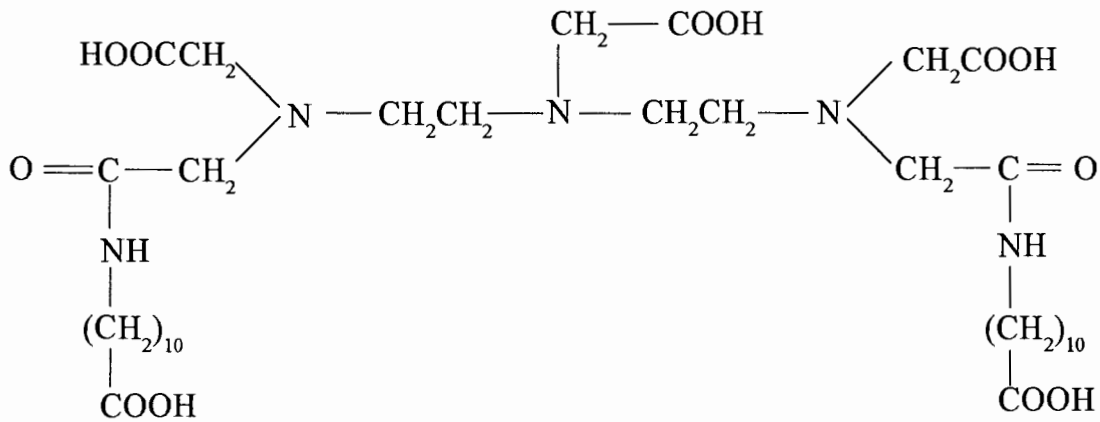

Puchel

On environmental issues, speciation has also proved to be a handy tool. Duffield *et.al.* [32] showed, by using ECCLES to simulate chemical speciation in blood plasma, that Puchel

(as shown above) would not be such a good plutonium chelation therapy. Intravenously administered CaDTPA however binds much better to Pu(IV) and is probably the best prompt treatment for plutonium contaminated people [32].

Radioactive waste storage is a controversial issue because plutonium and other waste products have such long half-lifes. Speciation can be used to predict how safe a particular storage area is [33]. Jarvis *et. al.* [34] commented on the transportation of plutonium around South Africa. They showed, using chemical speciation, that an accident causing contamination of South-Africans was very unlikely. If plutonium were to be released into the marine environment the physical spreading of PuO_2 is minimal and is largely non-bioavailable to marine organism.

1.4 Chemical speciation and the blood plasma

The human body consists of cells which are surrounded by an aqueous medium. Since 70% of the body is water, life is sustained by reactions between metal-ions and ligands which occur *in vivo* in this medium. Studying the reactions between metal-ions and ligands is therefore needed to understand more of the biochemistry in the human body [22].

The delivery of radioactive nuclides such as ^{153}Sm, ^{99m}Tc and ^{186}Re to the bone by bone seeking ligands is well known. Calculating the speciation for a particular ligand in blood plasma will tell whether a complex will survive the competition of metal-ions and ligands occurring naturally in blood plasma. If so, the ligand will be able to deliver the radionuclide to the bone and may be successful in the treatment of painful bone metastases. The computer program ECCLES [35] predicts the speciation of metal ions or ligands in biological fluids like blood plasma. ECCLES stands for **E**valuation of **C**onstituent **C**oncentrations in **L**arge **E**quilibrium **S**ystems. May *et. al.* [35] wrote this program to simulate the nature of the metal ion binding to low-molecular-weight ligands (LWL) in human blood plasma seeing that they play such an important role in biological systems [36]. This program uses the fact that the percentage distribution of transition-metal ions among LWL is not controlled by protein binding to bypass the exclusion of protein-metal equilibria. The distribution of Ca(II), Mg(II), Mn(II), Fe(III), Cu(II), Zn(II) and Pb(II) amongst 5000 complexes formed with 40 or more ligands is computed, clearly justifying

the use of a computer to speed up calculations. Binary and ternary complexes (like MLL' and MLL'L'' where L,L' and L'' are different ligands binding to the same metal ion) are also taken into account. Introducing a new ligand as a pharmaceutical requires that the program's database of formation constants be expanded by constants describing the complexation of the ligand with the various metal ions (including the metal ion used as source of radiation) in order to elucidate the *in vivo* behaviour of the radiopharmaceuticals, like it was done for ^{153}SmEDTMP in blood [5].

Constants for important blood plasma metal-ions with EDTMP as well as those for Sm(III) and all blood plasma ligands were added to the database. Speciation calculations with ECCLES showed that EDTMP effectively competes with blood plasma ligands such as citrate for Sm(III) and thus ^{153}Sm is likely to be successfully delivered to the bone. ^{166}Ho on the other hand forms a weaker complex with EDTMP [7] and therefore may be complexed by plasma citrate accounting for the high levels of ^{166}Ho in the blood of the baboon model [6]. As previously mentioned, ^{166}Ho would possibly treat some tumours more effectively. ^{166}Ho has the advantage that a higher dose is delivered in a shorter period. The results of the baboon tests showed that a bone to background (cardiac blood pool) uptake for ^{166}Ho-EDTMP, was 69% in comparison to 91 % ^{153}Sm-EDTMP [6]. In this case ECCLES confirmed that ^{166}HoEDTMP would not survive blood plasma even though the difference between the values of logK for the formation of ML for Ho and Sm is only 1.2. This is due to the fact that Ho(III) is a smaller ion than Sm(III) and therefore the complexation between Ho(III) and EDTMP is weaker due to steric hindrance. This allows citrate to compete more effectively for Ho(III) in blood plasma. It might therefore be worthwhile developing more suitable bone localising ligands for ^{166}Ho which will have a similar biodistrubution as ^{153}SmEDTMP. In this respect the choice of the radionuclide (of which the half-life and radiation emissions dictate its radiobiological effects) and the bone localising agent (of which the biochemical properties dictate its pharmocokinetics and biodistrubution) determine the therapeutic success of the modality [37].

Computer simulation (ECCLES) was used to confirm results achieved with ^{153}Sm- and ^{166}HoEDTMP as possible radiopharmaceuticals as had been tested in baboons [7]. Computer simulation may now be considered to be a screening method before pre-clinical and clinical trails. This research is useful as now it is not necessary to test all the available ligands with a radioactive lanthanide (normally this type of metal-ion has radioactive

isotopes that are suitable for radiation in humans) in baboon tests. It is expensive to manufacture the radioactive isotope and the required concentration of the injected metal-ion can only be estimated. Unnecessary and expensive baboon tests (to which there is growing objection) are reduced. The minimum of baboon tests are now needed and the best concentrations are known beforehand. There is also the possibility of predicting side effects of the treatment in advance. In the case of ^{153}SmEDTMP it was predicted that a stripping of Zn(II) out of the body via the urine would occur. This was later confirmed by urine tests. Patients may thus need to receive Zn additives while being treated with ^{153}SmEDTMP [7].

Another example where ECCLES was used is the previously mentioned article by Duffield *et. al.* [32]. ECCLES calculated the distribution of Pu(IV) in normal blood plasma showing that it complexes with citrate. The competition of the studied chelation therapy ligand with citrate for Pu(IV) gave an indication of how successful Pu(IV) would be mobilised from the blood and excrete it. Jones *et.al.* [28] investigated the mobilisation of cadmium from blood plasma using ECCLES.

1.5 Research objectives.

To assist in the understanding of the function of a ligand in blood plasma, its speciation may be calculated. The purpose of this thesis is to construct blood plasma speciation models for the three diphosphonate ligands, using the program ECCLES [35]. Various techniques were used to arrive at the constants needed. From the results achieved by ECCLES a ligand is chosen and tested together with ^{166}Ho(III) as a radiopharmaceutical in the baboon model.

The complexation of APD, MDP and HEDP with various metal ions was studied in 0.15M NaCl (the approximate ionic strength of blood plasma) and at 37°C [39]. The calculated formation constants assist in predicting the speciation of metal ions and the ligands in human blood plasma. Important metal-ions in blood plasma complexed by these ligands are Ca(II), Mg(II) and Zn(II), and these equilibria must be studied. The aim is to find a suitable ligand to complex Ho(III) and Sm(III) in blood plasma in such a way that it will survive competition from blood plasma ligands and release the metal-ion at the bone. The

formation constants of these metal-ions with each of the ligands are thus required to complete the blood plasma model. Because of reasons given below formation constants for the lanthanides fall beyond the scope of this thesis but will be completed at a later stage. The three metal-ions Ca(II), Mg(II) and Zn(II) and their complexation with the three ligands have been studied extensively in this work.

1.5.1 Techniques used to derive complexation constants

The main technique used in this dissertation for determining formation constants was potentiometric titrations. The data is fed to the library of computer programs, ESTA which was written to fit the titration curve to a series of complexation reactions chosen by the user. From this the best protonation and complexation constants are calculated for a particular system [5]. For Zn(II), Ho(III) and Sm(III) precipitates formed between pH = 4 and pH = 7. Potentiometry proved therefore to be inappropriate for the calculation of the complexation of Zn(II), Ho(III)and Sm(III) with these ligands. Another technique was required.

Polarography is able to use lower concentrations of the metal-ion and thus avoids precipitation. It can measure low concentrations of metal-ions very accurately as well as the reduction potential by differential pulse polarography. With this technique two possible complexes are studied viz. labile or non-labile [38]. The data is treated on a computer program called ML-SPEC [38] or CV-FIT. From this the constants for Zn(II) with the three ligands were derived.

A comparison of these two techniques was necessary to ascertain whether both gave similar results. A system in which no precipitate forms at the required potentiometric concentrations using a metal-ion that is polarographically active was studied. As Ca(II) and Mg(II) are not polarographically active, Cd(II) was studied with HEDP.

1.5.2. NMR studies on the complexation sites involved in these ligands

The three ligands chosen have the diphosphonate group in common. Starting with MDP, the most simple ligand, the idea was to study how a 'tail' will affect the complexation (APD), what effect the amino group has (APD) and what contribution the hydroxy group

makes to the complexation (HEDP). Potentiometry and polarography describe the thermodynamics of these systems in solution. These two experimental techniques do not describe the structure of the complex. An NMR-study on a complex may yield a 'visual' picture of the solution structures. This was attempted using ^{13}C and ^{31}P NMR. Ultimately we hope that answers to some of the questions posed in this thesis may lead to a radiopharmaceutical that will not only have pain palliation applications but also be useful in the treatment of secondary bone metastases .

1.5.3. Layout of this dissertation

This dissertation will be presented in the order of the five main techniques viz. potentiometry, polarography with the comparative study between these two, NMR studies, ECCLES simulation and baboon studies. For each section the material will be reported in this order. The sections discussed will be Theoretical background, Experimental, Results and Discussion and Conclusion.

2. Theoretical Background

2.1 Potentiometry as a tool to derive formation constants

The measurement of metal-ligand formation constants is nowadays considered as almost routine although there are still difficulties involved in determination of reliable values [47]. Potentiometry is often used as a technique to calculate formation constants but the same chemical systems studied by different research groups often result in considerable discrepancies in their results. It is considered by some to be necessary to evaluate calculated constants by a second technique to verify the results. In this work polarography was used to support constants found by potentiometry.

In this study the potentiometric data was analysed using the ESTA (**E**quilibrium **S**imulation by **T**itration **A**nalysis) suite of computer programs as described by P.M. May *et al.* [47,48,49]

ESTA imposes the conditions of mass-balance in the standard way by equating calculated total concentrations with real (analytical) concentrations:

(The meanings of the symbols are listed in Appendix A1)

$$T_i^r = T_i^c, \quad I=1,\ldots,NC \tag{1}$$

where

$$T_i^c = [X_i] + \sum_{j=1}^{NJ} r_{ji}\Gamma_j\beta_j\prod_{n=1}^{NC}[X_n]^{r_{jn}} \tag{2}$$

$$T_i^v = \frac{C_i^v V^o + \sum_{m=1}^{NB} C_{im}^B \upsilon_m}{V^o + \sum_{m=1}^{NB} \upsilon_m} \tag{3}$$

$$\Gamma_j = \left(\prod_{n=1}^{NC}\gamma_n^{r_{jn}}\right) \Big/ \gamma_j \tag{4}$$

The potential of the electrode can be written in the form

$$E_k = E_k^o + E_k^{IS} + E_k^{LJ} \tag{5}$$

where E_k^o is the electrode response intercept, E_k^{IS} the electrode selectivity and E_k^{LJ} the

liquid-junction potential.

Electrode selectivity

Unlike some programs [50,51] ESTA accommodates the well-known effects of interfering ions. It uses the Eisenman equation [52] as a basis to derive eq (6). It has the advantage that suitable choices for α and K_{ki} can be made.

$$E_k^{IS} = S_k \log[\{X_k\}^{1/\alpha} + \sum_i (K_{ki}\{X_i\}^{z_k/z_i})^{1/\alpha}]^{\alpha} \tag{6}$$

Liquid-junction potential

Unlike [50,51] the liquid-junction term E_k^{LJ} is not taken constant but is derived from the Henderson equation as described by Biedermann and Sillén [53]. It has the form

$$E_k^{LJ'} = -(RT/F)\ln(1+d[X_H]/I) \tag{7}$$

where I is the concentration of the background univalent electrolyte. This is used to correct for liquid-junction potential changes in the calibration of glass electrodes. The Henderson [54] equation (eq 8), itself is used to predict potentials across junctions of different univalent electrolytes at constant ionic strength.

$$E_k^{LJ'} = \frac{-RT}{F} \times \frac{\sum_i \gamma_i^s\{S_i^s\} - \lambda_i^b\{S_i^b\}}{\sum_i z_i(\lambda_i^s\{S_i^s\} - \lambda_i^b\{S_i^b\})} \times \ln\frac{\sum_i \lambda_i^s z_i\{S_i^s\}}{\sum_i \lambda_i^b z_i\{S_i^b\}} \tag{8}$$

For the purposes of this dissertation there was no liquid-junction and it was therefore not necessary to employ this correction.

Activity coefficients

For the calculation of activity coefficients the most common extension to the Debye-Hückel formula has been used.

$$-\log \gamma = \frac{Az^2\sqrt{I}}{1 + Ba\sqrt{I}} + cI \tag{9}$$

Conversion into thermodynamic constants

Equations (2), (6) and (8) require "thermodynamic" values of the parameters β_j, E_k^o, K_{ki} λ_i^s and λ_i^b, *i.e.*, those that are defined with respect to a standard state based on reactions occurring at infinite dilution in water at zero ionic strength. However, it is established practise to work with conditional constants (${}^I\beta_j$, ${}^IE_k^o$, ${}^IK_{ki}$ ${}^I\lambda_i^s$, ${}^I\lambda_i^b$) which refer to some other ionic strength (I). The formation constants reported are thus conditional formation constants characterised by the medium in which they were determined. Such constants can be converted into the corresponding thermodynamic values in the following way:

$$\beta_j = {}^I\beta_j/{}^I\Gamma_j$$

${}^I\Gamma_j$ is defined as in eq. (4). Eq. (6) now yields:

$$E_k^{IS} = s_k \log^I \gamma_k + s_k \log\left\{ [X_k]^{1/\alpha} + \sum_i \left(\frac{K_{ki}({}^I\gamma_i[X_i]^{z_k/z_i}}{{}^I\gamma_k} \right)^{1/\alpha} \right\}^{\alpha}$$

The supplied value of ${}^IE_k^o$ and the ion selectivity coefficients are converted into thermodynamic values as follows:

$$E_k^o = {}^I E_k^o - s_k \log {}^I\gamma_k$$

$$K_{ki} = {}^IK_{ki}({}^I\gamma_k/({}^I\gamma_i)^{z_k/z_i})$$

The supplied ionic conductivities to be used in the calculation of E_k^{IJ} are treated similarly:

$$\lambda_i^s = {}^I\lambda_i^s/{}^I\gamma_i^s, \qquad \lambda_i^b = {}^I\lambda_i^b/{}^I\gamma_i^b$$

Conditional constants are to be supplied by the program user. The same values (say, for electrode potential) are calculated for any point in the titration which actually has the reference ionic strength.

Solution of mass-balanced equations

The *NC* mass-balance equations (m.b.e.) eq.(1), can be solved for any *NC* unknowns as long as all the other parameter are known. There are *NC* free concentrations that can be determined. If one of the free concentrations has been measured experimentally, the remaining free concentration and one other parameter (such as υ_m, β_j and Γ_i^r) can be calculated. It follows that the procedure for solution of the m.b.e. falls into two categories. First the equations are solved for *NC* free concentrations without any reference to the electrode equation. Next the electrode potential can be obtained by substitution into eq. (5), (6) and (9). In the second category, it is necessary to solve the electrode equation to obtain the free

electrode-ion concentrations, $[X_k]$, (given an observed potential, E_k), before solution of the m.b.e. Solving the electrode equation for $[X_k]$ requires a knowledge of all the free concentrations. It is therefore necessary to implement an iterative solution of this equation and the m.b.e.

A Newton-Raphson procedure is generally the most efficient way to solve the m.b.e. The equations can be setup in terms of the absolute values of the unknowns except for the free concentrations, $[X_k]$, and formation constants, β, for which natural logarithms are more convenient. The equations can rapidly solved by forward and backward substitution. If a failure in the Newton-Raphson procedure occurs in those tasks for which the only unknowns are free concentration , the slower but more robust secant method [55] can be used to solve the equations.

Initial estimates

It is well known that the efficiency of the Newton-Raphson method is considerably improved if good initial estimates can be obtained for the unknowns. There are two classes of unknowns. The first is the free concentration of the components which have to be derived from the electrode equations otherwise they are difficult to estimate. Secondly, there are those unknowns which are experimental parameters such as total titrand concentration and titrand volume. Formation constants can also be included in this class. Generally it is possible to estimate reasonable initial values in this instance.

At the first and second titration points, initial estimates for the unknown values of the second type are readily calculated from experimental values. Electrode potentials are available and initial estimates of the corresponding free electrode-ion concentration can thus be calculated. Initial estimates of all parameters at the third and each subsequent point of a titration are best obtained by linear extrapolation of the solution from the previous two points. This based on the change in electrode potential.

This approach to simulate titration data is optimised by algorithms. Simultaneous optimisation of n_p parameters p_r, (where p_r may be β_j, E^o_k, s_k, V^o, C^v_i, or C^b_{im}) is performed by minimising an objective function, U, defined as

$$U = (N - n_p)^{-1} \sum_{n=1}^{N} n_e^{-1} \sum_{q=1}^{n_c} w_{nq} \, (y_{nq}^{obs} - y_{nq}^{calc})^2 \qquad (10)$$

where y_{nq}^{obs} and y_{nq}^{calc} may be either a T_{nq} or an E_{nq}. Weights are introduced by w_{nq} [49].
The Gauss-Newton method is the most frequent approach used for minimising U, as is used in ESTA. In general, given good initial estimates and a reasonable well behaved system, the Gauss-Newton method described above performs extremely well. It often converges in 3-6 cycles. Unfortunately the solution is sometimes obviously unsatisfactory (for example produce a shift vector with a upward gradient). If the shifts are not too excessive a Levenberg-Marquardt [56] method may be applied to reduce them otherwise the program will terminate. When the estimates of the parameter being refined are judged to be sufficiently close to the solution., standard deviations of the parameters may be calculated from

$$\sigma_r = \left[\frac{U \times G_{rr}}{N - n_p}\right]^{1/2} \tag{11}$$

where $\mathbf{G}=\mathbf{H}^{-1}$

Correlation coefficients can be calculated by using the formula

$$r_{sr} = \frac{G_{sr}}{(G_{ss}G_{rr})^{1/2}} \tag{12}$$

and the Hamilton R-factor, R^H, is given by

$$R^H = \left[\frac{U}{\sum_{n=1}^{N} n_e^{-1} \sum_{q=1}^{n_c} w_{nq}(y_{nq}^{obs})^2}\right]^{1/2} \tag{13}$$

and its limit by

$$R_{\text{lim}}^H = \left[\frac{U}{\sum_{n=1}^{N} n_e^{-1} \sum_{q=1}^{n_c} w_{nq}(y_{nq}^{obs})^2}\right]^{1/2} \tag{14}$$

Program description

ESTA accommodates chemical systems of up to 10 components forming up to 99 complexes.

Titrations involving up to three electrodes and three burettes are permitted. The program permits corrections of titration data affected by liquid-junction potentials and imperfect ion-selectivity of electrodes. The ESTA library contains program modules, which perform one or more kind of calculations (specified as a different "task"). The modules that have been used will be described.

ESTA1: *the simulation mode*

By setting up and solving the mass-balance equations, ESTA1 can determine, on a point-by-point basis, single values for almost any titration parameter. The calculations fall into two categories: (i) species-distribution calculations and (ii) potentiometric titration calculations. The latter include determination of emf values, formation constant estimates, total analytical concentrations , initial vessel concentrations and initial burette concentrations. This program most commonly used to generate formation function values (task ZBAR), deprotonation function values (task QBAR) and protonation values (NBAR). ZBAR can be described as the number of ligands bound per metal ion at a certain pH value. QBAR is the number of protons lost by the ligand due to complexation taken at a certain pH value. NBAR is the number of protons bound per ligand at a certain pH value in the absence of complexation. These functions can be mathematically described as follows: (The meanings of symbols are listed in Appndix A1)

The protonation formation constant is described as

$$\overline{Z_H} = \frac{T_H - H + OH}{T_{Lig}} \tag{15}$$

and the metal formation function is defined as

$$\overline{Z_M} = \overline{Z} = \frac{T_L - A(1 + \sum_n \beta_{LH_n} H^n)}{T_M} \tag{16}$$

where $A = (T_H - H + OH) / \sum_n \beta_{LH_n} H^n$. $\overline{Z_H}$ is plotted against pH and $\overline{Z}$ against pA = -log A, as can be derived from the equations 15 and 16.

The deprotonation function is defined as

$$\overline{Q} = \frac{T_H^{\star} - T_H}{T_M} \tag{17}$$

where $T_H^{\star}$ is the calculated total concentration of protons in the system at the observed pH ignoring the presence of all metal complexes. The following two mass balance equations are solved for $T_H^{\star}$ and T_L.

$$T_H^{\star} = H - OH + \sum_{j=1}^{NJ} r[M_p L_q H_r] \tag{18}$$

$$T_L = L + \sum_{j=1}^{NJ} q[M_p L_q H_r] \tag{19}$$

where p = 0.

By using this program graphs can be drawn of pH vs $\overline{Z_H}$ or $\overline{Q}$ and $\overline{Z}$ vs pA where the observed and calculated functions can be compared and E_k^{obs} , E_k^{calc} evaluated respectively. If the calculated and observed curves match each other closely in the pH region of interest, the proposed model of formation constants can be accepted. $\overline{n}$ is used together with $\overline{Q}$ to identify species like MLOH at high pH values not included in the ESTA2A model.

ESTA2: *the optimisation modules.*

There are two optimisation programs, ESTA2A and ESTA2B, differing only in the way data is weighted [49]. They are used when it is desired to determine, for one or more parameters, the "best" values, based on a least-square procedure applied to a whole system of titrations. In this way the following parameters can thus be refined: formation constants, vessel and burette concentrations, electrode slope and initial vessel volume. It is possible to group together, over any combinations of titrations, local parameters of the same type and with the same value so that they are refined together as a single parameter.

The approach is to model with ESTA2 the formation constants untill the best values for the standard deviations and Hamilton factors are reached. After this hurdle is crossed the proposed model of formation constants is tested by QBAR or ZBAR comparisons.

2.2 Polarography as a tool to derive formation constants

Two types of complexes can be distinguished according to the polarographic time scale viz. labile and non-labile. Complexes that have a quick exchange rate between the metal-ion and its ligand if compared to the polarographic time scale are classified as labile. It follows that the polarographically active peak is that of the metal-ion. The peak height and shift in peak potential as compared to different pH values is observed. For non-labile systems the exchange rate between metal-ion and ligand is slow relative to the polarographic time scale. What is observed is the peak corresponding to the reduction of the complex if polarographically active. The peak height is a function of the concentration of the active redox species which is characterised by a peak potential. Thus as the pH of the solution is changed the concentration of the species present in the solution changes and this change is reflected in a change in the polarographic peak height. The peak height as compared to pH values as well as the peak potential is observed. The pH region where the particular complex is predominant will show the peak height small at the lowest pH of this region, will rise to a maximum as the pH increases, decrease again and finally disappear. A new peak corresponding to another complex is now formed.

The computer program ML-SPEC and its update, CV-FIT, was written by Cukrowski and co-workers [38, 102] to treat the polarographic data and calculate formation constants from it. The programs calculate formation constants for complexes that are labile as described above.

Labile complexes

The program ML-SPEC is able to treat a system in which more than one ligand is co-ordinated to a central metal-ion and where there is a region of pH in which one complex is the predominant species present in the solution. To do this the Lingane equation [57], at 25°C, viz.

$$(E_{½})_c - (E_{½})_s \cong \frac{0.0591}{n} \log K_c - j \frac{0.0591}{n} \log C_x \qquad (1)$$

was used in a modified form (the subscripts "c" and "s" refer to the complex and free metal ion respectively). For CV-FIT, which calculates labile and non-labile complexes together the shift in in peak potential (Eq. (1)) caused by the formation of metal complexes and can be

calculated as follow

$$\Delta E_p = E_p(M_{Free}) - E_p(M_{Comp}) = \left(\frac{RT}{nF}\right) x \ln\left[\frac{M_{Free}(1)}{M_{Free}(2)} x \frac{c_a(2)}{c_a(1)}\right] \quad (2)$$

If the reduction current is sampled at a fixed interval of a mercury droplife-time then $c_a(2)$ / $c_a(1)$ can be replaced by $i_p(M_{Comp})$ / $i_p(M_{Free})$. For the ith pH(i) value the term $M_{Free}(1)$ can be substituted by $M_T(i)$ because $M_{Free}(1)$ is equivalent to the total metal ion concentration $M_T(i)$ at each pH(i) value of the solution after *i*th consecutive additions of sodium hydroxide in the absense of complexes. Eq. (2) can thus be rearranged to the folowing

$$\Delta E_p(i) - \left(\frac{RT}{nF}\right) x \ln\left(\frac{i_p(M_{Comp})(i)}{i_p(M_{Free})(i)}\right) = \left(\frac{RT}{nF}\right) x \ln\left(\frac{M_T(i)}{M_{Free}(i)}\right) \quad (2a)$$

However the program ML-SPEC, used to generate initial values for CV-FIT, is used where protonated complexes are formed and where one such complex will be the predominate species in a particular pH region, the equilibrium may be written as has been done previously

$$M + jL + bH \leftrightarrow ML_jH_b$$

and the Lingane expression can be readily expanded to:

$$\Delta E_{peak} - \frac{RT}{nF}\ln\left(\frac{i_c}{i_s}\right) = \frac{RT}{nF}\ln \beta_{MLH_b} + j\frac{RT}{nF}\ln [L] + b\frac{RT}{nF}\ln [H]. \quad (3)$$

In this equation (expanded for general use and not only for titration point *i*), M represents the metal-ion, L the ligand and the brackets denote molar concentrations as the experiment is performed at constant 0.15 mol.dm^{-3} ionic strength (charges on ions are omitted for simplicity as well as the subscripts "c" and "s" used which refer to the complexed and free metal ion respectively). ΔE_{peak} is the difference in the DPP (Differential Pulse Polarography) peak potentials between the simple metal-ion and the complexed ion. RT/*n*F has the usual meaning and i_s and i_c represent the peak currents for the simple and complexed metal-ion, respectively. Eq. (3) still holds if hydroxide is considered as a ligand and [H] is thus replaced by [OH] in (3). If complexes of the form ML_j are being considered, *b* becomes zero and Eq. (3) simplifies to the usual form of the Lingane equation. This approach is similar to that used by Fisher and Hall [58] although the program ML-SPEC and especially CV-FIT is extended to present graphical representation of achieved results as well as the capability of comparing calculated peak potential curves, for a chosen model, with the real peak potentials. (Almost like Zbar curves for potentiometry). From this fit, a standard deviation can be calculated.

By substitution and rearranging Eq. (3) as has been done in [59] the complexation constant for a chosen complex species (fixed j and b values) can be calculated for each data point (Eq. 5).

$$\Delta E_{peak} - \frac{0.06154}{n} \log\left(\frac{i_c}{i_s}\right) = \frac{0.06154}{n} \log\beta_{ML_jH_b} + j\frac{0.06154}{n} \log[L] - b\frac{0.06154}{n} pH \qquad (4)$$

which gives

$$\log\beta_{ML_jH_b} = \log\left(\frac{i_c}{i_s}\right) + j \log[L] - b\ pH - \frac{n}{0.06154} (\Delta E_{peak}) \qquad (5)$$

The value for log[L] at a certain pH is calculated from the known pK_a values for the ligand by the general equation :

$$K_{LH_x}/[H^+] = [LH_{x-1}]/[LH_x] \qquad (6)$$

If the constant calculated by Eq. 5 holds in a certain pH region, the complex formed is probably as chosen. This is further confirmed by graphical representation of the shift of the polarographic peak as a function of calculated free ligand concentration and of pH. This also helps in the interpretation of the electrochemical processes occurring at the mercury micro electrode and in identifying the complex species within a certain pH region. Complexes are identified from the slope of the graph representing potential shift against pH which is given in mV per pH unit. In such a given region the predominant form of the ligand is known and the shift in potential is visible as the slope of the graph. At 37 °C the term RT/nF is equal to about 61.54 mV, and since the number of electrons involved in the reduction of the M(II) species (where M(II) represents Cd(II) or Zn(II)) at the mercury drop is two, the slope should be 30.8 mV per pH unit per proton involved in the reaction. If the slope is 61.5 mV a proton transfer of two would have been proposed for the electrochemical process taking place. From the above gathered information the complex can be deduced out of the general equation of the reaction occurring at the electrode:

$$MLH_{x-y}^{n-y-2} + yH^+ + 2e^- \leftrightarrow M(Hg) + H_xL^{n+} \qquad (7)$$

The amount of ligand per metal ion is taken as one for simplicity. The way to proceed is from right to left. MLH_{x-y}^{n-y-2} is the unknown and can be found by substituting x, y (number of protons involved int he titration) and n (charge on a deprotonated ligand). Equation 7 will

now reveal the reaction taken place at the electrode. In support of the found result a Lingane approach can be used. The slope of ΔE_{peak} vs log[L] in this pH region should exhibit a constant value of 31 mV per log[L] unit, which would indicate the formation of a metal complex involving one molecule of the ligand only [38].

Non-labile complexes

The first section of ML-SPEC deals with non-labile complexes according to the polarographic time scale. Two peaks are observed on a polarogram at the same time at a particular pH value of the sample solution studied. The concentration of the complex is calculated from the decrease in the polarographic peak height for the metal ion, since

$$C^{i}_{M_xL_yH_z} = C^{i}_{M_{Total}} - C^{i}_{s} \tag{8}$$

According to Cukrowski *et al.* [60]. *I* represents the *i*th polarogram with two peaks observed, that of the metal ion and its complex. $c^{i}_{M\ tot}$ is the total metal ion concentration in the *i*th solution on which an *i*th polarogram was recorded, c^{i}_{MLH} is the concentration of the complex $M_XL_YH_Z$ (negative Z values represent hydroxide ions) and c^{i}_{s} is the concentration of the hydrolysis product of the metal ion i.e. the species M_XH_Z. The concentration of ligand c^{*i}_{Ltot} not bonded to the metal ion is calculated from

$$c^{*i}_{L_{Total}} = c_{L_{Total}} - yc^{i}_{M_xL_yH_z} \tag{9}$$

At each pH value and thus for each polarogram, a trial concentration of free ligand c^{i}_{L} is calculated from

$$c^{*i}_{L_{Total}} = c^{i}_{L}(1 + K_1[H^+]^i + K_1K_2[H^+]^{2i} + ...) \tag{10}$$

where K_1, K_2, ... represent stepwise protonation constants for the ligand. Trial concentrations of free metal ion, c^{*i}_{s} and of the complex $c^{*\,i}_{MLH}$ are calculated. From this a trial value for the formation constant is obtained.

$$\beta^{i}_{n} = \frac{c^{*i}_{M_xL_yH_z}}{(c^{*i}_{s})^X(c^{i}_{L})^Y(H^{i})^Z} \tag{11}$$

The appropriate mass-balance equations are solved

$$M_{Total} = \sum X\, M_XL_YH_Z \tag{12}$$

$$L_{Total} = L_{free} + \sum Y M_X L_Y H_Z \quad (13)$$

for metal-ligand complexes thought to be present in the solution. The calculated formation constants and known formation constants for complexes are incorporated. The known constants are kept fixed during solving of the mass balance equations. Corrections for hydrolysis of metal ion is allowed during the iteration to find the best values for the trail formation constants. The latter normally applies to high pH values.

2.3 NMR studies of complexes

Over the years the study of complexation by NMR techniques has proved to be very useful. For example, for DTPA, the determination of the sequence of protonation on nitrogen and carboxyl sites was contested by Langer [61] and Sawyer [62]. Sawyer proved by using NMR that nitrogen sites were protonated preferentially before the carboxyl groups.

The approach of such a study is to titrate a ligand or complex in its deprotonated form with acid and record NMR spectra at various pH values. The observations made, are related to shifts in various peaks corresponding to a C-, H- or P-atom in the ligand. If enough data points are gathered the order of protonation can be followed, the structure of the complex found and even an estimate of the protonation or complexation constants in favourable systems may be determined.

To a first approximation one can assume that the chemical shifts for a proton, carbon or phosphorous atom will be affected mostly by a change in chemical environment occurring only one bond length away. It follows that the position of a proton signal can be given (at any pH) by eq. 1

$$\delta = N_A\delta_A + N_B\delta_B \quad (1)$$

where N_A, N_B, δ_A and δ_B are, respectively, the mole fractions (N) and the chemical shifts (δ) of the protonated (A) and non-protonated (B) forms. Therefore the basic δ_B's can be taken at pH = 12 and δ_A at pH = 2. The fraction (*f*) of time that a particular site is protonated can be defined as

$$f_i = \frac{\delta - \delta_B}{\delta_A - \delta_B} \quad (2)$$

where i refers to the various donor sites, for example, two different nitrogen atoms and two different carboxyl groups.

In following the chemical shifts of a particular signal one finds a point of inflection where $\delta = 1/2(\delta_A + \delta_B)$ or where the concentrations of the protonated and non-protonated forms are equal. Here it is possible to calculate the dissociation constants, because if in general

$$K_a = \frac{N_B[H^+]}{N_A} \tag{3}$$

then $pK_a = pH$ (since $N_A = N_B$). Similarly the NMR data can be used to calculate the formation constants for protonated complexes do in most cases. If the formation constants for example ML, MLH and MLH_2 are not separated by more than two log units the NMR technique for log K determination will fail [63].

The structure of a complex or possible structures for a complex can be determined if the atom on the ligand which is bound firmly to the metal ion can be distinguished. This will generally be where the biggest shift in NMR peak will occur.

Some cases are unclear even where it is possible to assign pK_a values to different protonation sites. For example the three carboxyl-carbon resonances (^{13}C NMR) in citrate [64] were found to shift in unison, *i.e.* there was no preferred site of protonation. In determining a structure of such a ligand complexed to a metal ion the spectra at low pH (no complexation) and high pH (where complexation has taken place) are recorded. A ligand to metal ratio of 1 : 2 is taken to ensure complexation is complete.Most of the times it is possible to point out, from the differences in the spectra before and after complexation, the peaks most effected by the complexation. In this particular case one of the carboxyl groups (the central carboxyl group) is unaffected by complexation and is therefore not participating in it. Further deductions about the structure of the complex depend on the proposed structures of the complex and will differ according to the system studied.

Phosphorous-31 NMR can also be used to study complexation phenomena. Since the ligands discussed in this dissertation have diphosphonate structures,useful information may be obtained. As example the complexation of NTMP (a nitrilo-triphosphonate) as described by Sawada *et al.* [65] is taken. The spectra of NTMP at pH values below 12 show only one peak on the ^{31}P NMR. Since NTMP has three phosphonate groups this fact indicates that the

proton exchange of NTMP is very fast. The three phosphorous atoms of NTMP are averaged and the chemical shift given by

$$\delta_P = \sum \delta_n X_{H_nL} \tag{4}$$

where δ_n and X_{H_nL} are the chemical shift and the proportion of each protonated or unprotonated species, H_nL (n = 0-5), respectively. By the use of the protonation constants, the individual chemical shift δ_n, was evaluated by non-linear regression. These δ_n values are plotted as a function of the number of protons bound to the ligand, n. For the complex formation the same is done and the pattern and pH dependence of δ_p is found to be similar. The chemical shift of the metal-ligand solution is written by a non-linear combination of the chemical shifts of each species present in the solution as

$$\delta_P = \sum \delta_n X_{H_nL} + \sum \delta_m X_{MH_mL} \tag{5}$$

where δ_m and X_{MH_nL} are the chemical shift and the ligand proportion of protonated and unprotonated complex, MH_mL, respectively. The chemical shift of each species of a complex, δ_m was evaluated by linear regression. These chemical shifts of complexes, δ_m are also plotted as a function of the number of protons, m, bound to the complex MH_mL. From this the formation constants are evaluated. In both the protonation and formation constant values good agreement with potentiometry was achieved.

Not only the chemical shift but also the broadening of an NMR peak can be used in interpreting the structure of a complex. In the case of NTMP [65] the $^{31}P\{^1H\}$ signal of the metal-ligand 1:1 mixture becomes quite broad in the region of the pH jump where ML and MLH are predominant. The broadening is largest at pH = log K_{MLH} where [ML] = [MLH]. However the ligand shows a sharp ^{31}P NMR shift in the whole range of pH. The broadening of the M:L = 1:1 solution in this pH region is interpreted in terms of a slow protonation equilibrium of the metal complex, ML + H ⇌ MLH, and will suggest a drastic change in the proposed structure of the complex. Under these conditions (M:L = 1:1), some portion of NTMP dissociates into free ligand. It was, however, confirmed by studies of solutions containing an excess of metal ion (M:L = 2:1) that the dissociation of the complex , ML ⇌ M + L, had little effect on the broadening of the signal. On the other hand, sharp signals indicate fast protonation equilibria and a different structure.

To conclude, a rapid and simple method of visualising the bonding mode of trivalent metal ions to ligands is by using Gd(III) as a line broadening agent in proton NMR spectra. Jarvis [66] used this approach to show that bonding of DHDECMP (dihexyl-N,N-diethylcarbamoylmethylene phosphonate) to trivalent metals is via the phosphoryl and not the amide centre. Being a highly paramagnetic, symmetrical metal ion, Gd(III) broadens but does not shift NMR peaks.The closeness of the proton(s) to the metal ion is in this case a function of the extent of the broadening. A comparison of the proton spectra of the ligand without the shift reagent with that of the Gd(III)-DHDECMP complex revealed the protons near the complexation centre and delivered the required result.

2.4 ECCLES modelling

Peter Letkeman [67] said "Have you ever wondered what it would be like to wear a 'virtual reality helmet' and so experience the microcosmic world of ions in solution?". This is what computer-modelling of metal speciation in human blood plasma does. It might not be a physical picture but it gives the bioinorganic chemist, by means of numbers, a snapshot of what is happening with the metal ions in the blood. It is a complex scene. It is known that human blood plasma contains 20 essential amino acids, 12 essential metal ions, at least another 100 ligands, numerous low molecular weight [LMW] complexes as well as α/β macro-globulins such as albumin (complexes Zn very efficiently).The absolute concentrations of metal complexes in blood plasma is determined by protein binding, but not the percentage distribution of transition metal ions amongst low molecular weight ligands [68].

Computer simulation of speciation calculations are important to show whether a metal ion or its complex will be toxic. The relative concentrations of toxic compounds can be found because of the mathematical ability of these simulations which have no limits to the concentrations employed. No detection limits and disturbance by instrumental techniques can hinder the process. The ability to handle all the metal ions and ligands at once was a limit until D.R. Williams *et al.* introduced ECCLES (**e**valuate **c**onstituent **c**oncentrations in **l**arge **e**quilibrium **s**ystems) [69]. It can handle up to 50 metal ions and 100 ligands simultaneously and produces the exact concentration of each complex in order of decreasing concentration and relative percentage of each component. The algorithm used to get these concentrations is as follow:

ECCLES algorithm.

It is required to find the free concentrations of the components (metal ions and ligands) in a multi component metal-ligand system at equilibrium. The concentration of each complex species is determined according to eq. 1. (the meanings of the symbols are listed in

$$S_j = \beta_j \prod_i X_i^{k(i,j)} \tag{1}$$

Appendix A2). An iteration process of the free concentrations improves the estimates until they satisfy the mass-balance equations for each component viz.

$$T_i = [X_i] + \sum_j S_j\, k(i,j).$$

A variety of optimisation techniques can be applied to the problem. A successive procedure of some of these techniques is followed

The first few iterations employ eq. 2.

$$X_{m,n} = \frac{T_m \cdot X_{m,o}}{X_{m,o} + \sum_j [G_j \cdot S_j \cdot k(m,j)]} \tag{2}$$

Where $G_j' = \prod_i (T_i / T_{i,c})^{k(i,j)} / (T_m / T_{m,c})$

and is an approximation for $G = \prod_i (X_i / X_{i,c})^{k(i,j)} / (X_m / X_{m,c})$

These first few iterations rapidly produce values in close proximity of the final solution. However the number of iterations is the limiting criterion here. Because of its vast number of computation needed, it is not employed exclusively. Once the application of eq. 2 is completed the program moves into an intermediate phase. The expression now used is that of Perrin and Sayce [70], rewritten as eq. 3

$$X_{m,n} = X_{m,o}[T_m / (T_m \cdot T_{m,c})^{1/2}] \tag{3}$$

It is used solely and uses considerably less computation time. As the solution is approached there is a fall off in convergence rate, as is usual with many successive-approximation techniques. At this stage eq. 4 is used to improve the rate of convergence in the final stages.

$$X_{m,u} = X_{m,o}(T_m \cdot T_{m,c}) \tag{4}$$

This completes the three-tier successive-approximation procedure which gives rapid convergence, but at the same time keeping the computer core-store requirements low.

Program description

Most constants for complexation of metal ions with amino acids and low-molecular-weight-complexes have been fed into the program by the authors [69]. These constants were found in the literature although corrections for ionic strength were employed using Debye-Hückel-type and van't Hoff-type extrapolations for temperature corrections. For other published constants, for which different values were reported, the authors took the average after critical evaluation. The constants that were still missing when the program was written were estimated using a variety of methods. These were based on linear free-energy-relation principles like the extension proposed by Sigel [71], the Irving-Williams rule, and educated guesses based on the authors' observation of chemical analogies. In the computation of the distribution of the metal ions other than Ca^{2+} among the low-molecular-weight complexes a range of plausible free concentrations for each, which bracketed an estimated average value, was taken [69]. Since mixed-ligand (ternary) complex formation occurs widely in systems containing metal ions and two or more different ligands [72] as many as possible ternary constants have been included in the program. Because of the expected dominant role of these complexes, estimates of a further 4000 ternary constants were made, employing relevant binary constants and stabilisation factors. In order to correct the ternary constants, which had been experimentally measured, for physiological conditions, a scaling operation was performed with each respective stabilisation factor using eq. 5 [73]. Here, $\Delta\log\beta_{MAB}$(model) is the scaled stabilisation factor applicable to the model (*i.e.* physiological) conditions

$$\Delta\log\beta_{MAB}(model) = \Delta\log\beta_{MAB}(expt.)\left[\frac{\beta_{MA_2}(model)\ .\ \beta_{MB_2}(model)}{\beta_{MA_2}(expt.)\ .\ \beta_{MB_2}(expt.)}\right]$$

$\Delta\log\beta_{MAB}$(expt) is the observed scaling factor [74] obtained under non-physiological conditions = $\log\beta_{MAB}$(expt) - ½[$\log\beta_{MA2}$(expt) + $\log\beta_{MB2}$(expt) - log2, β_{MAB} is the formation constant of the ternary complex, MAB, formed between a metal, M, and two ligands, A and B, β_{MA2} and β_{MB2} are the cumulative formation constants of the binary complexes, MA_2 and MB_2. (expt) refers to experimental constants determined under non-physiological conditions and (model) applies to formation constants measured at or corrected to model conditions.

The procedure first invokes the program MIX to prepare input data for the program ECCLES. The user defines the system in terms of its components and their respective concentrations and MIX generates the intermediate data file by performing three tasks. These are (i) the selection of the applicable binary formation constants for the system in question, (ii) the calculation of formation constant estimates for all ternary complex species that may be assumed to exist according to the chosen binary formation constants and (iii) the substitution, adjustment or extension of these constant estimates in respect of those for which experimental data has been collected. The MIX program produces an output file that becomes the complete input for ECCLES. ECCLES is run and delivers the relative concentrations of all species at equilibrium.

2.5 Baboon tests with ^{166}Ho-APD

Baboon tests are carried out to validate the predictions made by ECCLES and as a precursor to clinical trails. Baboons are widely used as analogues for humans due to their similar physiology [46]. The *in vivo* distribution of a radionuclide can only be predicted to a certain extent by ECCLES. To see if the complex indeed survives blood plasma, is not filtered by the liver (colloids can be retained by the liver) and its bone uptake is as predicted can only be done with a human analogue [46].

Lin has showed in his review article on diphosphonates [75] that the binding of alendronate (4-Amino-1-hydroxybutylidene-diphosphonate) in other words (ABD) to serum albumin is calcium-dependant. The binding to albumin helps in the transport of the diphophonates to bone tissue. This would imply that the addition of Ca(II) is necessary as proved to be the case with other drugs such as pamindronate (APD) used as a anti-osteoporosis agent. However the amount of APD needed in our case is only 1E-05 M which is orders of magnitude smaller than that used for the above drugs. For the baboon test it was decided not to investigate the calcium-dependence.

The preparation of the sample for the test has to be done carefully since these tests are expensive and the time available for them limited. It has to be shown that the solution to be injected into the baboon is indeed fully complexed [43] using ECCLES at first at the

theoretical level. To show complexation on laboratory scale, two techniques are employed. The first is thin layer chromatography. The chromatographic plates are not developed but merely scanned on a radioscanner which detects the patterns of activity across the chromatographic plate [44].

The second method is liquid chromatography on a sephadex column. Sephadex is a polysaccharide resin which is employed as a mild ion-exchanger. It has the advantage that it does not denature proteins as other ion-exchangers do. Carboxymethyl Sephadex retains free metal ions like ^{166}Ho. A packed column of this resin contains carboxy groups to complex the metal ions. By keeping the free metal ions and letting the complexed ions go through, the resin can show how complete the complexation is by the following equation [45]

$$\%\ complex\ yield\ =\ 100\ x\left[1-\frac{Isotope\ activity\ after\ elution}{Isotope\ activity\ before\ elution}\right]$$

The next step is to validate a new drug on well-established experimental animal models e.g. baboons. The baboon is phylogenetically close to humans and therefore permits more meaningful extrapolation of results [46]. Because the animals are large, a good model for use in nuclear medicine techniques can be achieved. All parameters of human physiology can be measured in the baboon model, from circulation (through e.g. arteries and the heart) to skeletal uptake. Some categories of research on the baboon model are as follows [46]:

i. Cardiology studies, where it finds application in the Wolff-Parkinson-White syndrome [76].

ii. Septic shock, where microvascular plasma leakage is detected [77].

iii. Detection of inflammatory lesions by scintigraphy and skeletal uptake of radiological cancer drugs [46] and various other studies.

The baboons available at the H.A. Grové Research Centre of the Department of Hospital Services are chacma baboons (*Papio ursinus*). The protocols prepared for research projects are screened by an internal ethics committee in accord with the legislation pertaining to the use of vertebrates in biomedical experiments. The centre only excepts research of a high standard and which is aimed at human and veterinary advancement. The centre supplies veterinarians which assist in the supporting procedures and the well-being of the animals [46]. The research animals are captured from private farms or nature reserves where they are considered problem animals. The baboons are numbered, blood evaluated, checked for infections, dipped in insecticide and placed in quarantine. After it is established that there are no heart abnormalities an ideal healthy biomedical research animal is available and housed in

an individual cage to avoid fighting [46].

Prior to an experiment the animal is tranquilized and brought from its cage to the preparation room where the appropriate anaesthesia is administered and a endotracheal tube inserted. The baboon is injected with a sterile solution which has a pharmaceutically acceptable composition. The dosage of radionuclide is at least 0.2 mCi per kilogram of body weight of the baboon [43]. This gives a figure of about 3 to 4 mCi per animal per injection. Fluids are routinely given through an intravenous cannula. The animal is unconscious for a few hours and kept under narcosis while the distribution of the activity is studied by γ-scintography. Kinetic studies are performed at the same time taking blood and urinal samples to understand more of the biodistribution of the radioactive drug. After completion of the experiments the animal is transferred to the postexperimental observation room where they are monitored and in due time discharged by a veterinarian.

3 Experimental

3.1 Synthesis of APD

The synthesis of 1-hydroxy-3-amine-propilylidenediphosphonic acid (APD) was based on the method of Worms *et al* [40]. 95 ml (1 mole) of $POCl_3$ was added to a three-necked flask containing 82 g (1 mole) of crystalline phosphorous acid (H_3PO_3). The mixture was stirred magnetically in a closed vessel for one hour in order to dissolve the acid. The flask was then fitted with a mechanical stirrer. A T-shaped glass rod was used as the stirring bar instead of an iron bar because of the HCl gas that is formed in the reaction. Care was also taken to protect the stirring apparatus from these corrosive gasses. To the solution prepared above, 41g (0.5 mole) of β-Alanine was added portion-wise while stirring fast with the mechanical stirrer. Each portion was added quickly to minimising the amount of HCl escaping. After the addition the sticky mixture was stirred at 98°C for 4 hours. A white foam was produced after which the mixture was stirred for an additional hour. Care was taken that the foam did not turn yellow because of localised heating. After stirring was complete, the flask was transferred to an ice bath where the product was hydrolysed with 300 ml of water. This reaction is exothermic and addition of water had to be done slowly. The resulting solution was transferred to a beaker and evaporated to 200 ml. It was cooled and left overnight in the freezer to crystallise. The crystals which formed were washed with a cold methanol/H_2O (1:1). The mother liquor was kept as precipitation continued while being kept in the freezer. 23 g (20 %) of product was collected in three fractions which all had a melting point of 231-232°C as has been reported [40].

To verify that the product synthesised is indeed APD, a double CHN analysis was performed on a few milligrams of the compound. The results are presented in Table 1. The calculated % of C,H and N, according to the chemical structure of the ligand, and the experimental results are similar enough to except APD as synthesised purely.

Table 1. CHN analysis of APD

	Experimental Result	*Calculated Value*
% C	15.19 ± 0.05	15.33
% H	4.59 ± 0.01	4.72
% N	6.06 ± 0.02	5.96

For the other two ligands used, HEDP and MDP, a similar analysis was performed. The results are given Table 2 and 3. Both were acquired commercially and dried prior to analysis and use.

Table 2. CHN analysis of HEDP

	Experimental Result	*Calculated Value*
% C	11.61 ± 0.02	11.66
% H	3.86 ± 0.05	3.91
% N	0.00	0.00

Table 3. CHN analysis of MDP

	Experimental Result	*Calculated Value*
% C	6.71 ± 0.03	6.82
% H	3.31 ± 0.06	3.44
% N	0.00	0.00

To find whether the correct concentration of ligand was reported a potentiometric analyses was carried out. Results for the various ligands are displayed in Table 4-6. The ESTA2A input files used to calculate these values are included in Appendix B2.

Tables 4-6 show that experimental values for the concentration of the ligands match the potentiometric calculated values. The experimental concentrations in all three cases were thus accepted.

Table 4. Results of the potentiometric analysis of APD.

Ligand	Experimental concentration of ligand	Potentiometric calculated concentration of ligand	Number of Data points	Hamilton R-factor
APD	0.0010256	0.0010228 ± 0.0000055	470	0.0107
	0.0011905	0.0011874 ± 0.0000061		
	0.0018367	0.0018404 ± 0.0000064		

Table 5. Results of the potentiometric analysis of MDP

Ligand	Experimental concentration of ligand	Potentiometric calculated concentration of ligand	Number of Data points	Hamilton R-factor
MDP	0.0010277	0.0010239 ± 0.0000025	600	0.00593
	0.0011929	0.0011906 ± 0.0000027		
	0.0018404	0.0018388 ± 0.0000030		

Table 6. Results of the potentiometric analysis of HEDP

Ligand	Experimental concentration of ligand	Potentiometric calculated concentration of ligand	Number of Data points	Hamilton R-factor
HEDP	0.0010256	0.0010190 ± 0.0000010	600	0.00235
	0.0011905	0.0011810 ± 0.0000011		
	0.0014894	0.0014876 ± 0.0000012		

3.2 Potentiometric Titrations

Potentiometric titrations for Ca(II)-, Mg(II)-, Zn(II)-, Ho(III)- and Sm(III)-L systems (where L represents the three possible ligands viz. APD, MDP and HEDP) as well as the Cd(II)-HEDP system were controlled by a Metrohm Titroprocessor 670 using a Metrohm 665 Dosimat and a combination glass electrode (Ag-AgCl reference). Electrode constants were calculated regularly using strong acid-strong base titration data. All titrations were performed under inert atmosphere using high purity nitrogen gas.

Solutions were held at a constant ionic strength of 0.15 mol.dm^{-3} NaCl and at a temperature of 37.0 ± 0.1 °C. The titrations were performed beginning at low and ending at high pH, adding 0.10 cm^3 aliquots of 0.050 mol.dm^{-3} NaOH (carbonate-free to avoid complexation of the latter with any of the metal-ions) in 0.10 mol.dm^{-3} NaCl. Protonation constants for each of the three ligands were calculated from data obtained from titrations of the ligands in the presence of various hydrochloric acid concentrations. These protonation constants were held constant in the metal-ligand titration data modelling. Three different metal:ligand ratios were used for each system.

The different compositions of the titration solutions are reported in Table 7-9

Table 7. Composition of experimental solutions for potentiometric studies with APD

Cation	Titration	0.15*M* NaCl (*ml*)	Metal ion solution (*ml*)*	0.01*M* APD (*ml*)	0.05*M* HCl in 0.10*M* NaCl (*ml*)
H	1	30		4	5
	2	30		5	7
	3	30		9	10
Ca(II)	1	30	2	4	5
	2	30	2	5	5
	3	30	2	10	5
Mg(II)	1	30	2	4	5
	2	30	2	5	5
	3	30	2	10	5
Sr(II)	1	30	2	3	5
	2	30	2	5	5
	3	30	2	10	5

Zn(II)	1	30	2	4	5
	2	30	2	5	5
	3	30	2	10	5
Sm(III)	1	30	1	4	5
	2	30	1	5	5
	3	30	1	10	5
Ho(III)	1	30	1	4	5
	2	30	1	5	5
	3	30	1	10	5

* Solutions made up as follows: 0.0181M $CaCl_2$ in 0.11M NaCl, 0.0202M $MgCl_2$ in 0.11M NaCl, 0.0209M $ZnCl_2$ - 0.11M NaCl, 0.022M $SrCl_2$ in 0.11M NaCl, 0.026M $SmCl_3$ in 0.05M HCl and 0.025M M NaCl and 0.027M $HoCl_3$ in 0.0476M HCl and 0.025M NaCl.

Table 8. Composition of experimental solutions for potentiometric studies with MDP

Cation	Titration	0.15*M* NaCl (*ml*)	Metal ion solution (*ml*)*	0.01*M* MDP (*ml*)	0.05*M* HCl in 0.10*M* NaCl (*ml*)
H	1	30		4	5
	2	30		5	7
	3	30		7	10
Ca(II)	1	30	2	4	5
	2	30	2	5	5
	3	30	2	10	5
Mg(II)	1	30	2	4	5
	2	30	2	5	5
	3	30	2	10	5
Ni(II)	1	30	2	4	5
	2	30	2	5	5
	3	30	2	10	5

Zn(II)	1	30	2	4	5
	2	30	2	5	5
	3	30	2	10	5
Sm(III)	1	30	1	4	5
	2	30	1	5	5
	3	30	1	10	5
Ho(III)	1	30	1	4	5
	2	30	1	5	5
	3	30	1	10	5

* Solutions made up as follows: 0.0181M $CaCl_2$ in 0.11M NaCl, 0.0202M $MgCl_2$ in 0.11M NaCl, 0.0178M $NiCl_2$ - 0.11M NaCl, 0.0209M $ZnCl_2$ in 0.11M NaCl, 0.026M $SmCl_3$ in 0.05M HCl and 0.025 M NaCl and 0.027M $HoCl_3$ in 0.0476M HCl and 0.025 M NaCl.

Table 9. Composition of experimental solutions for potentiometric studies with HEDP

Cation	Titration	0.15M NaCl (*ml*)	Metal ion solution (*ml*)*	0.01*M* HEDP (*ml*)	0.05*M* HCl in 0.10*M* NaCl (*ml*)
H	1	30		4	5
	2	30		5	7
	3	30		7	10
Ca(II)	1	30	2	4	5
	2	30	2	5	5
	3	30	2	10	5
Mg(II)	1	30	2	4	5
	2	30	2	5	5
	3	30	2	10	5
Zn(II)	1	30	2	4	5
	2	30	2	5	5
	3	30	2	10	5

Cd(II)	1	30	2	4	5
	2	30	2	5	5
	3	30	2	10	5
	4	30	2	13	5
Sm(III)	1	30	1	4	5
	2	30	1	5	5
	3	30	1	10	5
Ho(III)	1	30	1	4	5
	2	30	1	5	5
	3	30	1	10	5

* Solutions made up as follows: 0.0181M $CaCl_2$ in 0.11M NaCl, 0.0202M $MgCl_2$ in 0.11M NaCl, 0.0214M $CdCl_2$ 0.11M NaCl, 0.0209M $ZnCl_2$ in 0.11M NaCl, 0.026M $SmCl_3$ in 0.05M HCl and 0.025 M NaCl and 0.027M $HoCl_3$ in 0.0476M HCl and 0.025 M NaCl.

The titrations were monitored for possible precipitates that might form in some of the systems. The pH region at which these precipitates occurred was noted and the corresponding data points ignored in further calculations. Data collected in non-precipitate pH regions were analysed by the ESTA library of programs [41]. Hydrolysis constants and pK_w were taken from the literature [42] and held constant during optimisation procedures. The model obtained for each system was tested for plausibility by comparing experimental and calculated formation and deprotonation curves.

Reagents.—Three ligands were used. APD was synthesised as described above, MDP and HEDP were obtained commercially. All three were dried at 90 °C and were found to be pure by (microanalysis see results above). Solutions of the ligands were made in 0.15 $mol.dm^{-3}$ NaCl by weighing dried amounts of ligand. Stirring for an hour ensured that all of the ligands (APD dissolves very slowly) dissolved in this medium. Fresh metal-ion solutions were employed in the titrations. These were made by dissolving reagent-grade chloride salts of the metal ions in distilled water and standardised by ICP atomic absorption spectroscopy. Where necessary, solutions were acidified to prevent hydrolysis. Fresh solutions of the titrant viz. 0.050 $mol.dm^{-3}$ NaOH in 0.10 $mol.dm^{-3}$ NaCl were regularly made using Merck titrisols. These solutions were made under inert atmosphere to avoid carbonate formation.

3.3 Polarographic titrations

Differential pulse polarograms were obtained with the use of an EG&G Princeton Applied Research Potentiostat/Galvanostat Model 273. A multimode electrode Model 303A SMDE was employed as the working electrode and used in the dropping mercury electrode mode with a drop time of 1s. A Ag-AgCl electrode and a platinum electrode (both EG&G PARC) were used as reference and auxiliary electrodes, respectively. A pulse height of 50 mV and a step height of 4 mV were used. The pH of the solution was measured to within 0.002 pH units with the use of a Beckman Φ72 pH meter and the corresponding combination glass bodied electrode (saturated calomel). The normal set-up of the Model 303A was modified to contain the pH electrode as well as the glass reaction vessel to have a water jacket. The temperature was thus controlled at 37 °C within 0.1 °C. As with the potentiometric titrations the solutions were kept at a constant ionic strength of 0.15 $mol.dm^{-3}$ NaCl. High purity argon was used for deaeration of sample solutions.

In a typical titration the polarographic cell contained metal-ion, Cd(II) or Zn(II) at 10^{-5} M in 0.15 $mol.dm^{-3}$ NaCl. The pH was lowered with hydrochloric acid to the starting value of pH 2. The reference potential and peak height of the metal-ion were established in this medium. The ligand (one of the three used in this dissertation) was introduced by addition of a standard solution to give three different ligand:metal ratios in the range of 3-100:1 in order to establish the correct speciation model. After recording a polarogram, the pH of

Table 10. Composition of experimental solutions for polarographic studies with APD.

			Metal ion		
		0.15M	solution	0.01*M* APD	0.15*M* HCl
Cation	Titration	NaCl (*ml*)	(*μl*)*	(*ml*)	(*ml*)
Zn(II)	1		50	10	
	2	5	50		5
	3	5	97.8		5
	4	7	40	5	0.7

* Solutions made up as follows: 0.0209M $ZnCl_2$ in 0.11M NaCl

Table 11. Composition of experimental solutions for polarographic studies with HEDP.

Cation	Titration	0.15M NaCl (*ml*)	Metal ion solution (*μl*)*	0.01*M* HEDP (*ml*)	0.15*M* HCl (*ml*)
Zn(II)	1		47.8	10	
	2		97.8	10	
	3	5	50		5
	4	5	97.8		5
	5	7	40	5	0.7
Cd(II)	1		50	10	
	2		100	10	
	3	5	50		5
	4	5	100		5
	5		110	0.0137g	15
	6	10	50	0.3	

* Solutions made up as follows: 0.0209M $ZnCl_2$ in 0.11M NaCl and 0.0214M $CdCl_2$ in 0.11M NaCl

the solution was adjusted upwards in steps of about 0.100-0.200 pH units, by addition of NaOH (0.15 $mol.dm^{-3}$) solution from an Eppendorf micropipet graduated to 0.1 μl, and a new polarogram recorded. In this way a set of between 40 to 50 polarograms of the species present in the solution was obtained as a function of pH. Polarograms of the metal-ion alone were also run in a similar way to identify possible metal hydroxide-species. Equilibrium for the metal-ligand solutions occurred within a few minutes.

A computer program ML-SPEC [38] and CV-FIT was used to calculate formation constants from the polarographic data. The section of the program used for Zn(II) and the lower pH regions of Cd(II) is that which deals with complexes which are labile on the polarographic time scale. Only one metal-ion peak is observed and the shift in peak potential as a function of pH is used to calculate the formation constant for a dominant species in a certain pH region. In the Cd(II)-HEDP system at high pH values, non-labile complexes are formed and are dealt with in another section of the program that calculates the formation constants from the appearance of a second peak (the non-labile complex under investigation). The composition of the titration solutions are listed in tables 10 to 12.

Table 12. Composition of experimental solutions for polarographic studies with MDP.

Cation	Titration	0.15M NaCl (*ml*)	Metal ion solution (*μl*)*	0.01*M* MDP (*ml*)	0.15*M* HCl (*ml*)
Zn(II)	1		50	10	
	2		56	10	
	3		63.5	10	
	4	5	50		5
	5	5	97.8		5
	6	7	40	50	0.7

* Solutions made up as follows: 0.0209M $ZnCl_2$ in 0.11M NaCl

3.4 NMR studies

Stock solutions of 0.05 mol.dm^{-3} HEDP and 0.05 mol.dm^{-3} $MgCl_2$ both in 99.7% D_2O were prepared. D_2O was used so that ^1H NMR spectra of the ligands and complexes formed could be obtained. However due to a fast exchange rate of the hydroxy-hydrogen on the ligand with the D_2O it was impossible to study the hydroxy-group's influence on complexation by ^1H NMR. The ionic strength of these solution were adjusted to 0.15 mol.dm^{-3} NaCl by addition of NaCl salt. 1 cm^{-3} samples were made in two series. The first series contained only the ligand adjusted to various pH values by 0.15 mol.dm^{-3} NaOH also in D_2O. The pH values were chosen according to the species distribution obtained from protonation constants for HEDP. The second series consisted of solutions where ligand and metal solutions were mixed in the ratio 1:1. The pH values of this series were chosen by the species distribution diagram obtained from the formation constants for the system Mg(II)-HEDP. Where precipitates formed these solution were rejected and the data in that pH region could not be collected.

For clear (no precipitate) solutions ^{31}P and ^{13}C NMR spectra were run on a 400 MHz Brücker Avance DRX400 spectrometer. Spectra were recorded at 37 ± 1 °C. ^{31}P chemical shifts were measured relative to an external orthophosphoric acid reference. D_2O was used as internal reference for ^{13}C. For the ^{31}P NMR spectra the number of scans taken with the

ligand alone were ± 60 but for the complex ± 200. The corresponding figures for the ^{13}C NMR were 400 and 4000. The latter is a time consuming procedure. To fit in with the little time available it was thought to increase the concentration of the ligand and metal-ion, fourfold which would reduce the number of scans 16 times. However at these elevated concentrations more precipitates were formed especially in the pH region of interest viz. 6-8.5 .

The D_2O used in these experiments had a purity of 99.7 % and was double distilled to give a conductivity of 1.3 μS. All reagent solutions used were made using this solution.

The composition of the NMR solutions are listed in Table 13.

Table 13. Composition of experimental solutions for NMR studies with HEDP.

Cation	Sample	0.15M NaOH (*μl*)	Metal ion solution (*ml*)*	0.05*M* HEDP (*ml*)	pH
H	1	275		1	2.014
	2	350		1	2.509
	3	500		1	3.108
	4	520		1	3.371
	5	569		1	5.027
	6	608		1	6.328
	7	630		1	6.775
	8	720		1	7.500
	9	850		1	8.606
	10	900		1	9.990
	11	1000		1	10.489
Mg(II)	1	300	0.5	0.5	2.988
	2	334	0.5	0.5	4.970
	3	440	0.5	0.5	5.959
	4	505	0.5	0.5	6.506
	5	555	0.5	0.5	6.995
	6	575	0.5	0.5	7.589
	7	605	0.5	0.5	8.094

8	622	0.5	0.5	9.091
9	638	0.5	0.5	9.987
10	645	0.5	0.5	10.501
11	700	0.5	0.5	11.50

* Solutions made up as follows: 0.15M $MgCl_2$ in D_2O

3.5 Preparation of ^{166}HoAPD for baboon test purposes

The complexation of Ho with APD was carried out in similar fashion to the description of the complexation of Ho to EDTMP as described by the Dow Chemical Co. patent [43].

Preparation of ^{166}Ho solution (48)

2.5 mg Ho_2O_3 was weight off in a quarts vial. The vial was sealed and placed in an aluminium can and irradiated in the SAFARI1 research reactor for 24 hrs at a neutron flux of 4 x 10^{13} neutron/cm^2.sec (equivalent of 10 megawatt). The can was opened in a hotcell and left to cool for a further 24 hrs. The vial was placed in a lead container and shipped to the laboratory were it was kept behind a lead window while being processed. The vial was opened by crushing the small quarts window on top. 100µl of a 2N HCl solution was added and heated at 60°C for 1 hr. 2 ml of water was used to rinse the $HoCl_3$ formed into the solution, making sure it is a homogeneous solution. As in most of this process syringes were used to add or transfer liquids, because of the small volumes dealt with and a lesser chance of spilling radioactive solutions.

Preparation and validation of ^{166}HoAPD

200 µl of the $^{166}HoCl_3$ solution was transferred to a 10 ml vial, containing a solution of 700 µl 1N NaOH in which 50 mg of APD was dissolved. The resulting mixture had an activity of ± 17.5 mCi. The pH was ~12. Two 0.5µl samples were taken and spotted on cellulose chromatographic plates. 235 µl of a 1N HCl solution was added to reduce the pH to ~ 7.8. The pH was checked with universal indicator strips. This was the stock solution from which samples were taken for validation of complexation and for the preparation of the 3 mCi injecting solution. Another two 0.5 µl samples were spotted on two different plates. The chromatographic plates were run in two different eluant mobile phases. The first one was a mixture of Pyridine, Ethanol and Water in a ratio of 1:2:4 and took 2 hrs to complete. The second contained Ammonia, Methanol and Water in the ratio of 1:10:20 and took 45 min to complete. The chromatographic plates were scanned by a radioscanner

while passing by the detector, recording a radiochromatogram scan [44]. The amount of activity was plotted vs. the channels as the chromatographic plate passed by. If a complex has formed it should be carried on the front of the mobile phase and therefore the activity should appear in a sharp peak near the end of the chromatogram. Reference runs were also recorded with $^{166}HoCl_3$ using both mobile phases. Here no ligand is present and the ^{166}Ho activity should remain at the origin. A sharp peak at the start of the chromatogram is expected.

Another way to validate if complexation has occurred is by using a small column of Carboxymethyl Sephadex (it retains all uncomplexed metal ions). This procedure was carried out according to Dormehl *et. al.* [44,45]

The column was prepared by putting 200 mg column of Carboxymethyl Sephadex in 20 ml of water and leaving it overnight to swell. While stirring, to give a homogenous suspension, 5 ml of the suspension was taken, put on a column and sucked dry.

20 µl of the stock solution was loaded on the column. The column was placed in an ionisation chamber, which had been zeroed for background measurement, and the activity measured. The column was washed (complex eluted) with 20 ml of saline (0.9% or 0.15M NaCl) and the activity measured. From the difference the percentage complex yield could be calculated.

Injection of baboons

0.5 ml of the ^{166}HoAPD stock solution was diluted with water to 1.5 ml to give a total activity of 9 mCi. Since the half-life of ^{166}Ho is 26.7 hrs and 1 ml is injected, the sample's activity would have decayed to 3 mCi the following day which is the dose injected into the baboon at the H.A. Grové Research Centre in Pretoria. The water used for dilution was highly purified to avoid sickness in the animal when administered with the solution. A sterile vial was used and the outside of the vial and lead container was sterilised by incubation at ± 121°C in an Autoclave apparatus for 40 minutes. The lead container was then placed in a, polystyrene containing, pot (normally used to transport radiological solutions) and taken to the H.A. Grové Research Centre.

At the centre a baboon (nr. P20/92) which had recovered sufficiently from previous radiological tests was chosen from the number of baboons kept at the centre. The personnel at the centre darted the animal with Ketamine HCl (± 10 mg/kg), weighed it (23.8 kg) and transferred it to the surveillance room The blood volume was estimated at

1.8 L via the equation 75.5 ml/kg. It was strapped on a bed with the γ-camera over head. To get a better understanding of the set-up, photo 5 is included.

Photo 5. Laboratory set-up used for baboon tests at the H.A. Grové research Centre.

An arterial line was fitted to the animal's leg and the narcotic, Sagatal 6%, administered intravenously via this device to keep the animal unconscious for the three hours needed to complete the study. The same line was used to inject the ^{166}HoAPD. The electrodes for the heart monitoring system were clamped to the body. At the arm another arterial line was fitted to take blood samples and add a diluted solution of saline. The bladder was emptied via a urinal catheter before the complex was introduced to study the excretion of ^{166}Ho more accurately. A reference blood sample was taken.

1 ml of the prepared ^{166}HoAPD was taken and registered 3.25 mCi in the ionisation chamber just before injecting. After injection the spread of the activity could clearly be seen on the camera. ^{166}Ho was monitored by a γ-camera (Siemens Orbiter), which was set at 85 keV (20 % window) to record the strongest γ-line of ^{166}Ho. To give an image, the dataprocessor (A^2/A^3 MDS) was used [44,46]. At the start, blood and urine samples were taken at 5 minute intervals. After 20 minutes, samples were taken every 30 minutes up to the two hour mark. At the three hour mark final samples were taken. Images were registered continuously but at two and three hours after administration static γ-scans were

taken at three positions viz. head, chest and pelvis. Computer enhanced images of this were recorded as the results. The blood and urine samples were taken back to the AEC and analysed in a multi-channel analyser. From this data the amount of ^{166}Ho in various parts of the body could be calculated.

4 Results and Discussion

4.1 Potentiometric titrations

4.1.1 Protonation formation constants

The protonation constants for APD, MDP and HEDP are shown in Tables 1-3. The accuracy of the results is illustrated by the Hamilton *R*-factor and shown graphically in the experimental and calculated formation curves (Figures 1 to 3).

Table 1 Protonation constants for APD

Cation	Equilibrium	Log K	Hamilton R factor
H^+	$H + L \rightleftharpoons HL$	10.95 ± 0.02	0.00845
	$H + HL \rightleftharpoons H_2L$	9.80 ± 0.03	
	$H + H_2L \rightleftharpoons H_3L$	6.01 ± 0.03	
	$H + H_3L \rightleftharpoons H_4L$	2.56 ± 0.04	

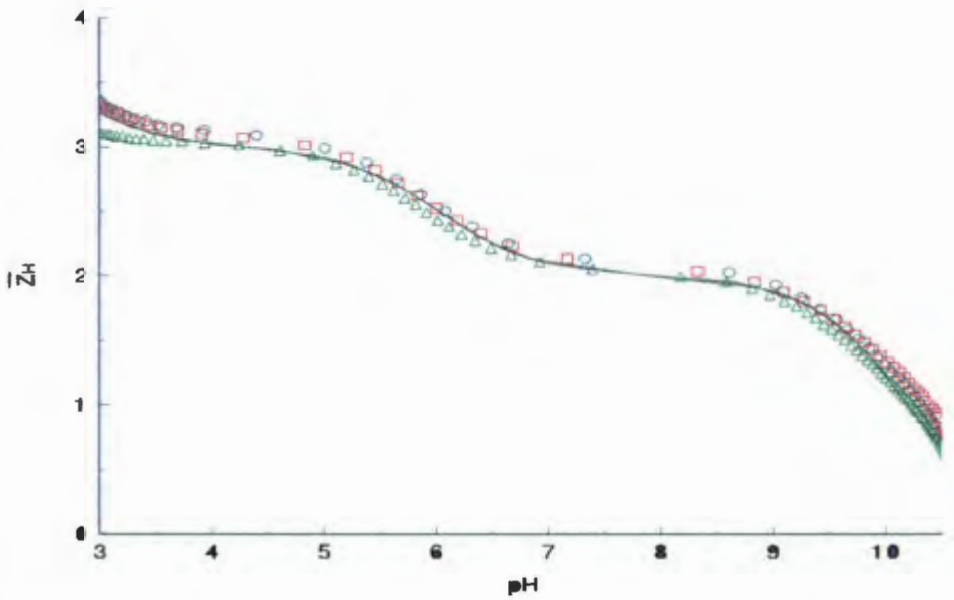

Figure 1. Experimental (points) and calculated (lines) formation curves for APD. $\overline{Z}_H$ is the formation protonation function. The separate titrations are presented by (○), (□) and (△).

The formation curves help to verify a certain chosen model, showing how well the data points, gathered in the potentiometric titration, fit the chosen model between pH = 4 and 10. This pH region is considered important when dealing with the simulation of blood plasma.

The best fit (experimental vs calculated $\overline{Z}_H$ values) displayed is that for the protonation model of HEDP. There is a significant difference between the models for HEDP and MDP vs APD. The species H_6L is not included in the model for APD. Inspection of species distribution curves indicates that H_6L would form at very low pH. When included it raised the standard deviations, Hamilton R-factor and the difference between experimental and calculated formation curves grew bigger. If the species H_5L was included in the model for MDP and HEDP the same observations were made. Leaving out the H_6L species in these models resulted in a slightly worse fit. This fact is demonstrated by Figure 4 which shows the model for HEDP without H_6L. The results of the modelling without H_6L is shown in Table 4. Visual comparison with Figure 3 explains why the model with H_6L is preferred.

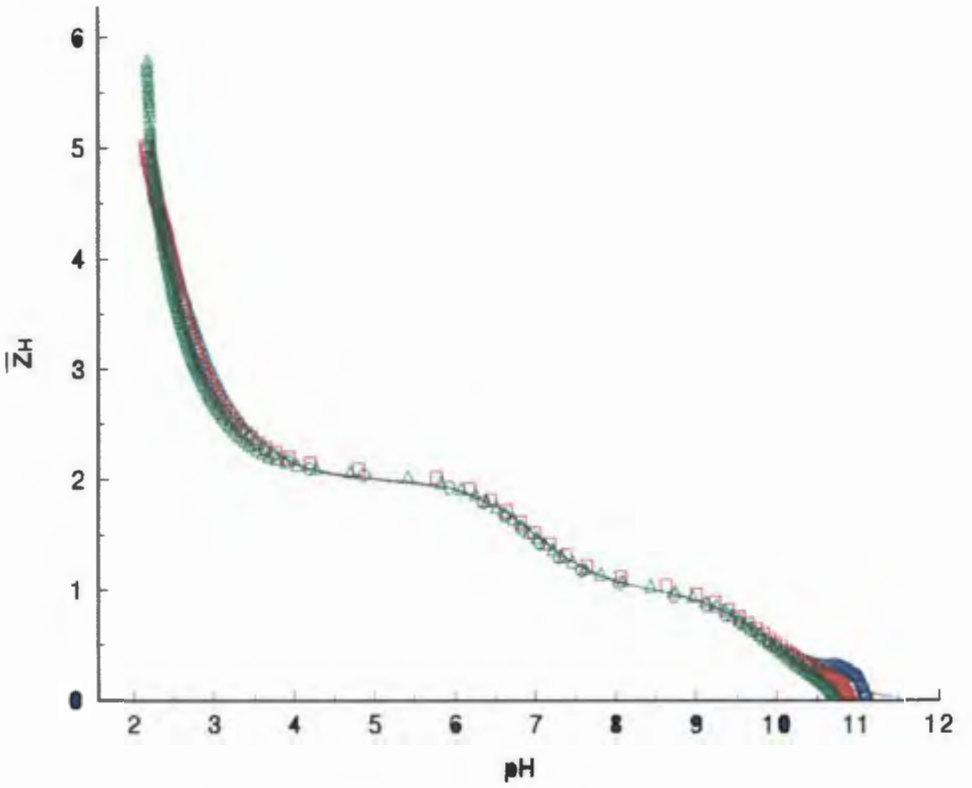

Figure 2. Experimental (points) and calculated (lines) formation curves for MDP. $\overline{Z}_H$ is the formation protonation function. The separate titrations are presented by (○), (□) and (△).

Table 2. Protonation constants for MDP

Cation	Equilibrium	Log K	Hamilton R factor
H^+	$H + L \rightleftharpoons HL$	9.97 ± 0.01	0.0138
	$H + HL \rightleftharpoons H_2L$	7.01 ± 0.01	
	$H + H_2L \rightleftharpoons H_3L$	3.26 ± 0.02	
	$H + H_3L \rightleftharpoons H_4L$	2.19 ± 0.05	
	$2H + H_4L \rightleftharpoons H_6L$	5.13 ± 0.05	

Table 3. Protonation constants for HEDP

Cation	Equilibrium	Log K	Hamilton R factor
H^+	$H + L \rightleftharpoons HL$	10.11 ± 0.005	0.00474
	$H + HL \rightleftharpoons H_2L$	6.81 ± 0.01	
	$H + H_2L \rightleftharpoons H_3L$	2.97 ± 0.01	
	$H + H_3L \rightleftharpoons H_4L$	2.43 ± 0.02	
	$2H + H_4L \rightleftharpoons H_6L$	4.66 ± 0.02	

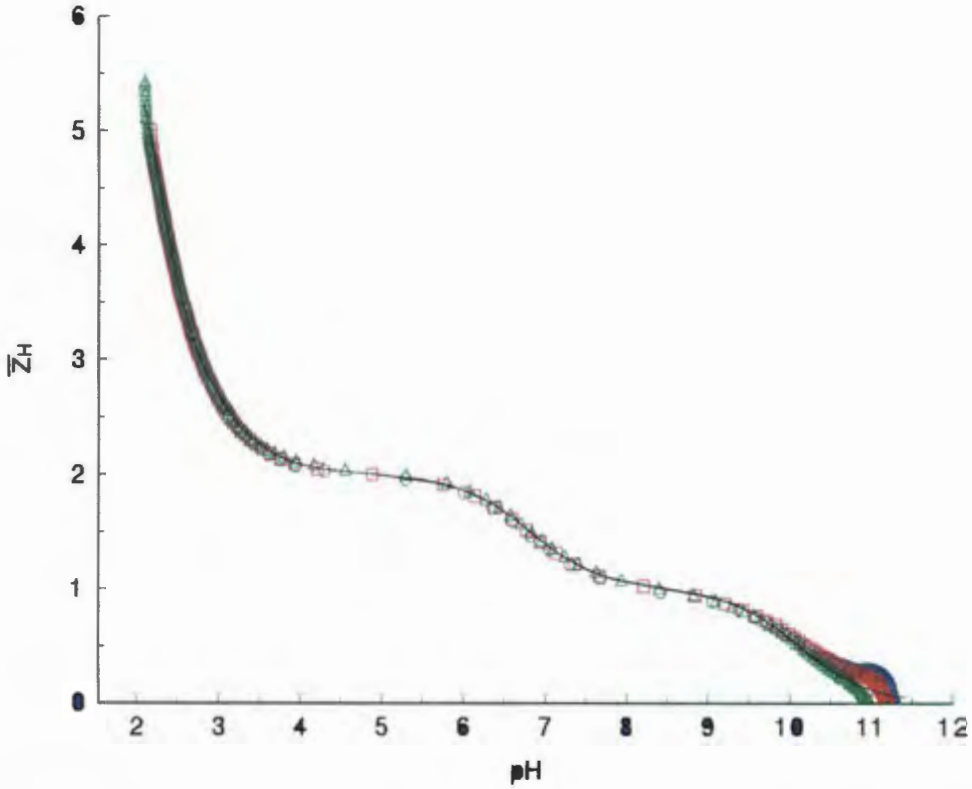

Figure 3. Experimental (points) and calculated (lines) formation curves for HEDP. $\overline{Z}_H$ is the formation protonation function. The separate titrations are presented by (○), (□) and (△).

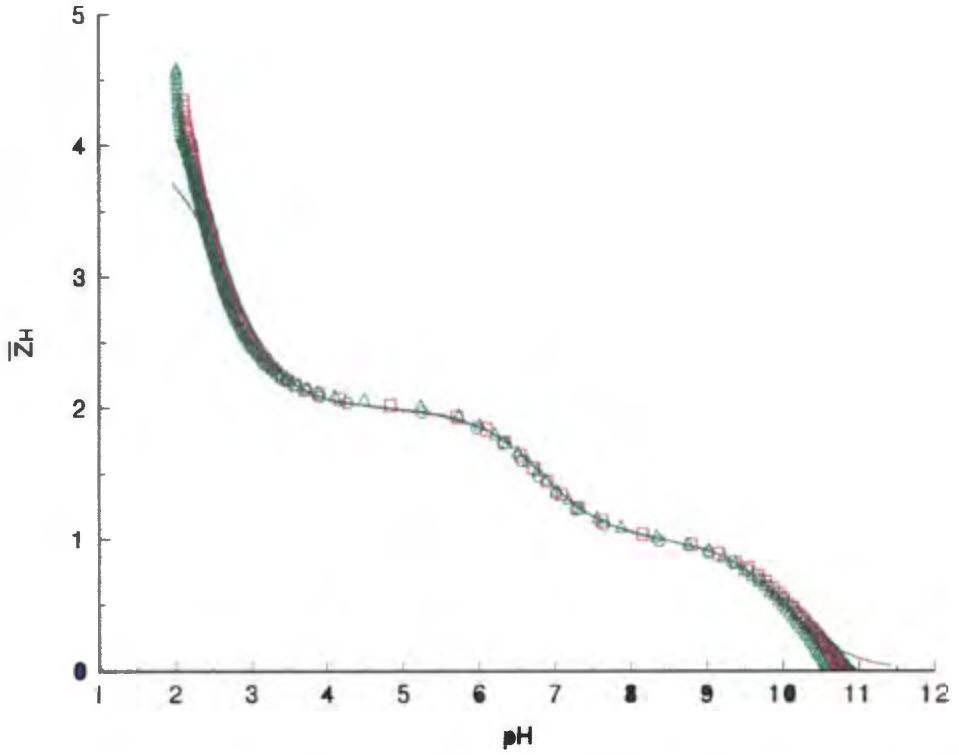

Figure 4. Experimental (points) and calculated (lines) formation curves for HEDP **excluding H_6L**. The separate titrations are presented by (O), (□) and (△).

Table 4. Protonation constants for HEDP without H_6L

Cation	Equilibrium	Log K	Hamilton R factor
H^+	$H + L \rightleftharpoons HL$	10.02 ± 0.01	0.00933
	$H + HL \rightleftharpoons H_2L$	6.82 ± 0.01	
	$H + H_2L \rightleftharpoons H_3L$	2.86 ± 0.02	
	$H + H_3L \rightleftharpoons H_4L$	2.48 ± 0.03	

For all the titrations 600 data points were used. The data points of each protonation titration are found in Appendix C1. All titration data gathered from titrating ligands with metal ions are found in Appendix C2-C4. Appendixes C1-C4 contain all the data points for E0 titrations (a titration between a strong base and acid done before and after a series of titrations to standardise the acid and to calculate the reference potential of the glass electrode) in between. The final outputs of the computer program ESTA2A reached for each model describing the protonation of a ligand are found in Appendix B2. The same type of output for E0 titrations are for reference in Appendix B1. Appendixes B3-B5 display metal ion - ligand complexation model output. (The data and input files are presented on micro floppy disk for easy access).

Previously reported values

Protonation constants for the ligands used in this study, are compared with literature values in Tables 5 and 6.

Table 5. Reported protonation constants for APD and HEDP

	APD		**HEDP**			
	This work	Kabachnik [79][a]	This work	Martell and Smith[b,c] [80]	Dietsche[d] *et. al.* [81]	Nash[e] *et.al.* [82]
Log K_1	10.95	10.8	10.11	10.98	10.60	9.12
Log K_2	9.80	9.9	6.81	6.75	6.89	6.20
Log K_3	6.01	5.83	2.97	2.33	2.5	2.20
Log K_4	2.56	2.55	2.43	(1.4)	<2	1.56
Log $K_{4.3}$						3.76
Log K_6			4.66			

[a] 0.1 mol.dm^{-3}, background electrolyte not stated, 25°C; [b]1.0 mol.dm^{-3} K^+, 25°C, [c]1.0 mol.dm^{-3} Na^+, 25°C; [d] 0.1 mol.dm^{-3} KCl, 25°C; [e]2.0 mol.dm^{-3} $NaNO_3$,25°C;

It is clear from these tables that the medium in which experiments are carried out, have an significant influence on the resultant constants. This was described by De Stefano *et. al.* [87]. Protonation constants in $(CH_3)_4NCl$ are significantly higher than those in KCl and NaCl, and follow the trend $(CH_3)_4NCl$ » KCl > NaCl. Furthermore with higher ionic strength, lower protonation values are expected.

For APD little literature is available. The values measured in this study are in close agreement with results reported in the literature [79] for similar conditions.

For HEDP a wider variation of protonation constants is seen. The values compiled by Martell [79] for β1 are higher than the value found here but Nash reports lower values. This could be explained by the use of KCl instead of NaCl as pointed out by De Stefano *et. al.*[86]. The constant would be expected to be lower in this case. For the next three protonation constants the opposite is true. The medium is now the same but a lower ionic strength is used causing higher values. A similar pattern is found for the values reported by Dietsche *et. al.*[81] although the difference is smaller. Here the ionic strength is lower than in this work but KCl

was used representing two opposing influences. The influence of a different medium is bigger and therefore one would expect the values of Dietsche to be higher than reported. All are in good agreement except the second protonation constant. Looking at the values (and considering the temperature difference) it is fair to say that the protonation constants reported here are in agreement with literature. However the first two references are both unsure about the fourth protonation constants. This might be explained by the use of the H_6L species as has been done here. The value for the third protonation constant is also slightly affected in a negative direction by the absence of this species (as shown above). The values found by Nash *et. al.*[82] are different. The background electrolyte used is 2.0 M $NaNO_3$. The protonation constants are therefore much smaller than reported by the others. In this case all values are proportionally smaller than reported here. Once again it is possible to argue that good agreement with literature has been attained.

The same tendency is noticeable for MDP. Martell [83] and others report higher, and Nash, lower values. The same arguments apply here. With the opposing effects of KCl vs ionic strength in Martell's values the theory outlined above is inconsistent. However the use of $(CH_3)_4NCl$ by Van der Linde *et. al.* [84] and Grabestetter *et. al.* [85] are consistent with the values reported here. Once again there is uncertainty in the fourth protonation constant. This could be explained by the absence of H_6L.

Table 6. Reported protonation constants for MDP

	This work	Martell, Smith[a,b] [83]	Nash *et. al.*[b] [82]	Van Der Linde *et. al.*[84][c]	Grabenstetter *et. al.* [85][c]
Log K_1	9.97	10.33	8.90	10.75	10.57
Log K_2	7.01	6.87	6.34	7.10	7.00
Log K_3	3.26	2.5	2.35	2.75	2.78
Log K_4	2.19	(1.7)	1.30		
Log $K_{4,3}$			3.65		
Log K_6	2.56				

[a] 0.1 mol.dm^{-3} K^+, 20°C; [b] 2.0 mol.dm^{-3} $NaNO_3$,25°C; [c] 0.1 mol.dm^{-3} $(CH_3)_4N^+$, 25°C.

However this is not the case in the values reported by Nash *et. al.*[82] which are, as expected, proportionally lower. For both HEDP and MDP, a standard deviation of 0.01 is reported for the fourth protonation constant. It is important to note that they included another equilibrium

in their model, seemingly to help with the fit, viz. Log $K_{4,3}$. This is the constant for the equilibrium: $2H + H_2L \rightleftharpoons H_4L$.

Perhaps it is this that helps the models to produce an accurate fourth protonation value.

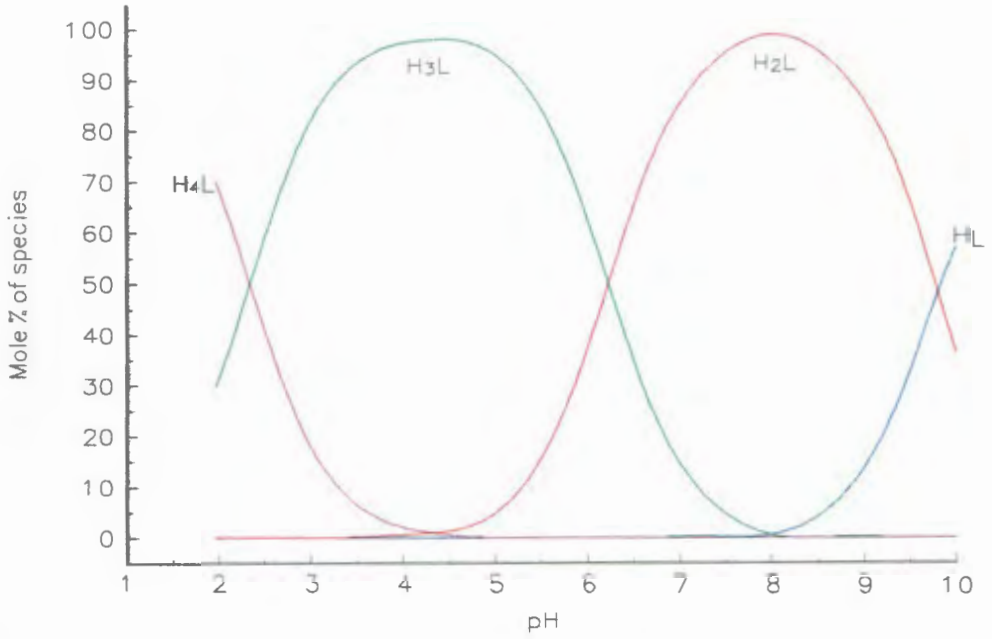

Figure 5. Species distribution curves for the protonation of APD at 37°C and 0.15 mol.dm^{-3} as calculated from protonation constants in Table 1. The initial APD concentration was 0.00184 mol.dm^{-3}.

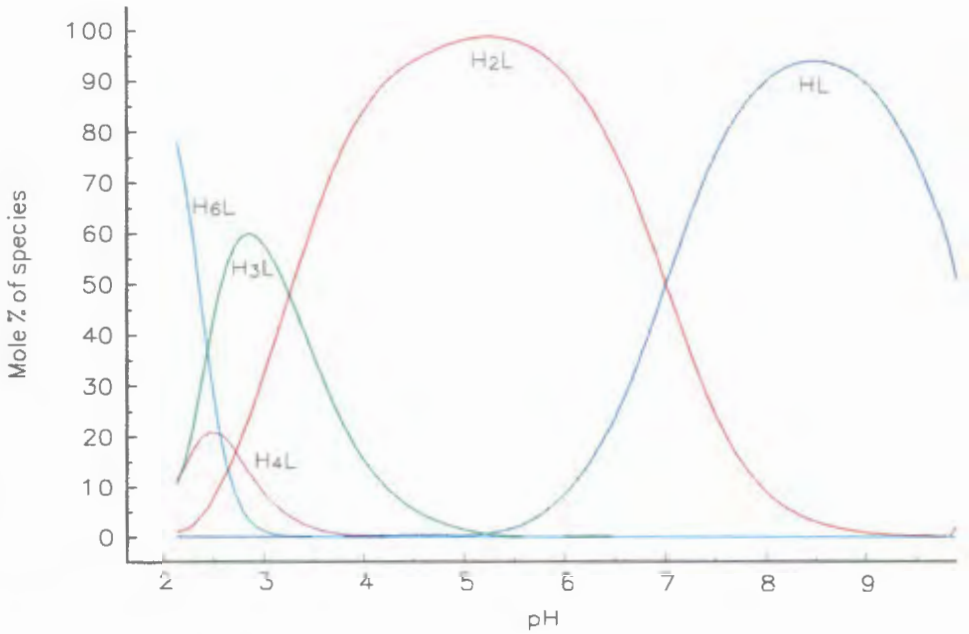

Figure 6. Species distribution curves for the protonation of MDP at 37°C and 0.15 mol.dm^{-3} as calculated from protonation constants in Table 2. The initial MDP concentration was 0.00184 mol.dm^{-3}.

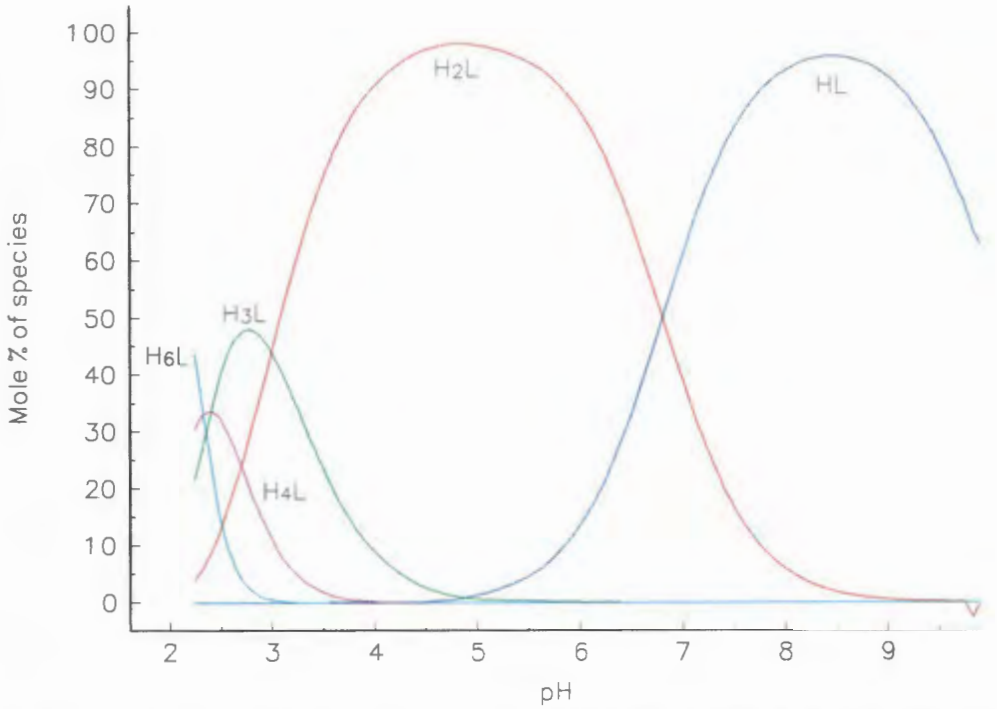

Figure 7. Species distribution curves for the protonation of HEDP at 37°C and 0.15 mol.dm^{-3} as calculated from protonation constants in Table 3. The initial HEDP concentration was taken as 0.00103 mol.dm^{-3}.

From the reported constants it is possible to draw species distribution curves for each of the ligands. These are shown in Figures 5 to 7. In blood plasma, which has a pH = 7.4, LH and LH_2 are the major species for MDP and HEDP while H_2L and, to a lesser extend, H_3L are the major species of APD.

The crossing of the lines, corresponding to two species for instance H_2L and HL in the HEDP model, coincide at the same pH where the inflections are visible in Figure 3 ($\overline{Z}_H$ vs pH). At first glance the curves for APD look totally different from the other two which have the same outline, although at low pH there is some difference visible. The similarity is mostly due to their structural resemblance, the same model applied and the similarity of the first three constants. APD however has a big structural difference in that it has an amine group which may also be protonated and deprotonated. This group is deprotonated last (at the highest pH) corresponding to the $H + L \rightleftharpoons HL$ equilibrium. The log K_1 value in this case is thus higher than for MDP and HEDP which lack this amine group. The value, for log K_2 of APD corresponds to deprotonation of the first of the diphosphonate groups' protons, as in the case of MDP and HEDP where this is reported by the log K_1 value. If these values are compared for APD and

MDP there is good agreement. The same applies for log K_3 of APD and log K_2 of MDP etc. Visually, the curves for APD are shifted one to the left, to ignore the effect of the amine group. For example, the H_2L curve of MDP or HEDP appears at the same pH as the H_3L curve of APD.

Between HEDP and MDP there is only a slight difference between all the constants reported. For instance, although the difference is small, the reported log K_1 value for HEDP is larger than that of MDP mainly due the inductive effect of the CH_3-group. The hydoxy group plays a secondary role withdrawing electrons from molecule and thus lowering the protonation constant.

4.1.2. Potentiometric formation constants for APD

The next sections will report formation constants calculated by potentiometric titrations for each of the ligands, starting with APD.

Results will be presented tabularly. Sometimes two models for the same system will be presented to show why a particular model was chosen. In these tables M will be used to represent the metal-ion, L the ligand and H protons. For clarity, the charges on the metal ions, ligands and complexes have been omitted. All data measured at 37 °C ± 0.1 °C and I = 0.15 mol.dm^{-3} NaCl. pK_w was fixed at 13.42 under these conditions [42].

Complexation of Ca^{2+} by APD

Table 7 contains the values calculated for the complexation of Ca(II) by APD. Two possible models were found. The output of the ESTA2A runs are included in Appendix B3 as are the rest of the ESTA2A outputs for the other APD complexation models. Potentiometric data points are shown in Appendix C2.

The only constant available in the literature is by Kabachnik *et. al.*[79] describing the equilibrium:

$$M + L + 2H \rightleftharpoons MLH_2 \qquad \text{Log } K = 23.55$$

Which compares well with the value for the same equilibrium reported in Table 7. The first model (perhaps unconventional) is preferred to the second because of the lower Hamilton factor and better deprotonation ($\overline{Q}$) curves.

Table 7. Formation constants for APD and Ca(II)

Cation	Equilibrium	Log K	Data points	Hamilton R factor
Ca(II)	$M + L + H \rightleftharpoons MLH$	16.65 ± 0.02	600	0.01019
	$2M + L \rightleftharpoons M_2L$	12.46 ± 0.03		
	$M_2L + H \rightleftharpoons M_2LH$	8.50 ± 0.04		
Ca(II)	$M + L \rightleftharpoons ML$	6.70 ± 0.03	600	0.01356
	$ML + H \rightleftharpoons MLH$	10.51 ± 0.03		
	$MLH + H \rightleftharpoons MLH_2$	6.80 ± 0.03		

The calculated and experimental $\overline{Q}$ curves vs pH are displayed for both models in Figure 8 and 9. The calculated and experimental formation ($\overline{Z}$) curves, for the first model, are displayed in a similar way in Figure 10. The deprotonation curves cast doubt on the vadility of the second model. The solid lines are much closer matched in Figure 8 by the points than in Figure 9. In Figure 8 the species presented in the model are evident from the following: There are inflections at $\overline{Q}$ = 0.5 and 1. From the dashed curve, $\overline{n}$ (the protonation state of the ligand in the absence of the metal ion), H_2L is the ligand species available for complexation. With $\overline{Q}$ = 0.5, one proton is released per two metal ions which means that M_2LH is the dominant species. For $\overline{Q}$ = 1 this proton is released (the 0.5 difference with the previous value represents one proton per two metal ions) leaving M_2L.

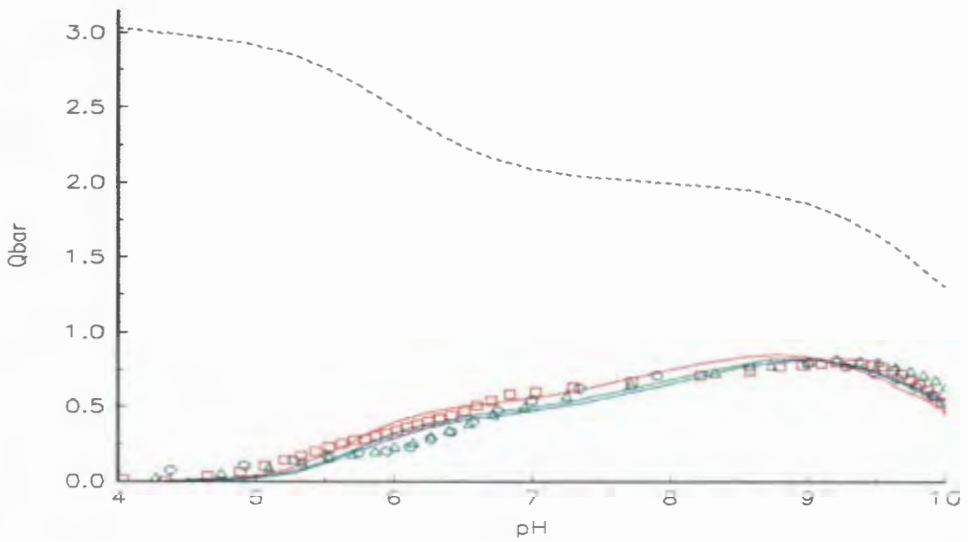

Figure 8 Experimental (points) and calculated (lines) deprotonation curves for Ca(II) complexation by APD. Qbar = $\overline{Q}$ and is the deprotonation function and the dashed line is the $\overline{n}$ curve. The three separate titrations were for the L:M ratio = 1:1 (O), L:M = 1:1.25 (□) and L:M = 1:2.5(△).

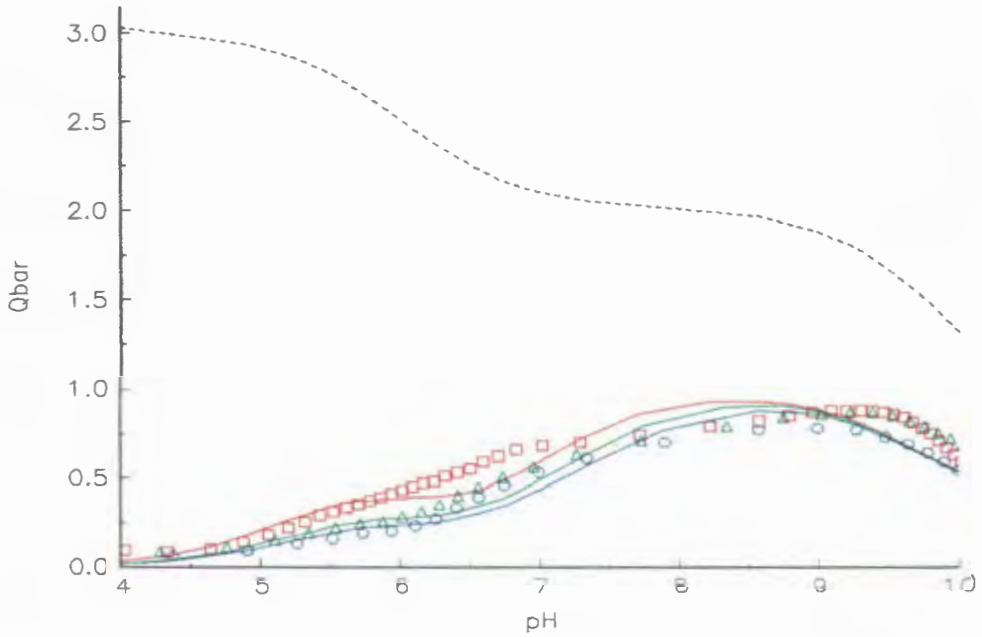

Figure 9. Experimental (points) and calculated (lines) deprotonation curves for Ca(II) complexation by APD. Qbar = $\overline{Q}$ and is the deprotonation function and the dashed line is the $\overline{n}$ curve. The three separate titrations are as shown in Fig. 8.

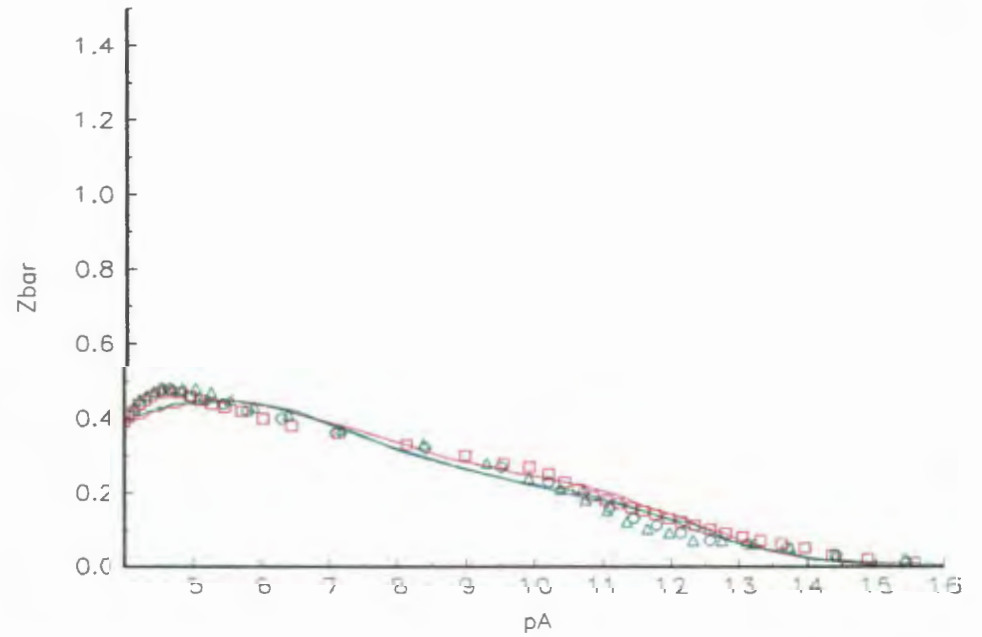

Figure 10. Experimental (points) and calculated (lines) formation curves for Ca(II) complexation by APD. Zbar = $\overline{Z}$ and is the formation function and pA is the negative logarithm of the free ligand concentration. The three separate titrations are as shown in Fig. 8.

The species distribution curves for the chosen model is displayed in Figure 11. From this it can be seen that the complexes attain maximum concentration at the pH values predicted by the deprotonation curves.

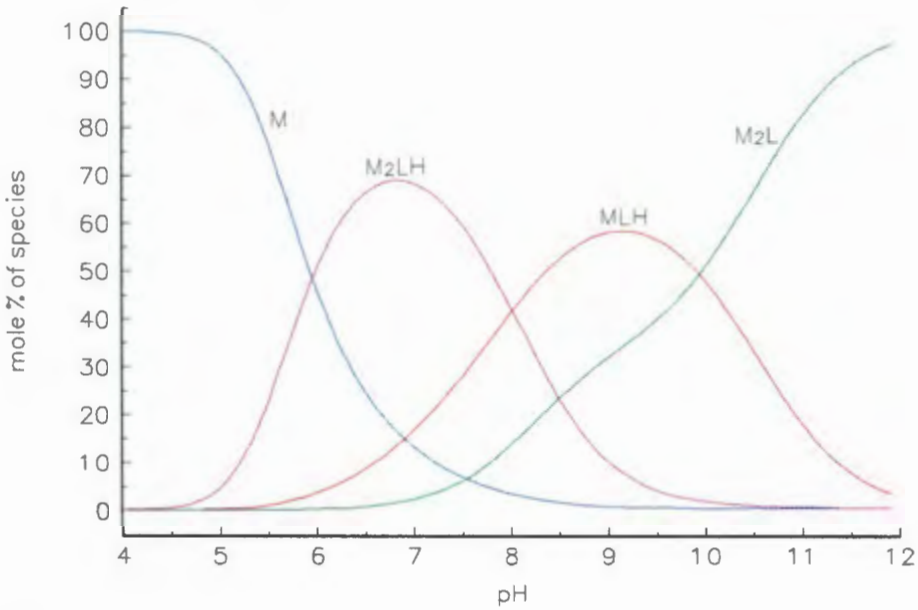

Figure 11. Species distrubution curves for the complexation of Ca(II) by APD at 37 °C and in 0.15 mol.dm^{-3} NaCl as calculated from formation constants in Table 7. 0.00213 M APD and 0.0077 M Ca(II).

Complexation of Mg(II) by APD

Table 8 displays the values found for two models achieved from titration data for the complexation of Mg(II) by APD. ESTA2A outputs are found in Appendix B3 and titration data points in Appendix C2.

Table 8 Formation constants for APD and Mg(II)

Cation	Equilibrium	Log K	Data points	Hamilton R factor
Mg(II)	$M + L \rightleftharpoons ML$	7.03 ± 0.03	600	0.01588
	$ML + H \rightleftharpoons MLH$	10.24 ± 0.03		
	$MLH + H \rightleftharpoons MLH_2$	6.77 ± 0.03		

Mg(II)	$M + L \rightleftharpoons ML$	6.90 ± 0.06	600	0.02004
	$ML + M \rightleftharpoons M_2L$	6.79 ± 0.07		
	$M_2L + H \rightleftharpoons M_2LH$	7.56 ± 0.05		

No constants were found in the literature for the complexation of Mg(II) by APD.

In this case the first model (conventional type) is preferred to the second (as in the case of APD and Ca(II)) because of the lower Hamilton factor, standard deviations and better deprotonation ($\overline{Q}$) curves. The calculated and experimental $\overline{Q}$ curves vs pH are displayed for both models in Figure 12 and 13. This difference in model between Ca(II) and Mg(II) might be due to the smaller size of the Mg(II) ion, forming stronger complexes (discussed later) and therefore preferring to complex one metal ion with one ligand. Ca(II) on the other hand forms a weaker complex and the ligand can accommodate two metal ions.

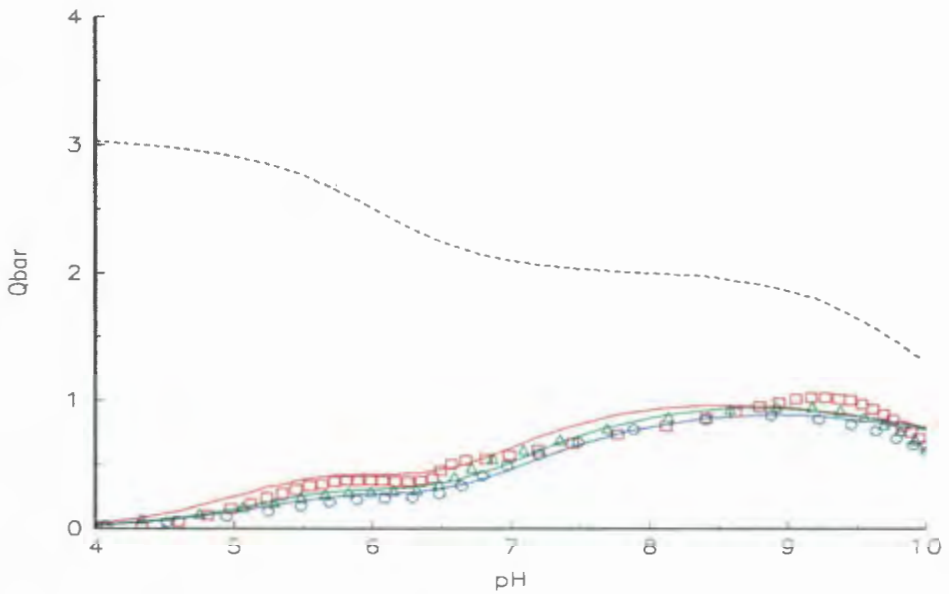

Figure 12. Experimental (points) and calculated (lines) deprotonation curves for Mg(II) complexation by APD (first model). Qbar = $\overline{Q}$ and is the deprotonation function and the dashed line is the $\overline{n}$ curve. The three separate tirations were for the L:M ratio = 1:1 (○), L:M = 1:1.25 (□) and L:M = 1:2.5 (△).

The calculated and experimental formation curves for the first model are displayed in a similar way in Figure 14. The deprotonation curves show that the second model is more plausible . The solid lines (calculated curves) are much closer matched in Figure 12 by the points (experimental curves) than in Figure 13.

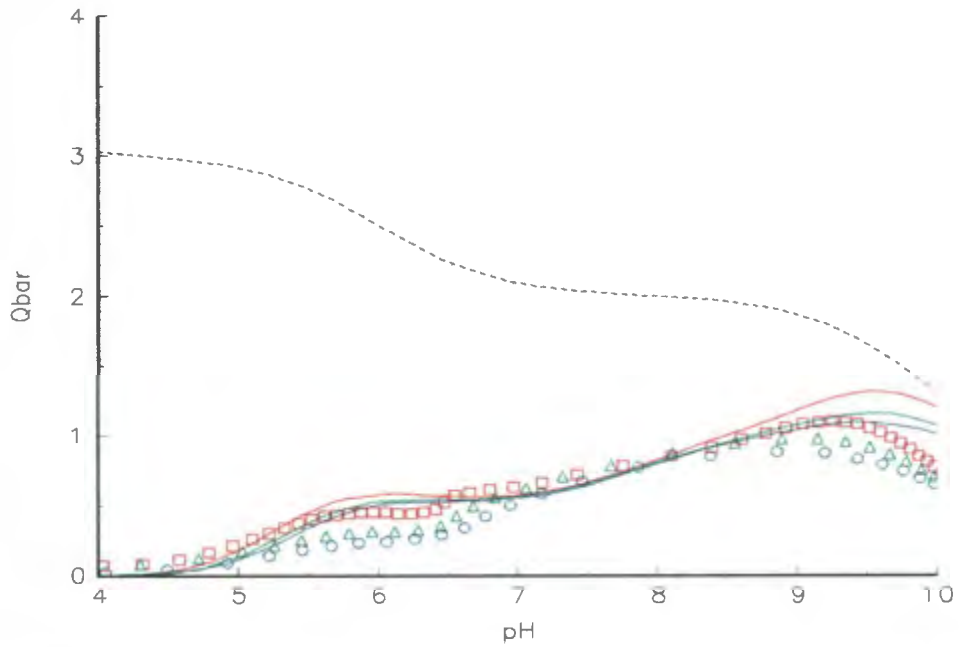

Figure 13. Experimental (points) and calculated (lines) deprotonation curves for Mg(II) complexation by APD (second model). Qbar = $\overline{Q}$ and is the deprotonation function and the dashed line is the $\overline{n}$ curve. The three separate tirations are as shown in Fig. 12.

In Figure 12 the difference with Figure 8 (APD and Ca(II)) is especially evident between pH = 5.5 to 6.5 where the $\overline{Q}$ curve is flattened for Mg(II) but climbing for Ca(II). For Mg(II) $\overline{Q}$ = 0.5 in this region and $\overline{n}$ shows that the ligand changes from H_3L to H_2L. This indicates that complexation occurs but not in a single species. At pH = 5.5 one would expect MLH_2 and unbound metal ion (M) species to be present lowering the $\overline{Q}$ value from 1 (which means that 1 proton is released on complexation. Together with the H_3L species this results in MLH_2) to 0.5. At pH = 6.5 the opposite is true, H_2L needs no release of protons to form MLH_2, thus $\overline{Q}$ should be 0. Another species is thus forming viz. MLH where $\overline{Q}$ = 1 applies. The $\overline{Q}$ = 0.5 is a compromise between them. In between (pH = 5.5 and 6.5) a combination of the two factors contributes to $\overline{Q}$ staying at 0.5 and MLH_2 is the major species. These observation are confirmed by the species distribution diagram, Figure 15. Between pH = 8 and 9 the explanation is simpler. $\overline{Q}$ = 1 and complexation with H_2L results in MLH. No competition by other species is evident here. At higher pH values, HL becomes the dominant ligand species where $\overline{Q}$ stays 1. For Ca(II), the $\overline{Q}$ values started to drop at pH = 10 showing the absence of ML and the involvement of M_2L.

The interesting aspect is that Ca and Mg could be explained by the same two models in each case but different ones were chosen. The strength of complexation for Ca(II) and Mg(II) by APD does not differ much although Mg(II) has a slightly higher first formation constant.

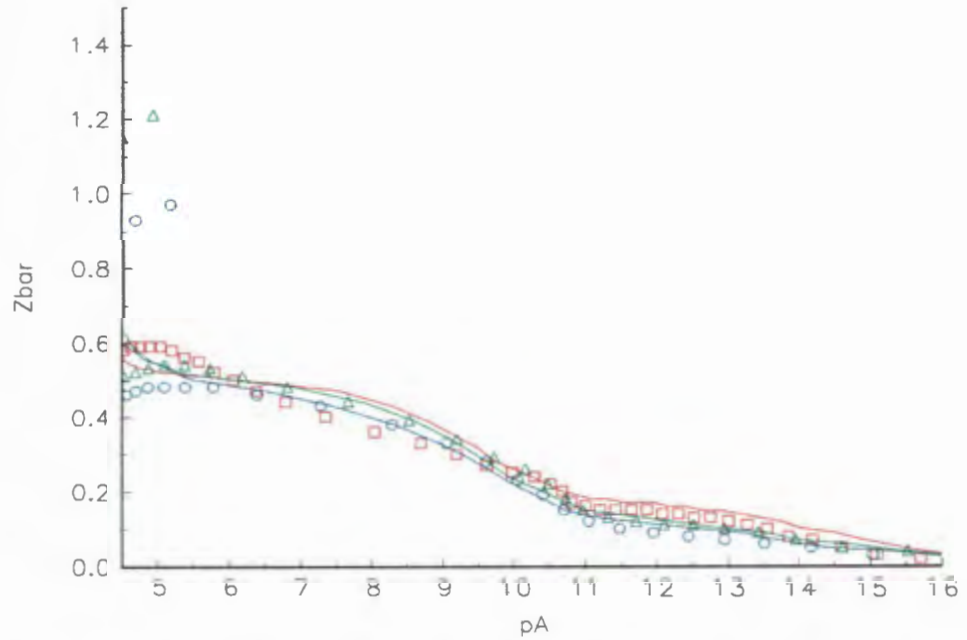

Figure 14. Experimental (points) and calculated (lines) formation curves for Mg(II) complexation by APD. Zbar = $\overline{Z}$ and is the formation function and pA is the negative logarithm of the free ligand concentration. The three separate titrations are as shown in Fig. 12.

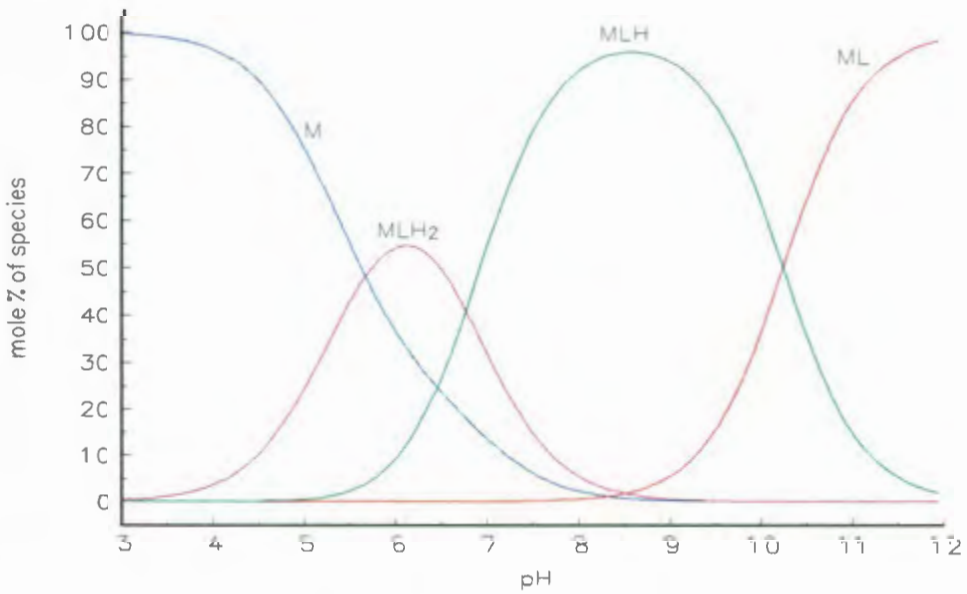

Figure 15. Species distrubution curves for the complexation of Mg(II) by APD at 37 °C and in 0.15 mol.dm^{-3} as calculated from formation constants in Table 8. 0.00213 M APD and 0.00086 M Mg(II).

Complexation of Sr(II) by APD

Another Alkaline Earth metal is Sr(II) which was studied to see whether it fits in with the model found for Ca(II), as we progress down this group. Sr(II) is also used as the active isotope in the radiopharmaceutical Metastron. This consist of $^{89}SrCl_2$ which is used in the pain palliation treatment of prostatic bone metastases. Here no phosphonate ligand is used to deliver the metal ion to the bone but it relies on phosphate in blood plasma, for which Sr(II) has a affinity, to deliver the radioactive isotope to the bone. The possible use of ^{89}SrAPD in this respect can be studied by ECCLES modelling as can the working of $^{89}SrCl_2$ and its side-effects, using the constants calculated here. Table 9 displays the values found for the best models achieved from titration data for the complexation of Sr(II) by APD. ESTA2A output in Appendix B3 and titration data points in Appendix C2.

Table 9 Formation constants for APD and Sr(II)

Cation	Equilibrium	Log K	Data points	Hamilton R factor
Sr(II)	$2M + L \rightleftharpoons M_2L$	9.22 ± 0.05	600	0.00937
	$M + L + H \rightleftharpoons MLH$	16.06 ± 0.01		
	$MLH + H \rightleftharpoons MLH_2$	7.64 ± 0.02		
	$M_2L + H \rightleftharpoons M_2LH$	10.30 ± 0.06		

No constants were found in the literature for the complexation of Sr(II) by APD.
Here the same species are reported as in the model for Ca(II) with the addition of MLH_2. The calculated and experimental $\overline{Q}$ curves vs pH are displayed in Figure 16. This fit of experimental vs calculated values is very similar to that achieved by Ca(II) and APD. As expected the first constant is lower than for Ca(II), following the trend Mg > Ca > Sr (in agreement with Ca < Mg < Zn [81] and the Irving-Williams series). This corresponds to the ionic radii increasing in the order: Mg(II) (0.66Å) < Ca(II) (0.99Å) < Sr(II) (1.12Å) The bigger the ion, the weaker the complexation. The important aspect is that the most plausible model here contained the same species as found for Ca(II) which verifies the unconventional type of model proposed. Sr(II) also accepts two metal ions bound per ligand (M_2L species) as was the case with Ca(II). This is surprising Sr(II) is even larger than Ca(II). This might indicate the stability of the M_2L species and the preference of these metal ions to form it.

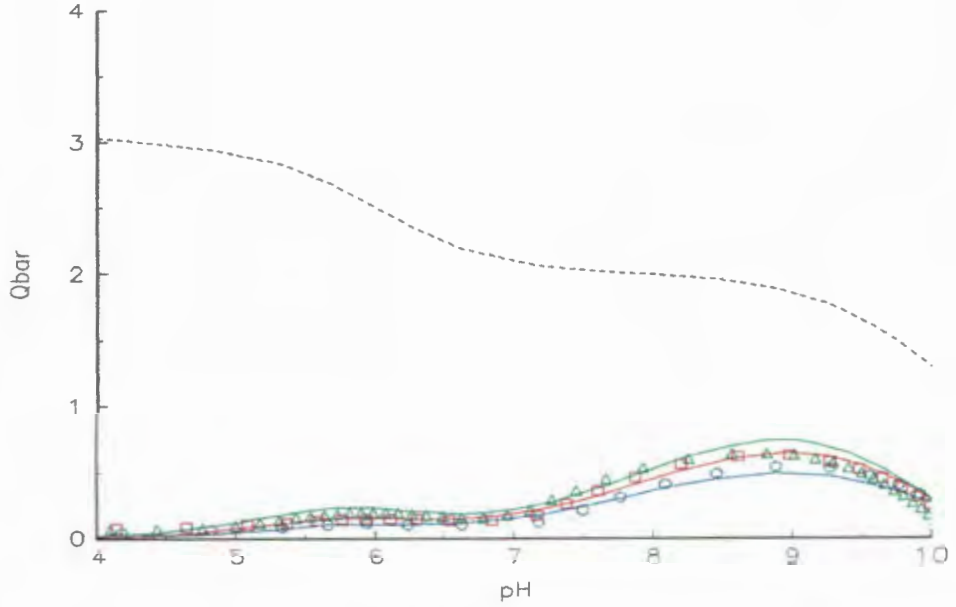

Figure 16. Experimental (points) and calculated (lines) deprotonation curves for Sr(II) complexation by APD. Qbar = $\overline{Q}$ and is the deprotonation function and the dashed line is the $\overline{n}$ curve. The three separate tirations were for the L:M ratio = 1:1 (○), L:M = 1:1.25 (□) and L:M = 1:2.5 (△).

Complexation of Zn(II) by APD

Table 10 displays the values found for the model achieved from titration data for the complexation of Zn(II) by APD. ESTA2A output is found in Appendix B3 and titration data points in Appendix C2. In both cases no suitable models were achieved.

Table 10 Formation constants for APD and Zn(II)

Cation	Equilibrium	Log K	Data points	Hamilton R factor
Zn(II)	$M + L \rightleftharpoons ML$	11.19 ± 0.05	**600**	0.03850
	$ML + H \rightleftharpoons MLH$	9.00 ± 0.07		
	$MLH + H \rightleftharpoons MLH_2$	5.82 ± 0.06		
	$ML + OH \rightleftharpoons MLOH$	2.64 ± 0.09		
Zn(II)	$M + L \rightleftharpoons ML$	12.20 ± 0.04	**566**	0.02658
	$ML + H \rightleftharpoons MLH$	8.79 ± 0.06		
	$MLH + H \rightleftharpoons MLH_2$	4.65 ± 0.06		
	$ML + OH \rightleftharpoons MLOH$	2.71 ± 0.06		

The main reason being the precipitate (seen as a 'milky' solution in the titration vessel) that forms between pH = 5 to 7.5. This precipitate might be due to neutral species (M_2L in the case of Zn(II) or MLH in the case of Ho(III) or Sm(III)) formed at the ligand and metal ion concentrations used. The data in this region of the titration are difficult to model. Removing data from this region results in cutting out the region of interest in our case (blood plasma has a pH round about 7.4). This is illustrated (second set of constants) to demonstrate the influence on the $\overline{Q}$ fit.

No constants were found in the literature for the complexation of Zn(II) by APD.

In this case neither model produces a satisfactory fit to the titration data points. This is clearly visible from the high Hamilton factors, standard deviations and poor deprotonation ($\overline{Q}$) curves. The calculated and experimental $\overline{Q}$ curves vs pH for the two models are respectively displayed in Figure 17 and 18. From Figure 18 it is evident that the cutting of the data points, corresponding to precipitation, is not successful in finding a better relation between the experimental and calculated $\overline{Q}$ curves although the Hamilton factor and standard deviations are significantly lower.

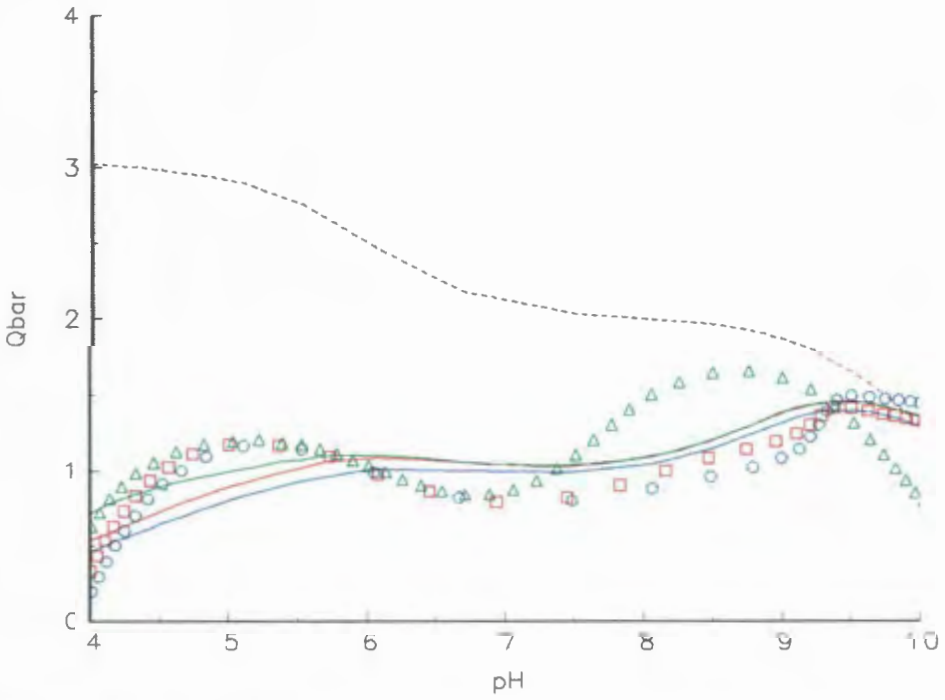

Figure 17. Experimental (points) and calculated (lines) deprotonation curves for Zn(II) complexation by APD. Qbar = $\overline{Q}$ and is the deprotonation function and the dashed line is the $\overline{n}$ curve. The three separate tirations were for the L:M ratio = 1:1 (○), L:M = 1:1.25 (□) and L:M = 1:2.5 (△).

Another way has to be found to bypass this precipitation problem. One is to have a higher ratio of ligand to metal resulting in lower metal ion concentrations. Potentiometry is not suitable with low metal ion concentrations but a technique like polarography is. The next section will contain formation constants determined by this technique. These values found here only serve as an indication for what to expect from this system and will not be used in blood plasma modelling.

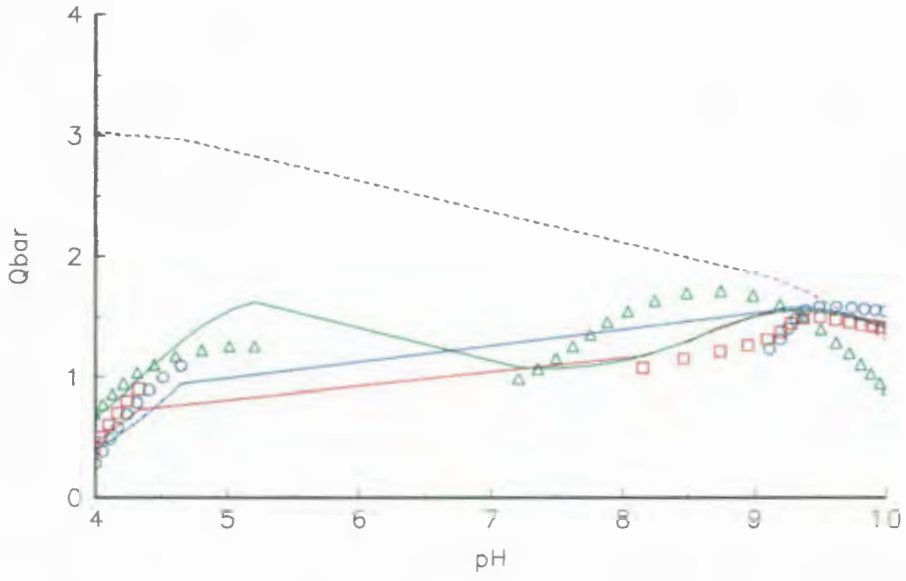

Figure 18. Experimental (points) and calculated (lines) deprotonation curves for Zn(II) complexation by APD. Qbar = $\overline{Q}$ and is the deprotonation function and the dashed line is then $\overline{n}$ curve. The three separate tirations as shown in Fig.17. Where precipitation occured the data points were cut.

Complexation of Ho(III) by APD

Table 12 displays the values found for the model achieved from titration data for the complexation of Ho(III) by APD. ESTA2A output is found in Appendix B3 and titration data points in Appendix C2. No suitable models were achieved. The main reason being the precipitate (as seen as a 'milky' solution in the titration vessel) that forms up till pH = 8 as was the case with Sm(III).

Table 11 Formation constants for APD and Ho(III)

Cation	Equilibrium	Log K	Data points	Hamilton R factor
Ho(III)	$M + L \rightleftharpoons ML$	13.81 ± 0.07	**1000**	0.02841
	$ML + H \rightleftharpoons MLH$	9.53 ± 0.09		
	$MLH + H \rightleftharpoons MLH_2$	4.29 ± 0.09		

No constants were found in the literature for the complexation of Ho(III) by APD.

The model is clearly provides no satisfactory fit to the titration data points as can be deduced from the high Hamilton factors, standard deviations and poor deprotonation ($\overline{Q}$) curves. The standard deviations values were slightly better than for Sm(III). The calculated and experimental $\overline{Q}$ curves are not displayed because they do not differ much from Figure 20. The conclusion is the same: an insufficient fit giving only semi-quantitative values. The value found for the first complexation constant is what was expected and agrees with the value for the complexation of Ho(III) by EDTMP, Log K_1 = 13.32 [5]. The species distribution curves for Ho(III) with APD, Figure 19, was used to explain results found in the baboon test and is therefore included.

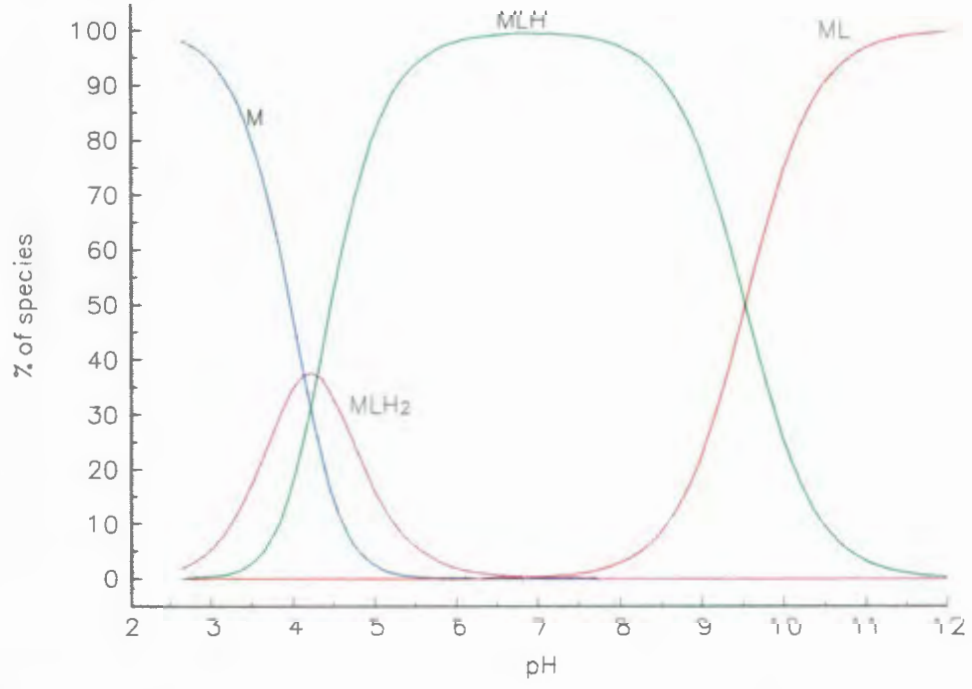

Figure 19. Species distrubution curves for the complexation of Ho(III) by APD at 37 °C and in 0.15 mol.dm^{-3} as calculated from formation constants in Table 11. 5 E-08 M APD and 1 E-06 M Ho(III)).

Complexation of Sm(III) by APD

Table 11 displays the values found for the model achieved from titration data for the complexation of Sm(III) by APD. ESTA2A output is found in Appendix B3 and titration data points in Appendix C2. No suitable models were achieved. The main reason being the precipitate (as seen as a 'milky' solution in the titration vessel) that forms up till pH = 8. Cutting out this area of precipitation will result in cutting out more than half of the titration and is therefore even worse than in the case of Zn(II).

Table 12 Formation constants for APD and Sm(III)

Cation	Equilibrium	Log K	Data points	Hamilton R factor
Sm(III)	$M + L \rightleftharpoons ML$	9.67 ± 0.10	**600**	0.02857
	$ML + H \rightleftharpoons MLH$	10.35 ± 0.12		
	$MLH + H \rightleftharpoons MLH_2$	7.22 ± 0.12		

No constants were found in the literature for the complexation of Sm(III) by APD.

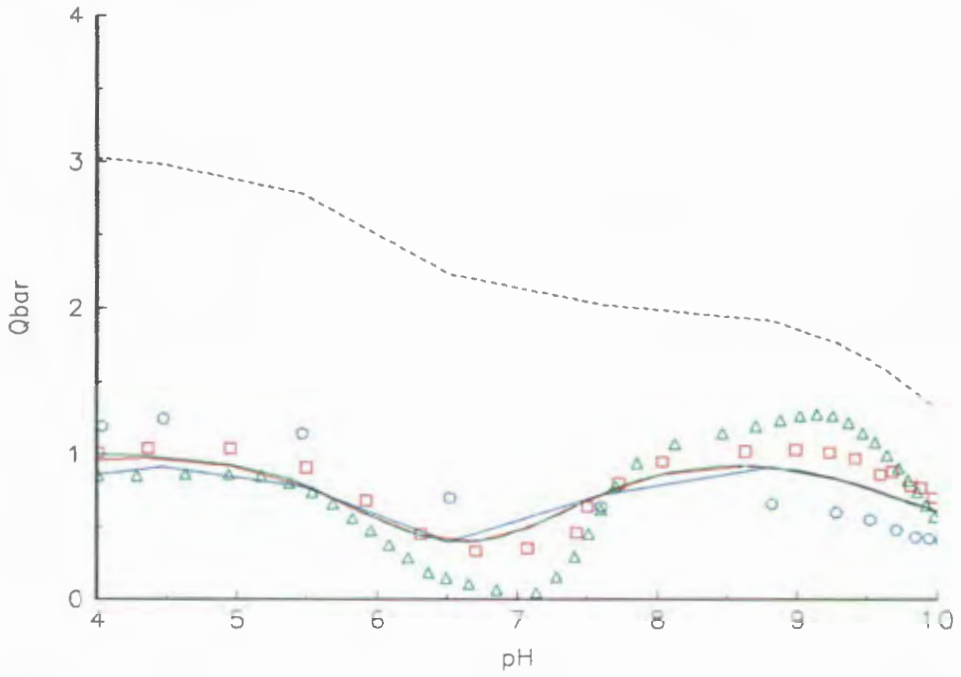

Figure 20. Experimental (points) and calculated (lines) deprotonation curves for Sm(III)) complexation by APD. Qbar = $\overline{Q}$ and is the deprotonation function and the dashed line is the $\overline{n}$ curve. The three separate tirations were for the L:M ratio = 1:1 (○), L:M = 1:1.25 (□) and L:M = 1:2.5 (△).

The model clearly provides no satisfactory fit to the titration data points as can be deduced from the high Hamilton factors, standard deviations and poor deprotonation ($\overline{Q}$) curves. The calculated and experimental $\overline{Q}$ curves vs pH are displayed in Figure 20. The cutting of data points proved to be fruitless as in the case of Zn(II). This was not even attempted and the estimate of the constants were established by taking all data points into consideration. Figure 20 shows that the fit is inefficient and these values are therefore only an indication and cannot be used in the blood plasma model. The value found for the first complexation constant is much lower than expected. The value for the complexation of Sm(III) by EDTMP is 14.44 [5]. The value for Zn(II) (this work) is 10.0. One would expect the value for Sm(III) to be higher because lanthanides are trivalent and will therefore have a stronger electrostatic effect than divalent Zn forming a stronger interaction with a ligand [87]. If the approximate value for Ho(III), log K_1 = 13.81 (this work), is considered the value also seems low. In the case of EDTMP, Sm(III) was complexed stronger than Ho(III) [5].

The relative relationship between formation constants of ligands containing negatively charged oxygen donor groups and log $K_1(OH^-)$ for the metal ions was described by Hancock and Martell [92]. Hancock and Martell [92] pointed out that there is a remarkable linear relationship between Log $K_1(L)$ and Log $K_1(OH)$ for negatively charged oxygen donor ligands. By plotting these values it is possible to find a linear fit and calculate a formation constant for a metal ion for which only the hydroxide constant is known. This approach was followed. Figure 20a contains the plot of these sets of constants against each other. The formation constants calculated so far (as well as by polarography) for Ca(II), Mg(II), Sr(II), Zn(II), Ho(III) and Cu(II) [93] were used. Formation constants for hydroxide species were taken from Martell [91]. The (□) resemble the real relationship. The line is the result of the linear regression which produced and regression factor (r) = 0.99. From the graph it is clear that Sm(III) should have a much bigger first complexation constant. From the regression a first formation constant of 13.0 is suggested. Ho(III) though fits in quite well with the other points as is proved by the high regression factor.

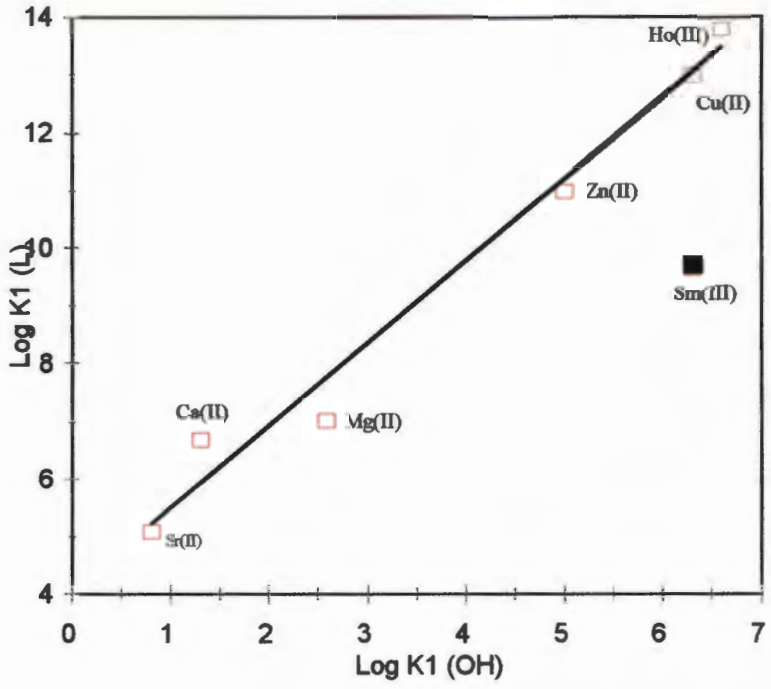

Figure 20a. Relationship between the stability of complexes of metal ions with APD and the affinity of the metal ion for the hydroxide ion. Ionic strength 0.15 mol.dm^{-3}. Note the linear relationship. Sm(III) does not fit on the curve therefore the constant calculated may not be accurate.

4.1.3. Potentiometric formation constants for MDP

The next section reports formation constants calculated by potentiometric titrations for the ligand MDP with various metal ions. Results will be presented tabularly, sometimes two models for the same complexation will be presented to show why a particular model was chosen. Again all data were measured at 37 °C ± 0.1°C and I = 0.15 mol.dm^{-3} NaCl. pK_w was fixed at 13.42 under these conditions [42].

Complexation of Ca(II) by MDP

Table 13 contains the values calculated for the complexation of Ca(II) by MDP. Two possible models were found. The output of the ESTA2A runs are included in Appendix B4 and potentiometric data points are shown in Appendix C3.

Table 13 Formation constants for MDP and Ca(II)

Cation	Equilibrium	Log K	Data points	Hamilton R factor
Ca(II)	$M + L \rightleftharpoons ML$	4.86 ± 0.01	**355**	0.00940
	$ML + H \rightleftharpoons MLH$	7.83 ± 0.03		
	$2M + L \rightleftharpoons M_2L$	8.39 ± 0.04		
Ca(II)	$M + L \rightleftharpoons ML$	4.96 ± 0.01	**355**	0.01107
	$ML + H \rightleftharpoons MLH$	7.87 ± 0.03		

Points up to pH = 4 were excluded as a slight precipitation was observed. In the case of the first titration (high metal concentration viz. L:M = 1:1) from pH = 8 onwards the precipitate reappeared. These values were exclude as well, visible in the ($\overline{Q}$) curves (Figure 21). Constants available in the literature are shown in Table 14.

Table 14. Reported formation constants for MDP and Ca(II)

	This work	Van Der Linde *et. al.*[84] [a]	Carroll *et. al.* [b] [88]	Dietche *et. al.* [b,c] [85] (For Cl_2MDP)
Log K_{ML}	4.86	5.97 (0.06)	4.70 (0.15)	4.71
Log $K_{MHL,MLHL}$	{2.71}	2.89 (0.08)	2.46 (0.04)	2.86
Log $K_{MLH,ML,H}$	7.83	{7.67}	{7.87}	{6.99}
Log $K_{M_2L/ML,M}$	3.54	3.84 (0.08)		

[a] 0.1 mol.dm^{-3} $(CH_3)_4N^+$, 25 °C; [b] 0.5 mol.dm^{-3} $(CH_3)_4N^+$, 25 °C; [c] 0.1 mol.dm^{-3} K^+, 25°C.
The values in normal brackets are the standard deviations. The values in {} brackets are calculated from the original reported values to give a better comparison. The reason for this, is the equilibrium used to describe a complex formation were different.

The last column in Table 14 is added only as an indication because it describes constants for the ligand Cl_2MDP.

The equilibria $ML + H \rightleftharpoons MLH$ has been used here.

However others use: $LH + M \rightleftharpoons MHL$. The values reported here compare well with the literature if the different media in which experiments were done are taken into account.

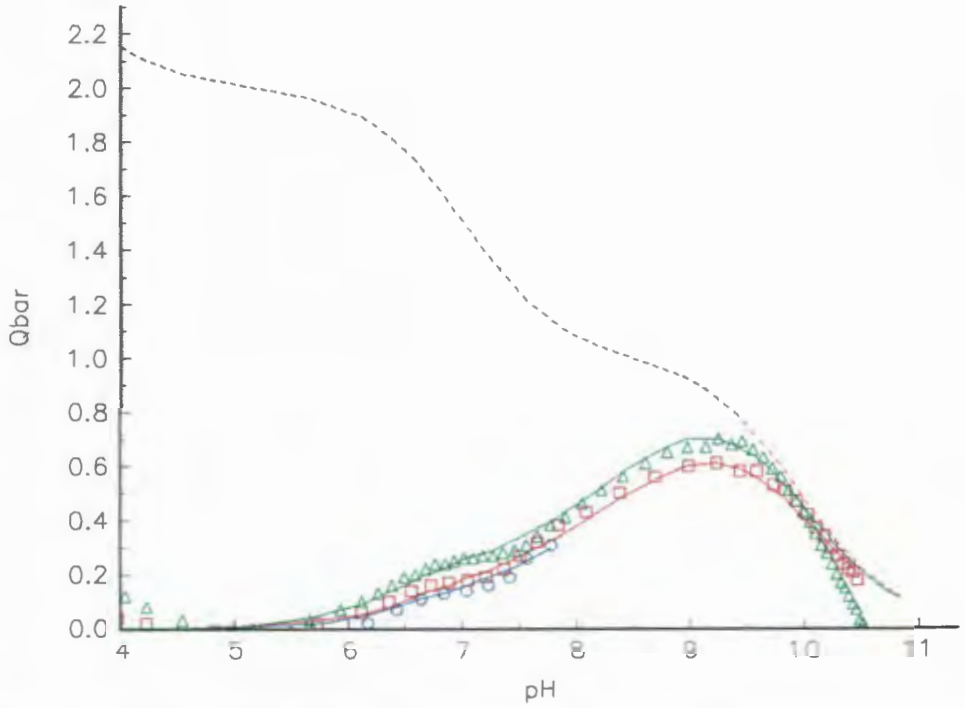

Figure 21. Experimental (points) and calculated (lines) deprotonation curves for Ca(II) complexation by MDP (first model, Table 13). Qbar = $\overline{Q}$ and is the deprotonation function and the dashed line is the $\overline{n}$ curve. The three separate titrations were of L:M = 1:1 (○), L:M = 1.25:1 (□) and L:M = 2.5:1(△) .

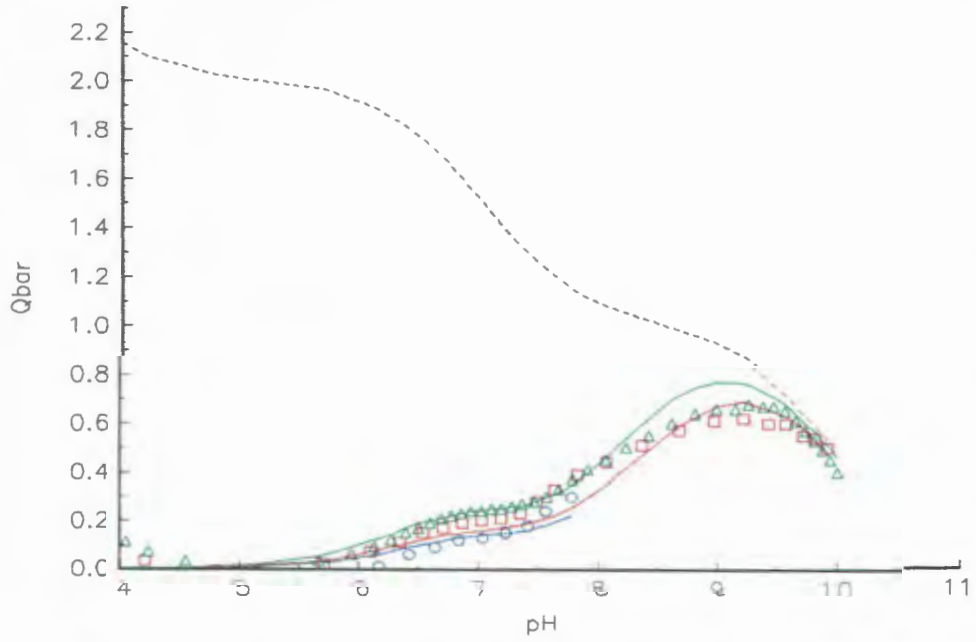

Figure 22. Experimental (points) and calculated (lines) deprotonation curves for Ca(II) complexation by MDP (second model, Table 13). Qbar = $\overline{Q}$ and is the deprotonation function and the dashed line is the $\overline{n}$ curve. The three separate titrations as shown in Fig. 21.

The values of Van der Linde *et. al.* [84] are higher due to the 0.1 mol.dm^{-3} $(CH_3)_4N^+$ background electrolyte [86]. They included the constant M_2L which has a value close to the one reported here. De Stefano *et. al.* [86] also pointed out that a higher ionic strength will result in lower formation constants. This partially would explain Carroll *et. al.* [88] and the relatively low values they reported. Here the standard deviations are larger, probably because of the exclusion of M_2L as can be seen in Table 12. The values by Dietsche *et. al.* [81] are in KCl and therefore a big difference is not expected.

The first model (which includes M_2L) is preferred to the second because of the lower Hamilton factor, standard deviations and better deprotonation ($\overline{Q}$) curves. The calculated and experimental $\overline{Q}$ curves vs pH are displayed for both models in Figure 21 and 22. The calculated and experimental formation curves, $\overline{Z}$, are presented in Figure 23. The deprotonation curves show a better fit for the first model. The solid lines (calculated curves) are much closer matched in Figure 21 by the points (experimental curves) than in Figure 22.

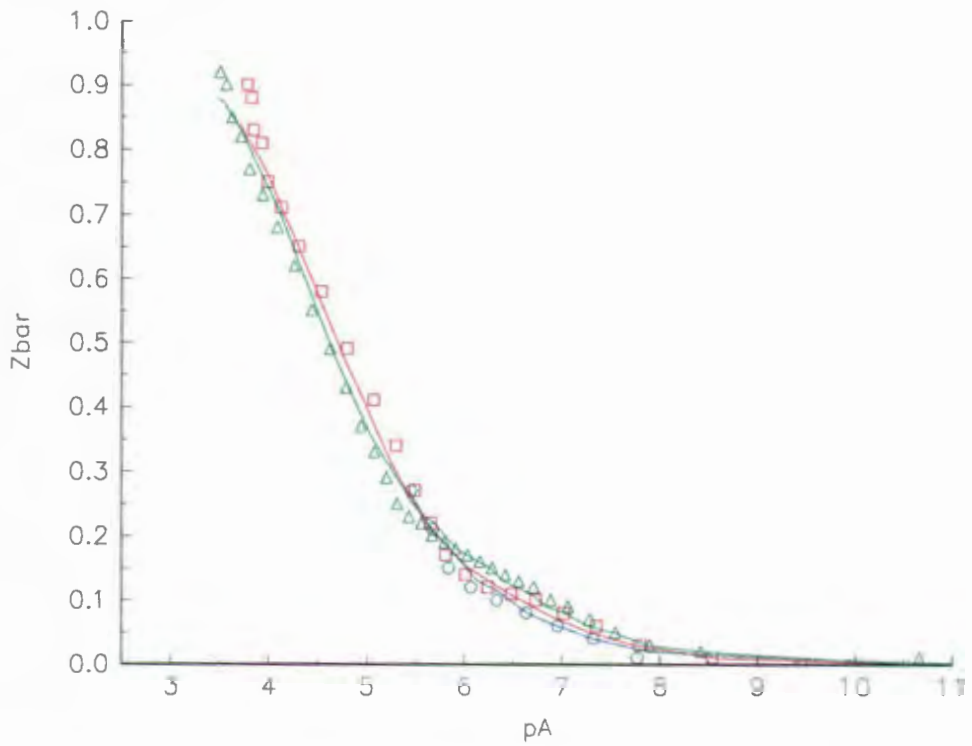

Figure 23. Experimental (points) and calculated (lines) formation curves for Ca(II) complexation by MDP. Zbar = $\overline{Z}$ and is the formation function and pA is the negative logarithm of the free ligand concentration. The three separate titrations were as for Figure 21.

From this figure the species present may be deduced from the following: Above pH = 10 the dotted line, $\bar{n}$, closely follows the $\bar{Q}$ curves. This means that no proton is left on the ligand while complexed thus making ML the dominant species. No MLOH is formed because $\bar{n}$ does not cross the $\bar{Q}$ curve (meaning more protons are released than the ligand normally has, indicating MLH_{-1}). Before pH = 5.5 no complexation occurs ($\bar{Q} = 0$). After pH = 6 the inflections of the $\bar{Q}$ curve flow one into another, indicating various complexes in competition viz. MLH and M_2L. The $\bar{n}$ curve also drops between pH = 6.5 and 8. This delivers a scenario equal to that described in Section 4.1.2 for APD and Mg(II), although different complexes are involved here.

The species distribution curves for the chosen model is displayed in Figure 24. From this it can be seen that the complexes attain maxima at the pH values predicted by the deprotonation curves. There is no single dominant species between pH = 5.5 and 9.5 as is visible from this graph.

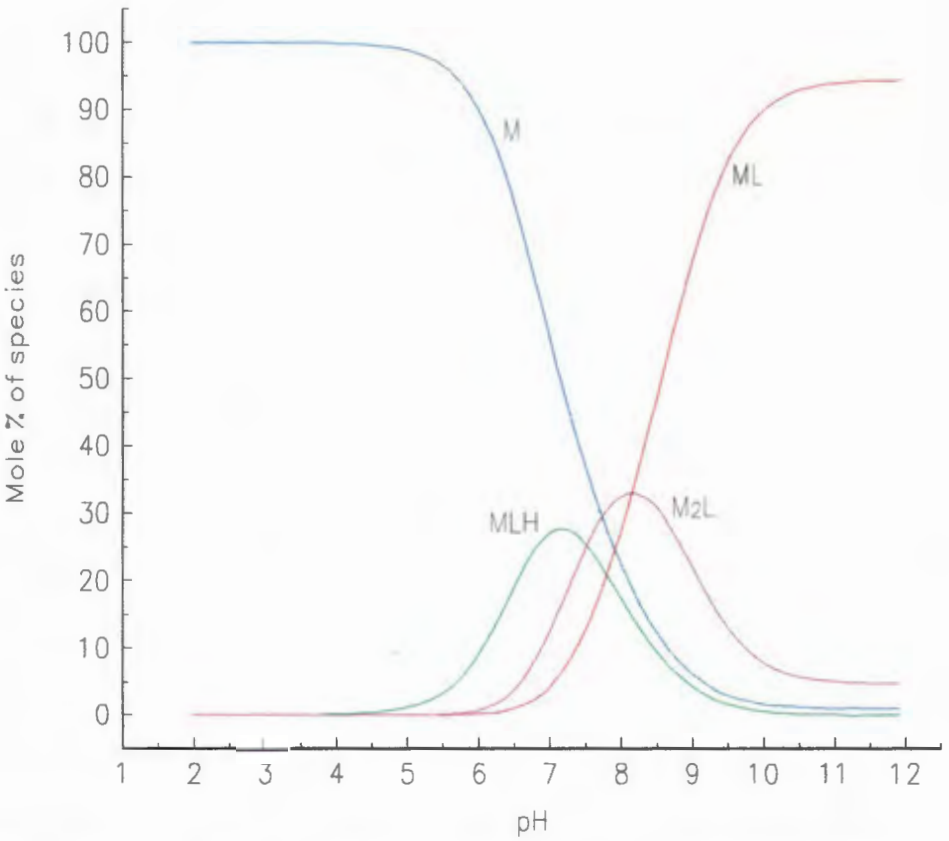

Figure 24. Species distrubution curves for the complexation of Ca(II) by MDP at 37 °C and in 0.15 mol.dm^{-3} as calculated from formation constants in Table 13. 0.00213 M MDP and 0.00077 M Ca(II).

Complexation of Mg(II) by MDP

Table 15 Formation constants for MDP and Mg(II)

Cation	Equilibrium	Log K	Data points	Hamilton R factor
Mg(II)	$M + L \rightleftharpoons ML$	5.68 ± 0.01	**91**	0.02009
	$ML + H \rightleftharpoons MLH$	7.56 ± 0.01		
	$2M + L \rightleftharpoons M_2L$	8.36 ± 0.08		
Mg(II)	$M + L \rightleftharpoons ML$	5.64 ± 0.01	**600**	0.01315
	$ML + H \rightleftharpoons MLH$	7.56 ± 0.03		
	$2M + L \rightleftharpoons M_2L$	8.46 ± 0.11		
Mg(II)	$M + L \rightleftharpoons ML$	5.71 ± 0.01	**91**	0.01971
	$ML + H \rightleftharpoons MLH$	7.57 ± 0.01		

Table 15 displays the values found for two models achieved from titration data for the complexation of Mg(II) by MDP. The best model is also displayed without excluding the data points at low and high pH values. No precipitation was observed but it was found that in this case the already good fit of the model to the data could be enhanced by excluding data points at pH levels where the glass electrode is more unstable. Only values between pH = 4 and 10 were taken. ESTA2A output is found in Appendix B4 and titration data points in Appendix C3.

In this case the first model is preferred to the second because of the lower standard deviations. The Hamilton R factor is lower for the latter. A better deprotonation ($\overline{Q}$) curve fit was also found. The calculated and experimental $\overline{Q}$ curves vs pH are displayed only for the first and third models in Figure 25 and 26. The curves match each other very well producing the best fit achieved so far. The cutting of the data helped to reduce the high standard deviation for the formation of M_2L in the second model. The third model is as good as the first. Only a slight difference in the two $\overline{Q}$ curves was observed. Very similar standard deviations and Hamilton factors were reported. The constants also are very similar, almost within the standard deviations. The same applies for the second model which has similar values.The first model (because it contains all the complexes and has the lowest standard deviations) is

therefore reported and used in the blood plasma model. The little difference in the models is explained by the species distrubution diagram, Fig.28. The calculated and experimental formation $\overline{Z}$ curves for the first model are displayed in Figure 27. The $\overline{Q}$ curves have the same shape as Ca(II) had with MDP, resulting in the same observations about the species dominating at various pH values.

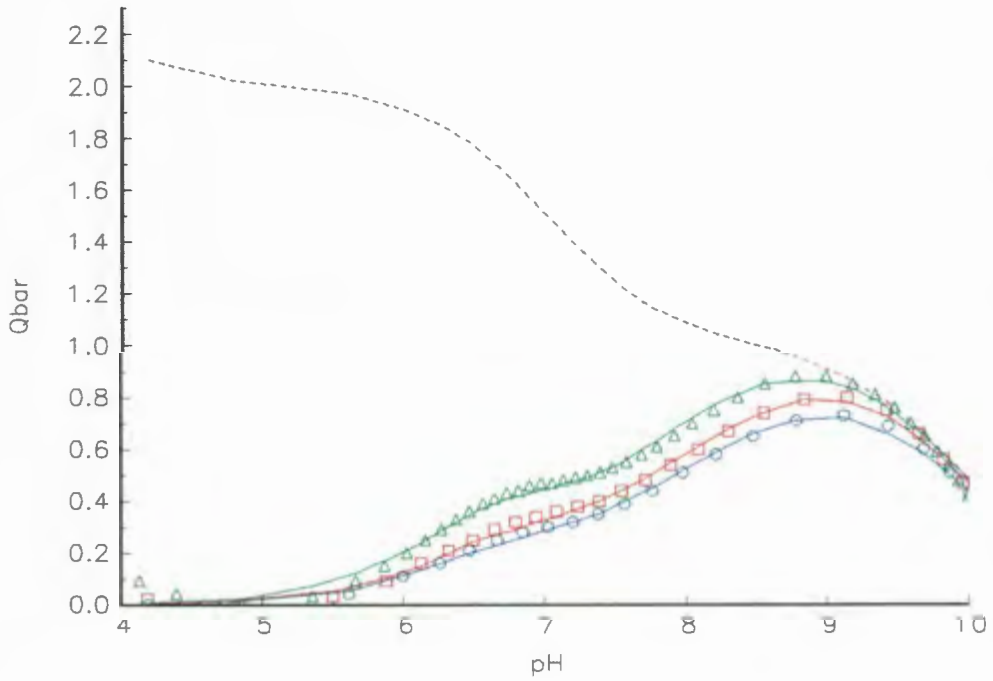

Figure 25. Experimental (points) and calculated (lines) deprotonation curves for Mg(II) complexation by MDP (for the first model). Qbar = $\overline{Q}$ and is the deprotonation function and the dashed line is the $\overline{n}$ curve. The three separate titrations were of L:M = 1:1 (○), L:M = 1.25:1 (□) and L:M = 2.5:1(△) .

Table 16. Reported formation constants for MDP and Mg(II)

	This work	Carroll *et. al.* [b] [88]	Dietche *et. al.* [85] [b] (For Cl_2MDP)
Log K_{ML}	5.68	5.78 (0.10)	4.75
Log $K_{MHL/M.HL}$	{3.27}	2.92 (0.05)	2.92
Log $K_{MLH/ML.H}$	7.56	{7.11}	{7.01}
Log $K_{M_2L/ML.M}$	2.68		

[b] 0.5 mol.dm^{-3} $(CH_3)_4N^+$, 25 °C; [c] 0.1 mol.dm^{-3} K^+, 25°C.The values in {} brackets are calculated from the original reported values to give a better comparison.

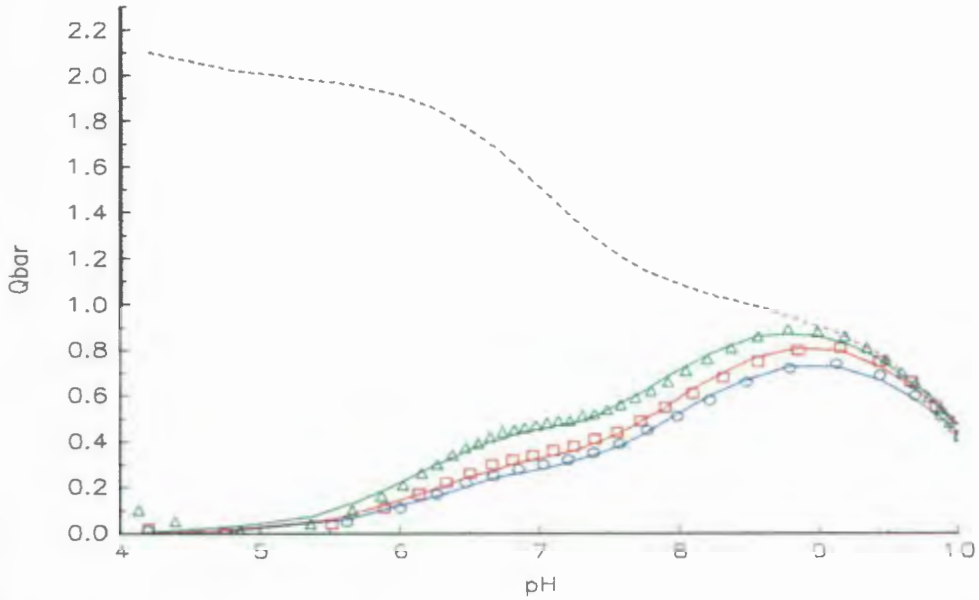

Figure 26. Experimental (points) and calculated (lines) deprotonation curves for Mg(II) complexation by MDP (for the third model). Qbar = $\overline{Q}$ and is the deprotonation function and the dashed line is the $\overline{n}$ curve. The three separate titrations are as shown in Fig. 25.

Once again the last column in Table 16 is added only as an indication because it describes constants for the ligand Cl_2MDP. The values reported here compare well with the literature if the different media in which experiments were done are taken into account. The values of Carroll *et. al.* [88] are slightly higher due to the 0.5 mol.dm^{-3} $(CH_3)_4N^+$ background electrolyte [86]. They did not included the constant M_2L which may cause the higher deviations. Only the second formation constant reported here seems to be a bit high. The values by Dietsche *et. al.* [81] are in KCl and therefore a big difference is not expected. Here Ca(II) and Mg(II) take the same model in contrast to APD. As proposed in Section 4.1.2 the formation of the M_2L complex is due to weaker complexation of the metal ion by the ligand. APD forms much stronger complexes than MDP, being just strong enough to form no M_2L in the case of MgAPD. MDP forms weaker complexes and M_2L appears in both cases. The same is true for HEDP although an extra species at high pH is formed viz. MLOH is formed for MgHEDP. The strength of complexation of MDP by Mg(II) is significantly higher than by Ca(II), agreeing with the Irving-Williams series [81].

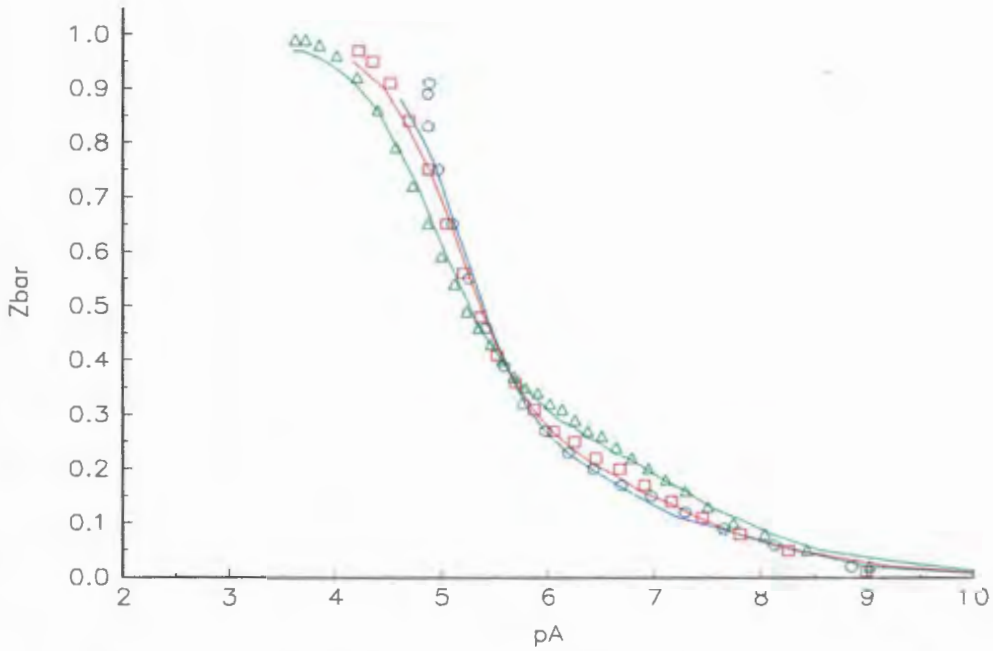

Figure 27. Experimental (points) and calculated (lines) formation curves for Mg(II) complexation by MDP. Zbar = $\overline{Z}$ and is the formation function and pA is the negative logarithm of the free ligand concentration. The three separate titrations were as for Figure 25.

The species distribution curves for the chosen model is displayed in Figure 28. An interesting aspect is how little of the species M_2L is formed. This explains why there is little difference between the fit for models which included or excluded it.

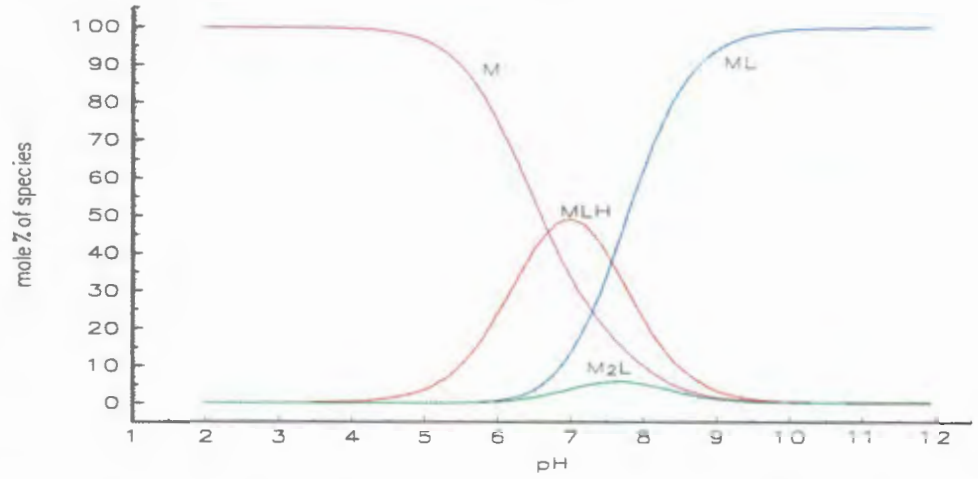

Figure 28. Species distrubution curves for the complexation of Mg(II) by MDP at 37 °C and in 0.15 mol.dm^{-3} as calculated from formation constants in Table 15. 0.00213 M MDP and 0.00086 M Mg(II).

Complexation of Zn(II) by MDP

Table 17 displays the values found for the model achieved from titration data for the complexation of Zn(II) by MDP. ESTA2A output in Appendix B4 and titration data points is found in Appendix C3. No suitable models were achieved. The main reason once again being the precipitate that forms between pH = 5 to 7.5. Cutting out this area of precipitation did not assist in achieving a plausible model.

Table 17. Formation constants for MDP and Zn(II)

Cation	Equilibrium	Log K	Data points	Hamilton R factor
Zn(II)	$M + L \rightleftharpoons ML$	8.19 ± 0.09	**575**	0.06438
	$ML + H \rightleftharpoons MLH$	7.35 ± 0.12		

No constants were found in the literature for the complexation of Zn(II) by MDP.
In this case the model produces no satisfactory fit to the titration data points at all. No calculated and experimental $\overline{Q}$ curves are displayed . Like in the complexation of Zn(II) by APD no improvement was made by excluding data. The pictures are the same (therefore not included). Polarography will be used to calculate the constants.

Complexation of Ni(II) by MDP

Another transition metal is Ni(II), close to Zn(II) which was studied to see whether it also forms precipitates with MDP as Zn(II) does. It does indeed form a precipitate as expected. Although the data points fit better into the model than with Zn(II). Table 18 displays the values found for the best model achieved from titration data for the complexation of Ni(II) by MDP. ESTA2A output is found in Appendix B4 and titration data points in Appendix C3.

Table 18. Formation constants for MDP and Ni(II)

Cation	Equilibrium	Log K	Data points	Hamilton R factor
Ni(II)	$M + L \rightleftharpoons ML$	7.27 ± 0.01	**103**	0.02970
	$2M + L \rightleftharpoons M_2L$	11.06 ± 0.03		
	$ML + OH \rightleftharpoons MLOH$	3.60 ± 0.03		

No constants were found in the literature for the complexation of Ni(II) by MDP.

Here two of the same species are reported as in the model for Ca(II) and Mg(II) with the addition of MLOH instead MLH_2 indicating a shift to a more basic system. From the calculated and experimental $\overline{Q}$ curves vs pH, Figure 29, it is evident that one of the species is MLOH. This can be deduced from the fact that the $\overline{n}$ curve crosses the $\overline{Q}$ curves indicating that the presence of more protons than can be supplied by the ligand. One proton is released on complexation while the ligand was already in the L form, forming an MLOH species. The same is true for Zn(II) where it looks as if MLOH could be included in the model although ESTA2A rejected it. This however might be because of the precipitation. The model for Ni(II) might be used as an indication for Zn(II) which has a worse fit with MDP than APD. The proton which is released by ML to form MLOH should be from the coordinated water seeing that no hydroxyl group is present in MDP. This is supported by the constants for MLOH viz. 3.60 and that for MOH (metal hydroxide), 3.7 which are similar. A full explanation of this phenomena is given in the next section (Section 3.1.4.) where the complexation of Mg(II) by HEDP is described.

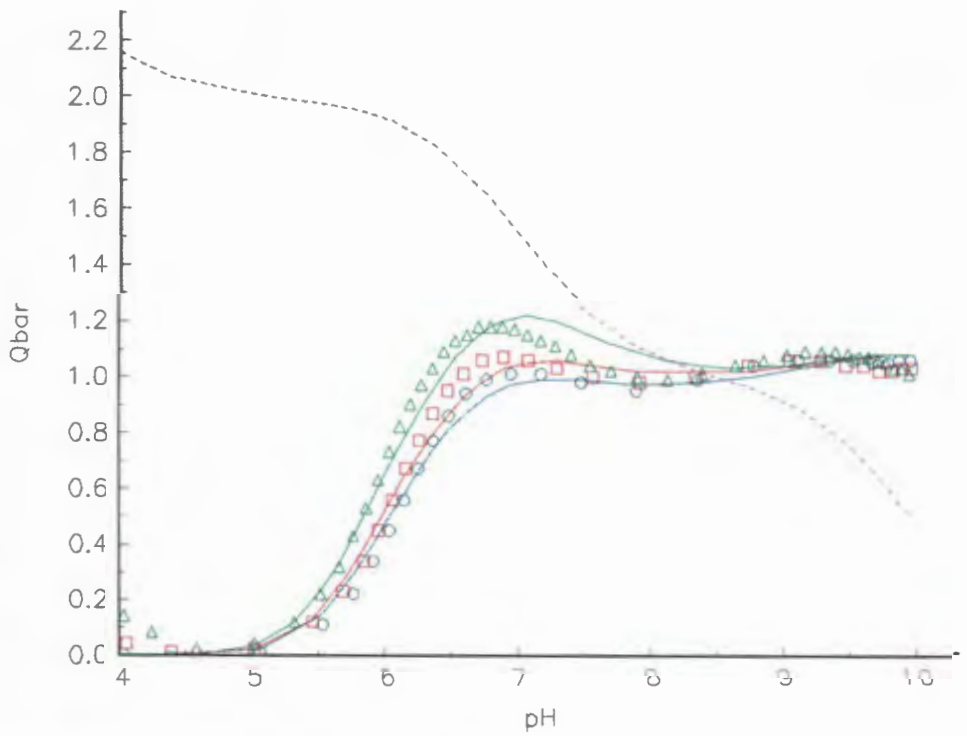

Figure 29. Experimental (points) and calculated (lines) deprotonation curves for Ni(II) complexation by MDP. Qbar = $\overline{Q}$ and is the deprotonation function and the dashed line is the $\overline{n}$ curve. The three separate titrations are as shown in Fig. 25.

Complexation of Sm(III) and Ho(III) by MDP

Table 19 displays the values found for the model achieved from titration data for the complexation of Sm(III) by MDP. ESTA2A output is found in Appendix B4 and titration data points in Appendix C3. No suitable models were achieved. The reason being the precipitate that forms belowl pH = 8.

As has been shown, precipitation causes problems which potentiometry is not able to overcome. The reason for the absence of any standard deviations lies in the fact that ESTA2A finds a correlation between the complexes. (See Appendix B4) These values are therefore only an indication. Here the first formation constant is much higher than that reported for APD with Sm(III).

Table 19 Formation constants for MDP and Sm(III)

Cation	Equilibrium	Log K	Data points	Hamilton R factor
Sm(III)	$M + L \rightleftharpoons ML$	14.71	**600**	0.02021
	$ML + H \rightleftharpoons MLH$	8.73		
	$MLH + H \rightleftharpoons MLH_2$	4.43		

ESTA2A was not able to find any model (how ever bad the fit might be) for titration data for the complexation of MDP by Ho(III). The main reason is again the precipitate that forms below pH = 8.

To find an estimate of the first formation constant the method of Hancock and Martell [93] was used once again. Figure 30 displays the relation of Log K_1(L) vs Log K_1(OH) for the metal ions Ca(II), Mg(II), Zn(II), Ni(II) and Sn(II) [84]; Log K_1(OH) form Martell [91]. The line represents the linear regression (r = 0.998) and the solid squares (■), the first formation constants for Sm(III) and Ho(III) from this regression. Here a value for Log K_1 = 9.3 is found for Sm(III) differing very much from the value reported above. For Ho(III) a first formation constant of 9.6 was found as displayed in Table 20. Table 20 also contains the estimated second formation constants for the complexation of Ho(III) and Sm(III) by MDP. It was estimated from the first formation constant in the following way. Log β_2 = Log K_{ML} + (Log K_{a1} - 1). The value for Log K_{MLH} is calculated from this value in the usual manner.

The values reported by Nash and Horwitz [82] for the complexation of Eu(III) by MDP were not used for either of the two formation constants. The values reported for Log K_1 = 4.04 and

Log K_{MLH} = 1.95. These values differ by more than five log units from what is reported here and cannot be explained in terms of different media used. The technique they used was solvent extraction. Assumptions in calculations made by these authors perhaps need to be tested. To support the higher values, Log K_1 = ±10, an analogue for MDP viz. hydrogen diphosphonate or pyrophosphoric acid is taken as an example. The values reported by Martell [91] for trivalent metal ions complex by pyrophophates are high viz. Log K_1 = 16.7 for La(III) etc.

Table 20. Estimated formation constants for MDP with Ho(III) and Sm(III)

Cation	Equilibrium	Log K
Ho(III)	M + L ⇌ ML	9.6
	ML + H ⇌ MLH	9.0
Sm(III)	M + L ⇌ ML	9.3
	ML + H ⇌ MLH	9.0

From this a higher formation constant for the complexation of MDP and HEDP by lanthanide ions than reported by Nash [82] is justified.

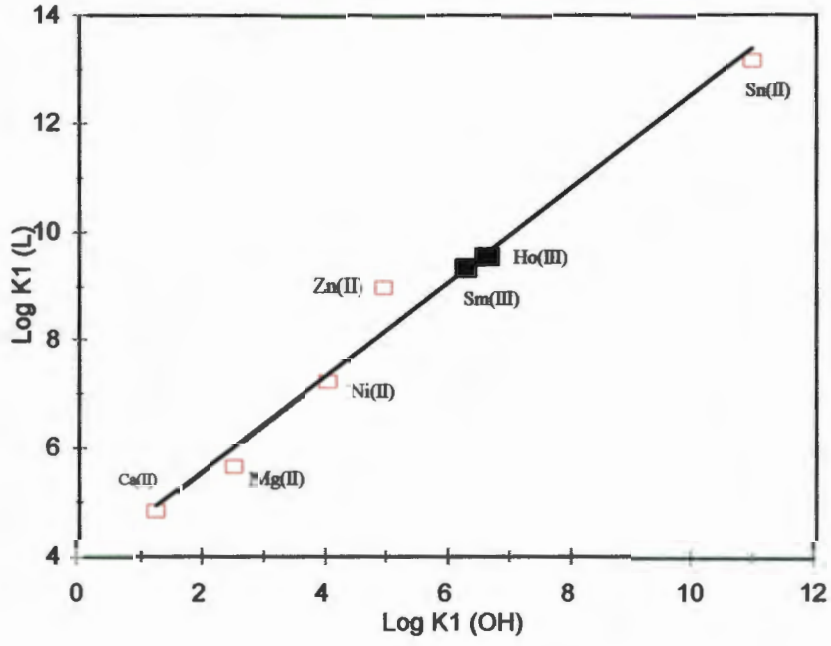

Figure 30. Relationship between stability of complexes of metal ions with MDP and the affinity of the metal ion for the hydroxide ion.

For MDP and ^{153}Sm(III), Simon *et. al.* [43] reported a high liver uptake. To get an idea of the species involved at pH = 7.4 a species distribution curve for MDP and Sm(III) has been drawn up from the values estimated in Table 20 which will be used to explain these results found in the literature [43] (Fig. 30a). This will be discussed in Section 4.4 on 'ECCLES models'.

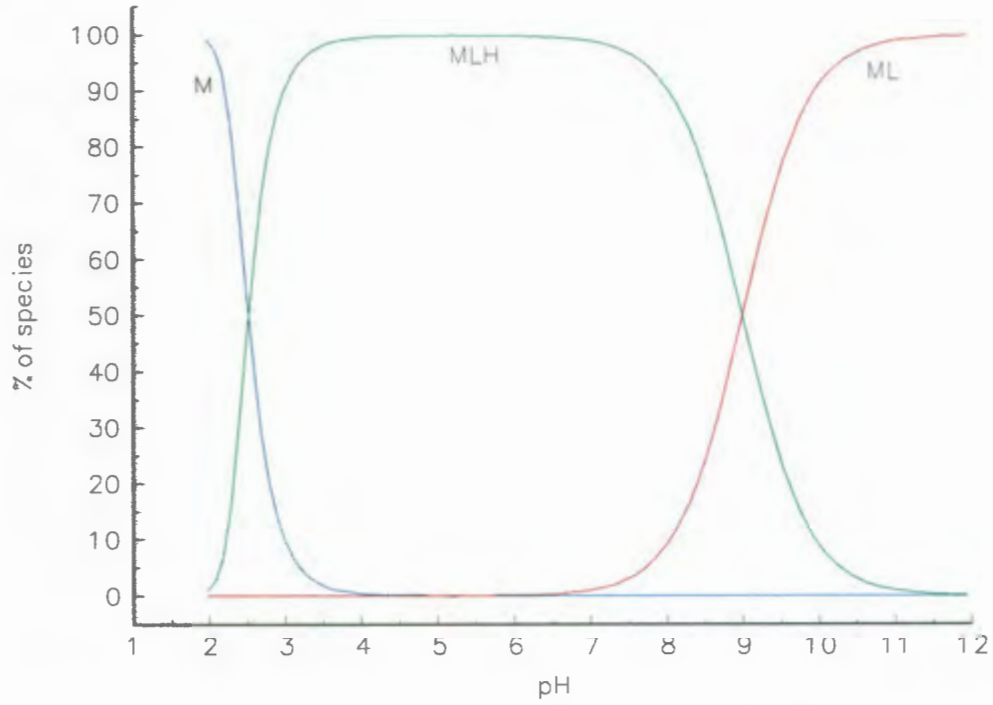

Figure 30a. Species distrubution curves for the complexation of Sm(III) by MDP at 37 °C and in 0.15 mol.dm^{-3} as calculated from formation constants in Table 20. 0.00213 M MDP and 0.00086 M Sm(III).

4.1.4. Potentiometric formation constants for HEDP

The next section reports formation constants calculated by potentiometric titrations for the ligand HEDP with various metal ions. Results will be presented tabularly. All data measured at 37 °C ±0.1°C and I = 0.15 mol.dm^{-3} NaCl. pK_w fixed at 13.42. Charges of metal ions, ligands and complexes have been omitted for simplicity.

Complexation of Ca(II) by HEDP

Table 21 contains the values calculated for the complexation of Ca(II) by HEDP. The output of the ESTA2A runs are included in Appendix B5 and potentiometric data points are in Appendix C4.

Table 21 Formation constants for HEDP and Ca(II)

Cation	Equilibrium	Log K	Data points	Hamilton R factor
Ca(II)	$M + L \rightleftharpoons ML$	5.34 ± 0.01	**88**	0.01957
	$ML + H \rightleftharpoons MLH$	7.83 ± 0.02		
	$ML + M \rightleftharpoons M_2L$	4.19 ± 0.02		

A large number of data points outside pH = 4 and 10 were cut out (as the pH electrode is less stable at very low and very high pH values) was done for the complexation of Mg(II) by MDP. The result is that a better fit is obtained as is displayed by the $\overline{Q}$ curves (Figure 31). From Figure 31 one can make the same observations as in previous cases about the species dominating and the justification of the absence of MLOH. Figure 32 contains $\overline{Z}$ curves. No 'backfanning' [90] (explained in the next section on HEDP and Mg(II)) is visible which would indicate MLOH or $ML(OH)_n$ species. In addition the $\overline{Q}$ curves do not cross the $\overline{n}$ curve. Constants available in the literature are shown in Table 22.

Table 22. Reported formation constants for HEDP and Ca(II)

	This work	Van Der Linde *et. al.* [a] [84]	Wada *et. al.* [a] [89]	Dietche *et. al.* [c] [85]	Carroll *et. al.* [b] [88]
Log K_{ML}	5.34	6.18 (0.03)	6.84	6.0	5.74 (0.10)
Log $K_{MHL/MLH}$	{3.14}	3.12 (0.06)	3.35	3.0	3.58 (0.14)
Log $K_{MLH/ML.H}$	7.83	{8.17}	{7.47}	{7.6}	{7.85}
Log $K_{M_2L/ML.M}$	4.19	4.63 (0.06)	5.36		

[a] 0.1 mol.dm^{-3} $(CH_3)_4N^+$, 25 °C; [b] 0.5 mol.dm^{-3} $(CH_3)_4N^+$, 25 °C; [c] 0.1 mol.dm^{-3} K^+, 25 °C.
The values in {} brackets are calculated from the original reported values to give a better comparison.

The values reported here compare well with the literature if the media in which experiments were done are taken into account.

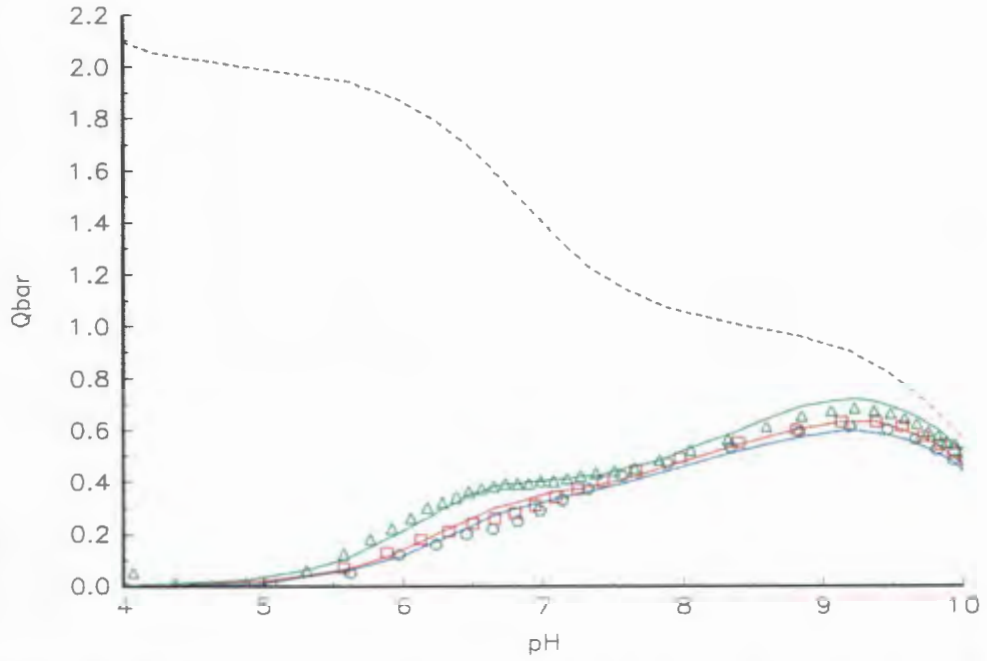

Figure 31. Experimental (points) and calculated (lines) deprotonation curves for Ca(II) complexation by HEDP. Qbar = $\overline{Q}$ and is the deprotonation function and the dashed line is the $\overline{n}$ curve. The three separate titrations were of L:M = 1:1 (O), L:M = 1.25:1 (□) and L:M = 2.5:1(△) .

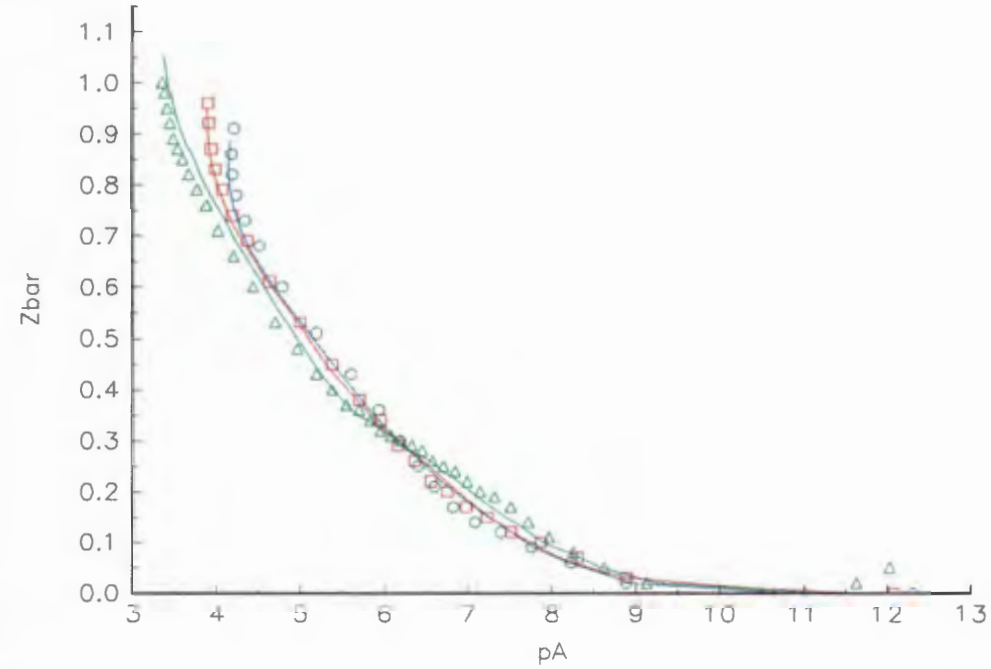

Figure 32. Experimental (points) and calculated (lines) formation curves for Ca(II) complexation by HEDP. Zbar = $\overline{Z}$ and is the formation function and pA is the negative logarithm of the free ligand concentration. The three separate titrations were as for Figure 31.

The values of Van der Linde *et. al.* [84] are once again higher due to the 0.1 mol.dm^{-3} $(CH_3)_4N^+$ background electrolyte [86]. For the same electrolyte Wada *et. al.* [89] report even higher values. It has to be said that these constants were published in 1972 and calculated not at various ligand to metal (L:M) ratios, like in this work, but at specific ratios different values were reported. The values tabled for Wada *et. al.* are for the ratio 2:1. If the ratio is lowered to 1:1 the value for Log K_1 for instance changes from 6.84 to 6.40 [89], comparing much better with the value 6.18, reported by Van der Linde [84]. Both included the constant M_2L which has a value close to the one reported here with the expected rise due to the background electrolyte. The reported standard deviations are higher than in this work indicating a better fit of the model to the data here. De Stefano *et. al.* [86] also pointed out that a higher ionic strength electrolyte will result in lower formation constants. This is derived from the Debye-Hückel type equation where $\log \beta \propto \log^T\beta - I^{1/2}$. This would explain the lower values by Carroll *et. al.* [88] and the even lower for those of Van der Linde and Wada. These values are higher than in this work, because of the $(CH_3)_4N^+$ background electrolyte [86]. Here the standard deviations are even bigger, probably because of the exclusion of M_2L. The values by Dietsche *et. al.* [81] were recorded in KCl which should, according to De Stefano *et. al.* [86], have give slightly higher values than in NaCl medium.

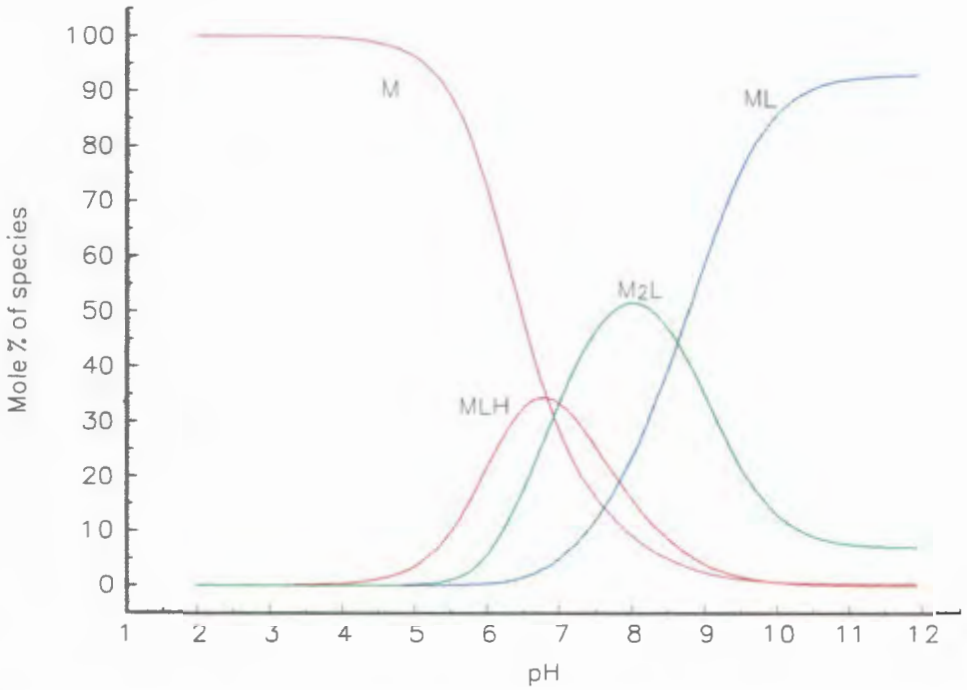

Figure 33. Species distrubution curves for the complexation of Ca(II)) by HEDP at 37 °C and in 0.15 mol.dm^{-3} as calculated from formation constants in Table 21. 0.00213 M HEDP and 0.00077 M Ca(II).

The species distrubution curves for the chosen model are now displayed in Figure 33. From this it can be seen that the complexes attain maximum concentration at the pH values predicted by the deprotonation curves. There is no single dominant species between pH = 5.5 and 9.5 visible from this graph.

Complexation of Mg(II) by HEDP

Table 23 displays the best model achieved from titration data for the complexation of Mg(II) by HEDP. Only the best model is displayed here. Only data points between pH = 4 and 10 were taken. ESTA2A output is found in Appendix B5 and titration data points in Appendix C4.

Table 23 Formation constants for HEDP and Mg(II)

Cation	Equilibrium	Log K	Data points	Hamilton R factor
Mg(II)	$M + L \rightleftharpoons ML$	6.03 ± 0.01	**96**	0.03054
	$ML + H \rightleftharpoons MLH$	7.48 ± 0.03		
	$ML + M \rightleftharpoons M_2L$	3.67 ± 0.04		
	$ML + OH \rightleftharpoons MLOH$	3.24 ± 0.03		

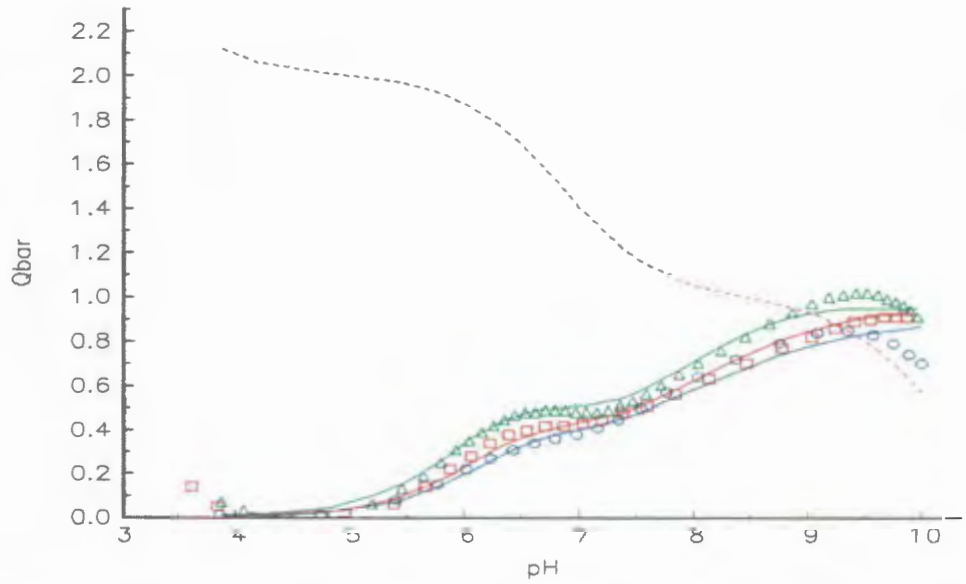

Figure 34. Experimental (points) and calculated (lines) deprotonation curves for Mg(II) complexation by HEDP. Qbar = $\overline{Q}$ and is the deprotonation function and the dashed line is the $\overline{n}$ curve. The three separate titrations were of L:M = 1:1 (○), L:M = 1.25:1 (□) and L:M = 2.5:1(△) .

The Hamilton factor might seem to be relatively high, if compared with previous reported values, but this is mainly due to the fewer data points used to fit the model. The standard deviations are low and the calculated and experimental $\overline{Q}$ curves (Figure 34) follow each other satisfactorily. The calculated and experimental formation ($\overline{Z}$) curves for the model are displayed in Figure 35. From Figure 34 one can make the same observations as in previous cases about the species dominating at various pH values.

There is a difference however at high pH where $\overline{Q}$ curves cross the $\overline{n}$ curve. This is the reason why MLOH was included in the model. Figure 35 also shows some backfanning indicating MLOH or $ML(OH)_n$ species. The term 'backfanning' was used *int. al.* by Jarvis *et. al.* [90] to explain the observation on $\overline{Z}$ graphs that the curves turn back at low pA (negative logarithm of the free ligand concentration) indicating that hydrolysis becomes important as the titration proceeds.

The question remains whether or not the hydroxyl group loses its proton to form MLH_{-1} or if the proton is released from a coordinated water molecule (MLOH). The equilibrium for the formation of MLOH can be written as: $ML + OH \rightleftharpoons ML(OH)$ (where $\text{Log } K = \text{Log } \beta_{MLOH} - \text{Log } \beta_{ML}$)

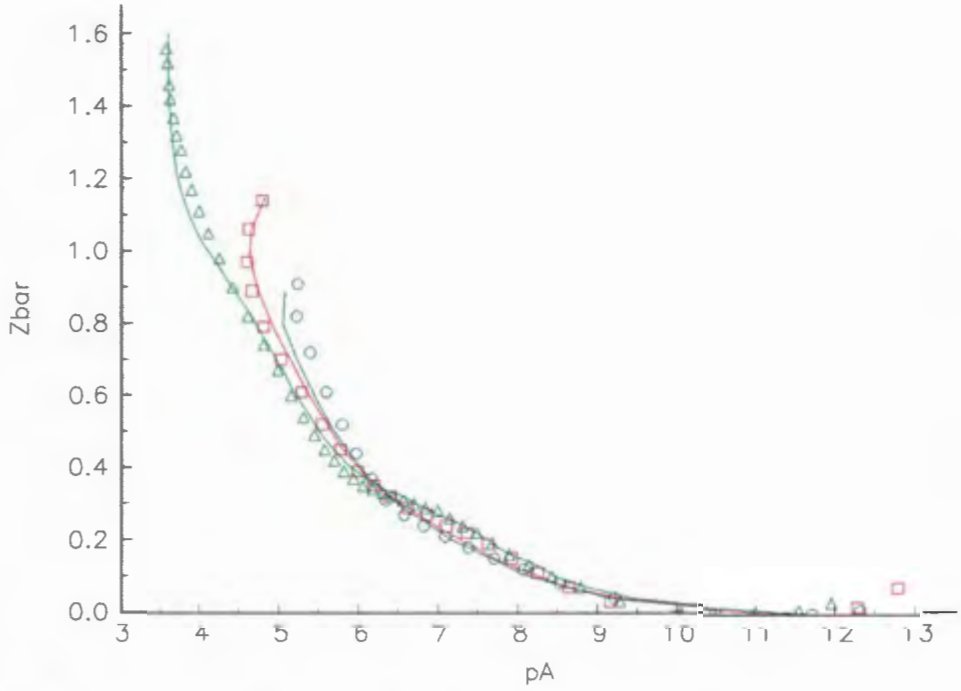

Figure 35. Experimental (points) and calculated (lines) formation curves for Mg(II) complexation by HEDP. Zbar = $\overline{Z}$ and is the formation function and pA is the negative logarithm of the free ligand concentration. The three separate titrations were as for Figure 34.

The value found for Log K = 3.24. If the proton was lost from a coordinated water molecule, we would not expect a value for the equilibrium constant very different from that of magnesium(II)hydroxide [64]. The literature [91] gives Log K = 2.58 for the equilibrium: M + OH ⇌ M(OH). Thus, the proton is released by the hydroxyl group. It would be impossible for the constant of the complex to be higher than that of the metal hydroxide if the proton were to be released by coordinated water.

Table 24. Reported formation constants for HEDP and Mg(II)

	This work	Carroll *et. al.* [b] [88]	Dietche *et. al.* [c] [85]	Wada *et. al.* [a] [89]
Log K_{ML}	6.03	6.39 (0.16)	6.17 (0.02)	7.30
Log $K_{MHL:M.HL}$	{3.40}	3.32 (0.06)	3.03 (0.02)	3.80
Log $K_{MLH:ML.H}$	7.48	{7.04}	{7.46}	{7.46}
Log $K_{MLOH:ML.OH}$	3.24			
Log $K_{M_2L:ML.M}$	3.67			3.7

[a] 0.1 mol.dm^{-3} $(CH_3)_4N^+$, 25 °C; [b] 0.5 mol.dm^{-3} $(CH_3)_4N^+$, 25 °C; [c] 0.1 mol.dm^{-3} K^+, 25°C. The values in {} brackets are calculated from the original reported values to give a better comparison.

The values by Wada *et. al.* [89] are expected to be the highest (0.1 mol.dm^{-3} $(CH_3)_4N^+$), Carroll *et. al.* [88] slightly lower due to higher ionic strength, 0.5 mol.dm^{-3}, and this work close to Dietsche *et. al.* [81] (0.1 mol.dm^{-3} KCl) [86]. Most did not include the constant M_2L which may cause the higher standard deviations. The MLOH complex also seemed to be neglegted in the literature so far. The strength of complexation for Mg(II) is significantly higher than for Ca(II) as in the case of MDP agreeing with the Irving-Williams series [81].

The species distrubution curves for the chosen model is displayed in Figure 36. From this the various complexes can be seen at the pH values predicted by the deprotonation curves. At high pH, MLOH becomes the predominant species.

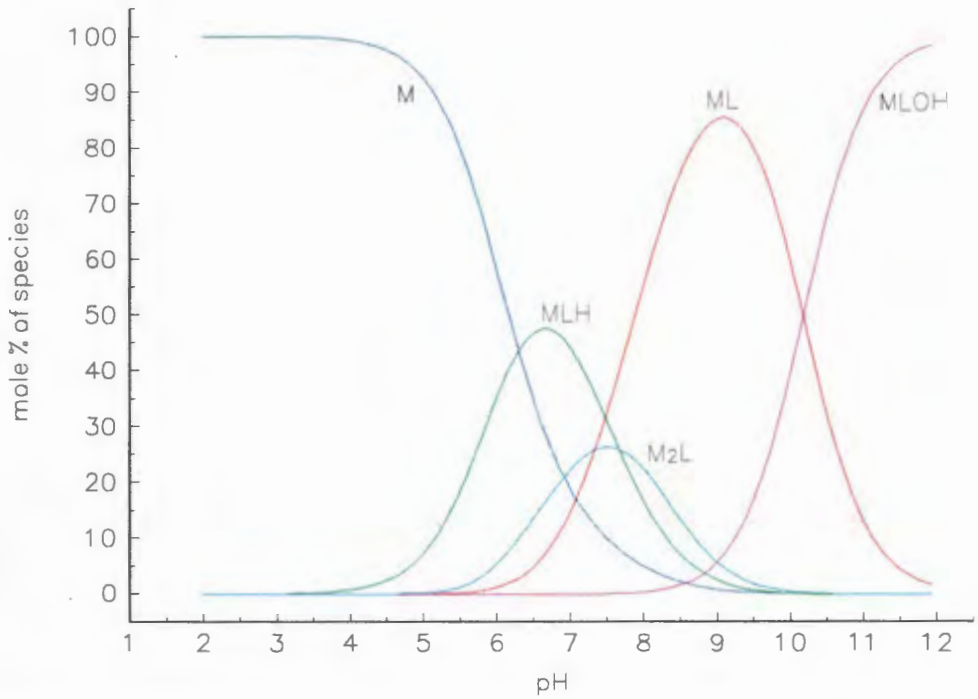

Figure 36. Species distrubution curves for the complexation of Mg(II)) by HEDP at 37 °C and in 0.15 mol.dm^{-3} as calculated from formation constants in Table 23. 0.00213 M HEDP and 0.00086 M Ca(II).

Complexation of Zn(II) by HEDP

Table 25 displays the values found for the model achieved from titration data for the complexation of Zn(II) by HEDP. ESTA2A output is found in Appendix B5 and titration data points in Appendix C4. No suitable models were achieved. The main reason once again being the precipitate that forms between pH = 5 to 7.5. Cutting out this area of precipitation was not helpfull in modelling.

Table 25 Formation constants for HEDP and Zn(II)

Cation	Equilibrium	Log K	Data points	Hamilton R factor
Zn(II)	$M + L \rightleftharpoons ML$	8.85 ± 0.02	**600**	0.02359
	$ML + M \rightleftharpoons M_2L$	4.72 ± 0.04		
	$ML + OH \rightleftharpoons MLOH$	4.38 ± 0.04		

Constants in literature for Zn(II) with HEDP were only reported by Dietsch *et.al.* [81] and will be discussed together with polarographic data. (For the first complexation constant they report Log K_1 = 8.19, comparing with the value reported here.)

The calculated and experimental $\overline{Q}$ curves are displayed in Figure 36a. This was the main reason to doubt the plausibility of the model. The Hamilton factor and standard deviations are reasonable. MLOH was included because of backfanning in the $\overline{Z}$ curve and crossing of the $\overline{n}$ curve by the $\overline{Q}$ curves. Polarography will be used to accurately calculate the constants.

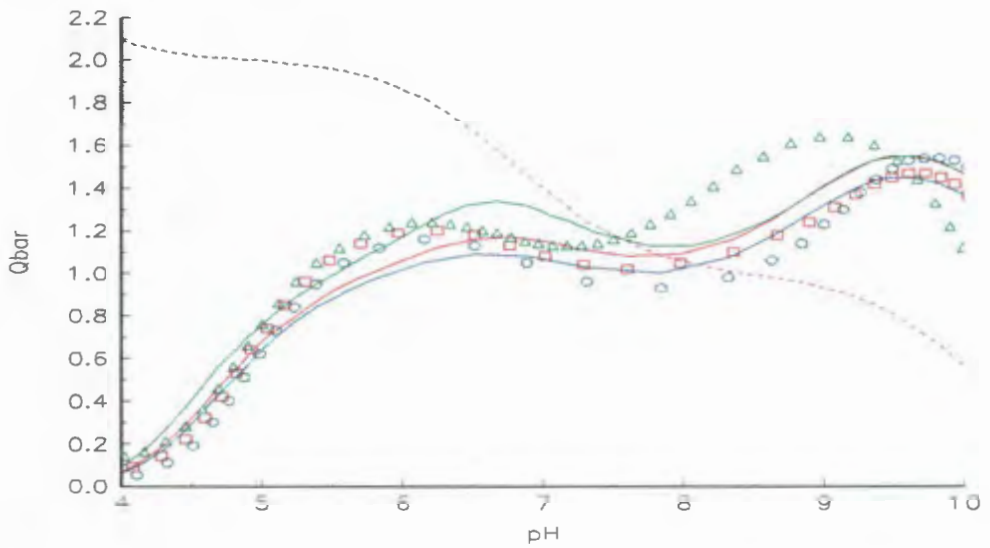

Figure 36a. Experimental (points) and calculated (lines) deprotonation curves for Zn(II) complexation by HEDP. Qbar = $\overline{Q}$ and is the deprotonation function and the dashed line is the $\overline{n}$ curve. The three separate titrations were of L:M = 1:1 (○), L:M = 1.25:1 (□) and L:M = 2.5:1(△) .

Complexation of Cd(II) by HEDP

Because of the use of polarography as a tool to derive complexation constants, a system had to be found to compare it with potentiometry. Such a system should include a polarographically active metal ion and one which forms no precipitates with the ligand at potentiometric ratios and concentrations. Such a system was found to be Cd(II) with HEDP. Table 26 displays the values found for the best model achieved from titration data for the complexation of Cd(II) by HEDP using all the 600 data points aquired with the normal L:M ratios used. ESTA2A output is found in Appendix B5 and titration data points in Appendix C4.

Table 26 Formation constants for HEDP and Cd(II)

Cation	Equilibrium	Log K	Data points	Hamilton R factor
Cd(II)	$M + L \rightleftharpoons ML$	7.39 ± 0.03	**600**	0.01333
	$ML + H \rightleftharpoons MLH$	7.31 ± 0.06		
	$MLH + H \rightleftharpoons MLH_2$	5.75 ± 0.06		
	$ML + M \rightleftharpoons M_2L$	5.77 ± 0.06		
	$ML + OH \rightleftharpoons MLOH$	3.14 ± 0.04		

No constants were found in the literature for the complexation of Cd(II) by HEDP.
The fit of the data to the model is not totally satisfactory but because of a good Hamilton factor and standard deviations and a reasonable agreement between calculated vs experimental $\overline{Q}$ curves (Figure 37) the model is acceptable. From this graph the species MLOH is very evident (the crossing of the curves). From the calculated vs experimental $\overline{Q}$ curves it seems that a complex is missing from the model to fit the calculated curve better to the data. From results with polarography at a ratio 30:1 this complex proved to be ML_2. From speciation calculations it was evident that only at a ratio higher than ratio 3:1 this species becomes predominant. Potentiometric titrations at this ratio was used to calculated this complexation constant. Table 27 presents results from this experiment.

Table 27 Formation constants for HEDP and Cd(II) ratio 3:1.

Cation	Equilibrium	Log K	Data points	Hamilton R factor
Cd(II)	$M + L \rightleftharpoons ML$	6.93 ± 0.04	**76**	0.020
	$ML + L \rightleftharpoons ML_2$	3.29 ± 0.07		
	$ML + 2H \rightleftharpoons MLH_2$	12.93 ± 0.05		
	$ML + M \rightleftharpoons M_2L$	6.06 ± 0.05		

Figure 38 displays calculated vs experimental $\overline{Z}$ curves and figure 39 the corresponding $\overline{Z}_H$ curves. From this it is evident that a plausible fit of data to the model has been achieved.

Table 28 displays the new values found for this model applied to the titration data for the L:M ratios normally used. The value for ML_2 found in Table 27 was kept fixed during the ESTA iterations, but although it is a minor species at this ratio, it still influences the other species

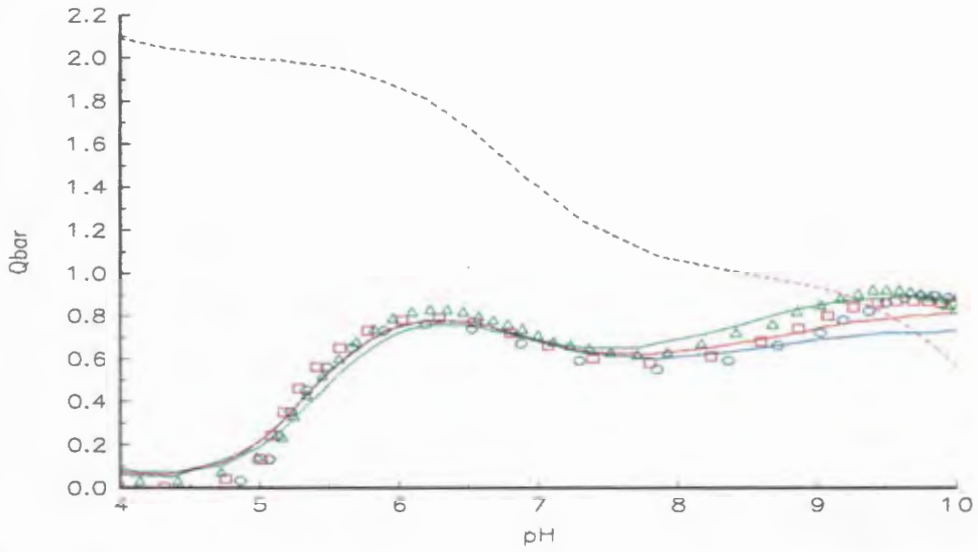

Figure 37. Experimental (points) and calculated (lines) deprotonation curves for Cd(II) complexation by HEDP. Qbar = $\overline{Q}$ and is the deprotonation function and the dashed line is the $\overline{n}$ curve. The three separate titrations were of L:M = 1:1 (○), L:M = 1.25:1 (□) and L:M = 2.5:1(△) .

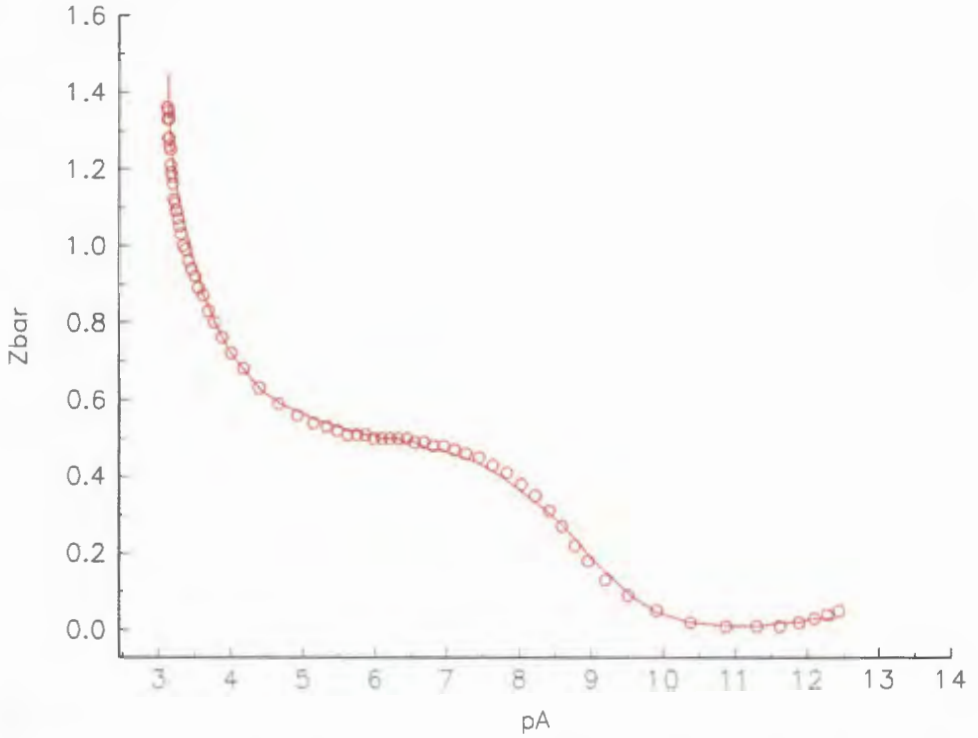

Figure 38. Experimental (points) and calculated (lines) formation curves for Cd(II) complexation by HEDP (For the ratio of L:M = 3:1). Zbar = $\overline{Z}$ and is the formation function and pA is the negative logarithm of the free ligand concentration.

formed in the same pH region. It therefore improves the $\overline{Z}$ fit dramatically. Data points corresponding to low and high pH values were cut to improve the fit even further. Interestingly enough the ML_2 species is prominent only at a ratio higher than 3:1. This explains why in the normal potentiometric ratios one could not find the species absent causing a slighty worse $\overline{Z}$ fit.

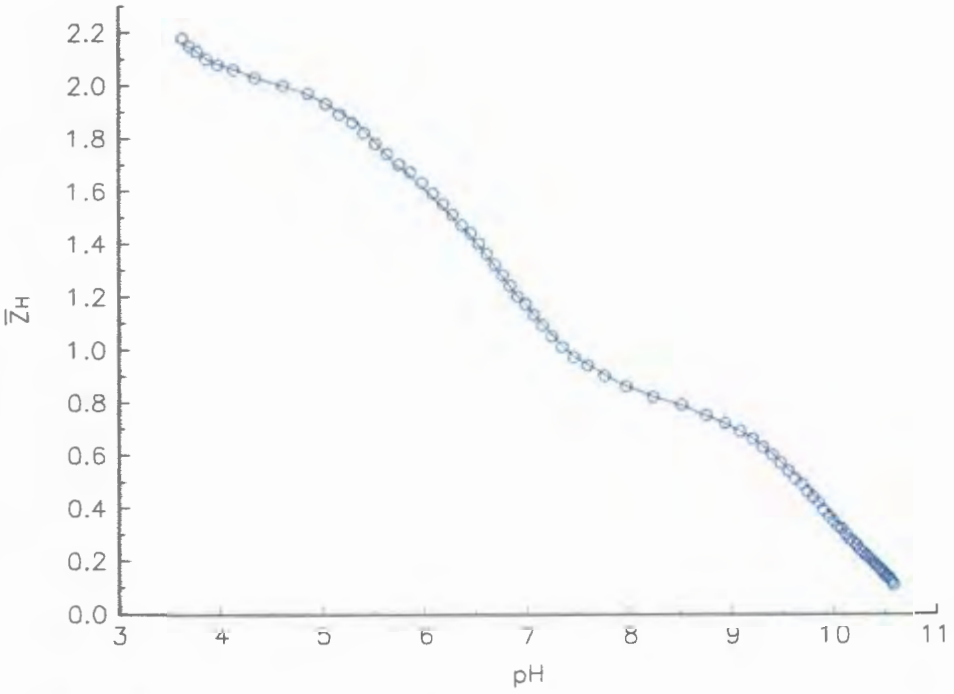

Figure 39. Experimental (points) and calculated (lines) protonation formation curves for Cd(II) complexation by HEDP (ratio 3:1). $\overline{Z}_H$ is the protonation formation function.

Table 28 New set of formation constants for HEDP and Cd(II)

Cation	Equilibrium	Log K	Data points	Hamilton R factor
Cd(II)	$M + L \rightleftharpoons ML$	7.10 ± 0.04	**165**	0.01566
	$ML + L \rightleftharpoons ML_2$	3.36 ± 0.06		
	$ML + 2H \rightleftharpoons MLH_2$	12.92 ± 0.06		
	$ML + M \rightleftharpoons M_2L$	5.89 ± 0.05		
	$ML + OH \rightleftharpoons MLOH$	3.86 ± 0.05		

Figure 39 shows the $\overline{Z}_H$ curves for this improved model and proves that it is plausible.

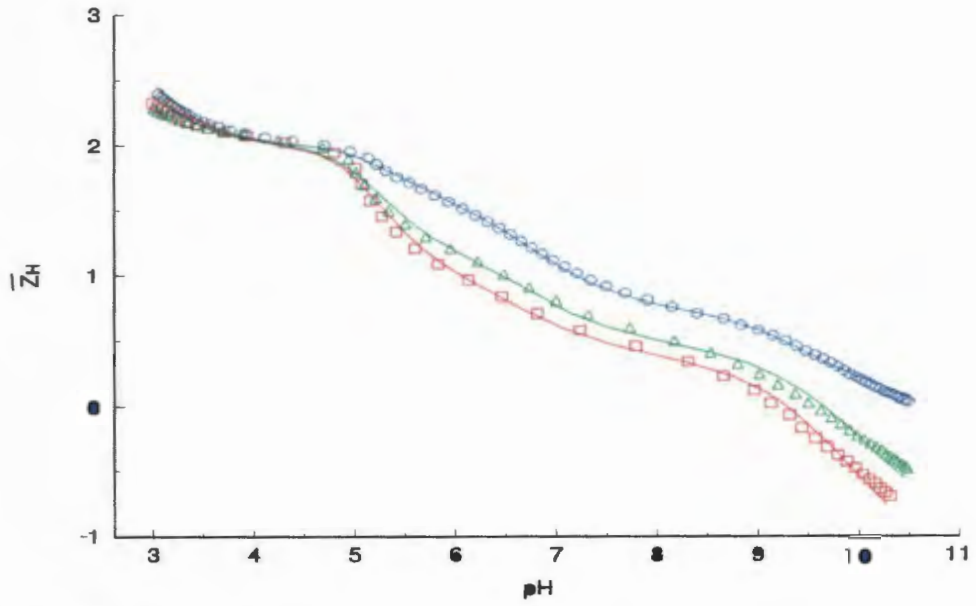

Figure 39. Experimental (points) and calculated (lines) protonation formation curves for Cd(II) complexation by HEDP. $\overline{Z}_H$ is the protonation formation function. The three curves are as shown in Fig. 37 and cover the normal potentiometric L:M ratios used.

For HEDP and Cd(II) the proton is released by coordinated water and not the hydroxyl group. The constant for ML(OH) is 3.14 but for M(OH) it is 3.9 [91]. The values are similar and the value for ML(OH) is smaller than for the metal hydoxide, making it possible that the proton is released from coordinated water.

The species distrubution curves for the chosen model is displayed in Figure 40. At high pH, MLOH becomes the predominant species. These graphs were calculated for a L:M ratio of 4:1. Fig. 40a displays the species distubution curves at a ratio 1:1 which illustrates how the species ML_2 changes from a predominant species (Fig. 40) to a insignificant one in Fig. 40a.

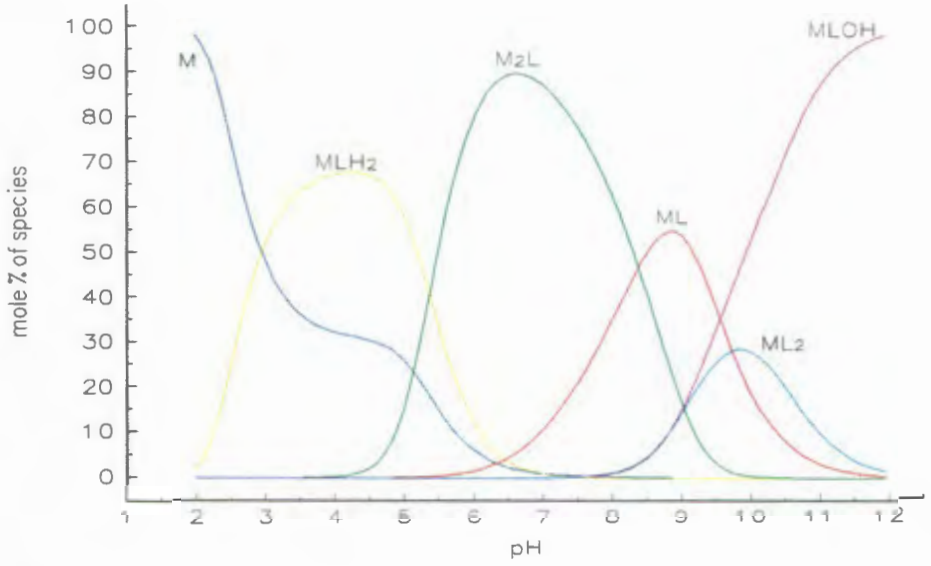

Figure 40. Species distrubution curves for the complexation of Cd(II) by HEDP at 37 °C and in 0.15 mol.dm^{-3} as calculated from formation constants in Table 28. L:M ratio = 3:1. Note the ML_2 species.

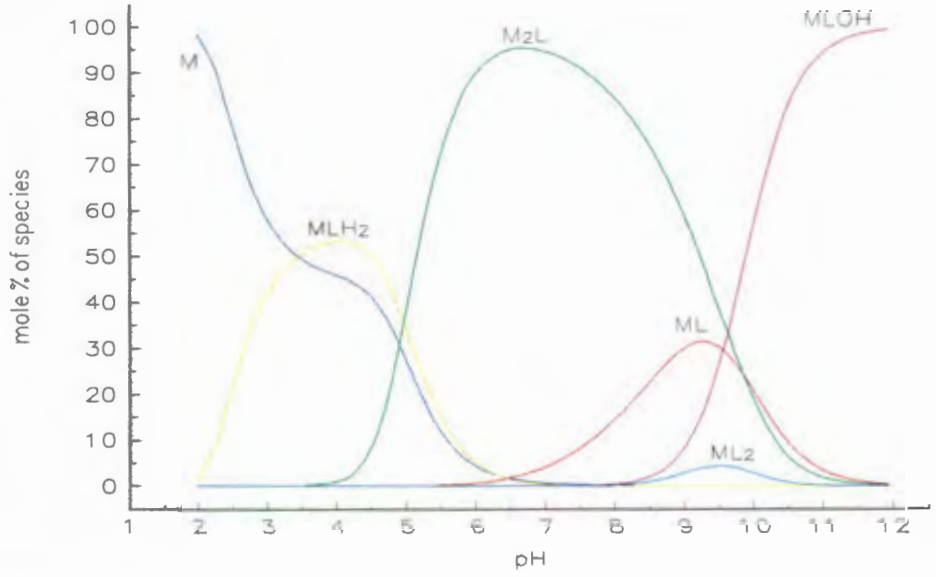

Figure 41. Species distrubution curves for the complexation of Cd(II) by HEDP at 37 °C and in 0.15 mol.dm^{-3} as calculated from formation constants in Table 28. L:M ratio = 1:1. Note the almost absence ML_2 species.

Complexation of Ho(III) and Sm(III) by HEDP

ESTA2A was not able to find any model (however bad the fit might be) for titration data for

the complexation of Ho(III) or Sm(III) by HEDP. The main reason is again the precipitation that forms below pH = 8.

To find an estimate of the first formation constant the approach of Hancock and Martell [93] was used once again. Figure 41 displays the relation of Log K_1(L) vs Log $K_1(OH^-)$ for the metal ions Ca(II), Mg(II), Zn(II), Cd(II) , Sr(II) and Cu(II) [80] and Sn(II) [84]; Log $K_1(OH^-)$ from Martell [91]. The line represents the best line (r = 0.994) and the solid squares (■), the first formation constants for Sm(III) and Ho(III) from this regression. The value of log K_1 for Sm(III) is 10.11 and 10.4 for Ho(III). Table 29 contains the estimated constants for the complexation of Ho(III) and Sm(III) by HEDP. The second formation constant was calculated from the first constant in the same manner as explained earlier. From this a species distribution curve can be obtained which can be used to explain results found in the literature for the absorption of the radiopharmaceutical ^{153}SmHEDP in the liver [43] (Figure 42).

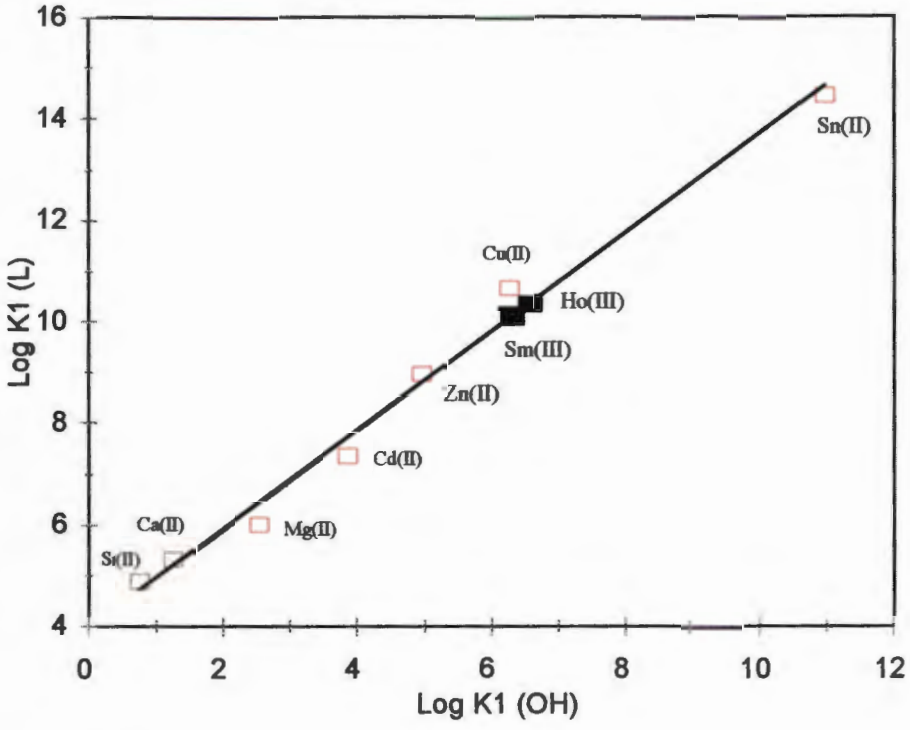

Figure 41. Relationship between stability of complexes of metal ions with HEDP and the affinity of the metal ion for the hydroxide ion.

Table 29 Estimated formation constants for HEDP and Ho(III) and Sm(III)

Cation	Equilibrium	Log K
Ho(III)	$M + L \rightleftharpoons ML$	10.4
	$ML + H \rightleftharpoons MLH$	9.1
	$M + L \rightleftharpoons ML$	10.1
	$ML + H \rightleftharpoons MLH$	9.1

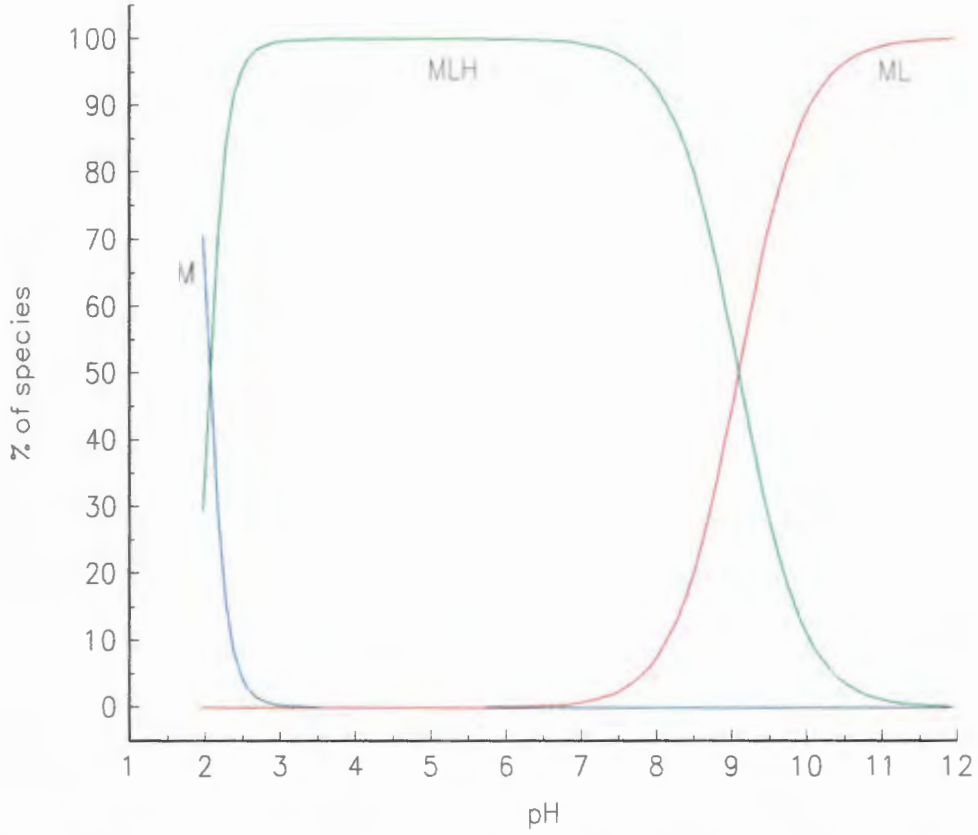

Figure 42. Species distrubution curves for the complexation of Sm(III) by HEDP at 37 °C and in 0.15 mol.dm^{-3} as calculated from formation constants in Table 28. HEDP = 0.00213 M and Sm(III) = 0.00086 M.

4.2 Polarographic results

Polarography was used for metal ions where precipitation occurred with the ligands, as described in Section 4.1 on potentiometric titrations. Ligand to metal ratios used were in the order of 1:1 and metal ions like Zn(II) formed precipitates with the ligands at these ratios and ligand concentrations. To confirm that formation constants derived from these two techniques are comparable, a system in which no precipitation at potentiometric ratios and a metal ion which is polarographically active is needed.

4.2.1 Polarographic results for the complexation of Cd(II) by HEDP

Such a system was found to be Cd(II) and HEDP. Experiments with different L:M ratios were carried out. Results from the experiment at ratio 27:1 will be presented here.

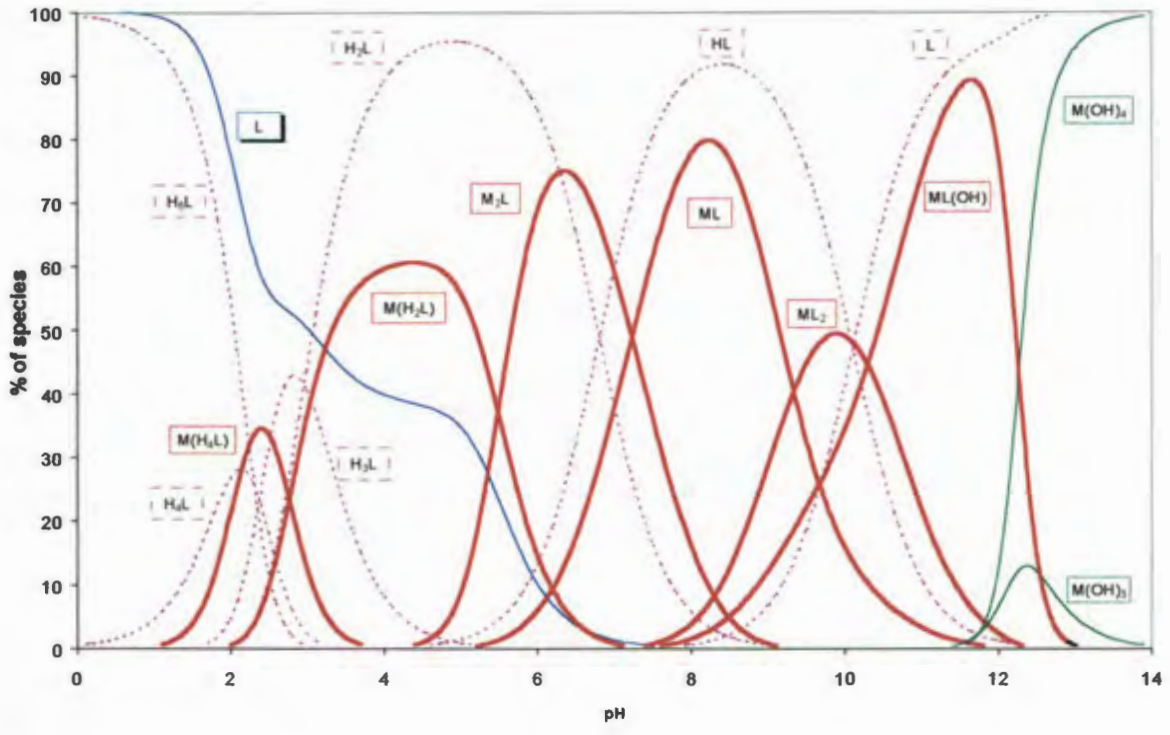

Figure 42. The species distribution diagram as a function of pH calculated from polarographic results. L:M ratio taken as 27:1 at 37°C and 0.15M NaCl background solution. (—) Represents fractions of cadmium complexes, (···) fractions of the total ligand and (—) represents the fractions of cadmium complexes with OH^-.

Fig. 42 represents the species distribution diagram for a ratio of 27:1. This will be used to discuss various tendencies further on.

In Fig. 43 the shift in the peak potential vs pH is shown. The regions where various protonated forms of the ligand HEDP predominate are marked in Fig. 43 to facilitate the discussion of the results that follow. It has been demonstrated [38] that when one metal species is predominant in the pH range where one form of ligand also predominates, then the slope of about 61 / n mV (at 37°C) per proton involved in the electrochemical reaction should be observed (n = number of electrons involved in electrochemical reaction). This value should be expressed per metal ion. In region II , between pH 5 and 6.8, a slope of 25 mV per pH unit is observed. It indicates the

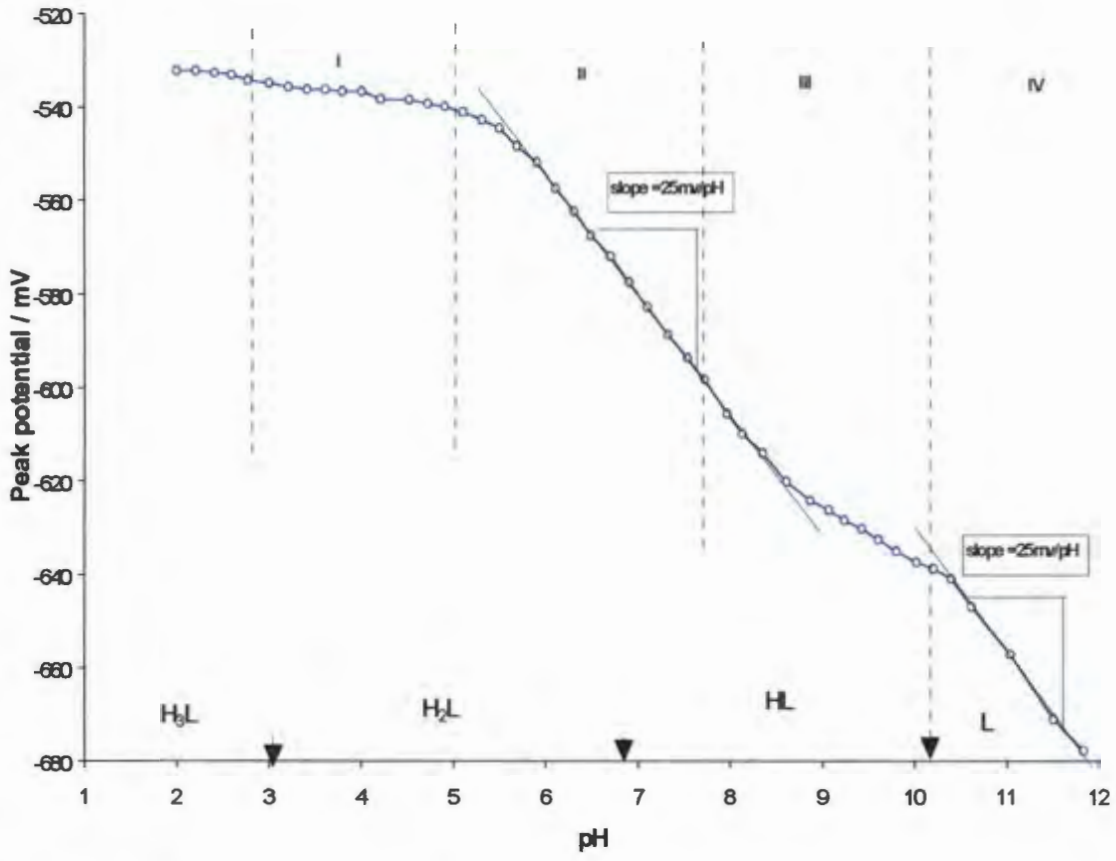

Figure 43. Shift in DP peak potential of cadmium complexes as a function of pH at 37°C and 0.15M ionic strength. All polarograms were recorded in one solution; adjusted to a particular pH given by data points indicated by (○). Dotted vertical lines indicate regions of interest.

presence of the polynuclear species M_2L which undergoes the following reaction

$$M_2L + 2H^+ + 2e^- \rightleftharpoons 2M(Hg) + H_2L \qquad \text{(Charges have been omitted for simplicity)}$$

in which two protons are involved to form the H_2L form of the ligand L. Per metal ion (and n =2) one would expect 30 mV for the two protons involved.

The species M_2L continues to dominate in region III although the predominant ligand form changes to HL at pH = 6.8. The slope would be expected to decrease (to 15 mV per pH unit) due to less protons formed in the electrochemical reaction.

$$M_2L + H^+ + 2e^- \rightleftharpoons 2M(Hg) + HL$$

However ML according to the reaction

$$ML + H^+ + 2e^- \rightleftharpoons M(Hg) + HL$$

also starts to form in this region, increasing the slope to an expected 30 mV. The resulting 25 mV is therefore observed. At higher pH (pH = 7.4) ML becomes the predominant species. However in this region (region III) the peak height decreases up to pH = 8 and then decreases sharply (Fig. 44) indicating that ML is still a labile species but ML_2 is non-labile. From the decrease in peak height it is possible to calculate the formation constant for ML and ML_2. The slope (peak potential) decreases to about 13 mV between pH 8.5 and 10.2 where the quasi-labile ML and non-labile species ML_2, predominate. In region IV the peak height starts to increase again (Fig. 44) and the measured slope of 25 mV indicates the MLOH species which undergoes the reaction

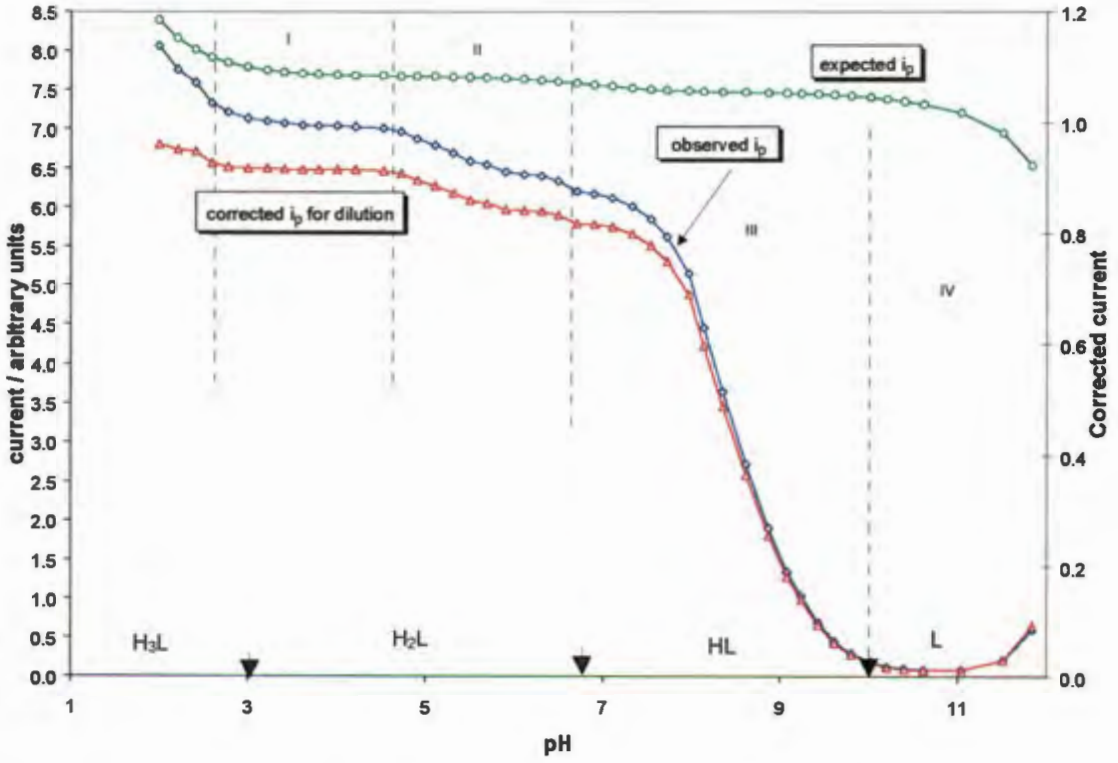

Figure 44. Variation in DP peak height vs. pH for the system described in Fig.43. (○) represents the expected peak height (a decrease in height is only caused by dilution), (◇) the observed peak (a decrease is caused by formation complexes) and (△) represents the peak height corrected for dilution which indicates whether a decrease in peak height is due to a complex formation reaction or not.

$MLOH + H^+ + 2e^- \rightleftharpoons M(Hg) + L.$

To conclude; Almost no shift was found for region I where MLH_2 and H_2L dominate respectively. This can be explained by the absence of protons in the following reaction

$$MLH_2 + 2e^- \rightleftharpoons M(Hg) + H_2L.$$

The relationship between the expected height of a peak i_c (this is calculated from the dilution factor in Eq. 2 ,section 2.2, assuming that no metal complexes are formed) and the observed height is plotted vs. pH as seen in Fig. 44. This is an important relationship because the expected and observed height are both used to calculate the formation constant in Eq. 2a, as a decrease in the corrected peak height will contribute to the shift in peak potential.

One can easily identify that prior to region 1, MLH_4 and MLH_2 complexes are formed because the corrected peak height curve shows a decrease. In region I the height stays constant indicating that no new complexes are formed and MLH_2 predominates in this region. In region II a new species, M_2L, is formed as indicated by the decrease in peak height and stays constant for a short period where it predominates (between pH 5.4 and 7.4). In region III the peak height decreases sharply. This is due to the formation of quasi-labile ML and non-labile ML_2 complexes. Although the shift in peak potential decreased in this region, the inclusion of the term describing the decrease in the corrected peak height in Eq. 2a made it possible to determine the formation constant not only for ML but also for ML_2. Region IV shows the rise in peak height as MLOH is formed.

To support the formation of the binuclear species M_2L and not MLH the shift in peak potential vs. Log $[L_{Free}]$ can be used [38] (see Fig. 45). Here the slope in region II is 15 mV per log$[L_{Free}]$ unit which clearly indicates that one ligand per two metal ions (or ½ a ligand per metal ion) is involved. (A slope of 30 mV indicates one metal ion per ligand). Proof to strengthen the suggested existence of the M_2L species, as deduced from potentiometry which has indicated this species to be important in the complexation of all three ligands studied, is provided by polarography. This is not only by a mathematical exercise (where a mathematical model is fitted to data points using a series of mass-balance equations shown in Fig. 46) but also by this interpretation of decreases in peak potentials. In region III the slope is 28 mV indicating the formation and predominant presence of the ML species. The slope decreases at higher log$[L_{Free}]$ (less negative values) or higher pH values due to the formation of non-labile complexes. A slope of 60 mV would have been expected for the ML_2 species if it was labile.

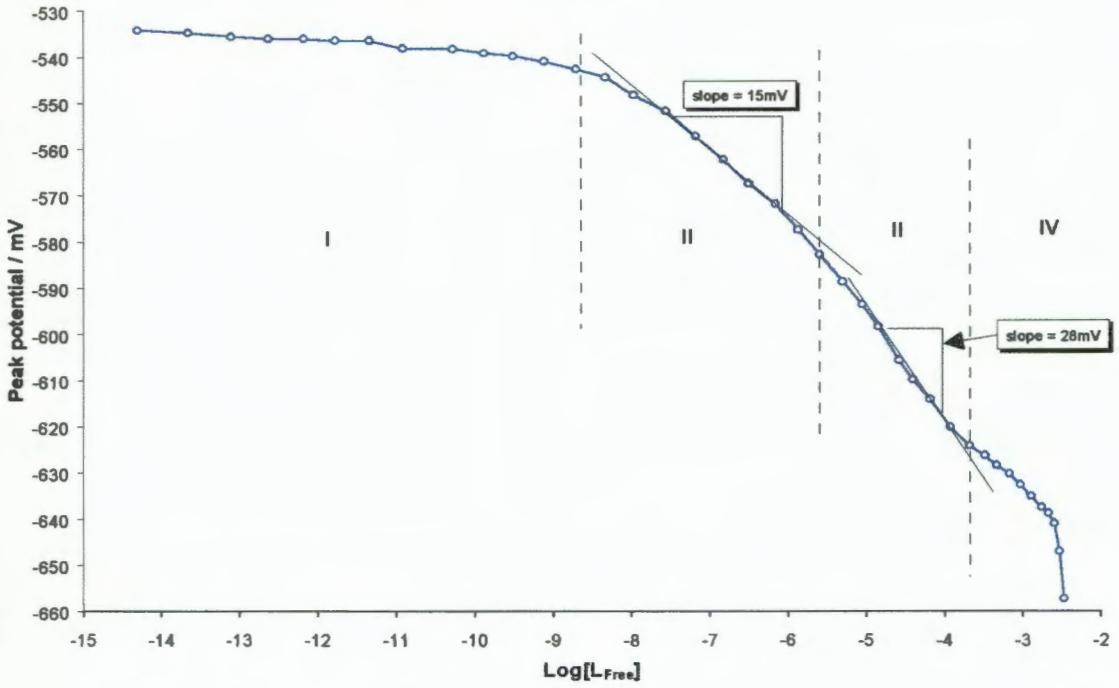

Figure 45. Shift in DP peak potential of cadmium complexes as a function of free ligand concentration calculated for each data point from recorded polarograms (see Fig.47).

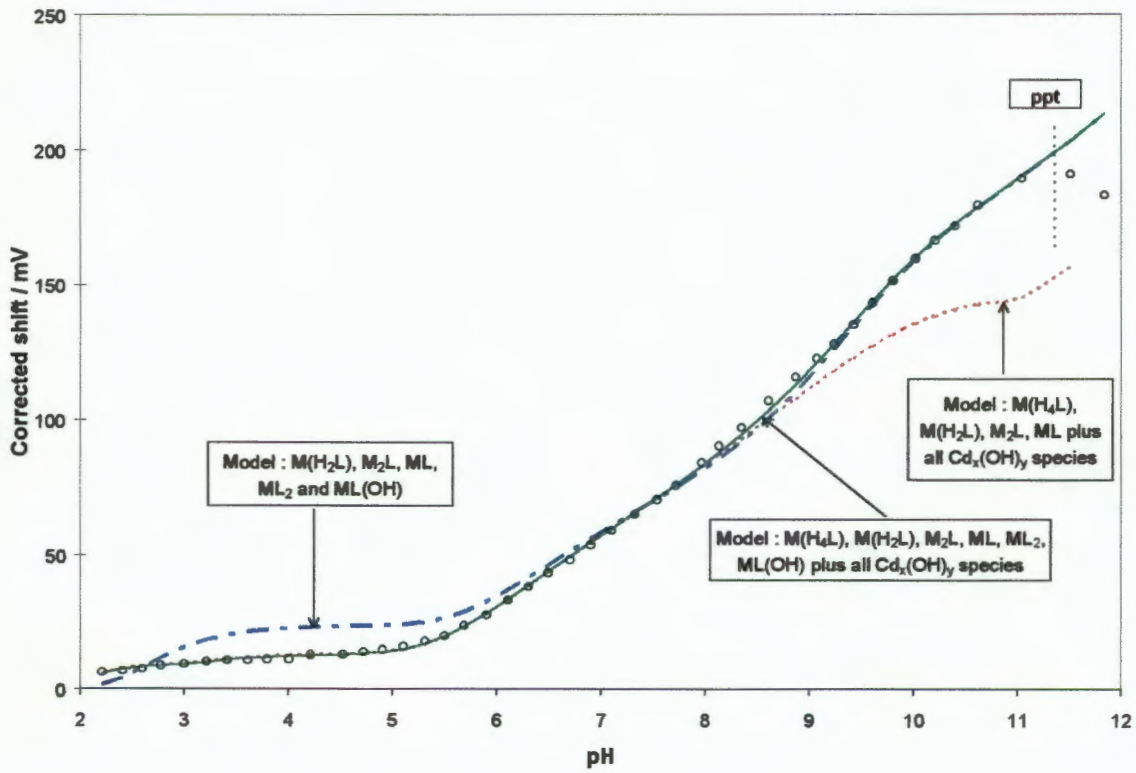

Figure 46. Experimental and calculated corrected shift in peak potential for the Cd-HEDP system. The corrected shift in the peak potential represents the left-hand side of Eq. 2a. The theoretical curve seen as (—) was calculated for the fully metal-ligand system. (—) and (····) represent theoretical curves calculated in the same way but excluding some complex from the model.

The calculated formation constant were refined using Eq. 2a. The expected shift in peak potential was calculated for each data point obtained for each pH(I) value obtained after the *i*th sodium hydroxide addition. The values achieved by Eq. 3 were used as starting values to calculated the theoretical curve. Throughout the calculations the formation constants for Cd(II) hydroxide species was kept fixed. The formation constants were refined by entering improved values by hand comparing the theoretical and corrected shift in peak potentials as can be seen in Fig. 46. The corrected shift in the peak potential is described by the left-hand side of Eq. 2a where the observed shift $\Delta E_p(I)$ at each *i*th pH(I) value is corrected by the logarithmic term from the relative decrease in the polarographic peak height caused by the change in the diffusion coefficient for each metal complex formed in the solution. Open circles in Fig. 46 represents the experimental points and the continuous line is the calculated corrected shift from Eq. 2a for all the complexes of cadmium with the ligand HEDP seen in Table 30 as well as the complexes with OH^-. The other lines present other models. If the model derived from potentiometry (without MLH_4), the dashed line, the theoretical corrected shift values are higher than the observed ones at low pH. This can be understood as potentiometry cannot calculate formation constants accurately at low pH. If ML_2 and MLOH are excluded the values for the theoretical corrected shift are too low if compare with the data points (dotted line).

Table 30 Formation constants for Cd(II) and HEDP derived by polarography

Cation	Equilibrium	Log K	Data points
Cd(II)	$M + L \rightleftharpoons ML$	7.18 ± 0.05	**46**
	$ML + L \rightleftharpoons ML_2$	3.28 ± 0.06	
	$ML + 2H \rightleftharpoons MLH_2$	12.37 ± 0.07	
	$MLH_2 + 2H \rightleftharpoons MLH_4$	5.53 ± 0.07	
	$ML + M \rightleftharpoons M_2L$	5.57 ± 0.07*	
	$ML + OH \rightleftharpoons MLOH$	3.76 ± 0.06	

*Note: It is important that the calculation of the formation constant for the non-labile, ML_2 species, was performed for the first time by Eq. 2a, using only the shift in labile peak potentials and drop in peak height.

In support of this a good agreement between potentiometry and polarography was achieved for the formation constant for the ML_2 species as well as all formation constants in general. Table 31 compares the two techniques by means of Log β values.

Polarography proved that a non-labile species existed at high pH. Potentiometry found this to be ML_2 found a formation constant for it. This was inserted into the polarographic model and by using Eq. 2a the theoretical corrected shift could be calculated from this. It proved after a few

iterations by hand that the potentiometric constant value reproducing the observed corrected shift the best value. This resulted in similar values for this constant. However for MLOH the similar constant was achieved totally independently by the two techniques.

Table 31. Comparison of results obtained by potentiometry and polarography for Cd(II) complexation by HEDP at 37 °C and I = 0.15 M NaCl.

Equilibrium	logß (potentiometry)	logß (polarography)
$M + L = ML$	7.10(4)	7.18(5)
$2M + L = M_2L$	12.99(3)	12.75(5)
$M + L + 2H = MLH_2$	20.02(3)	19.55(5)
$M + L + 4H = MLH_4$	Not found	25.08(3)
$M + L + OH = MLOH$	10.94(3)	10.94(3)
$M + 2L = ML_2$	10.46(5)	10.46(5)

It is now possible to understand the kind of results that are achieved by this technique. Fig. 47 shows polarograms recorded at various pH values to indicate the shift in peak potential (to more

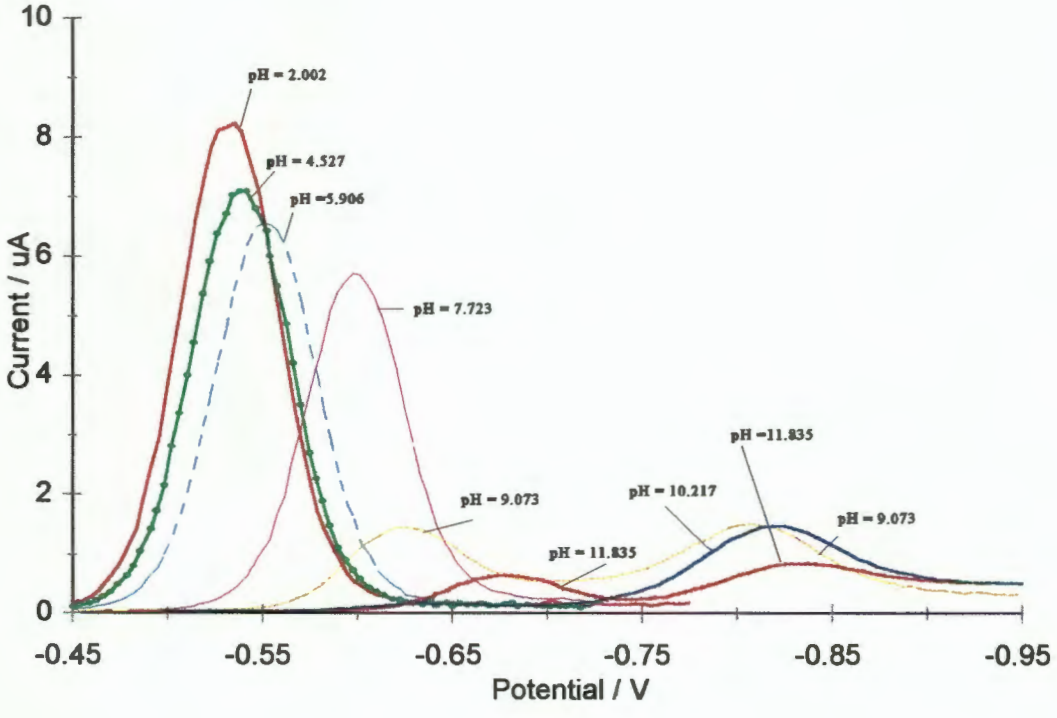

Figure 47. Polarograms recorded at various pH values indicating the shift in peak potential and decrease of peak height indicating the formation of Cd-HEDP complexes. Note the second peak appearing at pH = 10 and the reappearance of the original peak at pH = 11.

negative value) and the decrease in peak height. This is as expected up to pH 7.723 when the shift increases and the peak height starts to drop dramatically. Here ML becomes the predominant species. When the pH is increased to 9.073, the labile peak decreases sharply and at pH = 10.217 it totally disappears. The second peak has already the same height as the labile peak at pH = 9.073 and corresponds to the non-labile species, ML_2. This peak is only briefly the major peak but at pH = 11.835 the original labile peak has reappeared. This is proof of the formation of the labile MLOH complex.

4.2.2 Polarographic results for the complexation of Zn(II) by HEDP

The next system to be studied was HEDP and Zn(II). Here a similar drop in peak height and shift in peak potential was recorded as for Cd(II). (See Appendix E2 to view the polarograms recorded at different pH values as in Fig.47). Although the second peak probably appears at higher pH it is at a potential where the ligand shows activity and it was therefore impossible to record at more negative potentials than -1.1 V .Peak potentials were therefore recorded only up to pH = 6.5. However from the Cd(II)HEDP system it was shown that by using Eq. 2a only the labile part is necessary to calculate all the formation constants (including the non-labile).

In Fig. 48 the shift in the peak potential vs pH is presented. The regions where various protonated forms of the ligand HEDP predominate are marked as before. A slope of about 30.7 mV per proton involved in the electrochemical reaction, expressed per metal ion, should be observed (two electrons involved for Zn(II)). In region II , between pH 4.5 and 5.7, a slope of 27 mV per pH unit is observed. It indicates the presence of the polynuclear species M_2L which undergoes the following reaction

$$M_2L + 2H^+ + 2e^- \rightleftharpoons 2M(Hg) + H_2L$$

Per metal ion, one would expect a 30 mV shift per pH unit for the two protons involved.
This changes in region III, up to pH 6.3, where ML predominates. This is visible from the slope of 59 mV for the reaction

$$ML + 2H^+ + 2e^- \rightleftharpoons M(Hg) + H_2L$$

The formation of ML occurs with Zn(II) at a lower pH as for Cd(II). This indicates that ML is a stronger complex for Zn(II)-HEDP. This will result in higher formation constants as is expected from the free linear energy plots (Section 4.1.4) for HEDP. This is in correspondence with the tendency that a higher first hydrolysis constant for a metal ion (Log $K(OH^-)$ Zn(II) > Log$K(OH^-)$

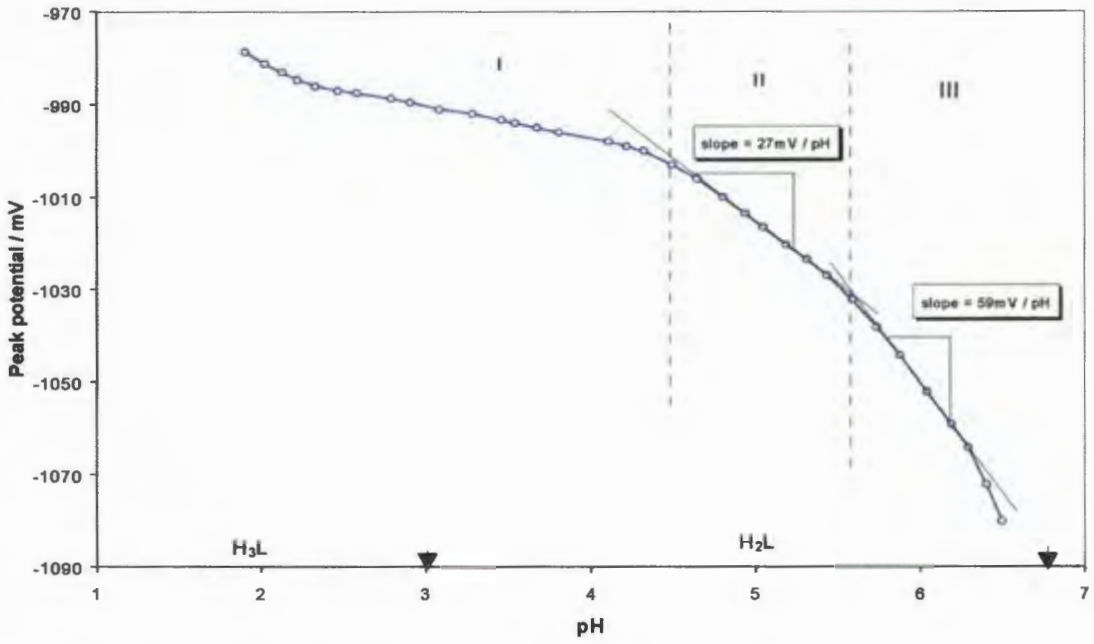

Figure 48. Shift in DP peak potential of HEDP-Zn(II) labile complexes as a function of pH at 37°C and 0.15M ionic strength. All polarograms were recorded in one solution; adjusted to a particular pH given by data points indicated by (○). Dotted vertical lines indicate regions of interest.

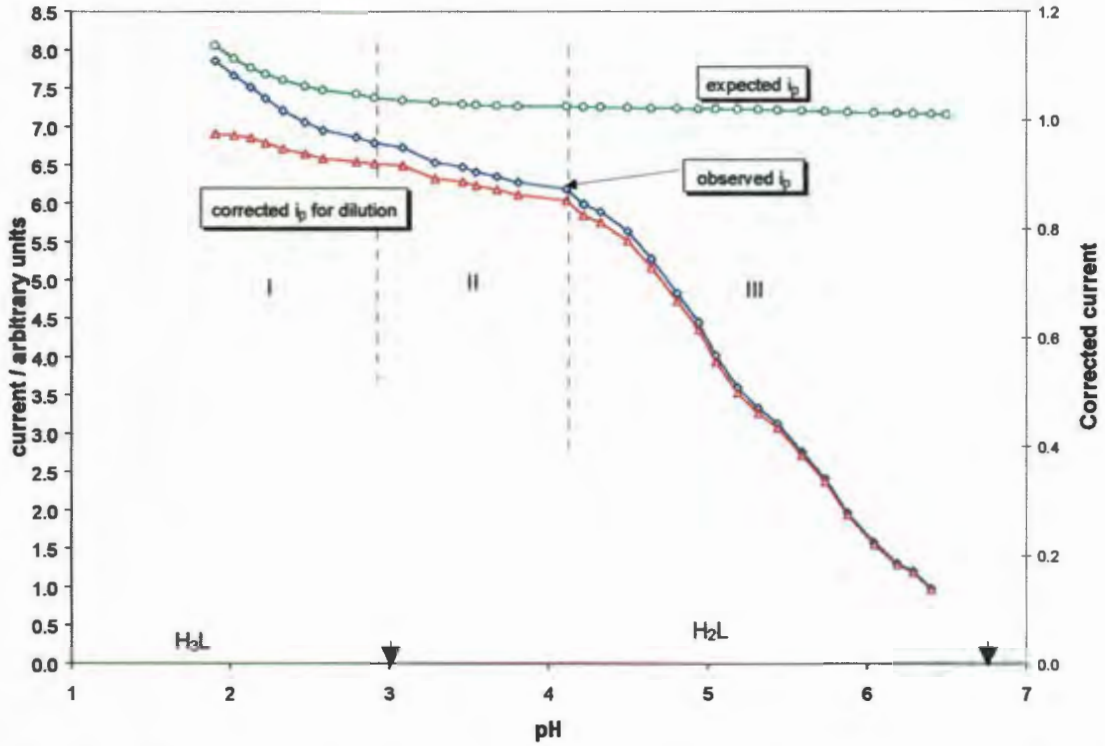

Figure 49. Variation in DP peak height vs. pH for the system described in Fig.48. (○) represents the expected peak height (a decrease in height is only caused by dilution), (◇) the observed peak (a decrease is caused by formation complexes) and (△) represents the peak height corrected for dilution which indicates whether a decrease in peak height is due to complex formation or not.

Cd(II)) will results in stronger complexes

To conclude; Almost no shift was found for region I where MLH_2 and H_2L dominate respectively. This can be explained by the absence of protons in the following reactions

$$MLH_2 + 2e^- \rightleftharpoons M(Hg) + H_2L.$$

At the start of region I however, pH = 1.9 to 2.4 there was a shift in potential. This can be explained by more protonated complexes viz. MLH_4, where H_6L (together with H_4L) predominate at lower pH value, according to the reaction

$$MLH_4 + 2H^+ + 2e^- \rightleftharpoons M(Hg) + H_6L.$$

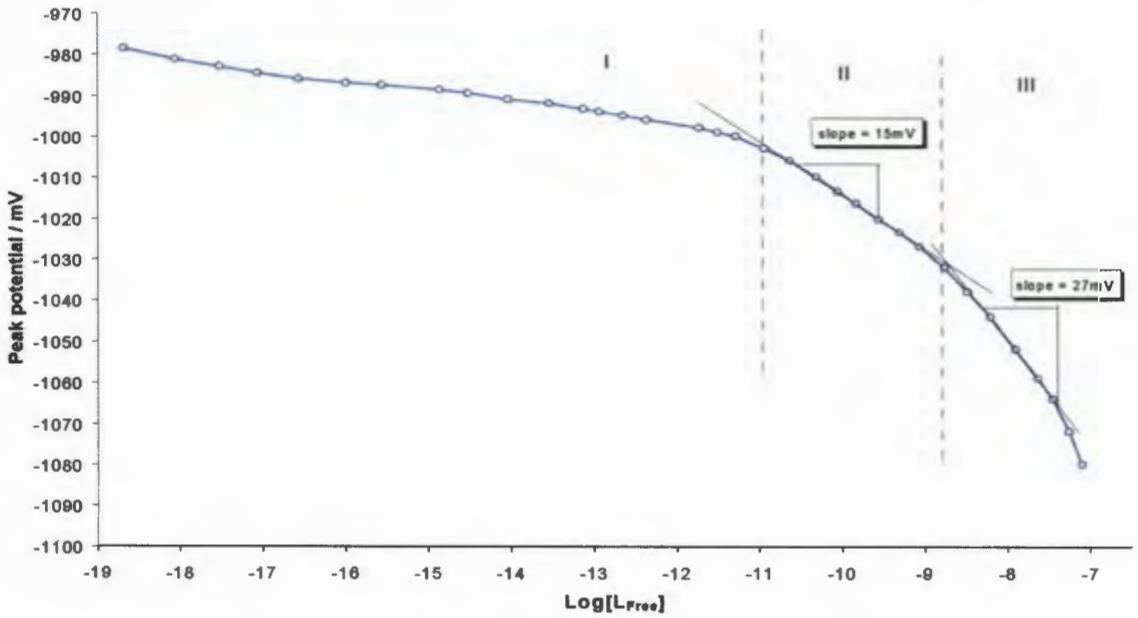

Figure 50. Shift in DP peak potential of zinc complexes as a function of free ligand concentration calculated for each data point from recorded polarograms (see Appendix E2).

The relationship between the expected height of a peak and the observed height vs. pH is plotted in Fig. 49. One can easily identify that in region I, MLH_4 and MLH_2 complexes are formed because the corrected peak height curve shows a decrease. Between pH = 2.5 and 3 however this curve tends to be horizontal, indicating that MLH_2 is the predominant species. In region II the ligand changes from H_3L to H_2L and the species M_2L starts to dominate. The peak height therefore drops but the decrease flattens off at pH = 3.8. In region III the peak height decreases significantly. This is due to the formation of the quasi-labile complex ML and possibly another non-labile complex that forms (not polarographically visible).

As was the case with HEDP and Cd(II), the formation of the binuclear species M_2L, and not MLH, is proven by the shift in peak potential vs. Log [L_{free}] graph shown in Fig. 50 [38]. Here the slope in region II is also 15 mV per log[L_{Free}] unit which clearly indicates that one ligand per two metal ions is involved in the electrochemical reaction. In region III the slope is 27 mV indicating the formation and predominant presence of the ML species.

The best mathematical model achieved to fit the data points, using a series of mass-balance equations, is shown in Fig. 51. Throughout the calculations, the formation constants for Zn(II) hydroxide species was kept fixed. The formation constants were refined by entering improved values by hand and comparing the curve of the theoretical corrected shift with the observed corrected shift in peak potentials as can be seen in Fig. 51.

Open circles in Fig. 51 represents the experimental points and the continuos line are the calculated corrected shift from Eq. 2a for all the complexes of Zn(II) with the ligand HEDP seen in Table 32 as well as the complexes with OH^-. The other lines represent other models where some of the complexes are missing. If MLH_4 (dashed curve) is excluded from the model, the dashed line indicates that at low pH the observed corrected shift values are higher than the theoretically (calculated) corrected shift in peak potentials. If MLOH is excluded (dotted line) the values for the theoretical corrected shift are too low at higher pH values if compared with the observed shift in peak potential.

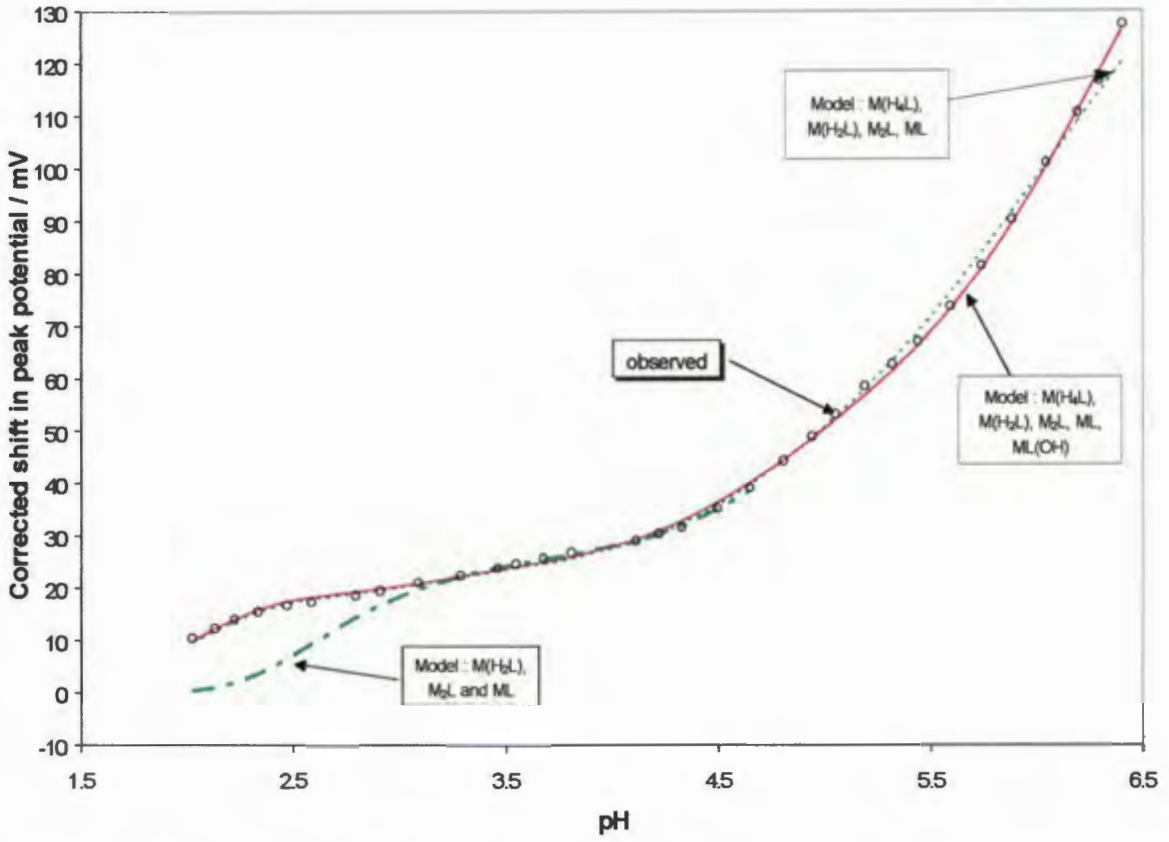

Figure 51. Experimental and calculated corrected shift in peak potential for the Zn(II)-HEDP system. The theoretical curve seen as (—) was calculated for the fully metal-ligand system. (—) and (··) represent theoretical curves calculated in the same way but excluding some complex from the model

Table 32 Formation constants for Zn(II) and HEDP derived by polarography

Cation	Equilibrium	Log K	Data points
Zn(II)	$M + L \rightleftharpoons ML$	10.30 ± 0.05	**25**
	$ML + 2H \rightleftharpoons MLH_2$	9.88 ± 0.05	
	$MLH_2 + 2H \rightleftharpoons MLH_4$	5.50 ± 0.03	
	$ML + M \rightleftharpoons M_2L$	6.16 ± 0.07	
	$ML + OH \rightleftharpoons MLOH^*$	7.43 ± 0.07	

* The MLOH species was not deduced from any previous plot. However this value is needed in the model as can be seen from Fig. 51 where the theoretical fit is improved by its inclusion. The value is nonetheless high if one considers Log K(OH^-) for Zn(II) to be 4.8. This value is therefore doubtful especially when only a few data points are available at pH values where MLOH predominates. It is also possible that other non-labile species are present.

To conclude Fig.52 represents the species distribution diagram for Zn(II)-HEDP, ratio of 58:1.

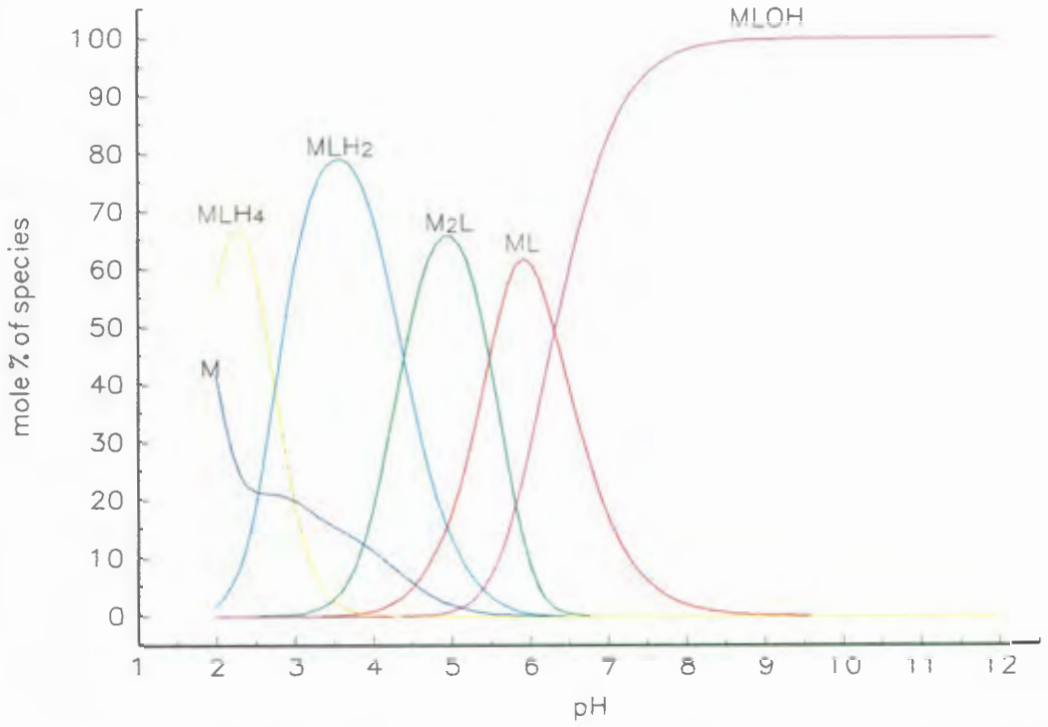

Figure 52. The species distribution curve as a function of pH calculated from polarographic results. L:M ratio taken as 58:1 at 37°C and 0.15M NaCl background solution. (—) Represents fractions of zinc complexes

4.2.3 Polarographic results for the complexation of Zn(II) by MDP

The next system to be studied was MDP and Zn(II). Here a similar drop in peak height and shift in peak potential was recorded. (See Appendix E3 to view the polarograms recorded at different pH values as in Fig.47). The second peak probably appears also at higher pH (above 6.5), at a potential where the ligand shows activity making it impossible to record polarograms.

In Fig. 53 the shift in the peak potential vs pH is presented. A slope of 30 mV per pH unit is observed in region II whereas a slope of about 30.7 mV expressed per metal ion should have been observed to indicate the species M_2L. M_2L is thus described by

$$M_2L + 2H^+ + 2e^- \rightleftharpoons 2M(Hg) + H_2L$$

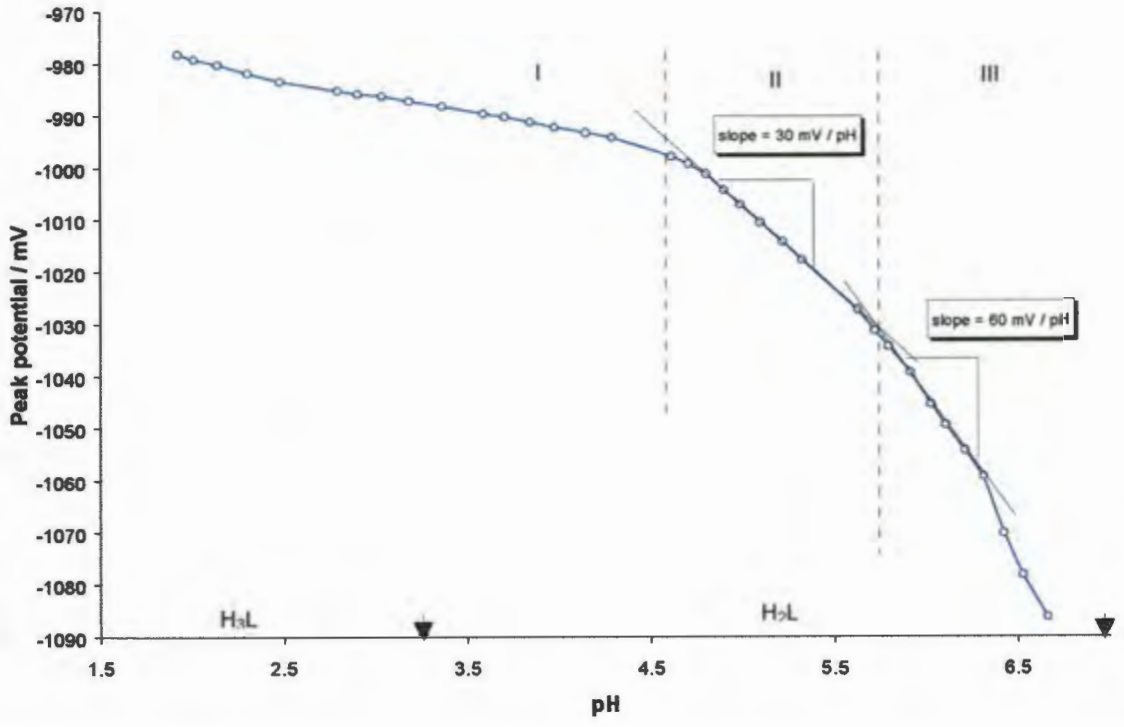

Figure 53. Shift in DP peak potential of MDP-Zn(II) complexes as a function of pH at 37°C and 0.15M ionic strength. All polarograms were recorded in one solution; adjusted to a particular pH given by data points indicated by (○).

In region III, up to pH 6.4, ML predominates. This is apparent from the slope of 60 mV for the reaction

$$ML + 2H^+ + 2e^- \rightleftharpoons M(Hg) + H_2L$$

The formation of ML for MDP occurs at almost the same pH as for HEDP. This indicates little difference between the complexation of MDP and HEDP. A small shift was found for region I where MLH_2 and MLH_4 dominate.

The relationship between the expected height of a peak and the observed height vs. pH is plotted, in Fig. 54. One can identify that in region I, MLH_4 and MLH_2 complexes are formed because the corrected peak height curve shows a decrease. In region II however this curve tends to be horizontal, indicating that MLH_2 is the predominant species. In region III the ligand changes from H_3L to H_2L and the species M_2L starts to dominate. The peak height therefore drops and continues to do so until it decreases sharply as ML (quasi-labile) starts to dominate.

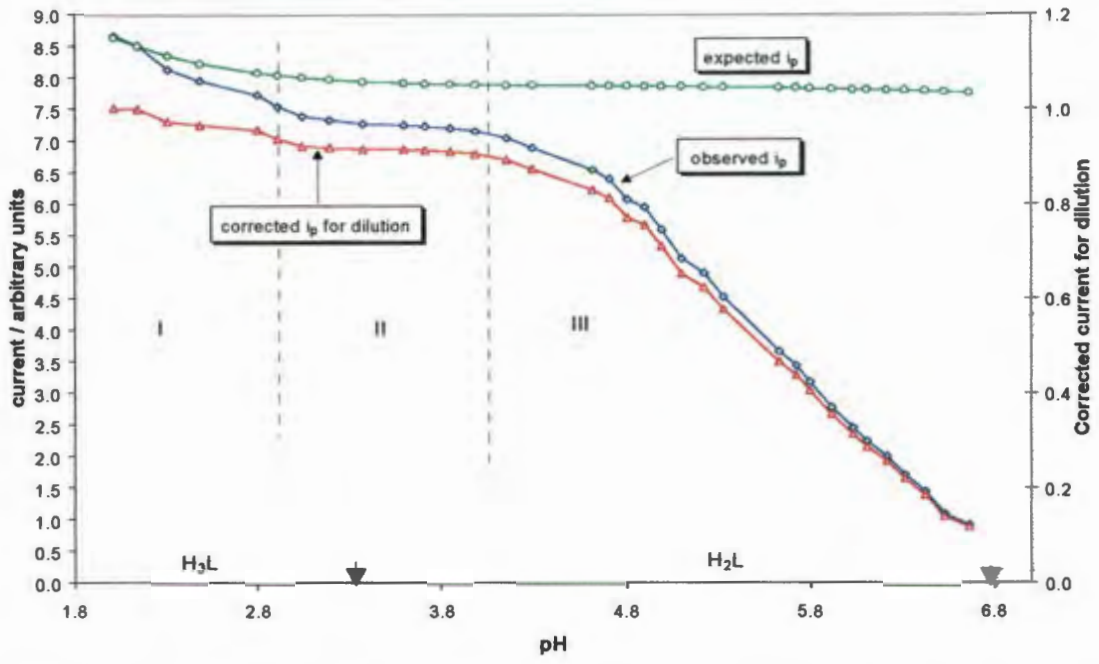

Figure 54. Variation in DP peak height vs. pH for Zn(II)-MDP. (○) represents the expected peak height (a decrease in height is only caused by dilution), (◇) the observed peak (a decrease is caused by formation complexes) and (△) represents the peak height corrected for dilution which indicates whether a decrease in peak height is due to complex formation or not.

The presence of the binuclear species M_2L is proven by the shift in peak potential vs. Log $[L_{free}]$ graph shown in Fig. 55 where a slope of 15 mV per log$[L_{Free}]$ unit in region II is observed. In region III the slope is 30 mV indicating formation of the ML species.

The best mathematical model achieved to fit the data points, using a series of mass-balance equations, is shown in Fig. 56, open circles representing the experimental points and the continuos line is the calculated corrected shift for all the complexes of Zn(II) with the ligand MDP, seen in Table 33. Other lines present other models where some extra complexes are included.

Table 33 Formation constants for Zn(II) and MDP derived by polarography

Cation	Equilibrium	Log K	Data points
Zn(II)	$M + L \rightleftharpoons ML$	9.94 ± 0.05	**25**
	$ML + 2H \rightleftharpoons MLH_2$	10.02 ± 0.05	
	$MLH_2 + 2H \rightleftharpoons MLH_4$	5.73 ± 0.03	
	$ML + M \rightleftharpoons M_2L$	5.56 ± 0.07	
	$ML + OH \rightleftharpoons MLOH^*$	7.46 ± 0.07	

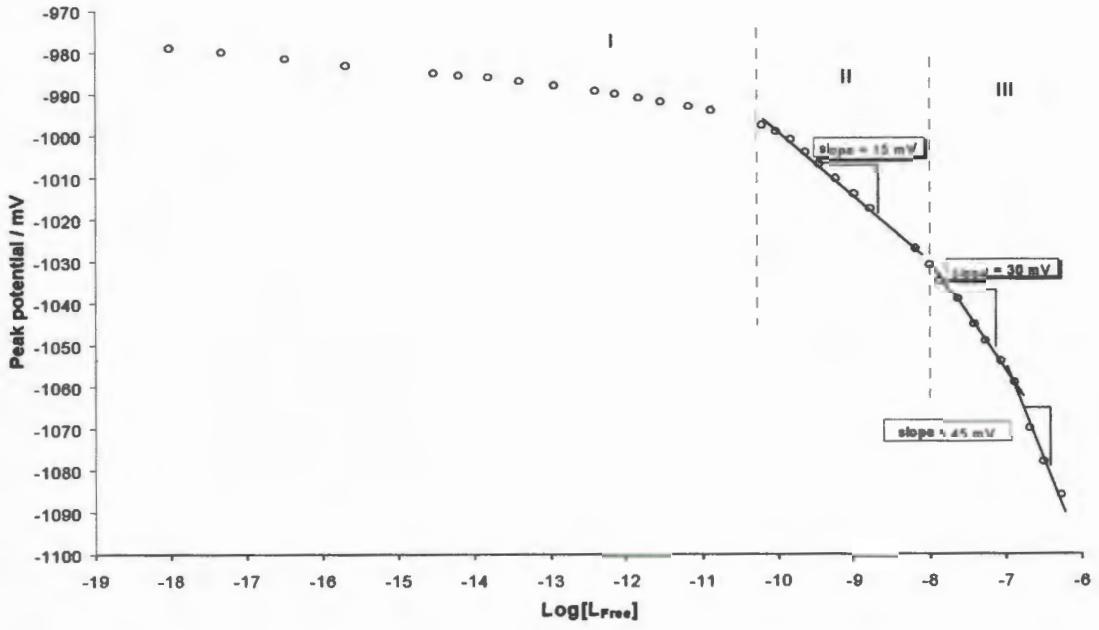

Figure 55. Shift in DP peak potential of zinc complexes as a function of free ligand concentration calculated for each data point from recorded polarograms (see Appendix E3).

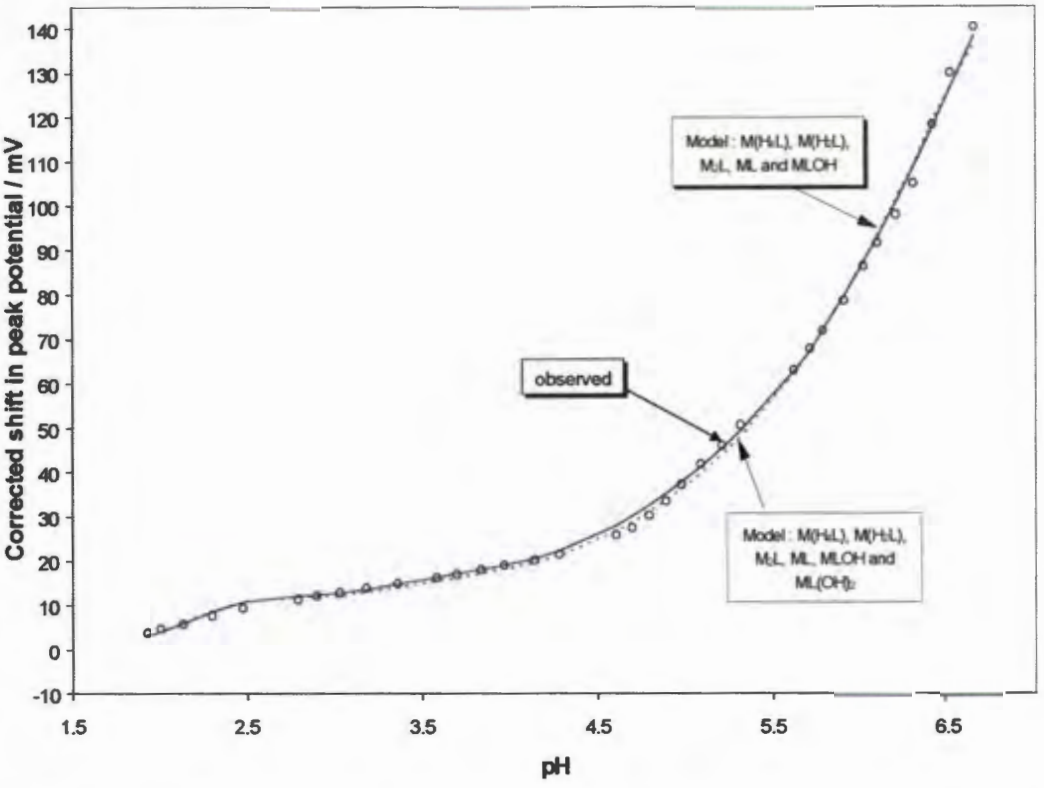

Figure 56. Experimental and calculated corrected shift in peak potential for the Zn(II)-MDP system. The theoretical curve seen as (—) was calculated for the fully metal-ligand system. (····) represents a theoretical curve calculated in the same way but including some extra complexes in the model.

* The MLOH species is needed in the model as can be seen from Fig. 56 where the theoretical fit is improved by its inclusion. However the constant calculated for it is high if one considers Log K(OH^-) for Zn(II) to be 4.8. This would normally indicate that a hydroxy group takes part in complexation. However MDP has no hydroxy group. This value is therefore doubtful which may be explained by the few data points available at this pH and other non-labile complexes formed in this pH region.

$ML(OH)_2$ however seems to have an adverse effect on the fit at lower pH and is not included.

To conclude Fig.57 represents the species distribution diagram for Zn(II)-MDP, ratio of 60:1.

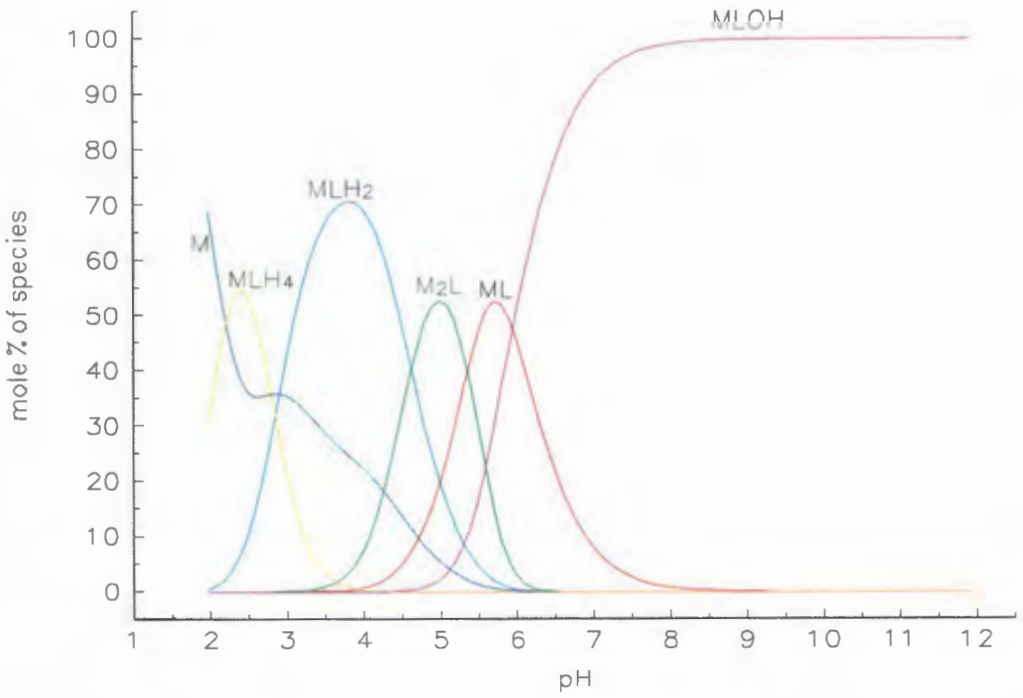

Figure 57. The species distribution curve as a function of pH calculated from polarographic results. L:M ratio taken as 60:1 at 37°C and 0.15M NaCl background solution. (—) Represents fractions of zinc complexes.

4.2.4 Polarographic results for the complexation of Zn(II) by APD

The next system to be studied was APD and Zn(II). Here a similar drop in peak height and shift in peak potential was recorded. (See Appendix E4 to view the polarograms recorded at different pH values as for Fig.47). The second peak probably appears at higher pH (pH ≥ 6), at a potential where the ligand shows activity and therefore making it impossible to record polarograms.

In Fig. 58 the shift in the peak potential vs pH is presented. A slope of 32 mV per pH unit is observed in region II. With APD however the ligand species, H_3L is still predominant. This corresponds with changing the complex species from M_2L to MLH_2 or M_2LH as shown by the following reactions.

$$M_2LH + 2H^+ + 2e^- \rightleftharpoons 2M(Hg) + H_3L$$

$$MLH_2 + H^+ + 2e^- \rightleftharpoons M(Hg) + H_3L$$

Both would have reported a theoretical shift of 31.5 mV / pH unit. From evidence of the $Log[L_{Free}]$ vs peak potential plot (Fig. 59) the M_2LH species is accepted. This excludes MLH_2 from the model which would normally form in this region. Therefore in region I, MLH_3 and not MLH_2, will dominate as indicated by the very small shift (almost zero slope) for this region.

$$MLH_3 + 2e^- \rightleftharpoons M(Hg) + H_3L \qquad \text{(No protons, no shift)}$$

At lower pH levels H_4L is the dominant ligand species. Here the shift is noticeable as explained by

$$MLH_3 + 2e^- + H^+ \rightleftharpoons M(Hg) + H_4L$$

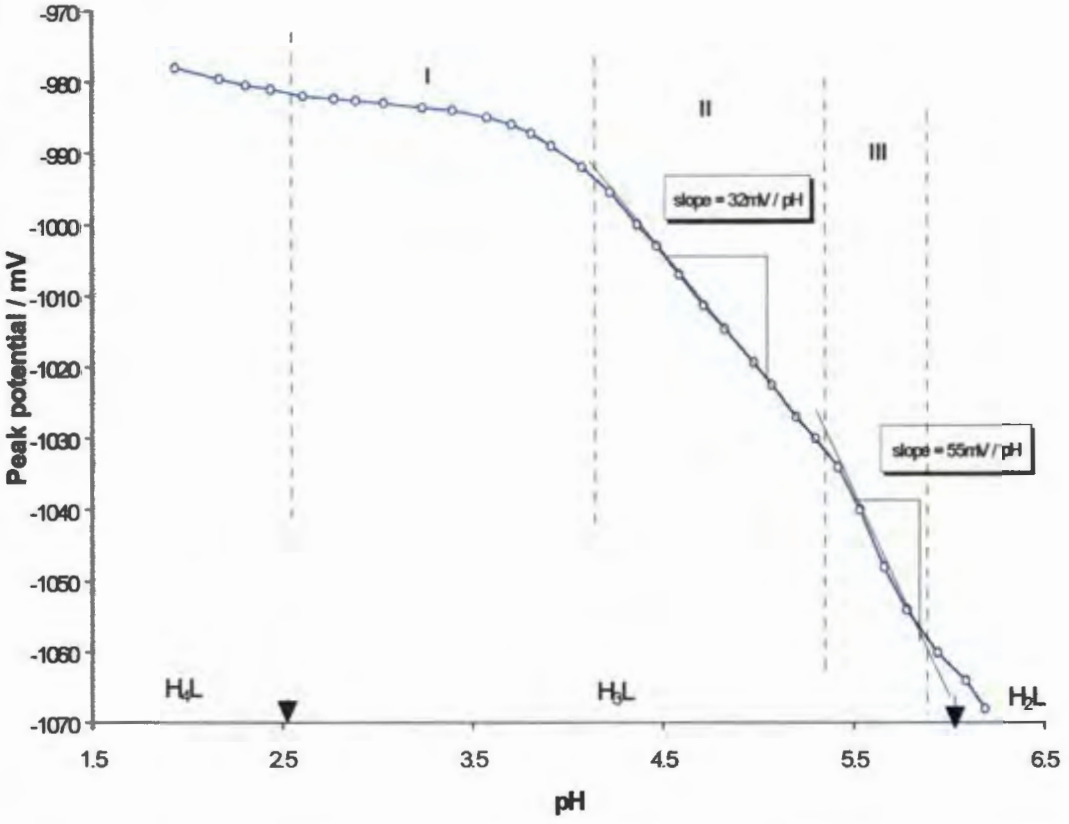

Figure 58. Shift in DP peak potential of APD-Zn(II) complexes as a function of pH at 37°C and 0.15M ionic strength. All polarograms were recorded in one solution; adjusted to a particular pH given by data points indicated by (○).

In region III, up to pH 5.8, MLH predominates. This is apparent from the slope of 55 mV for the reaction

$$MLH + 2H^+ + 2e^- \rightleftharpoons M(Hg) + H_3L$$

The formation constant for ML is calculated from the last few data points. No data is available to calculate less protonated species like MLOH. The big difference between the complexation of MDP and HEDP on the one hand and APD on the other is once again evident.

The presence of the binuclear species M_2LH, is proven by Fig. 59 where a slope of 13 mV, and not 30 mV, per $\log[L_{Free}]$ unit is observed in region II. M_2L is thus absent. If the peak potential was plotted vs $\text{Log}[HL_{Free}]$ a slope of 30 mV would possible have resulted and delivered direct prove of M_2LH. In region III the slope of 30 mV indicates the formation of the MLH species. A similar drop in peak height was observed as was the case with Zn(II) and MDP as well as HEDP. The drop was more equally spread and no deduction could be made from it.
This was also the best mathematical model to fit the data points. Formation constants for the complexes of Zn(II) with the ligand APD, are presented in Table 34.

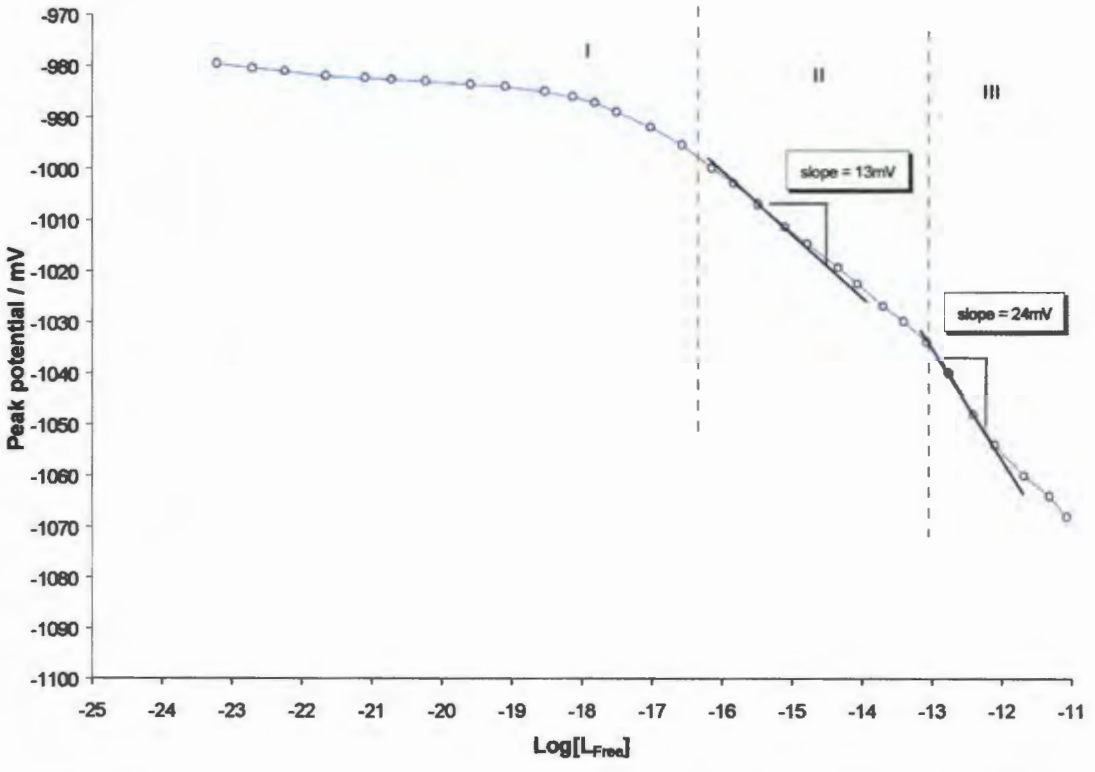

Figure 59. Shift in DP peak potential of zinc complexes as a function of free ligand (APD) concentration calculated for each data point from recorded polarograms.

Table 34 Formation constants for Zn(II) and APD derived by polarography

Cation	Equilibrium	Log K	Data points
Zn(II)	$M + L \rightleftharpoons ML$	14.55* ± 0.05	**33**
	$ML + H \rightleftharpoons MLH$	6.33 ± 0.07	
	$ML + 3H \rightleftharpoons MLH_3$	14.80 ± 0.07	
	$MLH + M \rightleftharpoons M_2LH$	4.86 ± 0.07	

* This is a high value for the ML species if one considers the Log $K(OH^-)$ vs Log $K_1(L)$ plot (Section 4.1.2) where a value for this constant equal to 12.5 would be expected. This value is therefore doubtful and may be explained by the few data points available at this pH. This is very possible as no next complex (etc. MLOH for HEDP and MDP) could be calculated. Uncertainty seems to be part of the last complex calculated by polarography.

The opposite is true for MLH where a value of 9-10 is expected as this is the value for the first protonation constant for APD. The small value might be due to the large value for ML.

To conclude Fig.60 represents the species distribution diagram for Zn(II)-APD, ratio of 60:1.

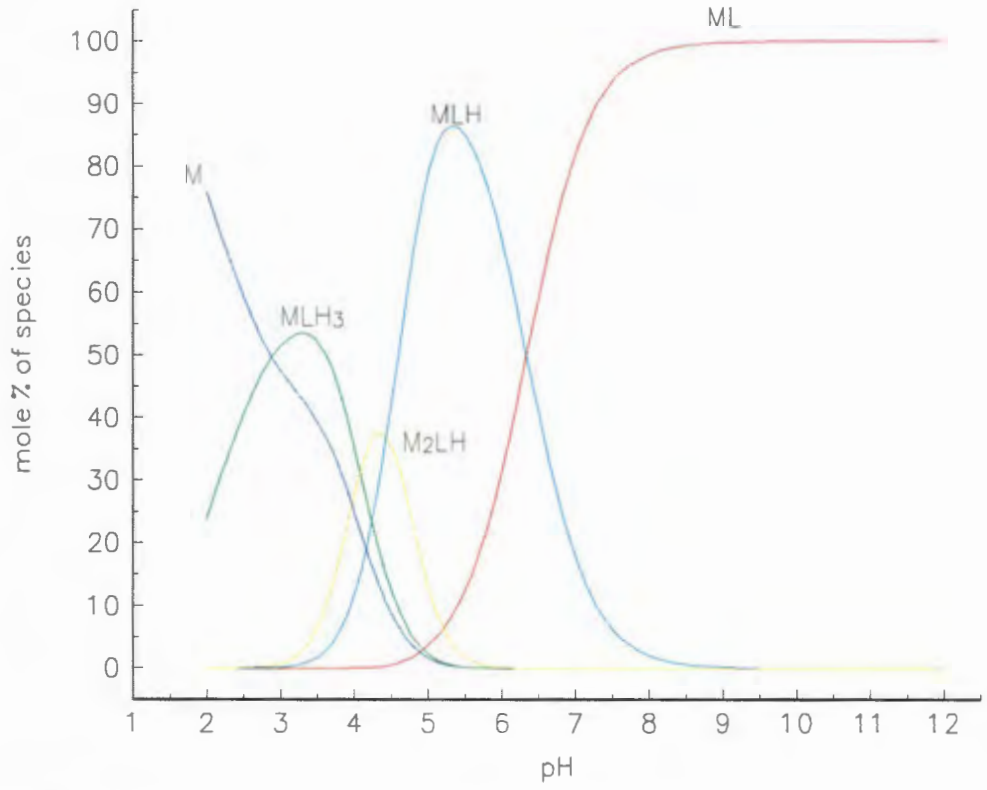

Figure 60. The species distribution curve as a function of pH calculated from polarographic results for Zn(APD). L:M ratio taken as 60:1 at 37°C and 0.15M NaCl background.

The data points (peak potential and peak height) recorded from each polarogram is included in Appendix D1 to D4 for each of the systems in the order as they were discussed in this chapter.

A summary of protonation and formation constants calculated is included in Table 1 (Appendix B0). This will facilitate the comparison of constants for the different ligands with each other as well as the identification of tendencies described in the following sections.

4.3 NMR results and proposed Structures

4.3.1 NMR studies

NMR has been used extensively to study the structure of metal complexes in solution [103]. Initially HEDP was studied using ^{31}P NMR. This is an ideal nucleus with which to study the complexation of HEDP as the phosphorous atom is near the site of complexation and the ^{31}P nucleus has a high NMR sensitivity. Phosphoric acid was used as an external reference. The $^{31}P\{^{1}H\}$ NMR spectrum of the ligand alone at low and high pH shows a single peak (the diphosphonate groups are symmetrical) at 20.4 ppm (pH = 2) and 20.2 ppm (pH = 10.5). This difference is within experimental error and as expected, no shift was recorded. The reason for this being the two bond distance of a proton from the P-atom. For example a big change in a phosphonate structure was studied by Li *et.al.* [100]. They observed only a 4 ppm difference in ^{31}P shift before and after the hydrolysis of thymidine 5-boranomonophosphate. (The tymidine-boranophophate bond breaks releasing boranophosphate). Others [99] confirmed that no shift was expected in this case. At high pH the oxygen next to the phosphorous might be protonated but the water solution is still negatively charged. Little changes in the environment surrounding the P-atom [101].

For complexed HEDP the following changes were observed: as the pH of the solution was increased the ^{31}P resonance shifted to 19.0 ppm (pH 3.0), 19.1 ppm (pH 5.0), 19.9 ppm (pH 7.0) and 20.0 ppm (pH 11.0). At the same time the peak became very broad indicating that the species in solution were fluxional. The change in chemical shift is very small and could be ascribed to experimental error. Although one would expect substantial shifting of the peak on complexation, it must be concluded that the complex is labile or fluxional by nature causing an absence of shift. It is thought that the metal ion associates and dissociates at a rate faster than the NMR time scale. For fast exchange with the ^{31}P nucleus, the lifetime of the molecule (complex) must be smaller than 12.3 msec (1 / (0.5 ppm * 162 MHz)(the ^{31}P frequency on a 400 MHz apparatus)) as only a shift of 0.5 ppm is observed. As the complexation grows stronger (higher pH) the deviation round the true value increases as there is more interaction between ligand and metal ion. This might explain the broadening of the peak at higher pH.

For HEDP, besides the phosphonate groups, the central hydroxyl group can be involved in metal ion coordination. In order to investigate this possibility, a ^{13}C NMR study was undertaken. However, in the case of HEDP coordination, the study was not entirely successful as at the necessary concentrations only small peaks were recorded by ^{13}C NMR. The results achieved are none the less reported in this short chapter. NMR spectra are included in Appendix F for reference. At the same high metal to ligand ratios, APD formed precipitates on complexation with Mg(II). No alternative system was studied. The ligand alone produced two peaks at 92.8 and 22.0 ppm with a peak height ratio of 1:3 at pH = 2. This corresponds to the hydroxy containing a tertiary carbon (a low field value is expected with three deshielding groups attached) and the primary CH_3-group (relatively high field because its one bond from deshielding groups). The ratio of 1:3 is in accordance with the tertiary versus the primary carbon. The complexed ligand produced even smaller peaks due to line broadening. At pH = 3 two peaks at 32.9 and 21.7 ppm in the same ratio as before were recorded. The peaks are just above the background noise and some uncertainty exists as to whether there is indeed a peak at 32.9 ppm. The tertiary carbon peak seems to have shifted almost 60 ppm upfield. For the primary carbon the shift is 0.3 ppm but as it is one bond away and not expected to be involved in complexation, this is reasonable. At pH = 5 the number of scans had to be increased to get any useful information. This was done by recording overnight and accumulating 5000 scans. The resulting spectrum contains three peaks at 60.0, 21.7 and 19.4 ppm. It seems that the peak of the primary carbon was split into two. The other peak at 60.0 ppm belongs to the tertiary carbon indicating a 30 ppm shift. This value is more acceptable than before and because of the number of scans is definitely a peak above background. This result indicates that the molecule is in slow exchange with regard to the ^{13}C resonances. In fact it is often observed that a fluxional molecule can be in slow exchange with respect to one nucleus but not with respect to another. In this case because there is a shift of 3062 Hz (30 ppm * 100.62 MHz), the lifetime of the molecule (complex) has to be smaller than 0.33 msec (1 / (30 ppm * 100.62 MHz) (^{13}C frequency on a 400 MHz apparatus)), for fast exchange. The lifetime of the complex will be larger than 0.33 msec if the exchange with this nucleus is slow (two peaks appear). If one considers that the complex had a lifetime smaller than 12.3 msec (the peak broadening for ^{31}P NMR) the lifetime of the complex should be in between 0.33 and 12.3 msec.

Because of the large change in chemical shift of the carbon attached to the hydroxyl group it is reasonable to propose that the hydroxyl group is involved in coordination. This conclusion is supported by the potentiometric results.

The use of ^1H NMR in this problem was not possible as the protons of interest were all labile and rapidly exchanged with the D_2O solvent [99].

4.3.2 Structure

The following are suggested structures for some of the protonated ligands and complexes identified either by potentiometry or polarography.

As noted in Section 4.1.1 a protonated species of ligand viz. H_6L is found for MDP and HEDP. It will probable exits for APD as well but at a pH lower than 2. Here it becomes difficult to use potentiometry accurately. On first impression it seems an unlikely species but it might be explained by the following sequence of proposed deprotonation.

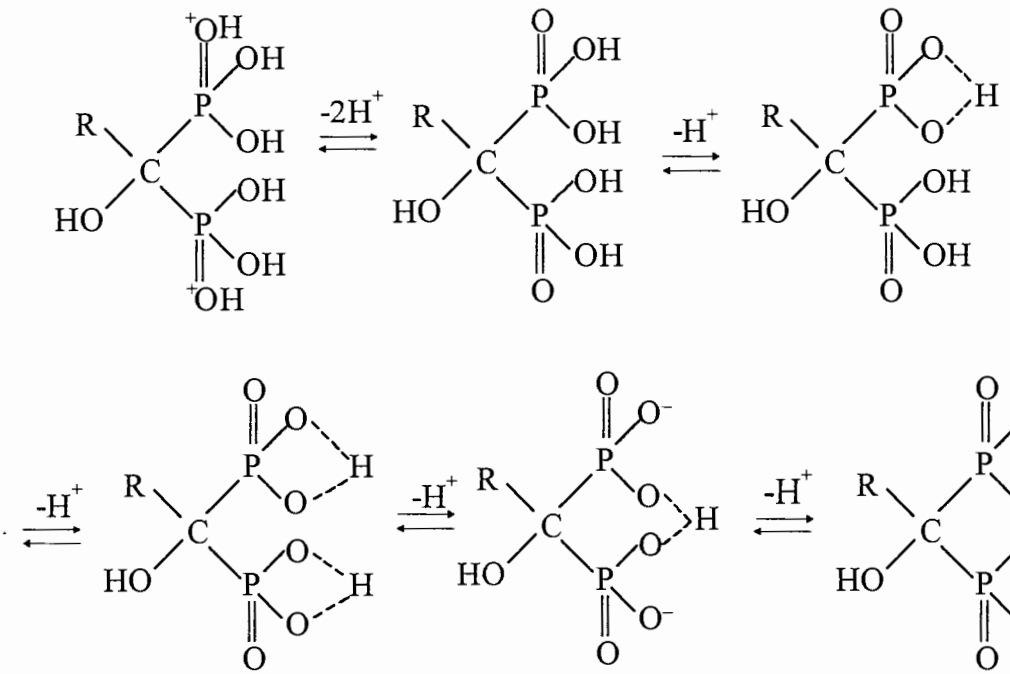

Where R can be H-, CH_3- or NH_2-CH_2-CH_2- . The OH can also be H in the case of MDP. The first species exists only at low pH values and looses both protons together. The rest of the sequence is in correspondence with Wada and Fernando [89].

For complex species these structures above are the starting point. MLH_2 (or MH_2L) should however differ from the fourth structure above. On each phosphonate group there

should be one protonated oxygen and a negatively charged oxygen that is participating in complexation. MDP should behave in all the complexes like a bidentate ligand which results in a six member ring with the metal ion. HEDP and APD have an extra hydroxy group which can take part in complexation. As described in Section 4.1.4 there is evidence that in the complexation of Mg(II) by HEDP the hydroxy group is deprotonated on formation of MLOH. This would indicate that the hydroxy group takes part in complexation. Further evidence comes from the stronger complexes HEDP forms with respect to MDP. The first formation constant for HEDP with most of the metal ions investigated is half a log unit higher than for MDP. The main difference between them is the hydroxy group. This would suggest that the hydroxy group takes part in complexation. One can postulate a possible structure for complexes with HEDP in general (structure I) and for octahedral metal ions, structure II. Both structures indicate that HEDP is a tridentate ligand. In structure II, the three remaining metal coordination sites are occupied by coordinated water molecules. The possibility also exists that each phosphonate group is bidentate. Whether this is the case in the ligands studied here can only be confirmed if it is possible to isolate the solid form of this complex and do an IR analysis on it. Oakes and Smith [98] postulated unidentate phosphonate groups for the ligand EDTMP using NMR evidence.

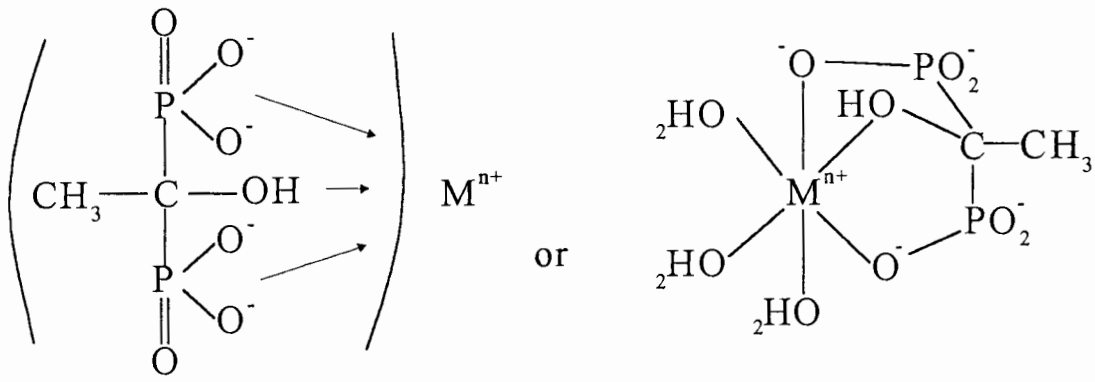

I II

Structures I and II would suggest an ML species but protonation can occur at the phosphonate sites to form the species MLH or MLH_2. For all the metal ions the pK_a of the

complex is inbetween the pK_{a1} and pK_{a2} of HEDP. This suggest that protonation of the complex takes place at one of the two phosphonate sites.

For APD, R=$CH_2CH_2NH_2$, which could also coordinate to a metal ion. The first formation constant for the various metal ions with ADP is more than one log unit higher than for HEDP. The only difference between APD and HEDP is the amino group. This strongly suggests that the amino group takes part in complexation. However it is impossible to have a structure where APD acts as a tetradentate ligand coordinating with the hydroxy as well as the amino group. This can easily be deduced by building a simple framework model and is also visible from structure III where APD is complexed to an octahedral metal ion.

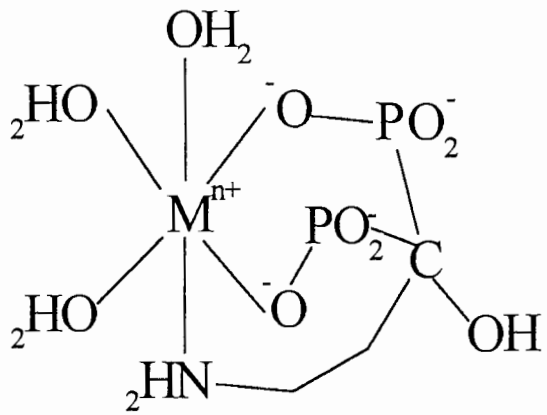

Structure III. Possible structure of ML for APD.

If one takes a tetrahedral metal ion it is even more difficult to accommodate four dentates. The contribution of an amino group to complexation is bigger than a hydroxide group as it is more basic. It is therefore still theoretically possible that APD will form stronger complexes (as is observed) than HEDP. Structure III is a suggested structure for the species ML. MLH would be a protonated form of this structure. For Ca(II), Sr(II) and Mg(II) the pK_a of the MLH complex is between pK_{a1} and pK_{a2} of APD. This is evidence for protonation taking place at the nitrogen centre. However for Zn(II), Ho(III) and Sm(III) the pK_a of the complex is below pK_{a2} of APD, indicating protonation at a phosphonate centre. This is in agreement with the tendencies found for EDTMP [7] and follow the trend that the less-stable complexes are protonated at a nitrogen which must entail metal-nitrogen bond rupture.

The structure of M_2L is something that has not been reported on very widely. Neither Van der Linden *et. al.* [84] nor Nash [82], who both include M_2L in there papers, report on its structure. If one accepts the structure III as that for the species ML, it follows that the second metal ion might involve the free hydoxide group and a second P-O^- dentate (the one not involved in complexation of ML). Structure IV proposes such a system.

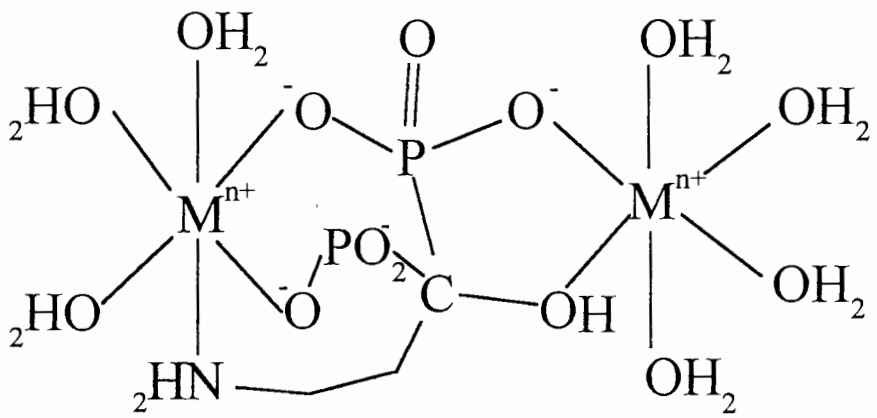

Structure IV. Possible structure of M_2L for APD

In structure IV the amino group can easily change from one metal ion to another. However if one suggests that each metal ion is bound to one a phosphonate group (no chelate rings can be formed by one phosphonate group to the same metal ion) each, the bonding between metal ion and ligand should be weak, resulting in low formation constants. For the ligand MDP, Log K values found for the equilibrium $ML + M \rightleftharpoons M_2L$ are low, ranging from 3.5 to 2.9 for Ca(II), Mg(II) and Ni(II) suggesting these weak bonds. However for HEDP the values are higher viz. 4.0 for Ca(II) to 5.9 for Cd(II). No weak bonds. For APD the values are even higher viz. 5.7 for Ca(II) and 6.8 for Mg(II). HEDP and APD might thus form M_2L species according to structure IV.

Another interesting aspect is that for MDP and HEDP, the formation constant for the M_2L species is higher for Ca(II) than Mg(II). This is the opposite of the normal stability order reported for Ca(II) and Mg(II). This indicates a stabilisation of some kind for Ca(II) or a destabilisation of Mg(II). The same tendency was reported by Wada and Fernando [89] for HEDP, however they explained this by the hydroxy group taking part in complexation of Ca(II) by HEDP. It has been shown here that in the case of Mg(II) and HEDP the hydroxy

group already takes part in complexation. Furthermore the same reversed order is found for MDP which has no hydroxy group. The reason given by Wada and Fernando [89] which was restated by Claessens and Van der Linde [84] can therefore not be true. Its seems that the reason is located in the structure of the complexes formed. The ligand probably does not 'fit' well around the small Mg(II) ion. Ca(II) has a radii of 0.99Å and Mg(II), 0.66Å. The same reason has been advanced for the observed reversal in stability order of EDTA [7]

4.4 *In vivo* Speciation by ECCLES

Since the uptake of ^{166}Ho by bone is rapid and completed in two to three hours after injection and metal uptake by proteins is slow, transferrin binding has been neglected in the blood plasma modelling of ^{166}Ho-APD. Jarvis *et. al.* [7] have shown that this assumption is valid for ^{153}Sm-EDTMP and ^{166}Ho-EDTMP. We shall also show that this assumption is valid for HEDP and Sm(III). Simulation calculations performed without the inclusion of transferrin binding, can be considered to model the speciation immediately after injection / administration i.e. before equilibrium with protein binding has been established. For Ho(III), transferrin cannot be included as the constants for the complexation of Ho(III) by transferrin is not available in the ECCLES database.

Fig. 61 shows the speciation of Ho-APD in the absence of protein binding.

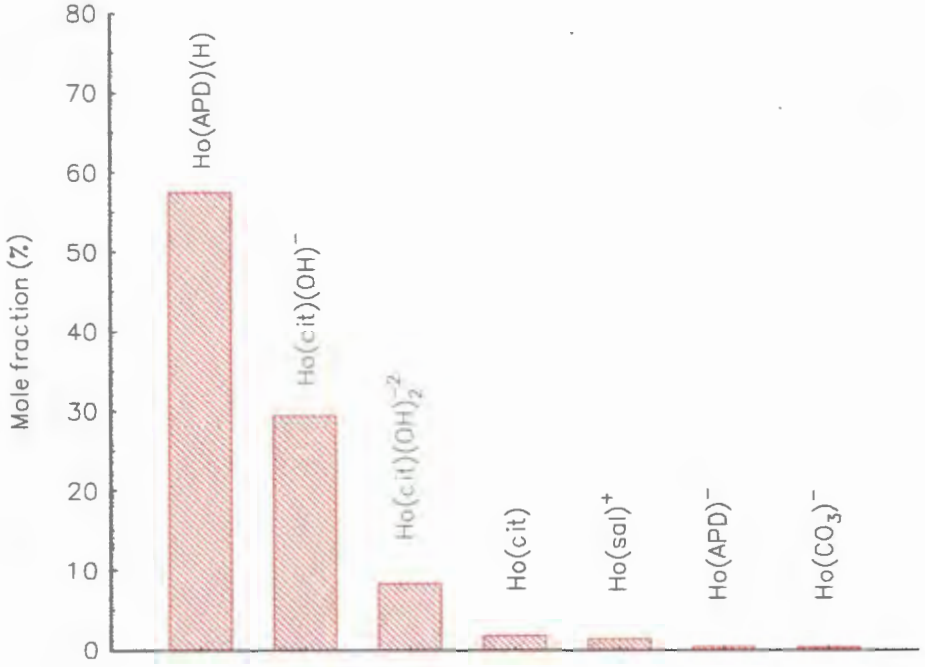

Figure 61. Speciation of Ho(III) in blood plasma with APD added; (Cit) = citrate and (sal) = salicylic acid (3-carboxy-3-hydroxy-pentane-1,5-dioic acid).

The output of the ECCLES runs can be found in Appendix G and the ECCLES input files in Appendix G1. (The concentrations taken are 8.5×10^{-5} mol.dm^{-3} for ligand and 2.0×10^{-6} mol.dm^{-3} for the metal ion). It is quite clear that, *in vivo*, citrate competes with APD for Ho(III). 58% of the Ho(III) remains bound to APD while citrate collects 38% in total. The remainder of the

Ho(III) is distributed between salicylic acid and carbonate. This explains the good bone uptake of Ho(III) in the baboon model (Section 4.5). Citrate it self can deliver Ho(III) to the bone but is less selective and in a longer time span. Neves *et. al.* [95] used ^{166}Ho(cit) as a bone localising agent. They describe colloid formation on complexation. This should be due to the neutral complex. However in blood plasma the complexes that are predominantly formed are $Ho(cit)(OH)^-$ and $Ho(cit)(OH)_2^{2-}$ (Appendix G) which are soluble. The neutral species, Ho(cit) accounts for only 4.3% (1.6/38 * 100%). Citrate will stay in the blood longer than APD and at some time pass through the bone blood vessels. Here it will be given of to the diphosphonate which can bind to the hydroxy apatite.

Hydroxy apatite forms a hexagonal crystal lattice in an elongated form on crystallization from a supersaturated solution of Ca(II), phosphate and hydroxide. All along the apatite crystals, grooves which run parallel with the C-axis of the crystal are formed. These grooves are the outside and are surrounded by the perivascular fluid from which the crystals are formed. The diphosphonate is believed to be taken up in this fluid and attach to these grooves via their strong affinity for Ca(II) which is part of this hydroxy apatite crystal structure. Whether or not a complex like SmEDTMP dissociates before absorption is not quite clear. Chirby *et. al.* [20] reported contradictory evidence. Jarvis *et. al.* [7] then proposed, after some insight by speciation modelling, a dual model where the SmEDTMP complex is absorbed on the bone followed by its dissociation allowing the uptake of Sm(III) into tumours.
From the ECCLES modelling (Appendix G) it is clear that citrate does not have the same affinity for Ca(II) as APD. It has lower formation constants, (i.e. Log K_1 = 3.2) and 23 % of the citrate remains as free citrate; 48% complexes with Ca(II) and 27% with Mg(II). Citrate should therefore cause less bone uptake than diphosphonates. In clinical trails using ^{166}Ho(III) and citrate, Neves *et. al.* [95] have shown this to be true. Because citrate is not exclusively selective for bone, Ho(III) will take more time to accumulate in the bone where it loses the Ho(III). This results in slow blood clearance and high accumulation in the kidneys. However it does not loose its property to deliver some Ho(III) to bone tissue complementing the bone delivering action of a diphosphonate.

It is interesting to compare the selectiveness of HoAPD with other diphosphonate-lanthanide combinations. Fig. 62 compares the speciation of HoAPD with that of SmEDTMP and HoEDTMP. The results show that HoAPD behaves different from SmEDTMP. For HoAPD the

complex Ln(Ligand)(H) predominates and almost no Ln(Ligand) is formed. This species is neutral in the case of APD and causes the high liver uptake in the baboon model (Section 4.5). In contrast to this SmEDTMP stays in the Ln(Ligand) form, 51% with 28 % in the Ln(Ligand)(H) species. Both complexes are not neutral because EDTMP has eight dissociable protons. Thus, the SmEDTMP system should not show high liver uptake. This is found in practise [6]. The total of these two metal species is important for the bone uptake. SmEDTMP scores 79%, HoAPD 58% and HoEDTMP 18% indicating the order of expected bone uptake for these three systems. This is confirmed by the reverse order found for the combined presence of Hocitrate species; 79% for HoEDTMP, 38% for HoAPD and 20% for SmEDTMP. Form this it can be concluded that HoAPD should have a better bone uptake and faster blood clearance than HoEDTMP. However the bone uptake is not as high as SmEDTMP and one would not expect a 91% bone uptake found for the latter [6]. Louw *et. al.* [6] reported only 65 % bone uptake for ^{166}HoEDTMP. This bone uptake is higher than the amount of Ln(Ligand)(H)$_x$ species calculated to be present in blood plasma. This discrepancy might be due to the bone seeking action, although low, of citrate.
An estimate of the ^{166}HoAPD bone uptake can be made from the speciation data. One would expect 85% uptake and a blood clearance close to SmEDTMP (closer to SmEDTMP than HoEDTMP).

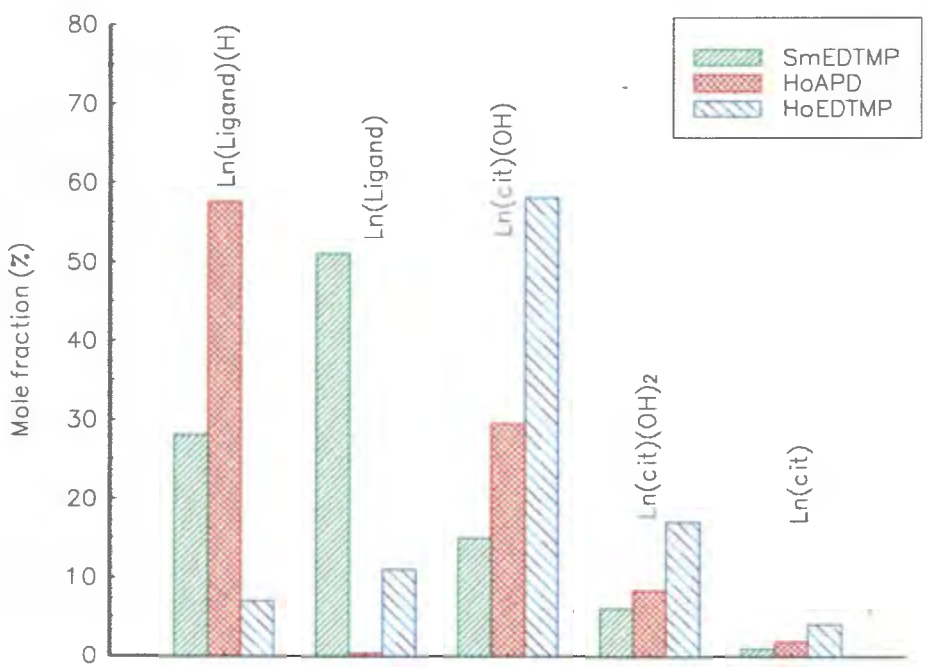

Figure 62. Comparison of speciation of Sm(III) and Ho(III) with EDTMP or APD in blood plasma.

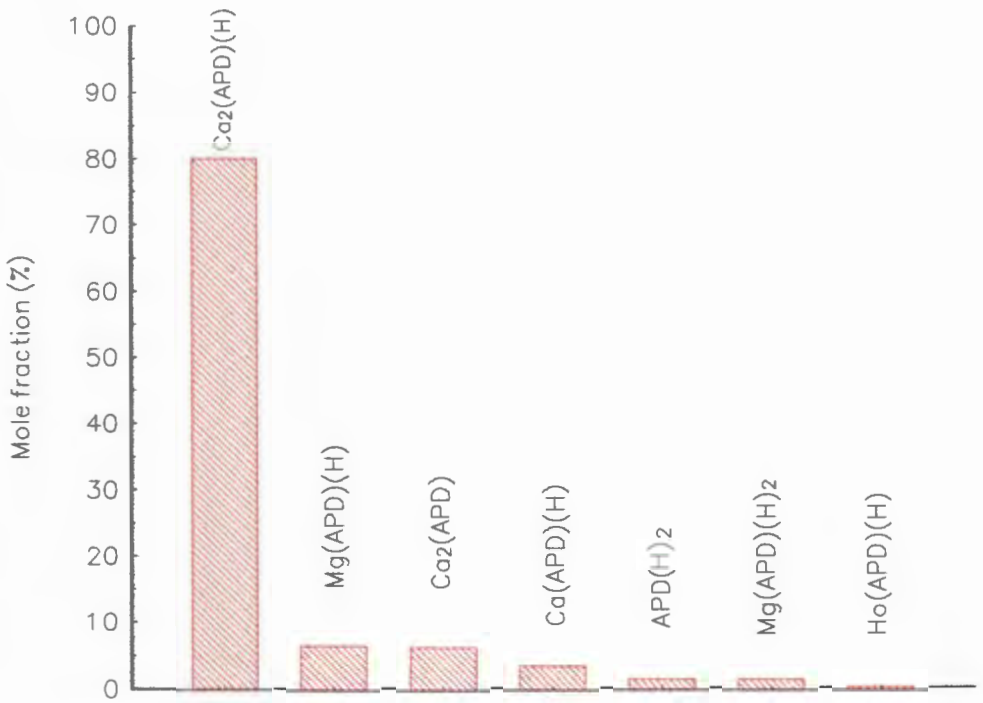

Figure 63. Speciation of APD in blood plasma. Charges have been omitted for simplicity.

The question remains why does APD not compete as effective as EDTMP for Ho(III) in the presence of citrate, even though the first complexation constant for HoAPD is taken at 13.81 and 14.44 for SmEDTMP.

One of the reasons might be APD's preference for Ca(II) illustrated by Fig. 63. Almost 90% of APD complexes to Ca(II) in blood plasma in various species, the major species is $Ca_2APD(H)$. The remaining APD is complexed by Mg(II) and Ho(III). It has to be remembered that these figures correspond to an injected ratio of Ligand:Metal = 50:1. None the less this will have an effect of the distribution of Ho(III) in blood plasma where such a high concentration of Ca(II) is present, compared to Ho(III). This explains why APD is used in the treatment for osteoporosis or malignant osteolytic bone disease [11]. APD mobilises Ca(II) efficiently and has the ability to bind to hydroxy apatite and stops via this process, the osteolytic resorption of bone.

Fig. 64. shows the speciation of HEDP and MDP in blood plasma calculated using the equilibrium constants given in Table 20 and 29 and the total component concentrations given in Appendix G. Here totally different species predominate with the free ligand concentration being significant.

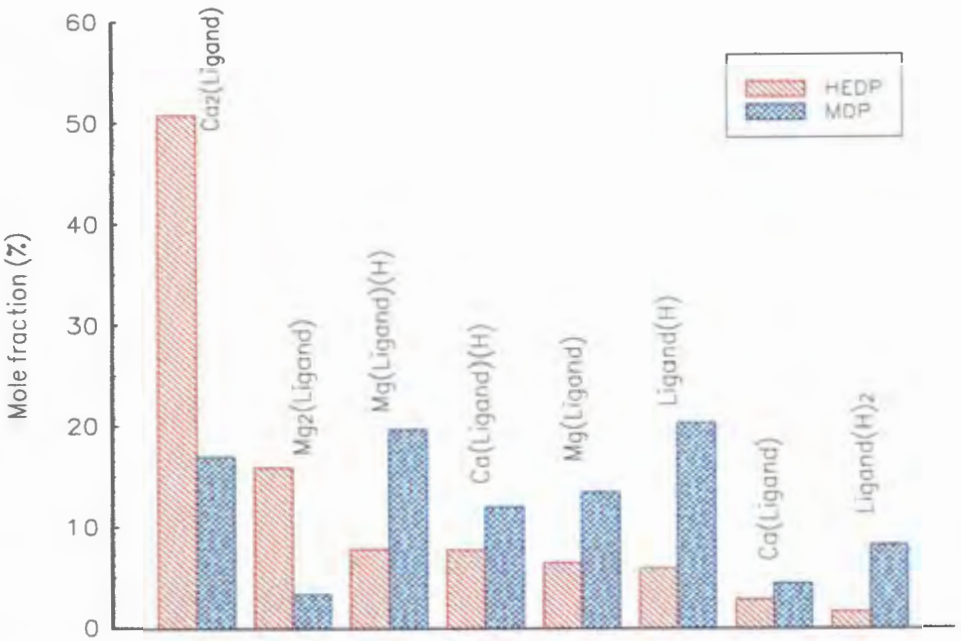

Figure 64. Comparison between the speciation of HEDP and MDP in blood plasma.

HEDP still mobilises Ca(II) the most (62%), with Ca_2HEDP the major species. This is quite different from MDP where the mobilisation is divided in three; Mg(II) takes 35%, Ca(II) 33% and 32% remains as free ligand or protonated ligand. In the case of HEDP only 8% stayed as ligand and for APD no free ligand was observed. This confirms the strength of the bonding of metal ions found in blood plasma with the three ligands. APD > HEDP > MDP. The hydroxy group plays a vital role in the first two ligands' stronger complexation. HEDP and MDP will therefore not be such good inhibitors of osteolytic processes.

As the formation constants for the complexation of Sm(III) by HEDP could be calculated (Section 4.1.3 and 4.1.4) and experimental results of ^{153}Sm with these ligands have been reported by Dow Chemicals [43] ECCLES modelling was performed for both MDP and HEDP (Appendix G). Fig. 65 shows the distribution of SmHEDP amongst low-molecular-weight compounds present in normal blood plasma. The speciation without transferrin can be assumed to be the situation shortly after the introduction of Sm(III) into blood plasma. Complexation of transferrin is kinetically slow and so the speciation in the presence of transferrin reflects the situation after a few hours. It can be seen that transferrin will eventually complex 88% of the remaining Sm(III) (that which is left after bone absorption). The relative percentages of the low-molecular-weight complexes of Sm(III) remain unchanged (Fig. 65).

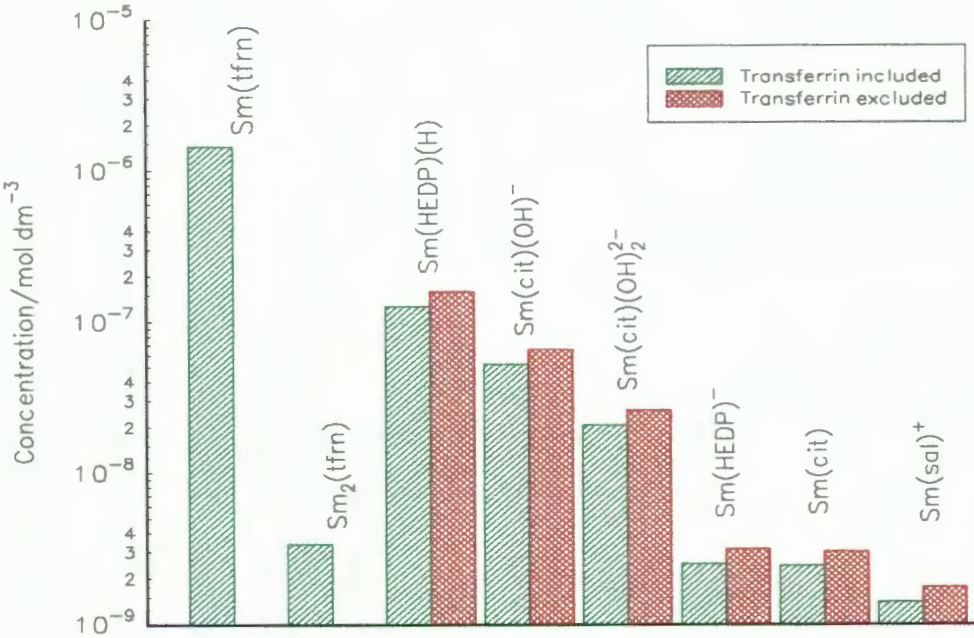

Figure 65. Speciation of SmHEDP in blood plasma. Tfrn = transferrin; the rest as previously defined.

As the relative speciation of species in blood plasma with or without transferrin is the same and bone uptake is supposedly complete within 2 to 3 hours, transferrin has been omitted from Fig. 66 for simplicity. Fig. 66 shows the various species Sm(III) should form with HEDP and MDP and other competing ligands in the blood plasma.

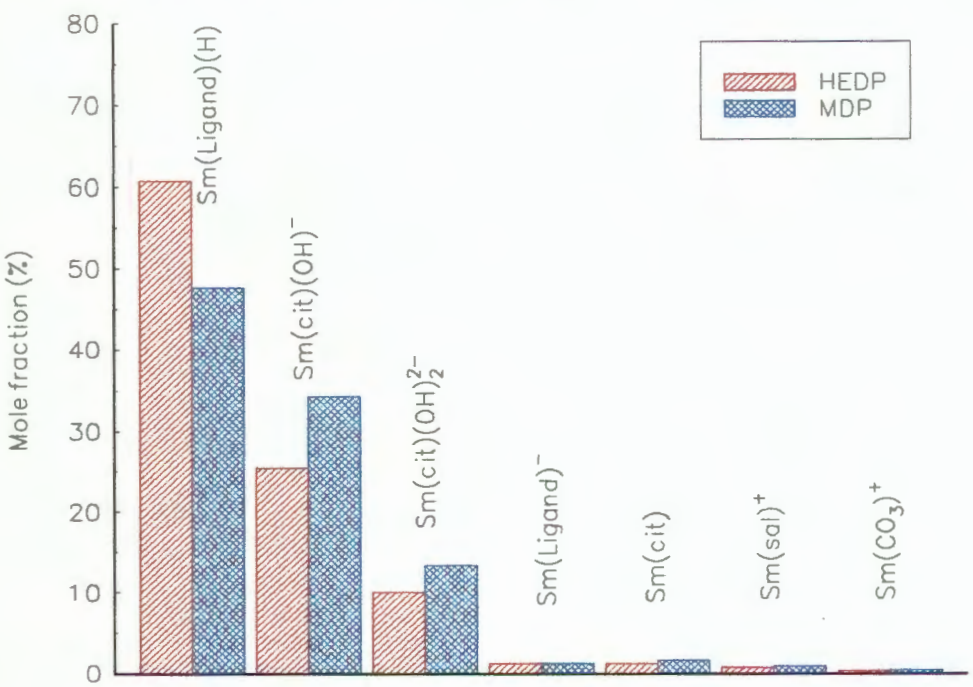

Figure 66. Speciation of Sm(III) in blood plasma with HEDP and MDP added.

Here the predominant species for both HEDP and MDP is the MLH species which is neutral. This explains why Dow Chemicals reported that 85% of the activity of ^{153}SmMDP and 35% of ^{153}SmHEDP injected into rats were taken up in the liver [43]. This is in agreement with what is found for ^{166}HoAPD (Section 4.5). A total of 61% of Sm stays bounded to HEDP while the percentage for MDP is 47%. This compares favourably with the 57% of APD. The other major competing species here is again citrate.

The question that arises is how it is possible that the percentages of complexed lanthanide in blood plasma for HEDP and MDP can be so close to APD although there is a three orders of magnitude difference in the first formation constant. (Log K_1 for APD = 13.81, Log K_1 for HEDP = 10.10, Log K_1 for MDP = 9.3) Two reason can be proposed. The first is the affinity of APD for Ca(II) which lowers the percentage of HoAPD(H). As has been discussed is this not the case for HEDP and MDP. The second is in the formation constants of Ho(III) and Sm(III) by citrate. For the species Sm(cit)(OH), Log K_1 = 13.91 and Sm(cit)$(OH)_2$, Log K_1 = 19.42. For Ho(III) these constants are 14.31 and 19.67 which makes a big difference to the competing ability of citrate. The fact that the concentration of citrate in blood plasma is 1.1×10^{-4} mol.dm^{-3} (1.4 times the concentration of ligand injected) enhances its competitiveness even further.

To conclude this section, an ECCLES calculation was done on the drug, Metastron ($^{89}SrCl_2$). Clinical trails on this therapeutical have been described in Porter *et. al.* [96]. The results of the calculation are given in Appendix G. Only two species, were found to be significant. APD was also include in the model but had no influence. 98.6 % of injected $SrCl_2$ in chloride medium is complexed by phosphate and only 1.4% by ascorbic acid. This might explain the success of Metastron in that it does not complex to the main *in vivo* chelator, citrate. Phosphate is used in the formation of hydroxy apatite but is a vital metabolic product in various other parts of the body. Although the tumours cells could be expected to have a higher metabolism and therefore would use more phosphate one would still expect a lower bone uptake than with diphosphonates, like ^{153}SmEDTMP, that are bone seekers par excellence. Robinson *et. al.* [97] have stated that Sm and Re diphosphonate compounds have a theoretical advantage over ^{89}Sr. It was hoped that APD would remain bound to Sr(II) in blood plasma and in this way enhance the bone uptake of Sr(II) using APD as its carrier. It is interesting to note that APD does not compete with phosphate at all although the formation constant for the species MLH in the complexation of Sr(II) by APD is 16.06. Phosphate however has a higher concentration (5 times) in blood plasma than APD.

Another aspect that makes Metastron less attractive is that it only emits β-rays. It is thus difficult to see if therapy reached the tumours and difficult to detect whether contamination occurs in hospitals. ^{153}Sm and ^{166}Ho are both γ-ray emitters and there is no problem detecting this. Another aspect is the long half-life of ^{89}Sr viz. 50.5 days. This means a patient is exposed to radiation for longer and has to be confined longer to hospital to avoid contamination. ^{153}Sm and ^{166}Ho have very short half-lives and once again minimising these effects.

4.5. Results from Baboon tests

The species distribution curves for APD and Ho(III) have been shown in the previous section. From this it is clear that APD will be present as the MLH complex at physiological pH. What is also evident is that Ho(III) is indeed bound by the ligand and should survive competition from blood plasma ligands. From a calculation with the program SPEC in the ESTA library, the species present at various pH values were calculated. The result at pH = 7.5 is include in Appendix H. The concentration taken for Ho(III) is 1 x 10^{-7} mol.dm^{-3} which is close to the concentration that would be injected. ^{166}Ho which is irradiated for 24 hrs has a high specific activity of 70 mCi per 2.5 mg Ho_2O_3 irradiated. If only 3 mCi is injected, the concentration in 1.9 L blood (baboon) is in the same region. This aspect that micrograms (100 μg) of a lanthanide (which is less toxic than other heavy metals) is injected for radiotherapy compared to chemotherapy where these heavy metals are used at milligram scale is the main reason why radiotherapy has little side effects if compared to chemotherapy.

The Ca(II) concentration was taken at 1 x 10^{-5} mol.dm^{-3} and 1 x 10^{-3} mol.dm^{-3} to verify that the ligand APD stays bound to the Ho(III). The ligand concentration is taken at 1 x 10^{-5} mol.dm^{-3}, a L:M ratio of 100:1. For both the concentrations of Ca(II), 99% of the Ho(III) stays bound to APD. Most of the Ca(II) stays as the free metal ion, while 2-3 % is bound to APD. 1% of the APD is bound to Ho(III) as expected from the 100:1 ratio. This theoretical evidence is supported by paper chromatography at high pH where ML is the dominant species. At physiological pH we know MLH is the dominant species and paper chromatography cannot distinguish between undissolved and uncomplexed species. Appendix H shows both these chromatograms. This result was achieved for both running solutions used. The sephadex column however provided the evidence that the Ho(III) is indeed complexed to APD. 96% of the activity was washed out by a saline solution indicating that the Ho(III) is not retained by the resin.

With both the theoretical and laboratory evidence proving that complexation does indeed occur an application was submitted to the ethical committee for a baboon test. Permission was granted and a solution consisting of 3.25 mCi ^{166}HoAPD was injected into baboon P20/92. The results are shown in recorded static images at 2 and 3 hours after injection, displayed in Photo 6 and 7 which do not differ very much. In each image three areas are covered viz. head, chest and pelvis. The red areas correspond to the tissue where the highest uptake of radiation

occurred. There seems to be a high bone uptake because the shoulder-knots, spine and some ribs are clearly visible. Because ^{166}Ho has a weak γ-ray (80 keV), a great amount of scatter occurs when an image of the emitted radiation of this isotope is recorded. A ray of this low energy is scattered by the tissue as it travels through it on its way to the camera.

Photo 6. Static γ-image recorded 2 hours after administration of ^{166}HoAPD.

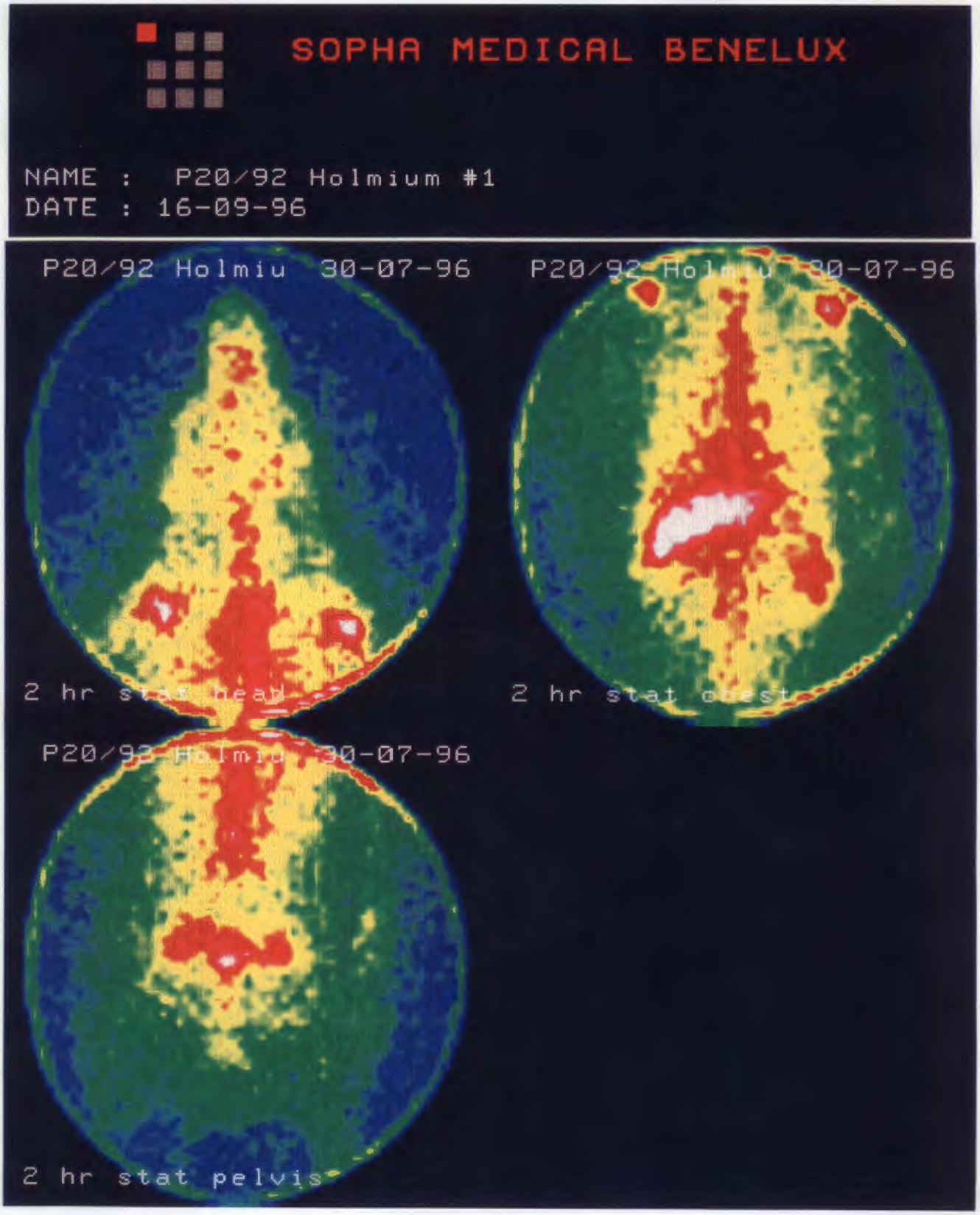

Photo 7. Static γ-image recorded 3 hours after administration of ^{166}HoAPD The images were recorded for the head, chest and pelvis. Note the white area in the image on the right which corresponds to the high uptake in the liver.

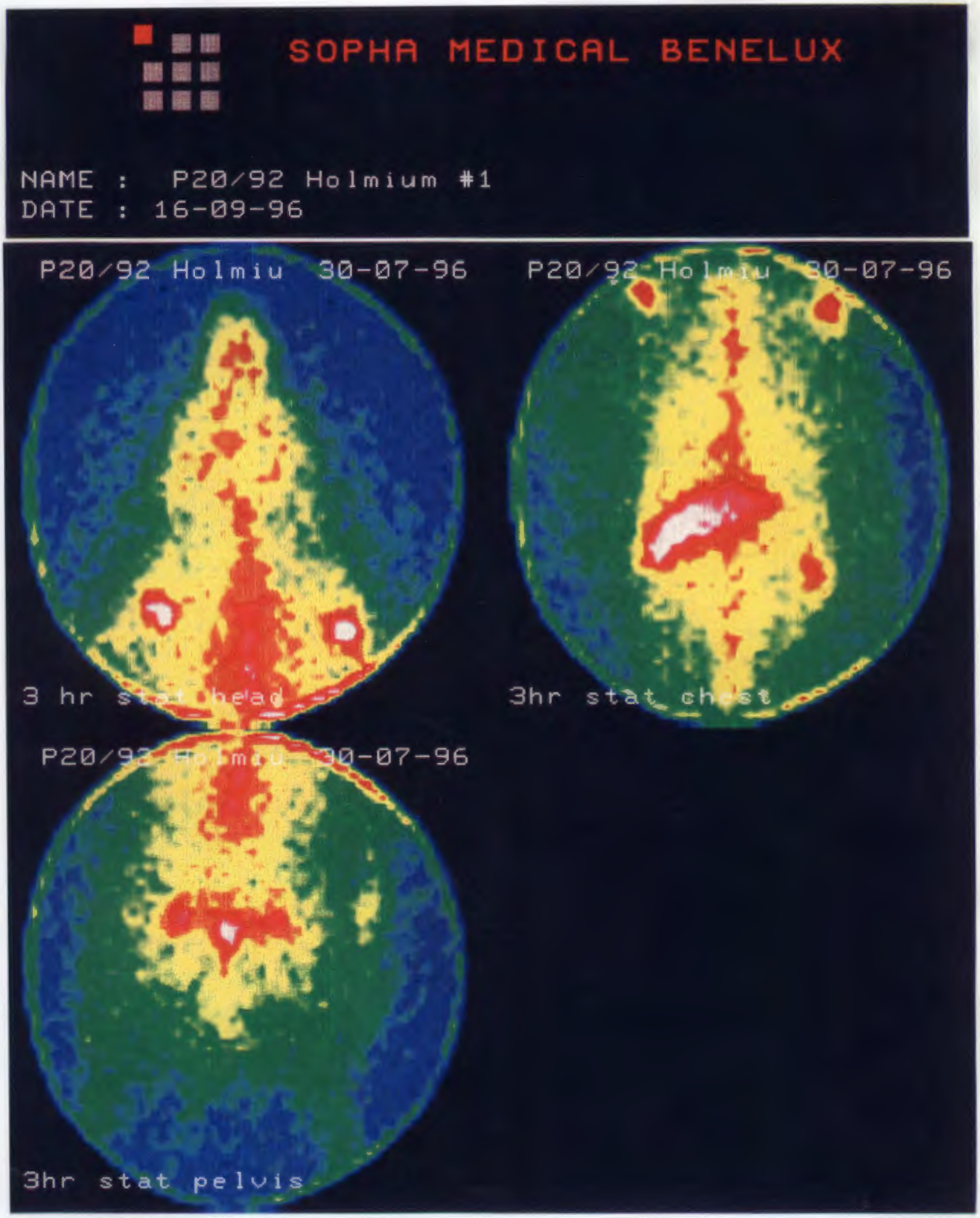

This results in an indistinct radiation pattern near the edges of the bone as was the case with ^{166}HoEDTMP. This is not only due to low bone uptake but the scatter of the γ-ray also contributes to an unclear picture. It is not possible to expect the sharp diference between bone and muscle as was achieved by ^{153}Sm and ^{99m}Tc (both have higher energy γ-rays). From ECCLES modelling it is evident that the competition of citrate with APD causes a bone uptake lower than that for ^{153}SmEDTMP. This together with the scattering explains the unclear picture above.

The interesting aspect visible is that a fair amount of radiation locates in the liver (second image). This is unfortunate because this liver uptake is unacceptable for any radiopharmaceutical designed for bone uptake and thus rules out the possibility that APD will be an effective carrier of Ho(III) to the bone. However, this liver uptake correlates well with that predicted by ECCLES. ECCLES predicted that MLH (HoAPD(H)) would be the dominant species at pH = 7.4 with 58% of the Ho(III) in this form. This is a neutral species as APD has a charge of -4. Because of the neutrality, a precipitation would be expected at higher concentrations. The low concentrations used here, 1 x 10^{-7} mol.dm^{-3}, probably prevents precipitation. Colloid formation may be possible. The liver filters and captures a great amount of these colloids. It is gratifying that the predictions by ECCLES are proved in practise. Uptake in the liver was expected even before the baboon test. The baboon test provided the evidence that this interpretation of the data produced by ECCLES was indeed correct.

The same is true for HEDP and MDP thus explaining why Simon *et. al.* of Dow Chemical Co. [74] found a high liver uptake in experiments done with these two ligands together with ^{153}Sm. They reported that 4 % of the total activity for ^{153}SmHEDP ended in the liver, where as 21 % went to the bone and 13 % remained in the blood. The rest must be in the kidneys and urine. For ^{153}SmMDP the liver uptake was 85 %, 2% in the bone and 0.2% remained in the blood. From the species distrubution curves (Section 4.1.3 and 4.1.4) and ECCLES modelling (Section 4.3) of these two ligands it is once again evident that the *in vivo* behaviour of radiopharmaceuticals and other drugs can be accuratedly predicted by ECCLES.

The dominant species at pH = 7.4 is the MLH species. This is for all these ligands a neutral species. One would expect with HEDP and MDP colloid formation and an uptake in the liver.

ECCLES once again proved that it is a very useful tool for the bioinorganic chemist, reducing the number of tests on animals and delivering an estimate of the result expected making it easier for the ethical committee to grant permission.

From the static images it is possible to calculate an estimate of the compartmental uptake in the three major areas in the body viz. bone, kidney and liver. This was done by comparing the activity recorded by the γ-camera on a certain organ and that in the soft tissue right next to it. The latter is taken as the background. For the bone three areas are used viz. head, spine and pelvis. For the kidney the left and right kidney are compared with the background and the liver on its own. The average activity for the bone, kidney and liver vs background and the resulting percent uptake in each of the organs vs background, after two hours, are reported in Table 35. The percentage compartemental uptake is calculated to compare the uptake in the different organs. The latter is only a indication if the data from which it is derived is considered. The background is calculated from tissue right next to the bone for instance. As explained, the scatter of ^{166}Ho's γ-ray will contribute to this factor, lowering the percentage uptake. Another contributing factor is the colloid form of the complex when moving through the body. This will result in a higher background recorded as the mobility of the complex is lower and more will be trapped in the tissue surrounding the bone.

Table 35. Percentage uptake in various organs of the baboon

Area	Activity	Background	% uptake	% compartemental uptake
Bone	461	333	58.1	26.3
Kidney	342	244	58.4	29.3
Liver	259	120	68.3	44.4

The only way to find a true reflextion of where the activity ended up is to do test with mice which are disected three hours after injection. Here an accurate measurement of the activity in various organs can be made. The result of such a test will be more correct.

During the baboon tests blood and urine samples were taken at various intervals. The blood samples were 2ml in volume. The blood volume of a baboon is calculated by the following equation : $V = 75.5 \text{ ml/kg} * m$ where m is the mass of the animal in kg. In our case this gives a total blood volume of 1.8 L. Fig. 67 contains the normalised blood activity curve for ^{166}HoAPD, ^{153}SmEDTMP and ^{166}HoEDTMP. The curve for ^{166}HoAPD is not very smooth as the other two (Louw *et. al.* [6]) because it is not an average of seven animals that is

taken. The curve for ^{166}HoAPD shows a fast blood clearance although it seems incomplete. In [6] the curves shown are also fitted at three hours, showing a lower activity than the data point would suggest. If ^{166}HoAPD is compared to ^{153}SmEDTMP the blood clearance is not as fast but beter than ^{166}HoEDTMP which had a slow blood clearance indicating an incomplete adsorption on the bone.

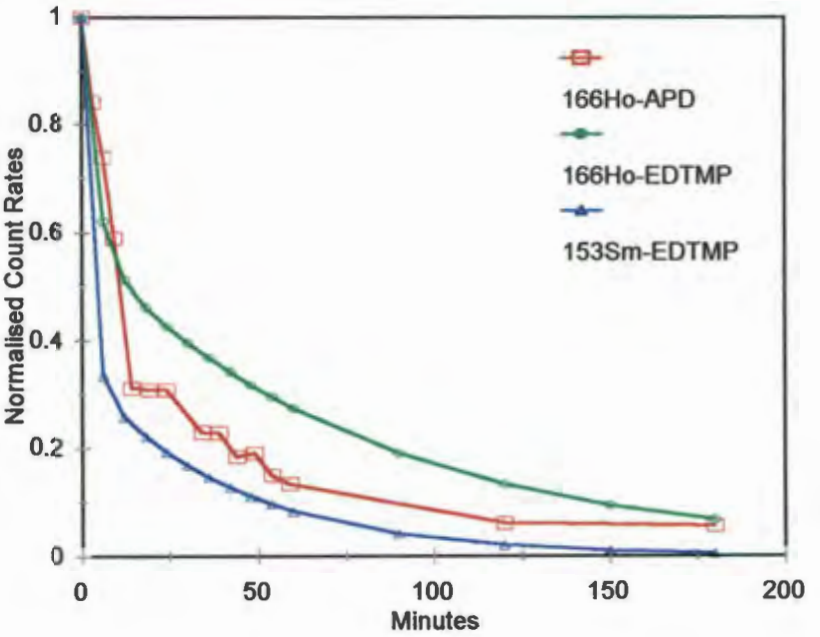

Figure 67. Normalised blood clearance curves for ^{166}HoAPD, ^{166}HoEDTMP and ^{153}HoEDTMP

The size of the urine samples are not standard because the bladder is emptied at specific times. Fig. 68 therefore shows the total accumulated activity taken from the bladder up till that point in time. These curves are normalised to the total activity injected in the blood. For ^{166}HoAPD it is a climbing curve almost flattening after two hours. For ^{153}SmEDTMP and ^{166}HoEDTMP the curves are smooth and higher. The reason for this is that with ^{166}HoAPD a high liver uptake occured leaving less activity to escape from the body. It is encouraging that a big portion of the activity found in the liver can be subtracted here. This indicates that more or less the same activity as for ^{153}SmEDTMP and ^{166}HoEDTMP gathered in the bone.

If the fit is displayed as activity per ml (Fig. 69) vs time a peak is found after 40 minutes. After two hours little more activity is excreted. This is in agreement with the blood curve which shows in this area that low levels of activity remained in the blood. At this time no additional activity is transferred to the bladder via the blood stream but should remain in the liver and bone.

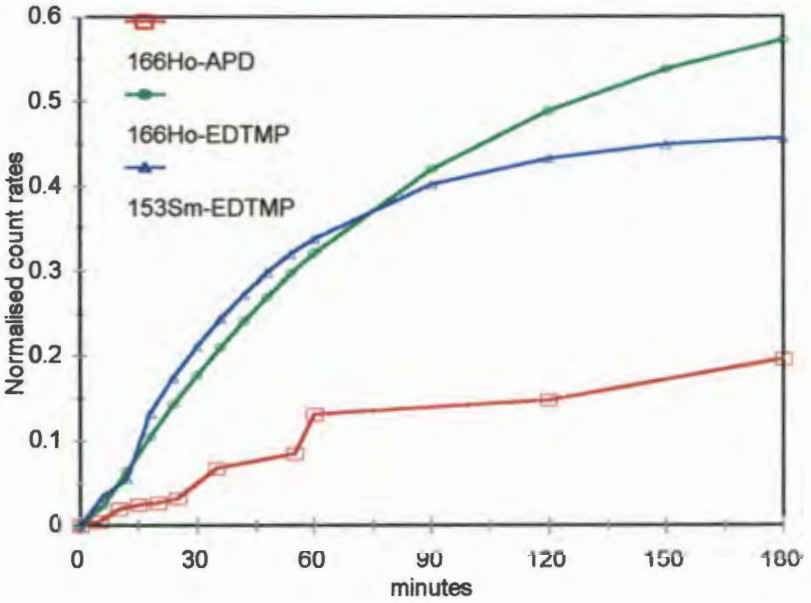

Figure 68. Normalised urine accumilation curve for for ^{166}HoAPD, ^{166}HoEDTMP and ^{153}HoEDTMP. Note the significant difference in height for ^{166}HoAPD.

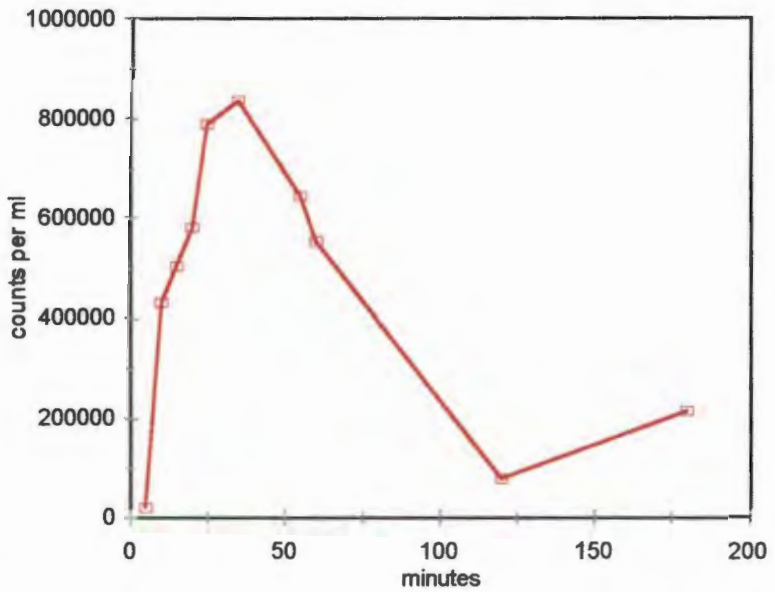

Figure 69. Counts per ml excreted in urine vs time. After 100 miutes most of the activity is excreted.

Rat tests

To confirm the results gathered with baboon tests and to verify the percentage bone uptake, rat tests were performed. ^{166}HoAPD was prepared as before and a dose of 1.64 mCi was injected in each of five rats. The rats were dissected after 24 hours and various parts of the body were weighed and their activity counted in an ionisation chamber. The results are presented in Table 36. To compare these results, a study of ^{166}HoEDTMP was done in parallel and previously found values for ^{153}SmEDTMP [6] are included. Although only certain sections of some organs, for instance only the femur was taken to represent bone, were counted, the percentage reported was calculated per gram of the tissue measured. The percentage reported is expressed in terms of the total activity injected. Corrections were made for decay of ^{166}Ho.

Table 36. Percentage uptake in various organs of rats.

Area	% uptake of injected activity per gram after 24 hours		
	^{166}HoAPD	^{166}HoEDTMP	^{153}SmEDTMP
Bone	0.310	0.903	1.72
Tissue around bone	0.026	0.009	-
Liver	1.815	0.005	-
Heart	0.080	0.004	-
Blood	0.203	0.002	-

Table 36 confirms the high liver uptake for ^{166}HoAPD. The bone to tissue ratio however is 10:1. This indicates a higher bone uptake (90%) than that calculated from the scintigraphic images for the baboon tests. This is however not three hours but 24 hours after injection. A great amount of activity has been washed out of the tissue into the urine by this time. A better comparison with the baboon tests would have been after three hours. Then no comparison with ^{153}SmEDTMP would have been possible which is essential as the metabolism of rats and baboons differ. For ^{166}HoEDTMP the ratio is even 100:1 indicating 99% uptake. One has to compare the 0.9% per gram of the injected dose located in the bone with that for ^{153}SmEDTMP viz. 1.72%. This shows that twice as much of the ^{166}Ho-activity is lost. This is due to the competition of citrate with EDTMP for Ho(III) preventing the uptake of ^{166}Ho in

the bone. Citrate locates its portion during this long time in the bladder where it is excreted. The final percentage per gram is thus lower.

For ^{166}HoAPD the bone uptake is only 0.3% of injected dose per gram. This is due to the high content in the blood (this also causes the activity in the tissue to be higher than expected) which could be the neutral species which is not caught by the liver. Because of the time waited one cannot propose that the bone uptake for ^{166}HoAPD is weaker than ^{166}HoEDTMP especially when baboon tests showed the contrary.

What is proved by this experiment is that the scatter of the weak γ-ray which ^{166}Ho emits contributes to a lower reported bone uptake gathered from scintigraphic images of baboons. Furthermore ^{166}HoAPD has a definite high liver uptake.

5. Future work

From the above it is clear that ^{166}HoAPD has a very promising bone uptake but due to the liver uptake it will not be an acceptable radiopharmaceutical. The reason for this, as described earlier, lies in the neutral species MLH that forms at physiological pH. If this problem could be overcome, clinical trial on humans may be pursued. One way to change the neutrality of the complex is to change the ligand slightly, not effecting the complexation centre but adding a charged group or groups. The ligand will then be more negatively charged and the complex MLH will have a negative charge.

Examples of what groups might be added are discussed next:

The first shows a Mannich reaction with APD to form a tetraphosphonate APDDMP (APD dimethylenephophonate).

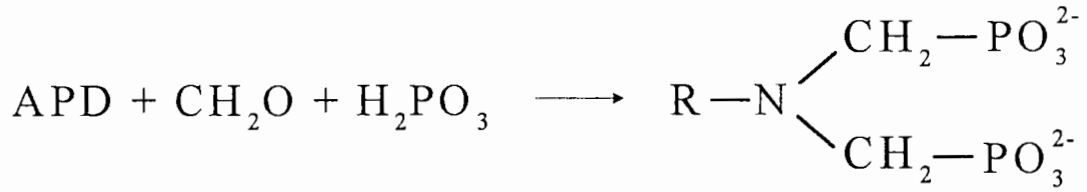

The new phosphonate groups (R = the rest of the APD molecule except for the amino group) may even take part in the complexation, improving the formation constants. The second alternative is to add a carboxyl group.

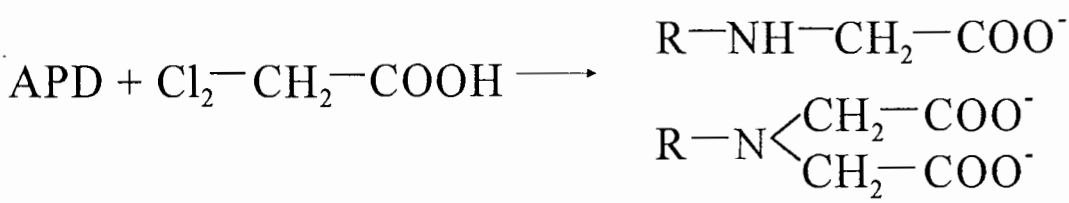

Here the product depends on whether one or two equivalent moles of reagent are used. Various other reagents like ethylene-oxide can also be used. Whether the complexation with each of these proposed ligands is strong enough can only be found by potentiometric titrations and ECCLES modelling.

Polarographic titrations.

It would be preferable to actually measure the formation constants for Ho(III) and Sm(III) with the various ligands. As potentiometry is not suitable, other techniques should be used. Lanthanides are not polarographically active but by means of competition between the lanthanide and another metal ions it might be possible to determine the formation constant with this technique. A metal ion is needed that is polarographically active and from which a high formation constant is expected (of the same order of magnitude as Sm(III) and Ho(III)). Cd(II) has a formation constant a few orders lower than these and will not be a suitable competitor for the ligand. Another possible metal ion is Pb(II), but unfortunately it forms a precipitate with the ligand at pH = 4.5 even at low concentrations. Another metal ion is Bi(III) but it has a very high acidity, limiting the area of study to the low pH range. Some other options are Sn(II) and Cu(II)

Another possible technique for measuring the Ho(III) and Sm(III) equilibria is spectrophotometry, but the ligands have no colour and are not UV active, therefore direct measurement is also not possible. Competition with another spectoscopically active ligand might be an option.

Crystal structures

To understand more the structures that the diphosphonate ligands upon complexation, a crystal structure is important. This is especially so for APD where there are some unexplained results (Section 4.3). The precipitate that forms during the potentiometric titrations of Zn(II) with APD may be isolated, analysed and crystallised. The precipitate might be re-crystallised out of solutions like methanol and acetonitrile.

In all these studies, the objective is to gain a greater insight into the complexation and *in vivo* speciation of Ho(III) so that better radiopharmaceuticals may be produced.

6. Conclusion

In this dissertation the main objective was to find a radiopharmaceutical which would employ ^{166}Ho(III) as its β-emitter to improve on the pain palliative effectiveness of radiopharmaceuticals like ^{153}SmEDTMP used in the treatment of bone cancer. This search involved three diphosphonate ligands viz. APD, MDP and HEDP which were studied to find whether they would selectively carry ^{166}Ho(III) to bone tissue. To achieve this one needs to know the formation constants for the complexation of Ca(II) and Mg(II), Zn(II) and Ho(III) with the ligands and use this information in a blood plasma model to predict the speciation of the proposed radiopharmaceutical. Glass electrode potentiometry was used to measure the formation constant for the complexation of Ca(II) and Mg(II) with all three ligands as well as the complexation of Ni(II), Sr(II), Cd(II), Sm(III) and Ho(III) with some of these ligands. An additional technique, polarography was used to calculated formation constants for the complexation of Zn(II) with all the ligands as precipitation occurred in these during the potentiometric study. The complexation of Cd(II) by HEDP was used to compare the two techniques and showed that the values found by both techniques are comparable. Where constants were found in literature good agreement with the measured constants was achieved. For the complexation of Sm(III) and Ho(III) by these ligands, a linear free energy relationship was employed to calculate the first formation constants. The previously found values were used in this relationship and provided some proof that the first formation constants (for each ligand) reported here, correlate well with each other as well as with literature values.

The speciation of Ho(III) and Sm(III) with these three ligands in blood plasma was then calculated by the program ECCLES using the constants determined in this study, together with the published blood plasma database [35]. The results suggested that Ho(III) and APD is a very promising systems. For the other ligands the results were not favourable. The ECCLES output was used as evidence in an application to an ethical committee before animal testing. A baboon test was carried out using ^{166}HoAPD. As in the case with HEDP and MDP (complexed to ^{153}Sm(III)), that have been tested before by others [43], a high liver uptake was recorded. However ^{166}HoAPD showed none-the-less a high bone uptake and fast blood clearance. These results were confirmed by rat tests with ^{166}HoAPD.

Based on the ECCLES results, the reason for this liver uptake is postulated to be a neutral species, MLH, forming at physiological pH. Furthermore the comparison between the radiopharmaceuticals ^{153}SmEDTMP, ^{166}HoAPD and ^{166}HoEDTMP (in decreasing order of bone uptake as measured in animal tests) could be reproduced by ECCLES modelling. The results showed that APD competes less effective for ^{166}Ho in blood plasma than EDTMP competes for ^{153}Sm but APD competes better for ^{166}Ho in blood plasma than EDTMP does.

The working of another existing radiopharmaceutical,Metastron ($^{9}SrCl_2$) could also be explained by ECCLES.

The main reason why only APD seemed suitable as a ligand for complexing Ho(III) is the higher formation constants of APD. The APD formation constants are higher than HEDP which are in turn higher than those of MDP. NMR studies were attempted on some complexes in solution to investigate the role of the hydroxy group (APD and HEDP) in complexation as it is believed that when taking part, it improves complexation. The complex however changes its structure at a rate faster than the NMR time scale delivering little useful information. From the strength of complexation for these ligands with various metal ions it is none-the-less postulated that the hydroxy group in HEDP as well as the amino group in APD takes part in complexation. As it is impossible for APD to be a tetradentate ligand; the hydroxy and amino group cannot be bound to an octrahedral metal ion at the same time. The hydroxy group might thus be bound to a second metal ion. This resulted in an idea on the structure for the most interesting species, M_2L, which is not found very often in literature but occurs frequently in the complexation of these ligands with the metal ions used. Polarography provided some clear evidence that this species indeed does exists. It was the first time that formation constants for a polynuclear species have been measured using this technique. It was also the first time in polarography that formation constants for non-labile species could be calculated using only peak potentials and peak heights for the labile part.

Although the main objective, to find a new radiopharmaceutical, was not reached, as ^{166}HoAPD is ineffective as a therapeutic agent due to its high liver uptake, it is now possible to design new ligands who might sustain the high bone uptake capabilities of APD but avoid its liver uptake.

7. References

1. I.C. Dormehl, W.K.A. Louw, N. Hugo, G.H. Beveley, A. Sweetlove and O.Knoesen, '^{153}Sm-EDTMP and ^{166}Ho-EDTMP as Systemic Radioisotopic Bone Therapeutic Agents: Experimental Pharmacokinetic and Biodistribution Studies in the Baboon Model', presented at the European Association of Nuclear Medcine Congress, Lausanne, Switserland, October 1993.
2. F. Hosain and R.P. Spencer, *Seminars in Nucl. Med.*,1992, **22**, No. 1, 11.
3. P.M. Boonenkamp *et. al.*, *Bone. Min.*, 1987, **2**, 29.
4. E.B. Silberstein, *Seminaars in Oncology.*,1993, **20**, No. 3, Suppl. 2, 10.
5. J.M. Wagner, N.V. Jarvis, *S. Afr. J. Chem.*,1995, **48**, 85.
6. W.K.A. Louw, I.C. Dormehl, A.J. van Rensburg, N. Hugo, A.S. Alberts, O.E. Forsyth, G. Beveley, M.A. Sweetlove, J. Marais, L.G. Lotter and A. van Aswegen, *Nucl. Med. and Biol.*, accepted for publication., 1996.
7. N.V. Jarvis, J.M. Wagner and G.E. Jackson, *J. Chem. Soc. Dalton Trans.*, 1995,1411.
8. R.G. Robinson, *J. Nucl. Med.* 1990, **31**, 1326.
9. R.J. Rumper, U. Yon Ryo and M.Jay, *J. Nucl. Med.*, 1991, **32**, No. 11, 2139.
10. A. Schoutens *et. al.*, *Calsified Tissue International*, 1988, **42**, 136.
11. B. Thürlimann, R. Morant, W.F. Jungi and A. Radziwill, *Support Care Cancer*, 1994, **2**, 61.
12. E. Deutsch, K. Lisbon and J.L. van der Heyden, 'Tc-99m Myocardial Imaging Agent' presented at the 2nd International Symposium on Technesium, Padua, Italy, September 1985.
13. T.G. Tji, H.A. Vink, W.J. Gelsema and C.J. de Ligny, *Appl. Radiat. Isot.*, 1990, **41**, No. 1, 17.
14. P.A. Dormstadt *et. al.*, *Radiology*, 1980, **136**, 209.
15. J.A. Bevan, A.J. Tofe, J.J. Benedict, M.D. Francis and B.L. Barnett, J. Nucl. Med., 1980, **21**, 961.
16. O.J. Degrossi, P. Oliveri, H.G. Del Rio, R. Labriola, D. Artagaveytia and E.B.Degrossi, *J. Nucl. Med.*, 1985, **26,** No. 10, 1135.
17. M.R.A. Khairi, P. Meunier, C. Edouard, *Calc. Tiss. Res.*, 1977, **22**, (Suppl) 355.
18. H.R. Mascon *et.al.*, *Seminars in Nucl. Med.*, 1992, **22**, No. 1, 33

19. M. Eisenhut, *Int. Jour. of Appl. Rad. and Iso.*, 1982, **33**, 99.

20. D. Chirby, S. Franck and D.E. Troutner, *Appl. Radiat. Isot.*, 1988, **39**, No. 6, 495.

21. W.F. Goeckeler, D.E. Troutner, W.A. Volkert, B. Edwards, J. Simon and D. Wilson, *Nucl. Med. Biol.*, 1986, **13**, 479.

22. D.M. Taylor and D.R. Williams,Trace Element Medcine and Chelation Therapy, 1995, The Royal Society of Chemistry, Cambridge.

23. J.R. Duffield and D.R. Williams, *Chemistry in Britain*, April 1989.

24. P. Vohra and F.H. Kratzer, *Poultry Sci.*, 1968, **47**, 699.

25. G.K.R. Makar and D.R. Williams, *J. Inorg. Nucl. Chem.*, 1977, **39**, 201.

26. J.A. Findlow *et. al.*, Proceedings of the third international conference on Bioinorganic Chemistry., *Rev. Trav. Chim. Pays Basque*, 1987, **106**, 403.

27. G.L. Christie, PhD thesis, University of Wales, 1983.

28. D.C. Jones, G.L. Smith, P.M. May and D.R. Williams, *Inorg. Chim. Acta*, 1984, **93**, 93.

29. Z.X. Huang *et. al.*, *Agents Actions*, 1982, **12**, 536.

30. H.J. Smith and H. Williams, Introdution to the Principles of Drug Design, 2nd edn., J. Wright, 1988, Essex..

31. S.R. Hurford *et. al.*, *Rev. Port. Quim.*, 1985, **27**, 423.

32. J.R. Duffield, P.M. May and D.R. Williams, *J. Inorg. Biochem.*,1984, **20**, 199.

33. D.R. Williams, *Analytical Proceedings*, 1989, **26**, 162.

34. N.V. Jarvis, P.W. Linder and P.W. Wade, 'Plutonium in the Marine Environment', presented at the Royal Soceity of SA., Cape Town, South Africa May 1994.

35. P.M. May, P.W. Linder and D.R. Williams, *J. Chem. Soc. Dalton Trans.*, 1977,588

36. G. Eichhorn, 'Inorganic Biochemistry', Elsevier, Amsterdam,1973.

37. W.A. Volkert *et. al.*, *J. Nucl. Med.*, 1991, **32**, 174.

38. I. Cukrowski *et. al.*, *Polyhedron*, 1995, **14**, No. 12, 1661.

39. P. Letkeman, *J. Chem. Edu.*, 1996, **73**, No. 2, 165.

40. Von K. H. Worms, H. Blum, H.U. Hempel, *Z. Anorg. Allg. Chem.*, 1979, **457**,214.

41. P.M. May, K. Murray, D.R. Williams, *Talanta*, 1988, **35**, No. 11, 825 and references therein.

42. A.E. Martell, R. M. Smith, Critical Stability Constants, Vol 3, Plenum, New York, 2nd print; 1989.

43. J. Simon, D.A. Wilson, J.R. Garlich and D.E. Troutner, Patent 899734, Dow Chemical Company, 1989.

44. I.C. Dormehl, W.K.A. Louw, N. Hugo, I. F. Redelinghuys and P.J. Fourie, *Am. J. Phys Imaging*, 1991, **6**, 176.

45. W.F.Goeckeler, B. Edwards, W.A. Volkert, R.A. Holmes, J. Simon and D. Wilson, *J. Nucl. Med.*, 1987, **28**, 495.

46. I.C. Dormehl, N. Hugo, G. Beverley, *Anesthesia & Pain Control in Dentistry*, 1992, **1**, No. 2, 109.

47. P.M. May, K. Murray and D.R. Williams, *Talanta*, 1988, **35**, No. 11, 823.

48. P.M. May, K. Murray and D.R. Williams, *Talanta*, 1985, **32**, No. 6, 483.

49. P.M. May, K. Murray and D.R. Williams, *Talanta*, 1988, **35**, No. 12, 927.

50. L.G. Sillén, *Acta Chem. Scand.*, 1964, **18**, 1085.

51. A. Sabatini, A. Vacca and P. Gans, *Talanta*, 1974, **21**, 53.

52. G. Eisenman, *Biophys. J.*, 1962, **2**, 259.

53. G. Briederman and L.G. Sillén, *Ark. Kemi*, 1953, **5**, 425.

54. P. Henderson, *Z. Phys. Chem.*, 1907, **59**, 118, 1908, **63**, 325.

55. N. Ingri, W. Kakolowics, L.G. Sillén and B. Warnqvist, *Talanta*, 1969, **14**, 1261; corrections, 1970, **15**, No. 3, p. xi.

56. M. Davies and I.J. Whiting in *Numerical Methods for Non-Linear Optimisation*, F.A. Lootsma (ed.), p 191. Academic Press, London, 1975.

57. J.J. Lingane, *Chem. Rev.*, 1941, **29**, 1.

58. J.F. Fisher and J. L. Hall, *Analyt. Chem.*, 1967, **39**, 1550.

59. J.F. Fisher, *ibid.*, 1962, **34**, 1094.

60. I. Cukrowski, E. Cukrowski, R.D. Hancock and G Anderegg, *Anal. Chim. Acta*, 1995, **312**, 307.

61. H.G. Langer, *Inorg. Chem.*, 1963, **2**, 1080.

62. D.T. Sawyer, J.E. Tackett, *J. Am. Chem. Soc.*, 1963, **85**, 309.

63. P.Letkeman, *J. Chem. Edu.*, 1979, **56**, No. 5, 348.

64. G.E. Jackson, *S. Afr. J. Chem.*, 1982, **35**, No. 3, 89.

65. K. Sawada, T. Araki, T. Suzuki and *K. Doi, Inorg. Chem.*, 1989, **28**, 2687.

66. N.V. Jarvis, *Solv. Extr. Ion Exch.*, 1991, **9**, No. 4, 697.

67. P.Letkeman, *J. Chem. Edu.*, 1996, **73**, 165.

68. D.R. Williams et. al., *Experentia*, 1976, **32**, No. 12, 1492.

69. P.M. May et.al., *J Chem. Soc. Dalton Trans.*, 1977, 588.

70. D.D. Perrin and I.G. Sayce, *Talanta*, 1967, **14**, 833.

71. H. Sigel, *J. Inorg. Nucl. Chem.*, 1975, **37**, 507.

72. P.S. Hallman, D.D. Perrin and A.E. Watt, *Biochem. J.*, 1971, **121**, 549.

73. Y. Marcus and I. Eliezer, *Co-ordination Chem. Rev.*, 1969, **4**, 273.

74. V.S. Sharma and J. Schubert, *J. Chem. Educ.*, 1969, **46**, 506.

75. J.H. Lin, *Bone*, 1996, **18**, No.2, 75.

76. I.C. Dormehl *et. al.*, *Nucl. Med. Comm.*, 1987, **8**, 803.

77. J.P. Pretorius et. al., 'The influence of tachycardia during shock on changes in cardiac volumes, Vienna Shock Forum, New York, 1989.

78. N. Parks et. al., *Blood*, 1993, **82**, No. 1, 318.

79. M.I. Kabachnik *et. al.*, *Bull. Acad. Sci. USSR.*, 1978, **27**, 374(433).

80. A.E. Martell and R. M. Smith, Critical Stability Constants, Vol. 6, Plenum, New York, 2nd ed. 1989, p 363.

81. P. Dietsche, T. Günther and M. Röhnelt, *Z. Naturforsch*,1976, **31c**, 661.

82. K.L. Nash and E.P. Horwitz, *Inorg. Chim. Acta*, 1990, **169**, 245.

83. A.E. Martell and R. M. Smith, Critical Stability Constants, Vol. 6, Plenum, New York, 2nd ed. 1989, p 361.

84. J.G.M. van der Linden and R.A.M.J. Claessens, *J. Inorg. Biochem.*, 1984, **21**, 73.

85. R.J. Grabenstetter, O.T. Quimby and T.J. Flautt, *J. Phys. Chem.*, 1967, **71**, 4195.

86. C. De Stefano, C. Foti and A. Gianguzza, *J. Chem. Research (S)*, 1994, 464.

87. H. Irving and R.J.P. Williams, *Nature*, 1948, **162**, 746.

88. R.L. Carroll and R.R. Iran, *J. Inorg. Nucl. Chem.*, 1968, **30**, 2971.

89. H.Wada and Q. Fernando, *Anal. Chem.*, 1972, **44**, No. 9, 1640.

90. N.V. Jarvis and J.M. Wagner, *Talanta*, 1994, **41**, No. 5, 747.

91. A.E. Martell and R. M. Smith, Critical Stability Constants, Vol. 4, Plenum, New York, 2nd print, 1989.

92. R.D. Hancock and A.E. Martell, *Chem. Rev.*, 1989, **89**, 1875.

93. J.R. Zeevaart and N.V. Jarvis, *unpublished work.*

94. K. Murray and P.M. May, Equilibrium Simulation for Titration Analysis Version 3.0, March 1989, (Manuaul included with the computer program ESTA).

95. M. Neves, M. Reis, F. Waerenborgh, E. Martinho and L. Patricio, *Inorg. Chim. Acta*, 1987, **140**, 359.

96. A.I. Porter *et. al.*, *Int. J. Radiation Oncology Biol. Phys.*, 1993, **25**, No. 5, 803.

97. R.G. Robinson, D.F. Preston, J.A. Spicer and K.G. Baxter, *Seminars in Nucl. Med.*, 1992, **22**, No. 1, 28.

98. J. Oakes and E.G. Smith, *J. Chem. Soc. Dalton Trans.*, 1983, 601.

99. L. Carlton, Personal Communications.

100. H. Li, C. Hardin, B.R. Shaw, *J. Am. Chem. Soc.*, 1996, **118**, 6606.

101. T.A. Modro, Personal Communications.

102. I. Cukowski, *Analytica Chimica Acta*, 1996, **336**, 23.

103. R.J.P. Williams, *Structure and Bonding*, 1982, **50**, 81-119

8. Appendixes

Appendix A1 : Theory

Appendix A2 : Theory

Appendix B0 : Summary of protonation and formation constants calculated by the three techniques used.

Appendix B1 : ESTA2A input files for E0-titrations

Appendix B2 : ESTA2A input files for protonation titrations

Appendix B3 : ESTA2A input files for complexation titrations with APD

Appendix B4 : ESTA2A input files for complexation titrations with MDP

Appendix B5 : ESTA2A input files for complexation titrations with HEDP

Appendix C1 : Titration data points of protonation titrations

Appendix C2 : Titration data points of complexation titrations with APD

Appendix C3 : Titration data points of complexation titrations with MDP

Appendix C4 : Titration data points of complexation titrations with HEDP

Appendix D1 : Polarographic titration data points for HEDP-Cd(II)

Appendix D2 : Polarographic titration data points for HEDP-Zn(II)

Appendix D3 : Polarographic titration data points for MDP-Zn(II)

Appendix D4 : Polarographic titration data points for APD-Zn(II)

Appendix E1 : Polarographic titration curves for HEDP-Cd(II)

Appendix E2 : Polarographic titration curves for HEDP-Zn(II)

Appendix E3 : Polarographic titration curves for MDP-Zn(II)

Appendix E4 : Polarographic titration curves for APD-Zn(II)

Appendix F : NMR spectra

Appendix G : ECCLES output

Appendix G1: ECCLES input files

Appendix H : Blood and Urine values

APPENDIX A1

T_i^c = calculated total concentration of component i

T_i^r = real (analytical) concentration of compenent i

$[X_i]$ = free concentration of component i

$[C_j]$ = concentration of complex j

$[S_i]$ = concentration of species i (component or complex)

$\{S_i\}$ = activity of species i (component or complex)

$\{S_i^s\}$, $\{S_i^b\}$ = activity of species i in the test solution and bridge solution, respectively

γ_i = activity coefficient of species i

β_j = thermodynamic formation constant of complex j

r_{ji} = stoichiometric coefficient of component i in complex j

NC = number of components appearing in complexes

NB = number of burettes

C_i^v = initial concentration of component i in titration vessel

C_{im}^B = concentration of component i in solution in burette m

v_m = volume added from burette m

V° = initial volume in vessel

s_k = electrode response slope

K_{ki} = selectivity coefficient of component i

z_i = charge on species i

R = the gas constant

T = absolute temperature

F = Faraday constant

I = ionic strengh

λ_i^S = ionic conductance of species i in the test solution

λ_i^b = ionic conductance of species i in the bridge solution

å = ionic size parameter

A, B = parameters in the Debye-Hückel equation

U = objective function to be minimized

R^H = Hamilton factor

n_p = number of parameters to be optimized

n_e = total number of electrodes

w_{nq} = weight of qth residual at nth point

y_{nq}^{obs} = observed variable of qth residual at nth point

y_{nq}^{calc} = calculated variable of qht residual at nth point

G = inverse Hessian

σ_r = standard deviations of the rth optimized parameter

r_{sr} = correlation coefficient of parameters s and r

APPENDIX A2

Meanings of symbols—*(a) Concentrations.*

S = the concentration of a complex species

X = the concentration of a component

T = the total concentration of a component

(b) Indices

i = the general index for components

j = the general index for complex species

m = the specific component index

p = the index for a metal ion component

q = the index for a ligand component

r = the index for a hydrogen ion component

(c) Superscripts.

c denotes a 'calculated' quantity

r denotes a 'real' quantity

o denotes an 'old' value in an iteration

n denotes a 'new' value in an iteration

(d) Parameters

k = the matix which defines the components and their multiplicity in a complex species.

M, L, H, β_{pqr} have their usual meaning.

Appendix BO

Table 1. Protonation and formation constants (log K) for MDP, HEDP and APD at 37 °C and I = 0.15 M NaCl.

Metal ion	Equilibrium	MDP	HEDP	APD	Method
H^+	$H + L = HL$	9.97(1)	10.11(1)	10.95(2)	Potentiometry
	$H + HL = H_2L$	7.00(1)	6.81(1)	9.80(2)	
	$H + H_2L = H_3L$	3.26(2)	2.97(1)	6.01(2)	
	$H + H_3L = H_4L$	2.19(5)	2.35(2)	2.56(3)	
	$6H + L = H_6L$	27.55(5)	26.98(2)		
Ca(II)	$M + L = ML$	4.86(2)	5.34(1)	6.70(2)	Potentiometry
	$ML + H = MLH$	7.83(3)	7.83(2)	10.51(3)	
	$ML + M = M_2L$	3.53(4)	4.19(2)	12.46(3)	
	$MLH + H = MLH_2$			6.80(3)	
	$M_2L + H = M_2LH$			8.50(4)	
Mg(II)	$M + L = ML$	5.68(1)	6.03(2)	7.03(3)	Potentiometry
	$ML + H = MLH$	7.56(2)	7.48(3)	10.24(3)	
	$ML + M = M_2L$	2.68(8)	3.67(4)		
	$MLH + H = MLH_2$			6.77(3)	
	$ML + OH = MLOH$		3.24(3)		

Table 1 (continued).

Metal ion	Equilibrium	MDP	HEDP	APD	Method
Sr(II)	$M + L + H = MLH$			16.06(1)	Potentiometry
	$2M + L = M_2L$			9.22(5)	
	$M_2L + H = M_2LH$			10.30(6)	
	$MLH + H = MLH_2$			7.64(2)	
Zn(II)	$M + L = ML$	9.94(5)	10.30(5)	14.55(5)*	Polarography
	$ML + H = MLH$			6.33(7)	
	$ML + 2H = MLH_2$	10.02(5)	9.88(5)		
	$MLH + 2H = MLH_3$			8.47(7)	
	$MLH_2 + 2H = MLH_4$	5.73(3)	5.50(3)		
	$ML + M = M_2L$	5.56(7)	6.16(7)		
	$MLH + M = M_2LH$			4.86(7)	
	$ML + OH = MLOH$	7.46(7)*	7.43(7)*		
Ni(II)	$M + L = ML$	7.27(1)			Potentiometry
	$ML + M = M_2L$	3.79(3)			
	$ML + OH = MLOH$	3.60(3)			
Sm(III)	$M + L = ML$	9.3	10.1		Linear Free
	$ML + H = MLH$	9.0	9.1		Energy Correlation
Ho(III)	$M + L = ML$	9.6	10.4	13.81(7)	LFEC /
	$ML + H = MLH$	9.0	9.1	9.53(9)	Potentiometry
	$MLH + H = MLH_2$			4.29(9)	

* Values calculated by polarography where these values are found to be higher than expected. This is possibly due to the few data points available to calculate the referrred to formation constants.

Table 2. Comparison of results obtained by potentiometry and polarography for Cd(II) complexation by HEDP at 37 ºC and I = 0.15 M NaCl.

Equilibrium	logß (potentiometry)	logß (polarography)
$M + L = ML$	7.10(4)	7.18(5)
$2M + L = M_2L$	12.99(3)	12.75(5)
$M + L + 2H = MLH_2$	20.02(3)	19.55(5)
$M + L + 4H = MLH_4$	Not found	25.08(3)
$M + L + OH = MLOH$	10.94(3)	10.94(3)
$M + 2L = ML_2$	10.46(5)	

APPENDIX B1:

E0 titrations; ESTA input file and output examples
See Disk 1

As the E0 titration is a regular exercise only an example of such an ESTA input file is include viz. CALSM.DAT in A:\APPENDB1. The ESTA2A output of such a file is attached on paper (for E0 titration E0950117.001 and E0950119.001). The data points in CALSM.DAT can be replaced by E0 titration data points found in Appendix C1 to C4 on Disk 2.

E0950117.001

```
*******    ******   *******    *****
*          *           *      *     *
*          *           *      *     *
******     *****       *      *******
*               *      *      *     *
*               *      *      *     *
*******   ******       *      *     *
```

PROGRAM ESTA2A VERSION 3.0

```
TASK OBJE  1        APD TITRATION 1 ELECTRODE CALIBRATION
MODL      H +1
CPLX 0  1 -13.4200  H +1(-1)
CONC
VESL IVOL     20.000  0 0
VESL H +1   .0119070  0 0
BUR1 H +1  -.0500000  0 0
ELEC
ZERO H +1    430.000    1
GRAD H +1     61.550    0
WGHT 1
VESL H +1   .0000250
BUR1 H +1  -.0000100
ZERO H +1       .250
GRAD H +1       .020
TITR RNDE      .0010
EOBS RNDE      .0800
DATA
```

TIMIZATION CYCLE 0
****
ERALL OBJE OBJECTIVE FUNCTION: 7.9559E+02 (N-R ITERATIONS: 171
CAL PARAMETERS:

TRATION NUMBER	OBJECTIVE FUNCTION	ZERO H +1
1	7.956E+02	430.000

JSS-NEWTON: INITIAL SLOPE = -7.0783E+02

/ENBERG-MARQUARDT:

PARAMETER	FRAC.	SLOPE	
4.300E+02	1.25	-7.0783E+02	0
4.300E+02	.86	-4.8630E+02	10

SLOPE AT PREDICTED SOLUTION = -1.5220E+02

```
TIMIZATION CYCLE  4     (CONVERGENCE)
******************
ERALL OBJE OBJECTIVE FUNCTION:      4.4167E+02         (N-R ITERATIONS:    983
CAL PARAMETERS:
---------------
TRATION    OBJECTIVE         ZERO
UMBER      FUNCTION          H +1
  1        4.417E+02      434.993
ANDARD DEVIATIONS:
------------------
TRATION                      ZERO
UMBER                        H +1
  1                           .396
 SIGNIFICANTLY CORRELATED PARAMETERS FOUND
MILTON R-FACTOR:    .02132
MILTON  R-LIMIT:    .00102
. OF TITRATIONS:     1           NO. OF POINTS:  100
op - Program terminated.
```

E0950119.001

```
*******    ******   *******    *****
*          *            *      *     *
*          *            *      *     *
******     *****        *      *******
*               *       *      *     *
*               *       *      *     *
*******   ******        *      *     *
```

PROGRAM ESTA2A VERSION 3.0

```
TASK OBJE  1        APD TITRATION 1 ELECTRODE CALIBRATION
MODL      H +1
CPLX 0  1 -13.4200  H +1(-1)
CONC
VESL IVOL     20.000  0 0
VESL H +1    .0119300  0 0
BUR1 H +1   -.0500000  0 0
ELEC
ZERO H +1     430.000    1
GRAD H +1      61.550    0
WGHT 1
VESL H +1    .0000250
BUR1 H +1   -.0000100
ZERO H +1        .250
GRAD H +1        .020
TITR RNDE       .0010
EOBS RNDE       .0800
DATA
```

```
TIMIZATION CYCLE  0
******************
ERALL OBJE OBJECTIVE FUNCTION:     1.7192E+03        (N-R ITERATIONS:    178
CAL PARAMETERS:
---------------
TRATION    OBJECTIVE        ZERO
UMBER      FUNCTION         H +1
  1        1.719E+03      430.000

USS-NEWTON:                  INITIAL SLOPE =  -3.0650E+03

VENBERG-MARQUARDT:           PARAMETER      FRAC.       SLOPE
                             4.300E+02       2.60   -3.0650E+03    0
                             4.300E+02        .92   -1.0847E+03   11

                             SLOPE AT PREDICTED SOLUTION  =   -7.0084E+02
```

```
'TIMIZATION CYCLE  5     (CONVERGENCE)
******************
'ERALL OBJE OBJECTIVE FUNCTION:      1.8667E+02          (N-R ITERATIONS:  1162
'CAL PARAMETERS:
---------------
TRATION    OBJECTIVE         ZERO
UMBER      FUNCTION          H +1
  1        1.867E+02       440.390
ANDARD DEVIATIONS:
------------------
TRATION                      ZERO
UMBER                        H +1
  1                           .258
 SIGNIFICANTLY CORRELATED PARAMETERS FOUND
MILTON R-FACTOR:    .01373
MILTON  R-LIMIT:    .00101
. OF TITRATIONS:     1            NO. OF POINTS:  100
op - Program terminated.
```

APPENDIX B2:

ESTA input files of protonation titrations with APD, MDP and HEDP

See Disk 1

The ESTA input files are presented in the same order as discussed in Section 4.1.1. The files contain the correct concentrations and E0 values.

APDH3.DAT

MDPHGR1.DAT

HEDPH.DAT
HEDPH1.DAT (excluding LH_6)

APPENDIX B3:

ESTA input files of complexation titrations with APD
See Disk 1

The ESTA input files are presented in the same order as discussed in Section 4.1.2. The files contain the correct concentrations and E0 values.

APDCa.DAT
APDCa1.DAT (2nd possible model)

APDMg1.DAT
APDMg.DAT (2nd possible model)

APDSr1.DAT

APDZn2.DAT
APDZn3.DAT (data points been cut)

APDHoGR.DAT

APDSm1.DAT

APPENDIX B4:

ESTA input files of complexation titrations with MDP

See Disk 1

The ESTA input files are presented in the same order as discussed in Section 4.1.3. The files contain the correct concentrations and E0 values.

MDPCa.DAT
MDPCa_T.DAT (excluding M_2L)

MDPMg1S.DAT
MDPMg1.DAT (uncut model)
MDPMg_S.DAT (excluding M_2L)

MDPZn.DAT

MDPNiS.DAT

MDPSm.DAT

APPENDIX B5:

ESTA input files of complexation titrations with HEDP

See Disk 1

The ESTA input files are presented in the same order as discussed in Section 4.1.4. The files contain the correct concentrations and E0 values.

HEDPCa.DAT

HEDPMgS.DAT

HEDPZn.DAT

CdHEDP1.DAT (titration 1, ratio L:M = 1:1.1)
CdHEDP2.DAT (titration 2, ratio 1.2:1)
CdHEDP3.DAT (titration 3, ratio 2.5:1)
CdHEDP4.DAT (titration 4, ration 3:1)

APPENDIX C1:

Titration data points of protonation titrations with APD, MDP and HEDP

See Disk 2

The titration data is presented in the same order as discussed in Section 4.1.1 with E0 titrations in between. Each E0 titration is applicable to the preceding protonation titrations.

APD_H.001
E0950313.001
APD_H.002 - APD_H.003
E0950314.001
MDPH.001 - MDPH.002
E0950403.001
MDPH.003
E0950404.001
MDPH_A.001 - MDPH_A.002
E0950406.001
HHEDP.001 - HHEDP.003
E0960630.001

APPENDIX C2:

Titration data points of complexation titrations with APD
See Disk 2

The titration data is presented in the same order as discussed in Section 4.1.2 with E0 titrations in between. Each E0 titration is applicable to the preceding complexation titrations.

APDCa.001 - APDCa.003
E0951018.001
APDMg.001 - APDMg.003
E0951019.001
SrAPD_B.001 - SrAPD_B.002
E0950112.001
SrAPD_C.001
E0950116.001
ZnAPD_D.001 - ZnAPD_D.003
E0950119.001
HoAPD_B.001 - HoAPD_B.003
E0950203.001
APDH0_D.001 - APDHo_D.002
E0950316.001
SmAPD_C.001 - SmAPD_C.002
E0950116.001
SmAPD_C.003
E0950117.001

APPENDIX C3:

Titration data points of complexation titrations with MDP
See Disk 2

The titration data is presented in the same order as discussed in Section 4.1.3 with E0 titrations in between. Each E0 titration is applicable to the preceding complexation titrations.

CaMDP.001 - CaMDP.004
E0950425.001
MgMDP.001 - MgMDP.003
E0950424.001
MDPZn.001 - MDPZn.002
E0950407.001
MDPZn.003
E0950410.001
MDPNi.001 - MDPNi.002
E0950411.001
MDPNi.003
E0950412.001

APPENDIX C4:

Titration data points of complexation titrations with HEDP
See Disk 2

The titration data is presented in the same order as discussed in Section 4.1.4 with E0 titrations in between. Each E0 titration is applicable to the preceding complexation titrations.

CaHEDP.001 - CaHEDP.003
E0950630.001
MgHEDP.001 - MgHEDP.003
E0950711.001
ZnHEDP.001 - ZnHEDP.003
E0950706.001
HEDPCd1.001 - HEDPCd1.003
E0951128.001
HEDPCdC.001
E0961118.001

APPENDIX D1:

Titration data points of complexation titrations of Cd(II) with HEDP

The titration data is presented as used in Section 4.2.1

Reference potential
pH = 2.270 -0.5265V 1.65E-06A

pH	Ep	Vtot	Ip	Iexpect	Ip/Iexpect
2.002	-532.1	0.000	8.058	8.39	0.960429
2.214	-532.1	0.370	7.759	8.156944	0.951214
2.412	-532.6	0.610	7.594	8.012574	0.94776
2.599	-533.0	0.780	7.336	7.913365	0.927039
2.779	-534.2	0.900	7.218	7.844801	0.9201
3.003	-534.8	1.000	7.140	7.788566	0.916728
3.216	-535.6	1.075	7.103	7.746916	0.916881
3.416	-536.1	1.115	7.080	7.724884	0.916519
3.616	-536.1	1.145	7.053	7.708443	0.914971
3.800	-536.5	1.165	7.044	7.69752	0.9151
4.009	-536.5	1.180	7.040	7.689349	0.915552
4.216	-538.2	1.190	7.030	7.683911	0.914899
4.527	-538.3	1.200	7.012	7.678481	0.913202
4.726	-539.2	1.205	6.970	7.675768	0.908052
4.909	-539.8	1.210	6.877	7.673058	0.896253
5.108	-541.0	1.215	6.793	7.670349	0.885618
5.314	-542.7	1.222	6.692	7.666561	0.872882
5.504	-544.4	1.230	6.593	7.662236	0.860454
5.690	-548.3	1.240	6.544	7.656836	0.854661
5.905	-551.8	1.255	6.454	7.64875	0.843798
6.109	-557.3	1.275	6.424	7.637996	0.841058
6.308	-562.3	1.300	6.403	7.624596	0.839782
6.495	-567.4	1.330	6.342	7.608578	0.833533
6.706	-571.9	1.370	6.208	7.587325	0.818207
6.903	-577.4	1.410	6.177	7.566191	0.816395
7.103	-582.7	1.450	6.127	7.545174	0.812042
7.328	-588.6	1.490	6.017	7.524273	0.799679
7.540	-593.6	1.520	5.849	7.508673	0.778966
7.723	-598.3	1.540	5.625	7.498309	0.750169
7.968	-605.6	1.560	5.160	7.487974	0.689105
8.135	-609.9	1.570	4.465	7.482817	0.5967
8.350	-614.0	1.580	3.660	7.477667	0.489457
8.609	-620.1	1.590	2.730	7.472524	0.365338
8.867	-624.2	1.600	1.914	7.467388	0.256315
9.073	-626.3	1.610	1.348	7.46226	0.180642
9.237	-628.4	1.620	1.046	7.457138	0.140268
9.428	-630.2	1.635	0.700	7.449469	0.093966
9.609	-632.6	1.655	0.460	7.439267	0.061834
9.802	-635.1	1.680	0.301	7.426555	0.04053
10.019	-637.5	1.720	0.195	7.406305	0.026329
10.204	-638.8	1.765	0.130	7.383656	0.017606
10.400	-641.0	1.825	0.102	7.353672	0.013871
10.618	-647.0	1.905	0.090	7.314069	0.012305
11.040	-657.2	2.125	0.090	7.20733	0.012487
11.510	-671.0	2.675	0.215	6.953632	0.030919
11.837	-677.8	3.675	0.613	6.535368	0.093797

1996-08-27
Total volume 12.95 ml
4.42E-03M HEDP + 1.65E-04M Zn (27:1)

APPENDIX D2:

Titration data points of complexation titrations of Zn(II) with HEDP

The titration data is presented as used in Section 4.2.2

7ml NaCl 0.15M + 40 ul Zn
pH = 5.042 -0.973V 1.09E-06A
700ul HCl 0.15M
pH = 1.900 -0.971V 1.40E-06A
pH = 1.900 -0.971V 1.39E-06A
5ml HEDP + 700ul (HCl en NaOH)

pH	Ep	Ip	Vadd	Vtot	Iexpect
1.908	-0.9795	7.81		13.44	7.81
2.026	-0.982	7.51	300	13.74	7.639476
2.131	-0.983	7.31	200	13.94	7.5298709
2.224	-0.985	7.28	150	14.09	7.449709
2.333	-0.986	7.22	150	14.24	7.371236
2.47	-0.987	7.17	150	14.39	7.2943989
2.585	-0.988	7	100	14.49	7.244058
2.793	-0.989	6.81	100	14.59	7.1944071
2.908	-0.099	6.79	100	14.69	7.1454323
3.086	-0.991	6.73	70	14.76	7.1115447
3.288	-0.992	6.53	60	14.82	7.082753
3.461	-0.993	6.47	40	14.86	7.0636878
3.546	-0.994	6.41	15	14.875	7.0565647
3.676	-0.995	6.35	15	14.89	7.049456
3.808	-0.996	6.27	23	14.913	7.0385838
4.111	-0.998	6.19	5	14.918	7.0362247
4.219	-0.999	5.99	10	14.928	7.0315113
4.326	-1	5.89	10	14.938	7.0268041
4.495	-1.003	5.64	13	14.951	7.0206943
4.647	-1.006	5.28	10	14.961	7.0160016
4.806	-1.01	4.83	10	14.971	7.0113152
4.939	-1.014	4.45	8	14.979	7.0075706
5.046	-1.018	4.02	6	14.985	7.0047648
5.188	-1.021	3.61	9	14.994	7.0005602
5.316	-1.024	3.34	9	15.003	6.9963607
5.436	-1.027	3.14	15	15.018	6.9893728
5.59	-1.032	2.77	20	15.038	6.9800771
5.736	-1.038	2.42	20	15.058	6.9708062
5.879	-1.045	1.98	10	15.068	6.96618
6.042	-1.052	1.59	15	15.083	6.9592521
6.19	-1.059	1.32	15	15.098	6.9523381
6.2492	-1.064	1.22	15	15.113	6.9454377
6.404	-1.072	0.988	15	15.128	6.938551
6.498	-1.08		15	15.143	6.931678

1996-03-14
5ml 0.01M HEDP + 40ul 0.0209M Zn in 13.440 ml
3.72E-03M HEDP + 6.22E-05M Zn (60:1)
Gestoor in hzn-4-st tot hzn-4-35

APPENDIX D3:

Titration data points of complexation titrations of Zn(II) with MDP

The titration data is presented as used in Section 4.2.3

7ml NaCl 0.15M + 40ul Zn
pH = 4.560 -0.972V 1.55E-06A
700ul HCl 0.15M
pH = 1.911 -0.974V 1.45E-06A
pH = 1.911 -0.975V1.45E-06A
5ml MDP 0.01M

pH	Ep	Ip	Vadd	Vtot	Iexpect
1.929	-0.978	8.95		12.74	8.95
2.018	-0.979	8.67	250	12.99	8.7777521
2.146	-0.98	8.52	200	13.19	8.644655
2.311	-0.981	8.07	250	13.44	8.4838542
2.487	-0.982	7.96	200	13.64	8.3594575
2.802	-0.984	7.73	250	13.89	8.2089993
2.909	-0.985	7.55	60	13.95	8.1736918
3.041	-0.986	7.4	60	14.01	8.1386867
3.191	-0.987	7.34	60	14.07	8.1039801
3.37	-0.988	7.28	60	14.13	8.0695683
3.595	-0.989	7.26	40	14.17	8.046789
3.709	-0.99	7.24	15	14.185	8.0382799
3.847	-0.991	7.21	15	14.2	8.0297887
3.981	-0.992	7.12	10	14.21	8.0241379
4.151	-0.993	7.06	15	14.225	8.0156766
4.292	-0.994	6.9	10	14.235	8.0100457
4.617	-0.998	6.55	5	14.24	8.0072331
4.709	-0.999	6.45	6	14.246	8.0038607
4.806	-1.001	6.08	6	14.252	8.0004912
4.902	-1.004	5.96	6	14.258	7.9971244
4.992	-1.008	5.6	6	14.264	7.9937605
5.101	-1.011	5.14	9	14.273	7.98872
5.222	-1.014	4.91	9	14.282	7.9836858
5.328	-1.018	4.54	9	14.291	7.9786579
5.631	-1.028	3.67	10	14.301	7.9730788
5.711	-1.031	3.45	8	14.309	7.9686211
5.798	-1.034	3.19	10	14.319	7.9630561
5.917	-1.039	2.79	25	14.344	7.9491774
6.03	-1.046	2.52	10	14.354	7.9436394
6.108	-1.05	2.25	5	14.359	7.9408733
6.215	-1.054	2.05	13	14.372	7.9336905
6.314	-1.59	1.72	13	14.385	7.9265207
6.425	-1.07	1.45	18	14.403	7.9166146
6.529	-1.078	1.1	20	14.423	7.9056368
6.664	-1.096	0.924	30	14.453	7.8892272

1996-03-13
5 ml MDP+ 40ul Zn in 12.74 ml
3.925E-03 M MDP + 6.562E-05 M Zn
Gestoor in mzn-2-st tot mzn-2-35

APPENDIX D4:

Titration data points of complexation titrations of Zn(II) with APD

The titration data is presented as used in Section 4.2.4

7ml 0.15M NaCl + 40ul Zn
pH = 5.371 -0.998V 6.16E-07A
700 ul 0.15M HCl
pH = 1.928 -0.973V 1.42E-06A
pH = 1.928 -0.974V 1.43E-06A
5ml 0.01M APD
pH = 2.051 -0.979V 8.70E-07A

pH	Ep	Ip	Vadd	Vtot	I expect
2.051	-0.979	8.7		12.74	8.7
2.175	-0.98	8.07	600	13.34	8.3086957
2.314	-0.981	7.96	200	13.54	8.1859675
2.444	-0.981	7.85	150	13.69	8.0962747
2.613	-0.982	7.76	150	13.84	8.008526
2.776	-0.982	7.65	100	13.94	7.951076
2.891	-0.983	7.62	50	13.99	7.922659
3.039	-0.983	7.58	50	14.04	7.8944444
3.24	-0.984	7.46	50	14.09	7.8664301
3.398	-0.984	7.37	25	14.115	7.8524973
3.579	-0.985	7.24	20	14.135	7.8413866
3.708	-0.986	7.17	10	14.145	7.8358431
3.81	-0.987	7.08	5	14.15	7.8330742
3.915	-0.989	6.98	5	14.155	7.8303073
4.075	-0.992	6.83	7.5	14.1625	7.8261606
4.223	-0.995	6.63	5	14.1675	7.8233986
4.365	-1	6.39	15	14.1825	7.8151243
4.469	-1.003	6.1	12.5	14.195	7.8082423
4.586	-1.007	5.46	12.5	14.2075	7.8013725
4.715	-1.012	5.19	15	14.2225	7.7931447
4.824	-1.017	4.51	15	14.2375	7.7849342
4.977	-1.021	4.31	10	14.2475	7.7794701
5.072	-1.024	4.13	20	14.2675	7.7685649
5.199	-1.027	3.62	25	14.2925	7.7549764
5.301	-1.03	3.26	10	14.3025	7.7495543
5.42	-1.034	2.82	15	14.3175	7.7414353
5.532	-1.04	2.75	20	14.3375	7.7306364
5.663	-1.048	2.33	20	14.3575	7.7198677
5.781	-1.054	1.98	20	14.3775	7.7091288
5.941	-1.06	1.65	30	14.4075	7.6930765
6.089	-1.064	1.27	30	14.4375	7.6770909
6.19	-1.068	1.12	20	14.4575	7.6664707

1996-03-15
5ml APD + 40 ul Zn in 12.740ml
3.925E-03M APD + 6.562E-05M Zn (60:1)
Gestoor in azn-5-st tot azn-5-33

APPENDIX E1-E4:

A selection of Polarograms recorded for each of the systems; Cd(II)-HEDP, Zn(II)-HEDP, Zn(II)-MDP and Zn(II)-APD in the same solution but at different pH levels

Polarograms recorded at various pH values for HEDP-Cd(II): Indicating shift in peak potential and drop in peak height.

Appendix E1

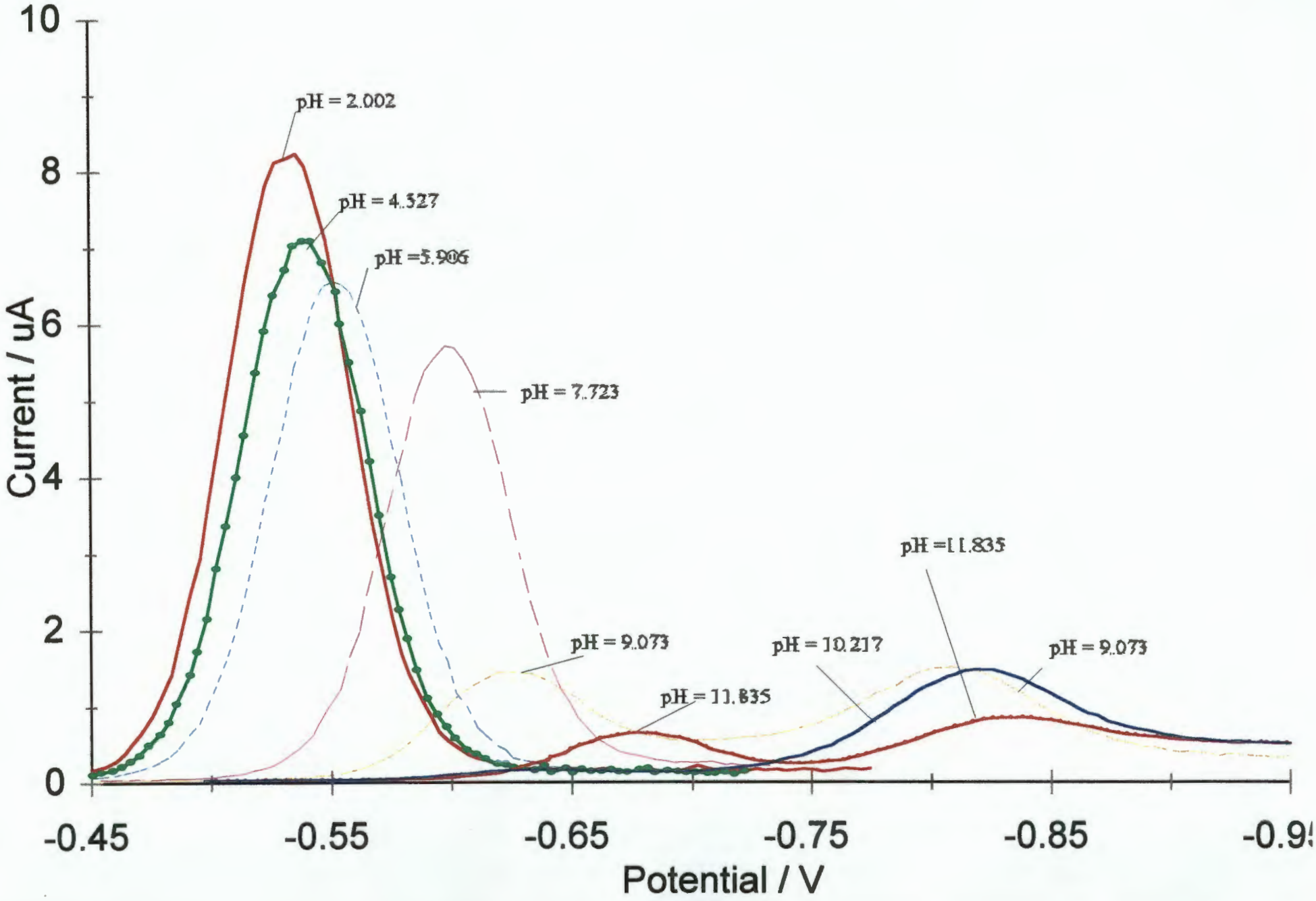

Appendix E2

Polarograms recorded at various pH values for HEDP-Zn(II): Indicating shift in peak potential and drop in peak height.

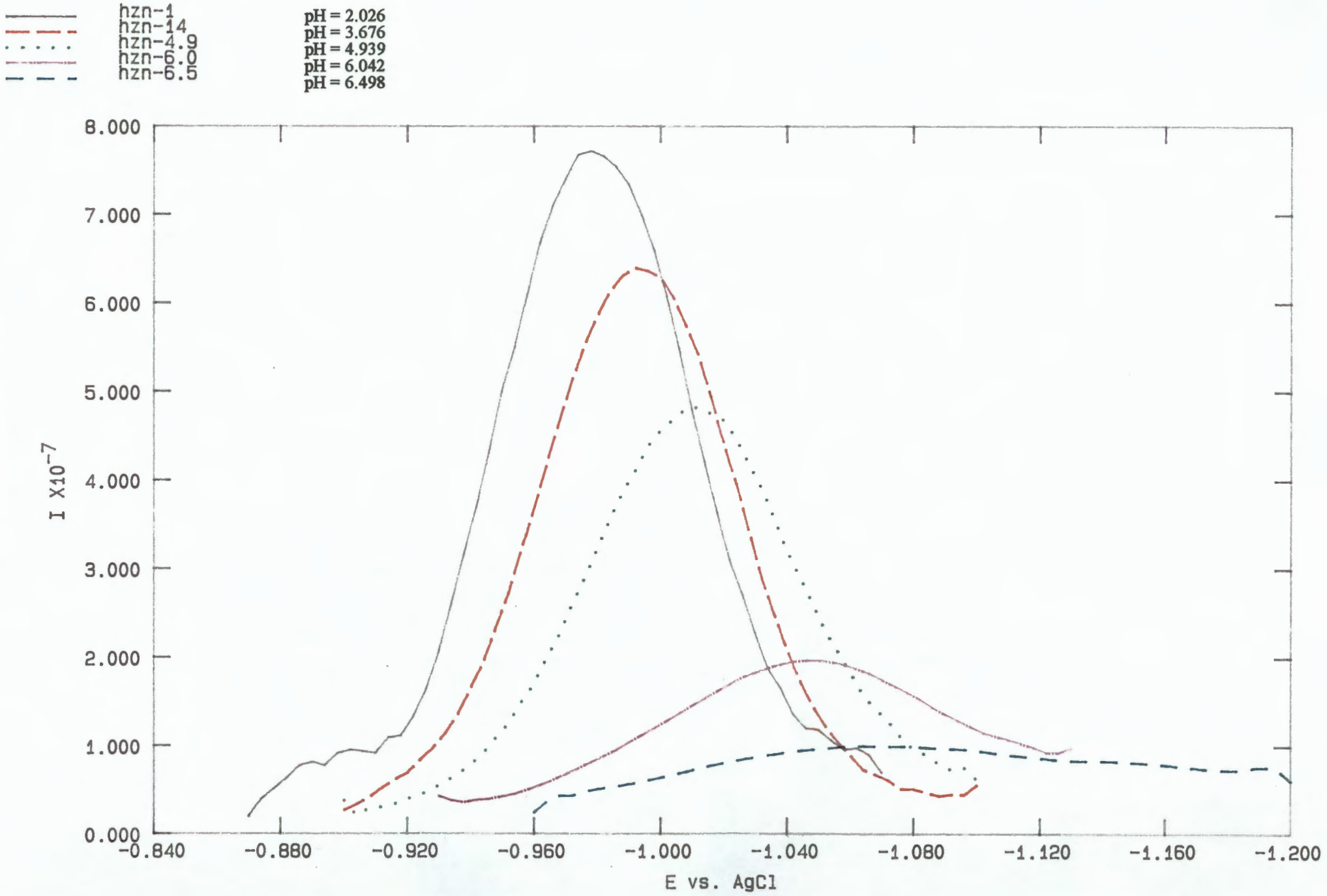

Polarograms recorded at various pH values for MDP-Zn(II): Indicating shift in peak potential and drop in peak height.

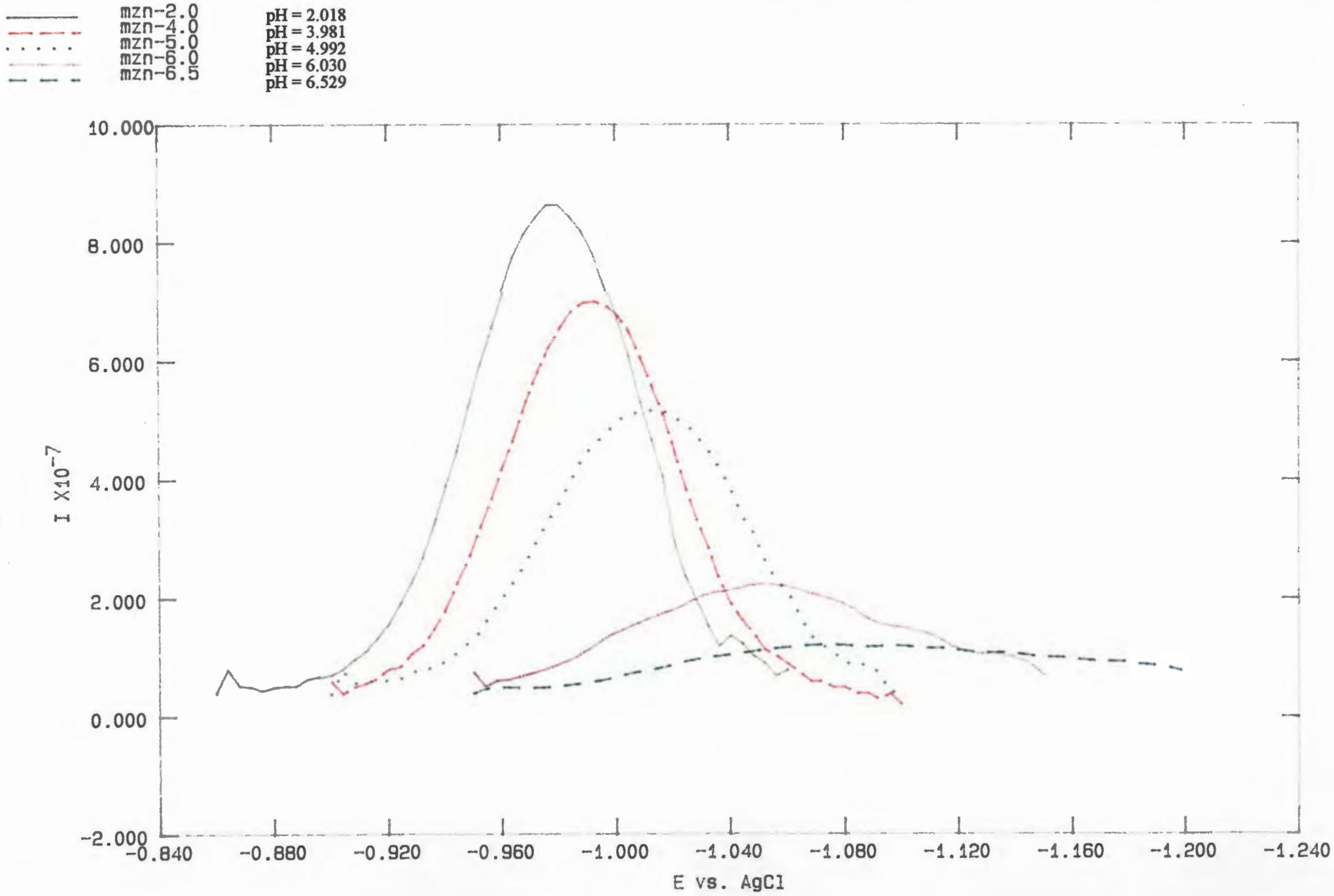

Appendix E3

Polarograms recorded at various pH values for APD-Zn(II): Indicating shift in peak potential and drop in peak height.

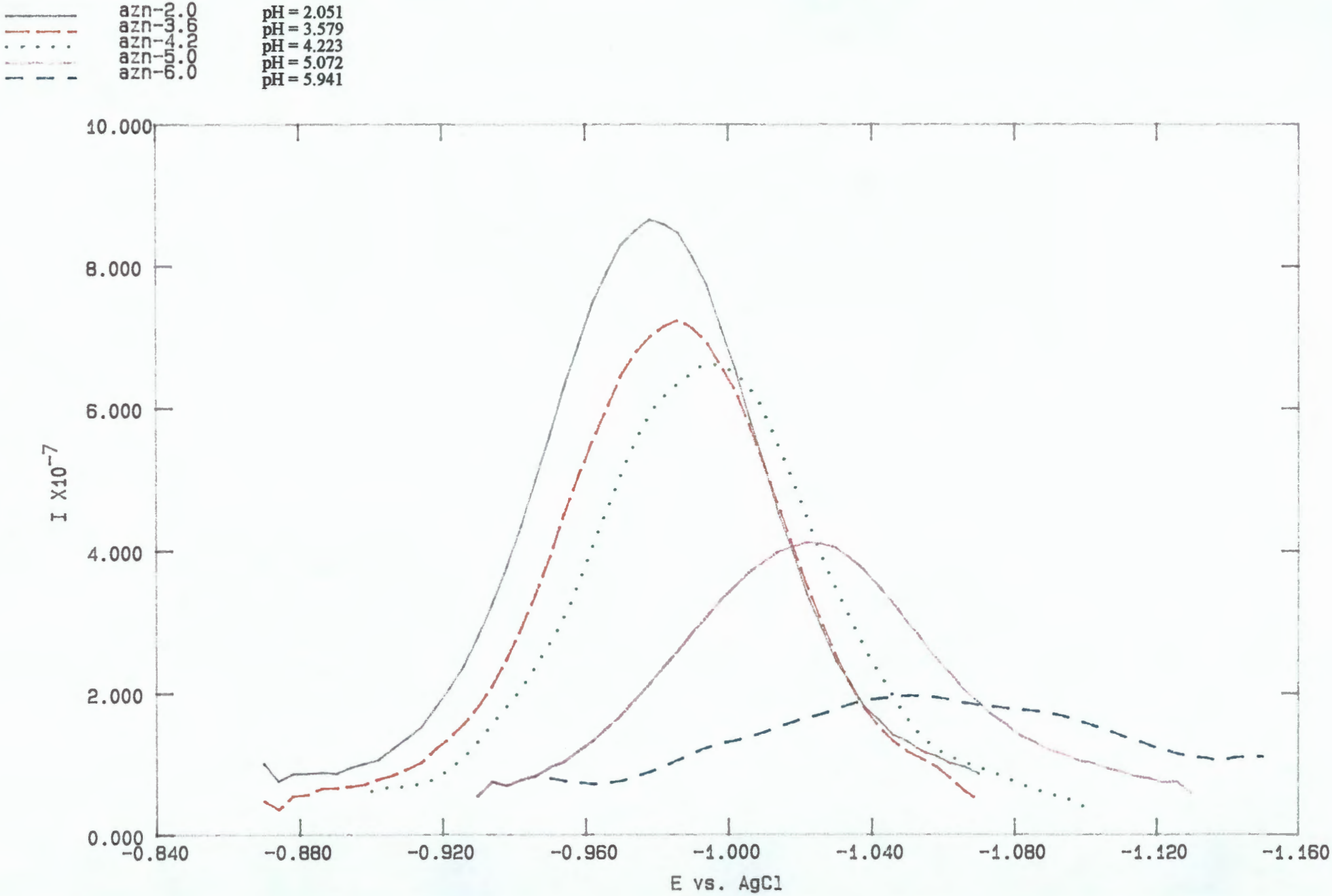

Appendix E4

APPENDIX F:

^{31}P and ^{13}C NMR spectra recorded for the system; Mg(II)-HEDP

The spectra are included in the following order

^{31}P of HEDP (pH = 2.0)
^{31}P of HEDP (pH = 10.5)
^{31}P of Mg(II)-HEDP (pH = 3.0)
^{31}P of Mg(II)-HEDP (pH = 5.0)
^{31}P of Mg(II)-HEDP (pH = 7.0)
^{31}P of Mg(II)-HEDP (pH = 11.0)
^{13}C of HEDP (pH = 2.0)
^{13}C of Mg(II)-HEDP (pH = 3.0)
^{13}C of Mg(II)-HEDP (pH = 5.0)

HEDP (0.05 M) pH 2.0 310 K.

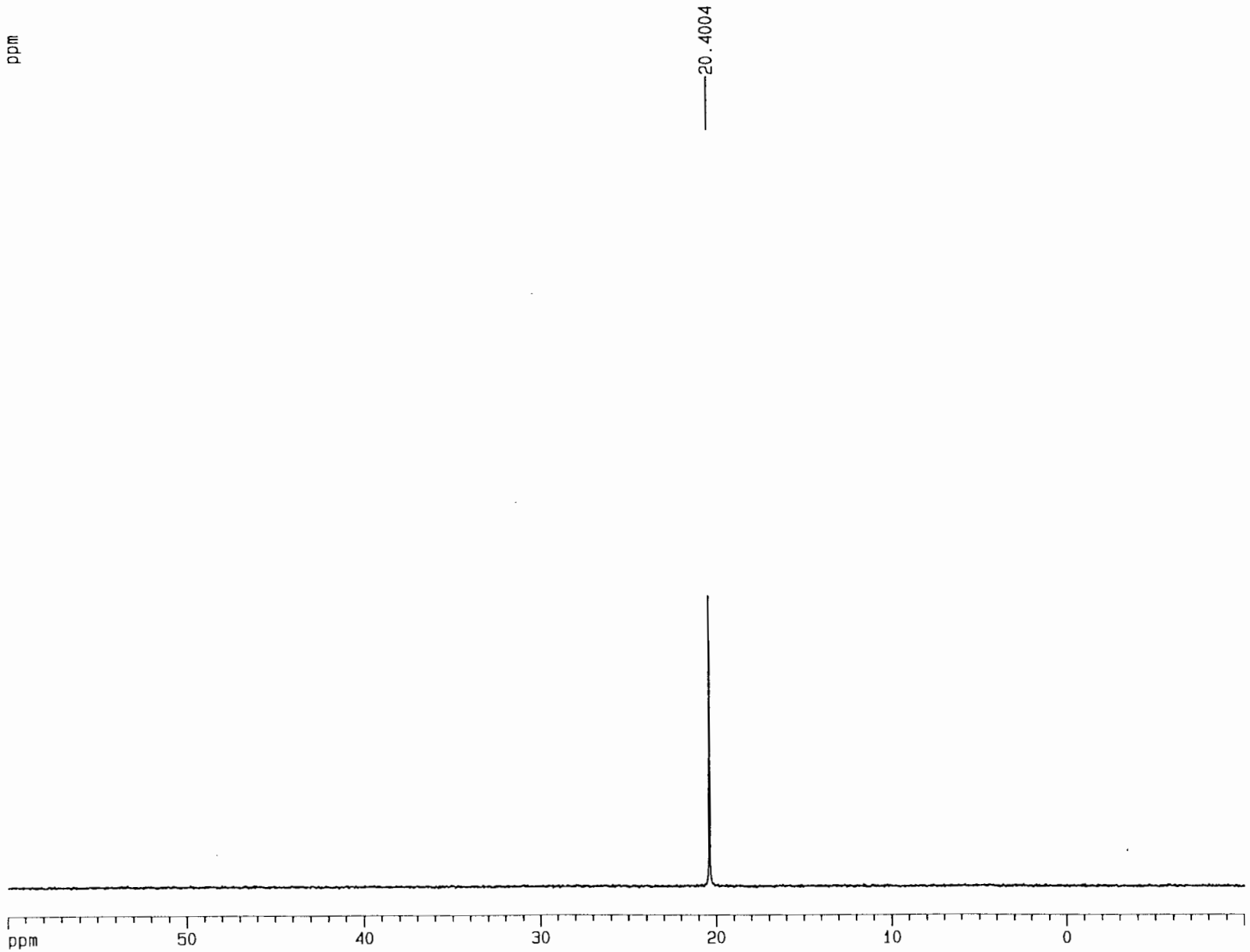

Current Data Parameters

NAME	AEC
EXPNO	6
PROCNO	1

F2 - Acquisition Parameters

Date_	960416
Time	12.15
INSTRUM	spect
PROBHD	5 mm Multinu
PULPROG	zgpg
TD	32768
SOLVENT	Tol
NS	64
DS	0
SWH	12953.368 Hz
FIDRES	0.395305 Hz
AQ	1.2648948 sec
RG	32768
DW	38.600 usec
DE	4.50 usec
TE	300.0 K
D12	0.00002000 sec
PL13	24.00 dB
D1	1.00000000 sec
CPDPRG2	waltz16
PCPD2	100.00 usec
SFO2	400.1328000 MHz
NUC2	1H
PL2	120.00 dB
PL12	22.00 dB
P1	13.50 usec
DE	4.50 usec
SFO1	161.9798930 MHz
NUC1	31P
PL1	-3.00 dB
D11	0.03000000 sec

F2 - Processing parameters

SI	32768
SF	161.9754877 MHz
WDW	EM
SSB	0
LB	2.50 Hz
GB	0
PC	0.10

1D NMR plot parameters

CX	21.00 cm
F1P	60.000 ppm
F1	9718.53 Hz
F2P	-10.000 ppm
F2	-1619.76 Hz
PPMCM	3.33333 ppm/cm
HZCM	539.91833 Hz/cm

HEDP (0.05 M) pH 10.5 310 K.

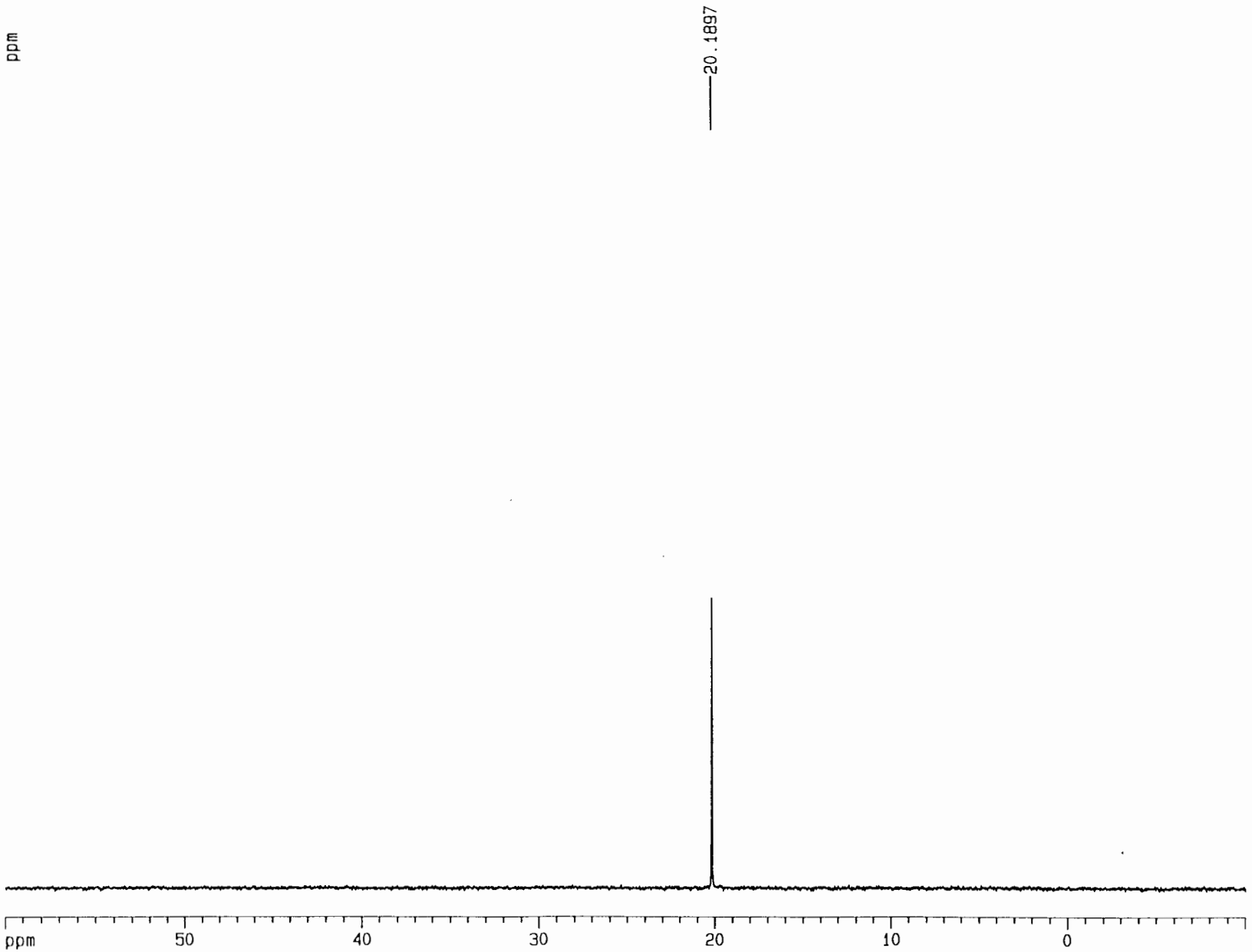

Current Data Parameters

NAME	AEC
EXPNO	5
PROCNO	1

F2 - Acquisition Parameters

Date_	960416
Time	12.10
INSTRUM	spect
PROBHD	5 mm Multinu
PULPROG	zgpg
TD	32768
SOLVENT	Tol
NS	48
DS	0
SWH	12953.368 Hz
FIDRES	0.395305 Hz
AQ	1.2648948 sec
RG	32768
DW	38.600 usec
DE	4.50 usec
TE	300.0 K
D12	0.00002000 sec
PL13	24.00 dB
D1	1.00000000 sec
CPDPRG2	waltz16
PCPD2	100.00 usec
SFO2	400.1328000 MHz
NUC2	1H
PL2	120.00 dB
PL12	22.00 dB
P1	13.50 usec
DE	4.50 usec
SFO1	161.9798930 MHz
NUC1	31P
PL1	-3.00 dB
D11	0.03000000 sec

F2 - Processing parameters

SI	32768
SF	161.9754877 MHz
WDW	EM
SSB	0
LB	2.50 Hz
GB	0
PC	0.10

1D NMR plot parameters

CX	21.00 cm
F1P	60.000 ppm
F1	9718.53 Hz
F2P	-10.000 ppm
F2	-1619.76 Hz
PPMCM	3.33333 ppm/cm
HZCM	539.91833 Hz/cm

HEDP (0.05 M) / Mg (0.05 M) / NaCl (0.15M) pH 3.0 310 K.

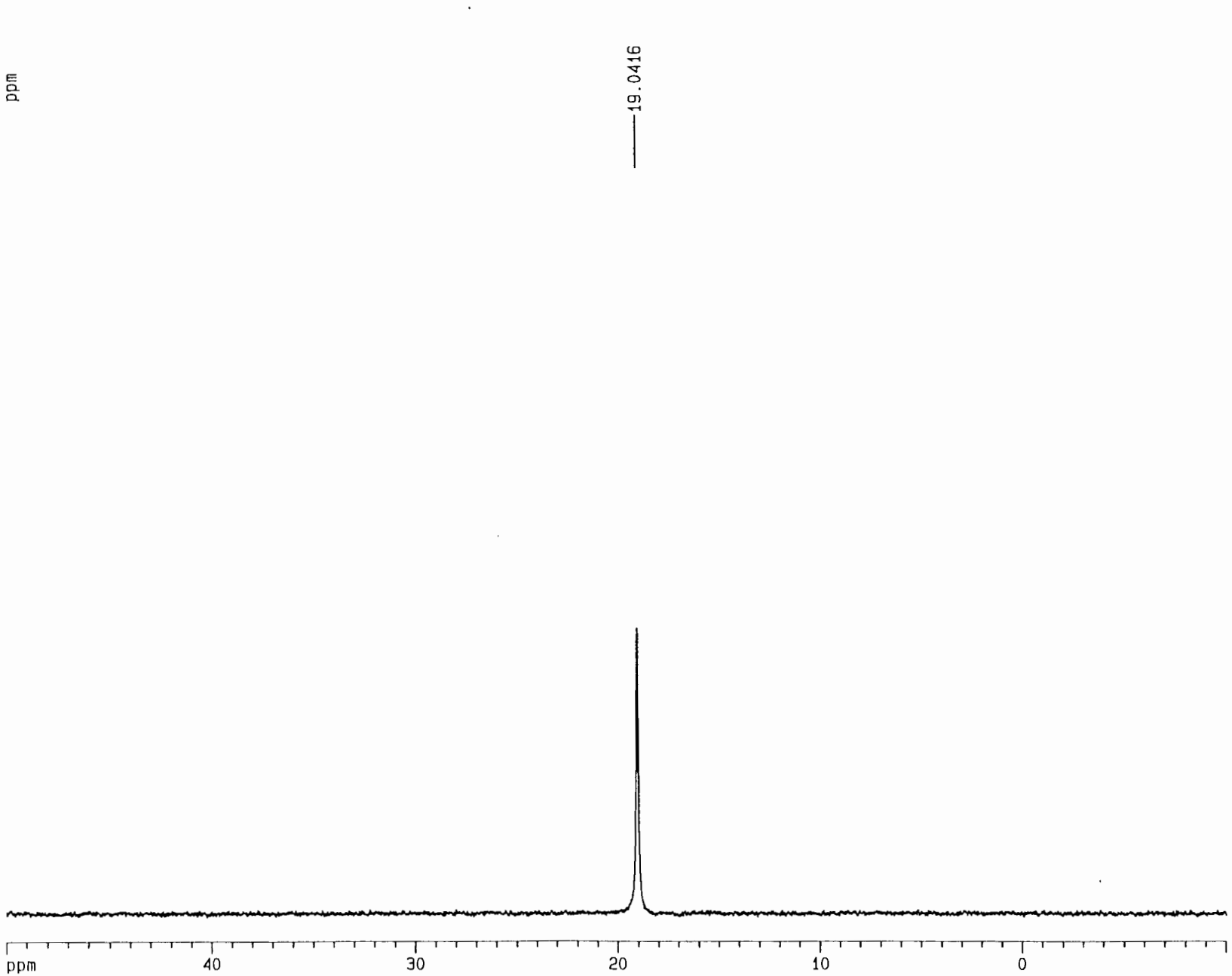

Current Data Parameters

NAME	AEC
EXPNO	7
PROCNO	1

F2 - Acquisition Parameters

Date_	960416	
Time	12.22	
INSTRUM	spect	
PROBHD	5 mm Multinu	
PULPROG	zgpg	
TD	32768	
SOLVENT	Tol	
NS	232	
DS	0	
SWH	12953.368	Hz
FIDRES	0.395305	Hz
AQ	1.2648948	sec
RG	32768	
DW	38.600	usec
DE	4.50	usec
TE	300.0	K
D12	0.00002000	sec
PL13	24.00	dB
D1	1.00000000	sec
CPDPRG2	waltz16	
PCPD2	100.00	usec
SFO2	400.1328000	MHz
NUC2	1H	
PL2	120.00	dB
PL12	22.00	dB
P1	13.50	usec
DE	4.50	usec
SFO1	161.9798930	MHz
NUC1	31P	
PL1	-3.00	dB
D11	0.03000000	sec

F2 - Processing parameters

SI	32768	
SF	161.9754877	MHz
WDW	EM	
SSB	0	
LB	2.50	Hz
GB	0	
PC	0.10	

1D NMR plot parameters

CX	21.00	cm
F1P	50.000	ppm
F1	8098.77	Hz
F2P	-10.000	ppm
F2	-1619.75	Hz
PPMCM	2.85714	ppm/cm
HZCM	462.78714	Hz/cm

HEDP (0.05 M), Mg (0.05 M), NaCl (0.15 M), pH 5 310 K.

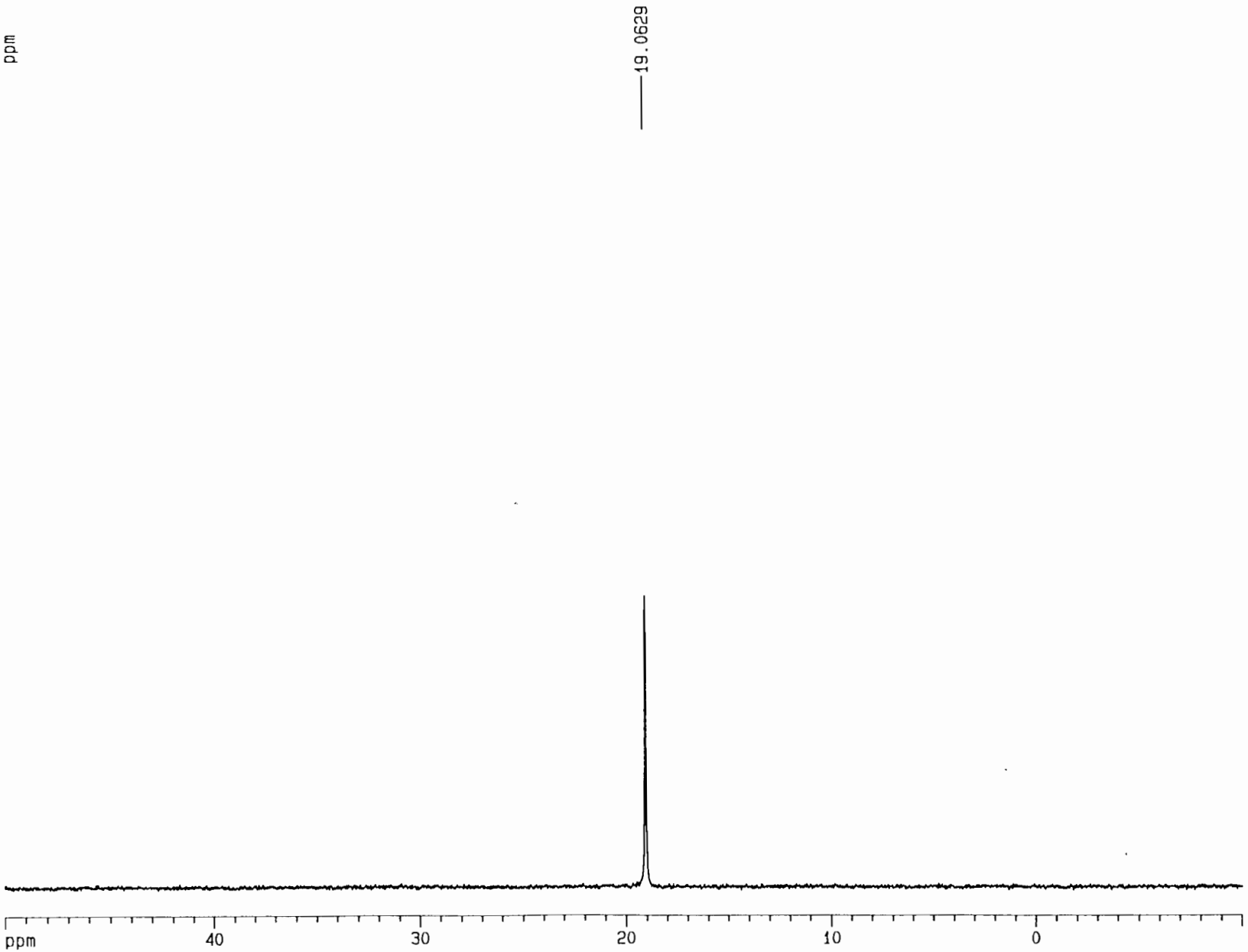

Current Data Parameters

NAME	AEC
EXPNO	9
PROCNO	1

F2 - Acquisition Parameters

Date_	960416
Time	13.19
INSTRUM	spect
PROBHD	5 mm Multinu
PULPROG	zgpg
TD	32768
SOLVENT	Tol
NS	80
DS	0
SWH	12953.368 Hz
FIDRES	0.395305 Hz
AQ	1.2648948 sec
RG	32768
DW	38.600 usec
DE	4.50 usec
TE	300.0 K
D12	0.00002000 sec
PL13	24.00 dB
D1	1.00000000 sec
CPDPRG2	waltz16
PCPD2	100.00 usec
SFO2	400.1328000 MHz
NUC2	1H
PL2	120.00 dB
PL12	22.00 dB
P1	13.50 usec
DE	4.50 usec
SFO1	161.9798930 MHz
NUC1	31P
PL1	-3.00 dB
D11	0.03000000 sec

F2 - Processing parameters

SI	32768
SF	161.9754877 MHz
WDW	EM
SSB	0
LB	2.50 Hz
GB	0
PC	0.10

1D NMR plot parameters

CX	21.00 cm
F1P	50.000 ppm
F1	8098.77 Hz
F2P	-10.000 ppm
F2	-1619.75 Hz
PPMCM	2.85714 ppm/cm
HZCM	462.78714 Hz/cm

HEDP (0.05 M), Mg (0.05 M), NaCl (0.15 M), pH 7 310 K.

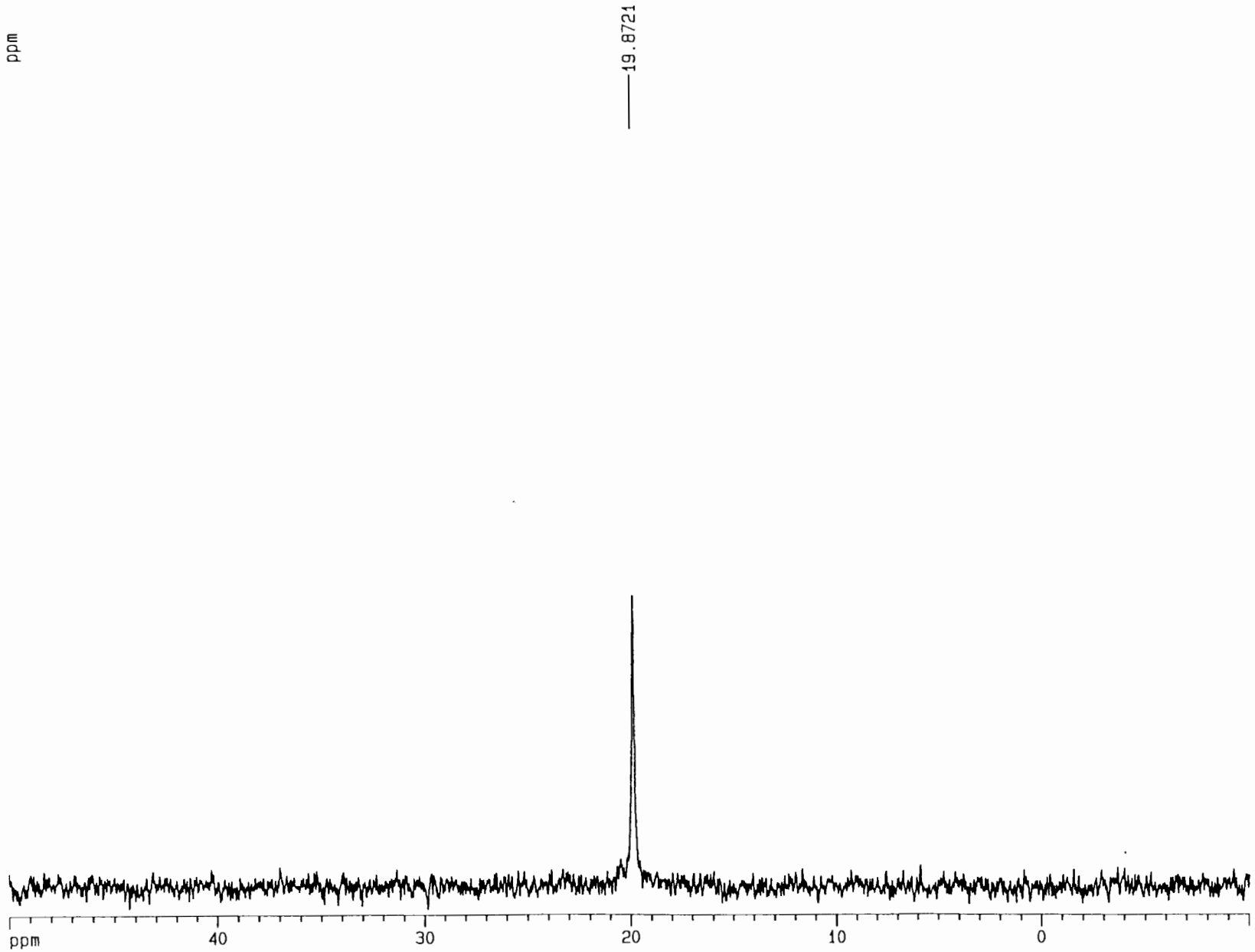

Current Data Parameters

NAME	AEC
EXPNO	10
PROCNO	1

F2 - Acquisition Parameters

Date_	960416
Time	13.29
INSTRUM	spect
PROBHD	5 mm Multinu
PULPROG	zgpg
TD	32768
SOLVENT	Tol
NS	208
DS	0
SWH	12953.368 Hz
FIDRES	0.395305 Hz
AQ	1.2648948 sec
RG	32768
DW	38.600 usec
DE	4.50 usec
TE	300.0 K
D12	0.00002000 sec
PL13	24.00 dB
D1	1.00000000 sec
CPDPRG2	waltz16
PCPD2	100.00 usec
SFO2	400.1328000 MHz
NUC2	1H
PL2	120.00 dB
PL12	22.00 dB
P1	13.50 usec
DE	4.50 usec
SFO1	161.9798930 MHz
NUC1	31P
PL1	-3.00 dB
D11	0.03000000 sec

F2 - Processing parameters

SI	32768
SF	161.9754877 MHz
WDW	EM
SSB	0
LB	5.00 Hz
GB	0
PC	0.10

1D NMR plot parameters

CX	21.00 cm
F1P	50.000 ppm
F1	8098.77 Hz
F2P	-10.000 ppm
F2	-1619.75 Hz
PPMCM	2.85714 ppm/cm
HZCM	462.78714 Hz/cm

HEDP (0.05 M), Mg (0.05 M), NaCl (0.15 M), pH 11 310 K.

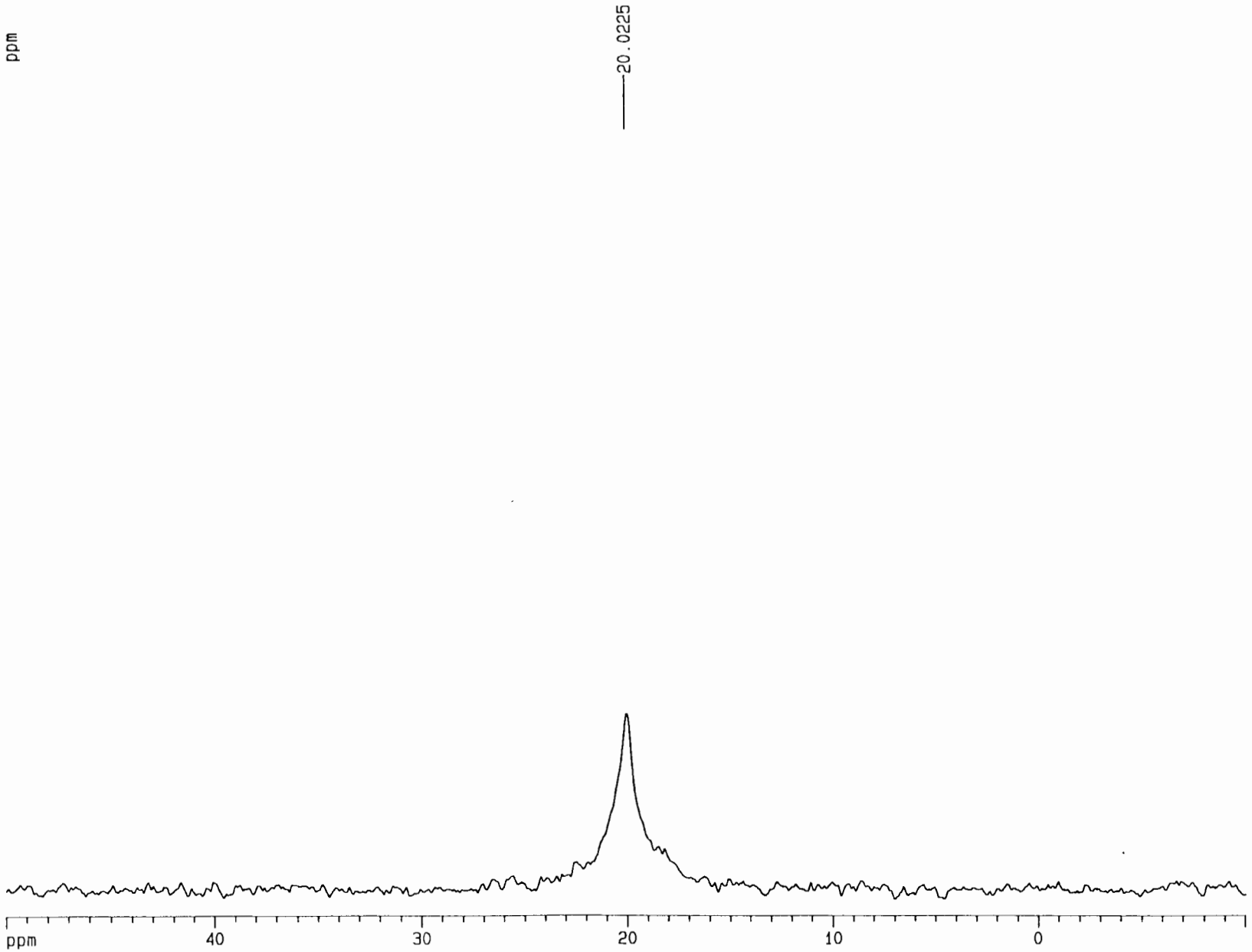

Current Data Parameters

NAME	AEC
EXPNO	11
PROCNO	1

F2 - Acquisition Parameters

Date_	960416
Time	13.43
INSTRUM	spect
PROBHD	5 mm Multinu
PULPROG	zgpg
TD	32768
SOLVENT	Tol
NS	272
DS	0
SWH	12953.368 Hz
FIDRES	0.395305 Hz
AQ	1.2648948 sec
RG	32768
DW	38.600 usec
DE	4.50 usec
TE	300.0 K
D12	0.00002000 sec
PL13	24.00 dB
D1	1.00000000 sec
CPDPRG2	waltz16
PCPD2	100.00 usec
SFO2	400.1328000 MHz
NUC2	1H
PL2	120.00 dB
PL12	22.00 dB
P1	13.50 usec
DE	4.50 usec
SFO1	161.9798930 MHz
NUC1	31P
PL1	-3.00 dB
D11	0.03000000 sec

F2 - Processing parameters

SI	32768
SF	161.9754877 MHz
WDW	EM
SSB	0
LB	25.00 Hz
GB	0
PC	0.10

1D NMR plot parameters

CX	21.00 cm
F1P	50.000 ppm
F1	8098.77 Hz
F2P	-10.000 ppm
F2	-1619.75 Hz
PPMCM	2.85714 ppm/cm
HZCM	462.78714 Hz/cm

HEDP (0.05 M) pH 2 / D20 310 K.

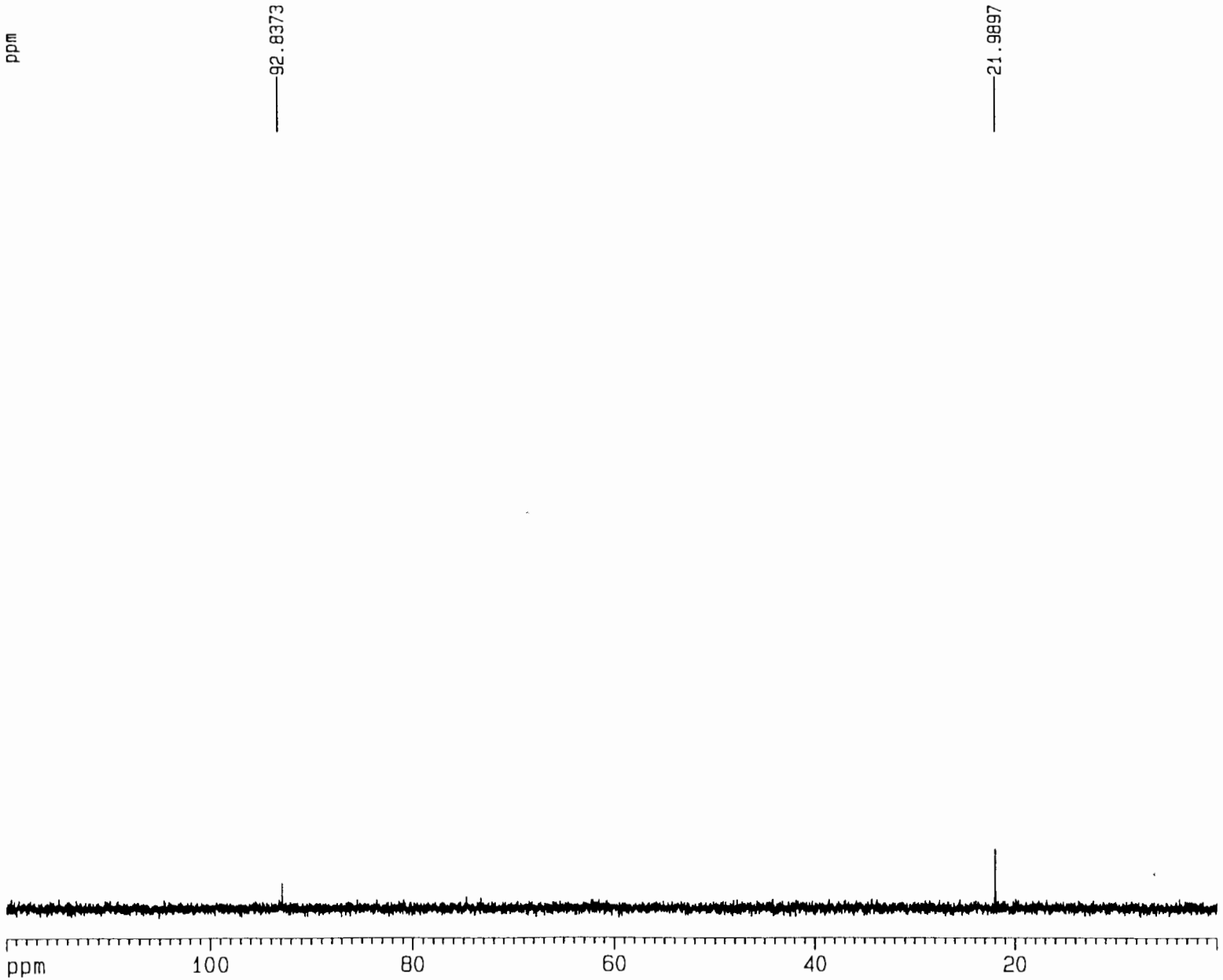

Current Data Parameters

NAME	AEC
EXPNO	2
PROCNO	1

F2 - Acquisition Parameters

Date_	960416
Time	10.43
INSTRUM	spect
PROBHD	5 mm Multinu
PULPROG	zgpg
TD	65536
SOLVENT	D20
NS	320
DS	0
SWH	30120.482 Hz
FIDRES	0.459602 Hz
AQ	1.0879476 sec
RG	16384
DW	16.600 usec
DE	4.50 usec
TE	310.0 K
D12	0.00002000 sec
PL13	24.00 dB
D1	5.00000000 sec
CPDPRG2	waltz16
PCPD2	100.00 usec
SFO2	400.1316005 MHz
NUC2	1H
PL2	20.00 dB
PL12	20.00 dB
P1	12.50 usec
DE	4.50 usec
SFO1	100.6247290 MHz
NUC1	13C
PL1	-3.00 dB
D11	0.03000000 sec

F2 - Processing parameters

SI	32768
SF	100.6125220 MHz
WDW	EM
SSB	0
LB	1.00 Hz
GB	0
PC	1.40

1D NMR plot parameters

CX	20.00 cm
F1P	120.000 ppm
F1	12073.50 Hz
F2P	0.000 ppm
F2	0.00 Hz
PPMCM	6.00000 ppm/cm
HZCM	603.67511 Hz/cm

HEDP (0.05 M) / Mg (0.05 M) / NaCl (0.15M) pH 3.0 310 K.

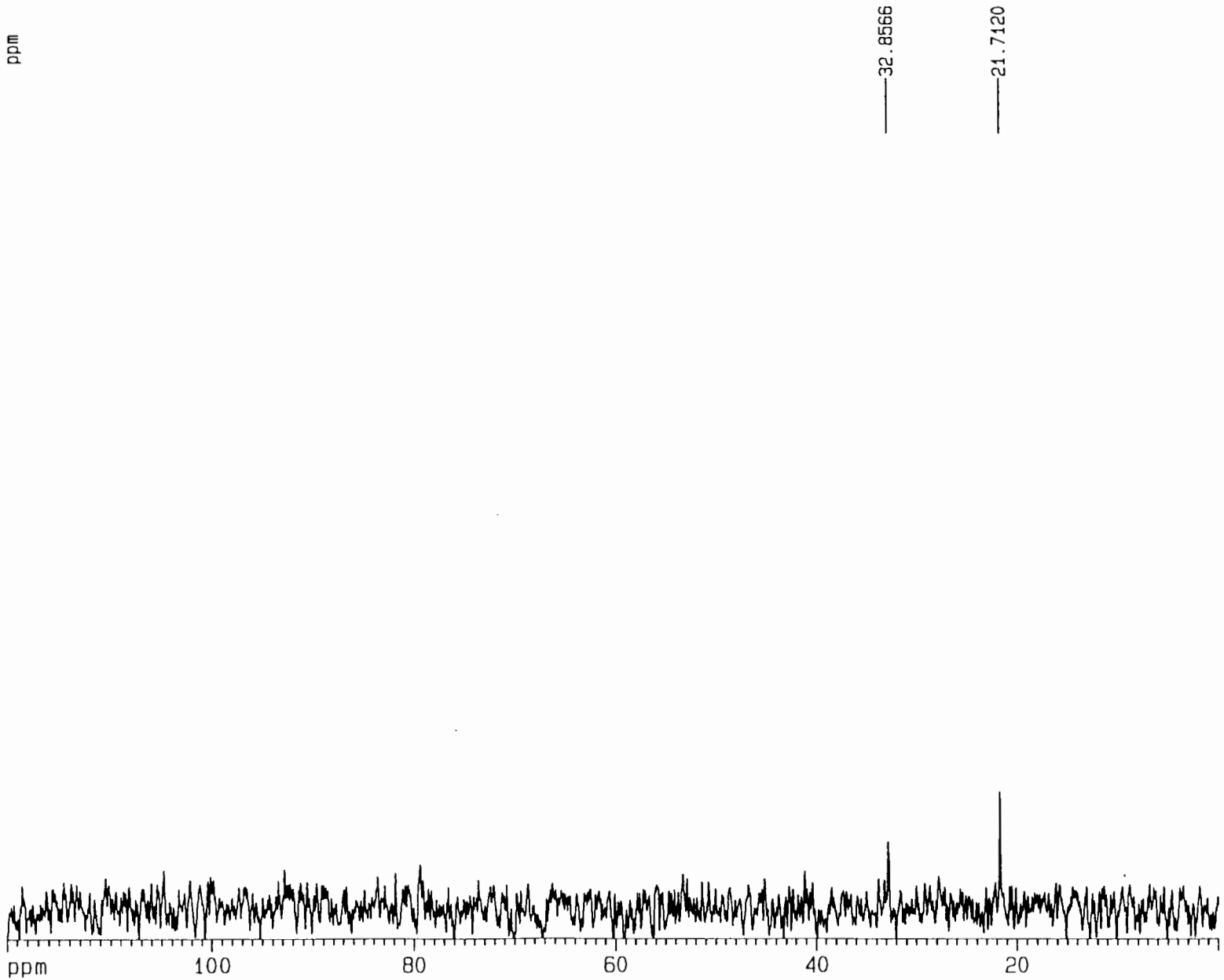

Current Data Parameters

NAME	AEC
EXPNO	8
PROCNO	1

F2 - Acquisition Parameters

Date_	960416
Time	15.03
INSTRUM	spect
PROBHD	5 mm Multinu
PULPROG	zgpg
TD	65536
SOLVENT	D20
NS	416
DS	0
SWH	30120.482 Hz
FIORES	0.459602 Hz
AQ	1.0879476 sec
RG	16384
DW	16.600 usec
DE	4.50 usec
TE	310.0 K
D12	0.00002000 sec
PL13	24.00 dB
D1	10.00000000 sec
CPDPRG2	waltz16
PCPD2	100.00 usec
SFO2	400.1316005 MHz
NUC2	1H
PL2	20.00 dB
PL12	20.00 dB
P1	12.50 usec
DE	4.50 usec
SFO1	100.6247290 MHz
NUC1	13C
PL1	-3.00 dB
D11	0.03000000 sec

F2 - Processing parameters

SI	32768
SF	100.6125220 MHz
WDW	EM
SSB	0
LB	10.00 Hz
GB	0
PC	1.40

1D NMR plot parameters

CX	20.00 cm
F1P	120.000 ppm
F1	12073.50 Hz
F2P	0.000 ppm
F2	0.00 Hz
PPMCM	6.00000 ppm/cm
HZCM	603.67511 Hz/cm

HEDP (0.05 M), Mg (0.05 M), NaCl (0.15 M), pH 5 310 K.

11 3397957 P.01

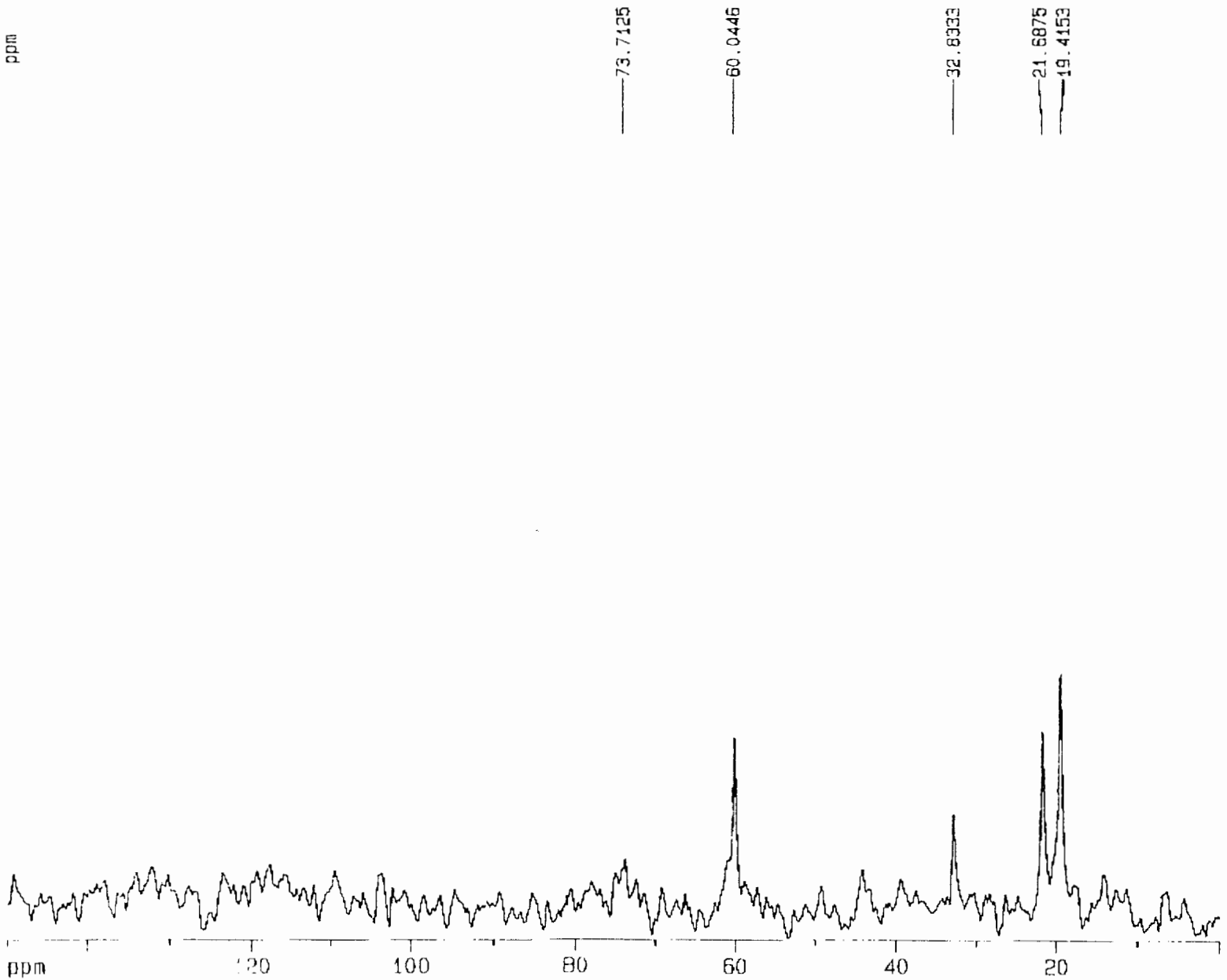

Current Data Parameters

NAME	AEC
EXPNO	13
PROCNO	1

F2 - Acquisition Parameters

Date_	960417
Time	5.24
INSTRUM	spect
PROBHD	5 mm Multinu
PULPROG	zgpg
TD	65536
SOLVENT	D2O
NS	4096
DS	0
SWH	30120.482 Hz
FIDRES	0.459602 Hz
AQ	1.0879476 sec
RG	16384
DW	16.600 usec
DE	4.50 usec
TE	310.0 K
D12	0.00002000 sec
PL13	24.00 dB
D11	10.00000000 sec
CPDPRG2	waltz16
PCPD2	100.00 usec
SFO2	400.1316005 MHz
NUC2	1H
PL2	20.00 dB
PL12	20.00 dB
P1	12.50 usec
DE	4.50 usec
SFO1	100.6247290 MHz
NUC1	13C
PL1	-3.00 dB
D11	0.03000000 sec

F2 - Processing parameters

SI	32768
SF	100.6125220 MHz
WDW	EM
SSB	0
LB	50.00 Hz
GB	0
PC	1.40

1D NMR plot parameters

CX	20.00 cm
F1P	150.000 ppm
F1	15091.88 Hz
F2P	0.000 ppm
F2	0.00 Hz
PPMCM	7.50000 ppm/cm
HZCM	754.59381 Hz/cm

APPENDIX G:

ECCLES modeling output

The ECCLES calculation output, with respect to the monitored components, is presented in the order used in Section 4.4

APD AND Ho(III)

```
****      ****      ****      *         *****     *****
         *         *          *         *         *
***      *         *          *         ****      *****
         *         *          *         *             *
****      ****      ****      *****     *****     *****
-------------------------------------------------------
```

```
><><><><><><><><><><><><><><><><><><><><><><><><><><><><><><><><><><><><><><><><><
>
>                       NORMAL PLASMA WITH ALL THE METALS
>
>
>  INCLUDING HO                                                            100392
>
><><><><><><><><><><><><><><><><><><><><><><><><><><><><><><><><><><><><><><><><><
```

```
JTPUT SUPRESSED.
DNITORED COMPONENTS:  HO+3 APD0
) SCAN REQUIRED.
:CLES DATA CHECKING PROCEDURES EMPLOYED.
IERE ARE 20 SPECIES WITH DEFINED CONCENTRATIONS.

ATA INPUT SUCCESSFULLY COMPLETED.
)TAL NUMBER OF COMPONENTS =  54  (LIMIT = 115 )
JMBER OF COMPONENTS WITH FIXED FREE CONCENTRATIONS = 13  (LIMIT = 15 )
)TAL NUMBER OF SPECIES =  4977  (LIMIT =  5000 )
)TAL NUMBER OF COMPONENTS ENTERED IN KEY ARRAY = 17347  (LIMIT = 18000 )

{PERIMENTAL PH =       7.398              CALCULATED LOG KW =    -13.3116
```

MONITOR COMPONENT HO+3 FREE CONC. = 2.5000E-11

SPECIES NO.	SPECIES CONC.		LOG STAB. CONST.	COMPOSITION.
1300	3.1989E-07	57.5%	23.34	APD0(1) HO+3(1) H +1(1)
1256	1.6349E-07	29.4%	14.31	CTA3(1) HO+3(1) OH-1(1)
1257	4.6284E-08	8.3%	19.67	CTA3(1) HO+3(1) OH-1(2)
1253	9.7623E-09	1.8%	7.17	CTA3(1) HO+3(1)
1268	7.6319E-09	1.4%	13.40	SLA2(1) HO+3(1)
1299	2.3602E-09	.4%	13.81	APD0(1) HO+3(1)
1274	1.4713E-09	.3%	6.26	CO32(1) HO+3(1)
1337	1.3876E-09	.2%	9.08	CTA3(1) LTA1(1) HO+3(1)
1254	1.3218E-09	.2%	10.88	CTA3(2) HO+3(1)
1324	7.6159E-10	.1%	14.10	CYS2(1) CTA3(1) HO+3(1)
1325	3.2609E-10	.1%	11.19	HIS1(1) CTA3(1) HO+3(1)
1345	2.6193E-10	.0%	10.10	CTA3(1) MLA2(1) HO+3(1)
1301	2.5530E-10	.0%	27.64	APD0(1) HO+3(1) H +1(2)
1329	1.6564E-10	.0%	9.09	SO42(1) CTA3(1) HO+3(1)
1263	1.2270E-10	.0%	5.70	OXA2(1) HO+3(1)
1326	9.3871E-11	.0%	13.34	LYS1(1) CTA3(1) HO+3(1)
1261	8.7412E-11	.0%	5.04	MLA2(1) HO+3(1)
1331	7.9950E-11	.0%	11.30	CYS2(1) LTA1(1) HO+3(1)
1258	5.2559E-11	.0%	3.08	LTA1(1) HO+3(1)
1327	4.6851E-11	.0%	11.49	TRP1(1) CTA3(1) HO+3(1)
1214	4.5931E-11	.0%	5.70	ARG0(1) HO+3(1)
1332	3.4231E-11	.0%	8.39	HIS1(1) LTA1(1) HO+3(1)
1323	3.3396E-11	.0%	11.89	ASP2(1) CTA3(1) HO+3(1)
1219	3.2219E-11	.0%	8.14	CYS2(1) HO+3(1)
1233	3.2142E-11	.0%	5.90	LEU1(1) HO+3(1)
1346	2.7497E-11	.0%	7.30	LTA1(1) MLA2(1) HO+3(1)
1236	2.2556E-11	.0%	5.90	MET1(1) HO+3(1)
1304	1.8788E-11	.0%	13.40	CYS2(1) HIS1(1) HO+3(1)
1336	1.7388E-11	.0%	6.29	SO42(1) LTA1(1) HO+3(1)
1225	1.6735E-11	.0%	11.21	GLY1(1) HO+3(1) OH-1(1)
1213	1.5916E-11	.0%	11.16	ALA1(1) HO+3(1) OH-1(1)
1218	1.5482E-11	.0%	5.69	CIT1(1) HO+3(1)
1339	1.5092E-11	.0%	12.31	CYS2(1) MLA2(1) HO+3(1)
1223	1.4863E-11	.0%	5.89	GLU2(1) HO+3(1)
1259	1.4567E-11	.0%	5.28	LTA1(2) HO+3(1)
1232	1.3782E-11	.0%	5.90	ILE1(1) HO+3(1)
1228	1.2785E-11	.0%	5.20	HIS1(1) HO+3(1)
1354	1.0550E-11	.0%	8.23	CTA3(1) PVA1(1) HO+3(1)
1243	9.8573E-12	.0%	4.63	THR1(1) HO+3(1)
1333	9.8543E-12	.0%	10.54	LYS1(1) LTA1(1) HO+3(1)
1318	9.5438E-12	.0%	11.31	CYS2(1) SO42(1) HO+3(1)
1249	8.0826E-12	.0%	3.20	SO42(1) HO+3(1)
1240	7.3421E-12	.0%	11.90	THR1(1) HO+3(1) H +1(1)
1224	6.8826E-12	.0%	12.31	GLY1(1) HO+3(1) H +1(1)
1241	6.7552E-12	.0%	16.29	THR1(1) HO+3(1) OH-1(2)
1211	6.7035E-12	.0%	5.90	ABA1(1) HO+3(1)
1340	6.4618E-12	.0%	9.40	HIS1(1) MLA2(1) HO+3(1)
1242	6.3343E-12	.0%	10.35	THR1(1) HO+3(1) OH-1(1)
1272	6.2500E-12	.0%	5.31	HO+3(1) OH-1(1)
1239	5.6833E-12	.0%	5.90	PRO1(1) HO+3(1)
1306	5.4086E-12	.0%	15.56	CYS2(1) LYS1(1) HO+3(1)
1226	5.3898E-12	.0%	16.63	GLY1(1) HO+3(1) OH-1(2)
1334	4.9183E-12	.0%	8.69	TRP1(1) LTA1(1) HO+3(1)

MONITOR COMPONENT APD0 FREE CONC. = 1.4622E-12

SPECIES NO.	SPECIES CONC.		LOG STAB. CONST.	COMPOSITION.
1281	6.8111E-05	80.1%	20.96	APD0(1) CA+2(2) H +1(1)
1297	5.5343E-06	6.5%	17.26	APD0(1) MG+2(1) H +1(1)
1280	5.3846E-06	6.3%	12.46	APD0(1) CA+2(2)
1279	2.9521E-06	3.5%	16.65	APD0(1) CA+2(1) H +1(1)
1276	1.3156E-06	1.5%	20.75	APD0(1) H +1(2)
1298	1.3035E-06	1.5%	24.03	APD0(1) MG+2(1) H +1(2)
1300	3.1989E-07	.4%	23.34	APD0(1) HO+3(1) H +1(1)
1277	5.3849E-08	.1%	26.76	APD0(1) H +1(3)
1290	8.8524E-09	.0%	20.18	APD0(1) ZN+2(1) H +1(1)
1296	8.1471E-09	.0%	7.03	APD0(1) MG+2(1)
1275	5.2127E-09	.0%	10.95	APD0(1) H +1(1)
1299	2.3602E-09	.0%	13.81	APD0(1) HO+3(1)
1301	2.5530E-10	.0%	27.64	APD0(1) HO+3(1) H +1(2)
1291	2.3940E-10	.0%	26.01	APD0(1) ZN+2(1) H +1(2)
1289	2.2131E-10	.0%	11.18	APD0(1) ZN+2(1)
1278	7.8206E-13	.0%	29.32	APD0(1) H +1(4)
1292	9.1821E-14	.0%	13.71	APD0(1) ZN+2(1) OH-1(1)
1294	1.4030E-17	.0%	25.38	APD0(1) FE+3(1) H +1(1)
1293	9.6605E-18	.0%	17.82	APD0(1) FE+3(1)
1286	6.8716E-19	.0%	21.07	APD0(1) CU+2(1) H +1(1)
1285	2.0654E-19	.0%	13.15	APD0(1) CU+2(1)
1283	1.1670E-19	.0%	18.30	APD0(1) NI+2(1) H +1(1)
1282	2.7227E-20	.0%	10.27	APD0(1) NI+2(1)
1284	3.3816E-21	.0%	24.16	APD0(1) NI+2(1) H +1(2)
1287	1.5457E-21	.0%	25.82	APD0(1) CU+2(1) H +1(2)
1295	1.0943E-21	.0%	28.67	APD0(1) FE+3(1) H +1(2)
1288	3.1838E-23	.0%	15.25	APD0(1) CU+2(1) OH-1(1)

WELL DONE ECCLES', SAID MORIARTY.

HEDP AND Sm(III)

```
****      ****      ****      *         *****     *****
            *         *         *         *         *
***         *         *         *         ****      *****
            *         *         *         *             *
****      ****      ****      *****     *****     *****
-------------------------------------------------------
```

```
><><><><><><><><><><><><><><><><><><><><><><><><><><><><><><><><><><><><><><><><><><><><><><><><
>
>                        NORMAL PLASMA WITH ALL THE METALS
>
>
>  INCLUDING SM                                                           100392
>
><><><><><><><><><><><><><><><><><><><><><><><><><><><><><><><><><><><><><><><><><><><><><><><><
```

JTPUT SUPRESSED.
ONITORED COMPONENTS: SM+3 HED4
O SCAN REQUIRED.
CCLES DATA CHECKING PROCEDURES EMPLOYED.
HERE ARE 20 SPECIES WITH DEFINED CONCENTRATIONS.

ATA INPUT SUCCESSFULLY COMPLETED.
OTAL NUMBER OF COMPONENTS = 54 (LIMIT = 115)
JMBER OF COMPONENTS WITH FIXED FREE CONCENTRATIONS = 13 (LIMIT = 15)
OTAL NUMBER OF SPECIES = 4977 (LIMIT = 5000)
OTAL NUMBER OF COMPONENTS ENTERED IN KEY ARRAY = 17352 (LIMIT = 18000)

XPERIMENTAL PH =   7.398   CALCULATED LOG KW =   -13.3116

MONITOR COMPONENT SM+3 FREE CONC. = 2.5000E-11

SPECIES NO.	SPECIES CONC.		LOG STAB. CONST.	COMPOSITION.
1291	1.5807E-07	60.7%	19.20	HED4(1) SM+3(1) H +1(1)
1256	6.6220E-08	25.4%	13.91	CTA3(1) SM+3(1) OH-1(1)
1257	2.6057E-08	10.0%	19.42	CTA3(1) SM+3(1) OH-1(2)
1290	3.1389E-09	1.2%	10.10	HED4(1) SM+3(1)
1253	3.0203E-09	1.2%	6.66	CTA3(1) SM+3(1)
1268	1.7504E-09	.7%	12.76	SLA2(1) SM+3(1)
1274	7.5457E-10	.3%	5.97	CO32(1) SM+3(1)
1327	4.1952E-10	.2%	8.56	CTA3(1) LTA1(1) SM+3(1)
1254	3.5658E-10	.1%	10.31	CTA3(2) SM+3(1)
1314	1.8502E-10	.1%	13.48	CYS2(1) CTA3(1) SM+3(1)
1315	9.0955E-11	.0%	10.63	HIS1(1) CTA3(1) SM+3(1)
1335	7.5628E-11	.0%	9.56	CTA3(1) MLA2(1) SM+3(1)
1319	4.8379E-11	.0%	8.56	SO42(1) CTA3(1) SM+3(1)
1263	3.9705E-11	.0%	5.21	OXA2(1) SM+3(1)
1261	2.9619E-11	.0%	4.57	MLA2(1) SM+3(1)
1316	2.4436E-11	.0%	12.76	LYS1(1) CTA3(1) SM+3(1)
1321	2.1769E-11	.0%	10.73	CYS2(1) LTA1(1) SM+3(1)
1258	1.9528E-11	.0%	2.65	LTA1(1) SM+3(1)
1214	1.4525E-11	.0%	5.20	ARG0(1) SM+3(1)
1317	1.3684E-11	.0%	10.95	TRP1(1) CTA3(1) SM+3(1)
1322	1.0701E-11	.0%	7.88	HIS1(1) LTA1(1) SM+3(1)
1233	1.0164E-11	.0%	5.40	LEU1(1) SM+3(1)
1219	9.6188E-12	.0%	7.62	CYS2(1) SM+3(1)
1336	8.8978E-12	.0%	6.80	LTA1(1) MLA2(1) SM+3(1)
1313	8.6934E-12	.0%	11.31	ASP2(1) CTA3(1) SM+3(1)
1225	7.6495E-12	.0%	10.87	GLY1(1) SM+3(1) OH-1(1)
1213	7.2749E-12	.0%	10.82	ALA1(1) SM+3(1) OH-1(1)
1236	7.1329E-12	.0%	5.40	MET1(1) SM+3(1)
1326	5.6919E-12	.0%	5.80	SO42(1) LTA1(1) SM+3(1)
1218	5.1265E-12	.0%	5.21	CIT1(1) SM+3(1)
1259	4.9358E-12	.0%	4.81	LTA1(2) SM+3(1)
1223	4.8876E-12	.0%	5.41	GLU2(1) SM+3(1)
1294	4.7196E-12	.0%	12.80	CYS2(1) HIS1(1) SM+3(1)
1241	4.4631E-12	.0%	16.11	THR1(1) SM+3(1) OH-1(2)
1232	4.3583E-12	.0%	5.40	ILE1(1) SM+3(1)
1228	4.0431E-12	.0%	4.70	HIS1(1) SM+3(1)
1329	3.9243E-12	.0%	11.73	CYS2(1) MLA2(1) SM+3(1)
1226	3.4800E-12	.0%	16.44	GLY1(1) SM+3(1) OH-1(2)
1243	3.4179E-12	.0%	4.17	THR1(1) SM+3(1)
1344	3.3018E-12	.0%	7.72	CTA3(1) PVA1(1) SM+3(1)
1249	3.2178E-12	.0%	2.80	SO42(1) SM+3(1)
1272	3.1324E-12	.0%	5.01	SM+3(1) OH-1(1)
1242	3.0318E-12	.0%	10.03	THR1(1) SM+3(1) OH-1(1)
1221	3.0242E-12	.0%	15.52	GLN1(1) SM+3(1) OH-1(2)
1323	2.8749E-12	.0%	10.01	LYS1(1) LTA1(1) SM+3(1)
1308	2.5104E-12	.0%	10.73	CYS2(1) SO42(1) SM+3(1)
1211	2.1198E-12	.0%	5.40	ABA1(1) SM+3(1)
1330	1.9291E-12	.0%	8.88	HIS1(1) MLA2(1) SM+3(1)
1240	1.8443E-12	.0%	11.30	THR1(1) SM+3(1) H +1(1)
1239	1.7972E-12	.0%	5.40	PRO1(1) SM+3(1)
1224	1.7288E-12	.0%	11.71	GLY1(1) SM+3(1) H +1(1)
1324	1.6100E-12	.0%	8.20	TRP1(1) LTA1(1) SM+3(1)
1248	1.4428E-12	.0%	10.19	VAL1(1) SM+3(1) OH-1(1)

MONITOR COMPONENT HED4 FREE CONC. = 9.9732E-09

SPECIES NO.	SPECIES CONC.		LOG STAB. CONST.	COMPOSITION.
1281	4.3151E-05	50.8%	9.53	HED4(1) CA+2(2)
1288	1.3516E-05	15.9%	9.70	HED4(1) MG+2(2)
1287	6.7127E-06	7.9%	13.51	HED4(1) MG+2(1) H +1(1)
1282	6.6677E-06	7.8%	13.17	HED4(1) CA+2(1) H +1(1)
1286	5.5570E-06	6.5%	6.03	HED4(1) MG+2(1)
1275	5.1392E-06	6.0%	10.11	HED4(1) H +1(1)
1280	2.4656E-06	2.9%	5.34	HED4(1) CA+2(1)
1276	1.3273E-06	1.6%	16.92	HED4(1) H +1(2)
1283	2.8108E-07	.3%	10.45	HED4(1) ZN+2(1)
1291	1.5807E-07	.2%	19.20	HED4(1) SM+3(1) H +1(1)
1289	8.9698E-09	.0%	9.15	HED4(1) MG+2(1) OH-1(1)
1290	3.1389E-09	.0%	10.10	HED4(1) SM+3(1)
1284	2.1923E-09	.0%	15.74	HED4(1) ZN+2(1) H +1(1)
1277	4.9547E-11	.0%	19.89	HED4(1) H +1(3)
1285	2.1036E-12	.0%	20.12	HED4(1) ZN+2(1) H +1(2)
1278	5.4585E-16	.0%	22.33	HED4(1) H +1(4)
1279	3.9012E-26	.0%	26.98	HED4(1) H +1(6)

HEDP, Transferrin and Sm(III)

```
****      ****      ****      *         *****     *****
            *         *         *         *         *
***         *         *         *         ****      *****
            *         *         *         *             *
****      ****      ****      *****     *****     *****
-------------------------------------------------------
```

```
><><><><><><><><><><><><><><><><><><><><><><><><><><><><><><><><><><><><><><><><><
>
>                       NORMAL PLASMA WITH ALL THE METALS
>
>
>  INCLUDING SM                                                        100392
>
><><><><><><><><><><><><><><><><><><><><><><><><><><><><><><><><><><><><><><><><><
```

```
JTPUT SUPRESSED.
)NITORED COMPONENTS:  SM+3 HED4
) SCAN REQUIRED.
:CLES DATA CHECKING PROCEDURES EMPLOYED.
IERE ARE 20 SPECIES WITH DEFINED CONCENTRATIONS.

\TA INPUT SUCCESSFULLY COMPLETED.
)TAL NUMBER OF COMPONENTS =  55   (LIMIT = 115 )
JMBER OF COMPONENTS WITH FIXED FREE CONCENTRATIONS = 13   (LIMIT = 15 )
)TAL NUMBER OF SPECIES =   4977   (LIMIT =   5000 )
)TAL NUMBER OF COMPONENTS ENTERED IN KEY ARRAY = 17360   (LIMIT = 18000 )

(PERIMENTAL PH =       7.398            CALCULATED LOG KW =     -13.3116
```

MONITOR COMPONENT SM+3 FREE CONC. = 2.0000E-11

SPECIES NO.	SPECIES CONC.		LOG STAB. CONST.	COMPOSITION.
1292	1.4547E-06	87.1%	25.49	TFRN(1) CO32(1) SM+3(1)OH-1(2
1291	1.2650E-07	7.6%	19.20	HED4(1) SM+3(1) H +1(1)
1256	5.2985E-08	3.2%	13.91	CTA3(1) SM+3(1) OH-1(1)
1257	2.0849E-08	1.2%	19.42	CTA3(1) SM+3(1) OH-1(2)
1293	3.3838E-09	.4%	49.88	TFRN(1) CO32(2) SM+3(2)OH-1(4
1290	2.5121E-09	.2%	10.10	HED4(1) SM+3(1)
1253	2.4166E-09	.1%	6.66	CTA3(1) SM+3(1)
1268	1.4004E-09	.1%	12.76	SLA2(1) SM+3(1)
1274	6.0362E-10	.0%	5.97	CO32(1) SM+3(1)
1329	3.3568E-10	.0%	8.56	CTA3(1) LTA1(1) SM+3(1)
1254	2.8536E-10	.0%	10.31	CTA3(2) SM+3(1)
1316	1.4805E-10	.0%	13.48	CYS2(1) CTA3(1) SM+3(1)
1317	7.2777E-11	.0%	10.63	HIS1(1) CTA3(1) SM+3(1)
1337	6.0513E-11	.0%	9.56	CTA3(1) MLA2(1) SM+3(1)
1321	3.8710E-11	.0%	8.56	SO42(1) CTA3(1) SM+3(1)
1263	3.1764E-11	.0%	5.21	OXA2(1) SM+3(1)
1261	2.3696E-11	.0%	4.57	MLA2(1) SM+3(1)
1318	1.9552E-11	.0%	12.76	LYS1(1) CTA3(1) SM+3(1)
1323	1.7415E-11	.0%	10.73	CYS2(1) LTA1(1) SM+3(1)
1258	1.5622E-11	.0%	2.65	LTA1(1) SM+3(1)
1214	1.1620E-11	.0%	5.20	ARG0(1) SM+3(1)
1319	1.0949E-11	.0%	10.95	TRP1(1) CTA3(1) SM+3(1)
1324	8.5609E-12	.0%	7.88	HIS1(1) LTA1(1) SM+3(1)
1233	8.1313E-12	.0%	5.40	LEU1(1) SM+3(1)
1219	7.6951E-12	.0%	7.62	CYS2(1) SM+3(1)
1338	7.1183E-12	.0%	6.80	LTA1(1) MLA2(1) SM+3(1)
1315	6.9559E-12	.0%	11.31	ASP2(1) CTA3(1) SM+3(1)
1225	6.1196E-12	.0%	10.87	GLY1(1) SM+3(1) OH-1(1)
1213	5.8200E-12	.0%	10.82	ALA1(1) SM+3(1) OH-1(1)
1236	5.7063E-12	.0%	5.40	MET1(1) SM+3(1)
1328	4.5536E-12	.0%	5.80	SO42(1) LTA1(1) SM+3(1)
1218	4.1012E-12	.0%	5.21	CIT1(1) SM+3(1)
1259	3.9486E-12	.0%	4.81	LTA1(2) SM+3(1)
1223	3.9101E-12	.0%	5.41	GLU2(1) SM+3(1)
1296	3.7757E-12	.0%	12.80	CYS2(1) HIS1(1) SM+3(1)
1241	3.5705E-12	.0%	16.11	THR1(1) SM+3(1) OH-1(2)
1232	3.4867E-12	.0%	5.40	ILE1(1) SM+3(1)
1228	3.2345E-12	.0%	4.70	HIS1(1) SM+3(1)
1331	3.1394E-12	.0%	11.73	CYS2(1) MLA2(1) SM+3(1)
1226	2.7840E-12	.0%	16.44	GLY1(1) SM+3(1) OH-1(2)
1243	2.7343E-12	.0%	4.17	THR1(1) SM+3(1)
1346	2.6419E-12	.0%	7.72	CTA3(1) PVA1(1) SM+3(1)
1249	2.5742E-12	.0%	2.80	SO42(1) SM+3(1)
1272	2.5059E-12	.0%	5.01	SM+3(1) OH-1(1)
1242	2.4254E-12	.0%	10.03	THR1(1) SM+3(1) OH-1(1)
1221	2.4194E-12	.0%	15.52	GLN1(1) SM+3(1) OH-1(2)
1325	2.2999E-12	.0%	10.01	LYS1(1) LTA1(1) SM+3(1)
1310	2.0083E-12	.0%	10.73	CYS2(1) SO42(1) SM+3(1)
1211	1.6959E-12	.0%	5.40	ABA1(1) SM+3(1)
1332	1.5433E-12	.0%	8.88	HIS1(1) MLA2(1) SM+3(1)
1240	1.4754E-12	.0%	11.30	THR1(1) SM+3(1) H +1(1)
1239	1.4378E-12	.0%	5.40	PRO1(1) SM+3(1)
1224	1.3831E-12	.0%	11.71	GLY1(1) SM+3(1) H +1(1)

MONITOR COMPONENT HED4 FREE CONC. = 9.9770E-09

SPECIES NO.	SPECIES CONC.		LOG STAB. CONST.	COMPOSITION.
1281	4.3168E-05	50.8%	9.53	HED4(1) CA+2(2)
1288	1.3521E-05	15.9%	9.70	HED4(1) MG+2(2)
1287	6.7153E-06	7.9%	13.51	HED4(1) MG+2(1) H +1(1)
1282	6.6702E-06	7.8%	13.17	HED4(1) CA+2(1) H +1(1)
1286	5.5591E-06	6.5%	6.03	HED4(1) MG+2(1)
1275	5.1412E-06	6.0%	10.11	HED4(1) H +1(1)
1280	2.4665E-06	2.9%	5.34	HED4(1) CA+2(1)
1276	1.3278E-06	1.6%	16.92	HED4(1) H +1(2)
1283	2.8119E-07	.3%	10.45	HED4(1) ZN+2(1)
1291	1.2650E-07	.1%	19.20	HED4(1) SM+3(1) H +1(1)
1289	8.9732E-09	.0%	9.15	HED4(1) MG+2(1) OH-1(1)
1290	2.5121E-09	.0%	10.10	HED4(1) SM+3(1)
1284	2.1931E-09	.0%	15.74	HED4(1) ZN+2(1) H +1(1)
1277	4.9566E-11	.0%	19.89	HED4(1) H +1(3)
1285	2.1044E-12	.0%	20.12	HED4(1) ZN+2(1) H +1(2)
1278	5.4606E-16	.0%	22.33	HED4(1) H +1(4)
1279	3.9027E-26	.0%	26.98	HED4(1) H +1(6)

'WELL DONE ECCLES', SAID MORIARTY.

MDP AND Sm(III)

```
****      ****      ****      *         *****     *****
         *         *         *         *         *
***      *         *         *         ****      *****
         *         *         *         *             *
****      ****      ****      *****     *****     *****
-------------------------------------------------------
```

```
><><><><><><><><><><><><><><><><><><><><><><><><><><><><><><><><><><><><><><><><
>
>                        NORMAL PLASMA WITH ALL THE METALS
>
>
>  INCLUDING SM                                                        100392
>
><><><><><><><><><><><><><><><><><><><><><><><><><><><><><><><><><><><><><><><><
```

```
UTPUT SUPRESSED.
ONITORED COMPONENTS:  SM+3 MDP0
O SCAN REQUIRED.
CCLES DATA CHECKING PROCEDURES EMPLOYED.
HERE ARE 20 SPECIES WITH DEFINED CONCENTRATIONS.

ATA INPUT SUCCESSFULLY COMPLETED.
OTAL NUMBER OF COMPONENTS =  54   (LIMIT = 115 )
UMBER OF COMPONENTS WITH FIXED FREE CONCENTRATIONS = 13  (LIMIT = 15 )
OTAL NUMBER OF SPECIES =  4977  (LIMIT =  5000 )
OTAL NUMBER OF COMPONENTS ENTERED IN KEY ARRAY = 17351  (LIMIT = 18000 )

XPERIMENTAL PH =       7.398            CALCULATED LOG KW =    -13.3116
```

MONITOR COMPONENT SM+3 FREE CONC. = 2.5000E-11

SPECIES NO.	SPECIES CONC.		LOG STAB. CONST.	COMPOSITION.
1293	9.2233E-08	47.6%	18.30	MDP0(1) SM+3(1) H +1(1)
1256	6.6220E-08	34.2%	13.91	CTA3(1) SM+3(1) OH-1(1)
1257	2.6057E-08	13.4%	19.42	CTA3(1) SM+3(1) OH-1(2)
1253	3.0203E-09	1.6%	6.66	CTA3(1) SM+3(1)
1292	2.3058E-09	1.2%	9.30	MDP0(1) SM+3(1)
1268	1.7504E-09	.9%	12.76	SLA2(1) SM+3(1)
1274	7.5457E-10	.4%	5.97	CO32(1) SM+3(1)
1329	4.1952E-10	.2%	8.56	CTA3(1) LTA1(1) SM+3(1)
1254	3.5658E-10	.2%	10.31	CTA3(2) SM+3(1)
1316	1.8502E-10	.1%	13.48	CYS2(1) CTA3(1) SM+3(1)
1317	9.0955E-11	.0%	10.63	HIS1(1) CTA3(1) SM+3(1)
1337	7.5628E-11	.0%	9.56	CTA3(1) MLA2(1) SM+3(1)
1321	4.8379E-11	.0%	8.56	SO42(1) CTA3(1) SM+3(1)
1263	3.9705E-11	.0%	5.21	OXA2(1) SM+3(1)
1261	2.9619E-11	.0%	4.57	MLA2(1) SM+3(1)
1318	2.4436E-11	.0%	12.76	LYS1(1) CTA3(1) SM+3(1)
1323	2.1769E-11	.0%	10.73	CYS2(1) LTA1(1) SM+3(1)
1258	1.9528E-11	.0%	2.65	LTA1(1) SM+3(1)
1214	1.4525E-11	.0%	5.20	ARG0(1) SM+3(1)
1319	1.3684E-11	.0%	10.95	TRP1(1) CTA3(1) SM+3(1)
1324	1.0701E-11	.0%	7.88	HIS1(1) LTA1(1) SM+3(1)
1233	1.0164E-11	.0%	5.40	LEU1(1) SM+3(1)
1219	9.6188E-12	.0%	7.62	CYS2(1) SM+3(1)
1338	8.8978E-12	.0%	6.80	LTA1(1) MLA2(1) SM+3(1)
1315	8.6934E-12	.0%	11.31	ASP2(1) CTA3(1) SM+3(1)
1225	7.6495E-12	.0%	10.87	GLY1(1) SM+3(1) OH-1(1)
1213	7.2749E-12	.0%	10.82	ALA1(1) SM+3(1) OH-1(1)
1236	7.1329E-12	.0%	5.40	MET1(1) SM+3(1)
1328	5.6919E-12	.0%	5.80	SO42(1) LTA1(1) SM+3(1)
1218	5.1265E-12	.0%	5.21	CIT1(1) SM+3(1)
1259	4.9358E-12	.0%	4.81	LTA1(2) SM+3(1)
1223	4.8876E-12	.0%	5.41	GLU2(1) SM+3(1)
1296	4.7196E-12	.0%	12.80	CYS2(1) HIS1(1) SM+3(1)
1241	4.4631E-12	.0%	16.11	THR1(1) SM+3(1) OH-1(2)
1232	4.3583E-12	.0%	5.40	ILE1(1) SM+3(1)
1228	4.0431E-12	.0%	4.70	HIS1(1) SM+3(1)
1331	3.9243E-12	.0%	11.73	CYS2(1) MLA2(1) SM+3(1)
1226	3.4800E-12	.0%	16.44	GLY1(1) SM+3(1) OH-1(2)
1243	3.4179E-12	.0%	4.17	THR1(1) SM+3(1)
1346	3.3018E-12	.0%	7.72	CTA3(1) PVA1(1) SM+3(1)
1249	3.2178E-12	.0%	2.80	SO42(1) SM+3(1)
1272	3.1324E-12	.0%	5.01	SM+3(1) OH-1(1)
1242	3.0318E-12	.0%	10.03	THR1(1) SM+3(1) OH-1(1)
1221	3.0242E-12	.0%	15.52	GLN1(1) SM+3(1) OH-1(2)
1325	2.8749E-12	.0%	10.01	LYS1(1) LTA1(1) SM+3(1)
1310	2.5104E-12	.0%	10.73	CYS2(1) SO42(1) SM+3(1)
1211	2.1198E-12	.0%	5.40	ABA1(1) SM+3(1)
1332	1.9291E-12	.0%	8.88	HIS1(1) MLA2(1) SM+3(1)
1240	1.8443E-12	.0%	11.30	THR1(1) SM+3(1) H +1(1)
1239	1.7972E-12	.0%	5.40	PRO1(1) SM+3(1)
1224	1.7288E-12	.0%	11.71	GLY1(1) SM+3(1) H +1(1)
1326	1.6100E-12	.0%	8.20	TRP1(1) LTA1(1) SM+3(1)
1248	1.4428E-12	.0%	10.19	VAL1(1) SM+3(1) OH-1(1)

MONITOR COMPONENT MDP0 FREE CONC. = 4.6226E-08

SPECIES NO.	SPECIES CONC.		LOG STAB. CONST.	COMPOSITION.
1275	1.7256E-05	20.3%	9.97	MDP0(1) H +1(1)
1290	1.6709E-05	19.7%	13.24	MDP0(1) MG+2(1) H +1(1)
1281	1.4489E-05	17.0%	8.39	MDP0(1) CA+2(2)
1289	1.1505E-05	13.5%	5.68	MDP0(1) MG+2(1)
1282	1.0234E-05	12.0%	12.69	MDP0(1) CA+2(1) H +1(1)
1276	7.0633E-06	8.3%	16.98	MDP0(1) H +1(2)
1280	3.7841E-06	4.5%	4.86	MDP0(1) CA+2(1)
1291	2.8635E-06	3.4%	8.36	MDP0(1) MG+2(2)
1286	9.4382E-07	1.1%	10.31	MDP0(1) ZN+2(1)
1293	9.2233E-08	.1%	18.30	MDP0(1) SM+3(1) H +1(1)
1287	1.0888E-08	.0%	15.77	MDP0(1) ZN+2(1) H +1(1)
1292	2.3058E-09	.0%	9.30	MDP0(1) SM+3(1)
1277	5.1412E-10	.0%	20.24	MDP0(1) H +1(3)
1288	1.1722E-11	.0%	20.20	MDP0(1) ZN+2(1) H +1(2)
1278	3.1126E-15	.0%	22.42	MDP0(1) H +1(4)
1283	8.6077E-19	.0%	7.27	MDP0(1) NI+2(1)
1285	3.2571E-21	.0%	10.76	MDP0(1) NI+2(1) OH-1(1)
1279	6.7181E-25	.0%	27.55	MDP0(1) H +1(6)
1284	5.3075E-33	.0%	11.06	MDP0(1) NI+2(2)

'WELL DONE ECCLES', SAID MORIARTY.

MDP, Transferrin and Sm(III)

```
*****      ****      ****      *         *****      *****
*         *         *         *         *          *
****      *         *         *         ****       *****
*         *         *         *         *              *
*****      ****      ****      *****     *****      *****
-------------------------------------------------------
```

```
<><><><><><><><><><><><><><><><><><><><><><><><><><><><><><><><><><><><><><><><><><><><><><><><><><><><><><<
<>
<>                        NORMAL PLASMA WITH ALL THE METALS
<>
<>
<>  INCLUDING SM                                                      100392
<>
<><><><><><><><><><><><><><><><><><><><><><><><><><><><><><><><><><><><><><><><><><><><><><><><><><><><><><<
```

```
OUTPUT SUPRESSED.
MONITORED COMPONENTS:  SM+3 MDP0
NO SCAN REQUIRED.
ECCLES DATA CHECKING PROCEDURES EMPLOYED.
THERE ARE 20 SPECIES WITH DEFINED CONCENTRATIONS.

DATA INPUT SUCCESSFULLY COMPLETED.
TOTAL NUMBER OF COMPONENTS =  55  (LIMIT = 115 )
NUMBER OF COMPONENTS WITH FIXED FREE CONCENTRATIONS = 13  (LIMIT = 15 )
TOTAL NUMBER OF SPECIES =  4977  (LIMIT =  5000 )
TOTAL NUMBER OF COMPONENTS ENTERED IN KEY ARRAY = 17358  (LIMIT = 18000 )

EXPERIMENTAL PH =       7.398           CALCULATED LOG KW =    -13.3116
```

MONITOR COMPONENT SM+3 FREE CONC. = 1.8000E-11

SPECIES NO.	SPECIES CONC.		LOG STAB. CONST.	COMPOSITION.
1294	1.3130E-06	90.0%	25.49	TFRN(1) CO32(1) SM+3(1)OH-1(2
1293	6.6429E-08	4.6%	18.30	MDP0(1) SM+3(1) H +1(1)
1256	4.7690E-08	3.3%	13.91	CTA3(1) SM+3(1) OH-1(1)
1257	1.8766E-08	1.3%	19.42	CTA3(1) SM+3(1) OH-1(2)
1295	2.7490E-09	.4%	49.88	TFRN(1) CO32(2) SM+3(2)OH-1(4
1253	2.1751E-09	.1%	6.66	CTA3(1) SM+3(1)
1292	1.6607E-09	.1%	9.30	MDP0(1) SM+3(1)
1268	1.2604E-09	.1%	12.76	SLA2(1) SM+3(1)
1274	5.4326E-10	.0%	5.97	CO32(1) SM+3(1)
1331	3.0213E-10	.0%	8.56	CTA3(1) LTA1(1) SM+3(1)
1254	2.5686E-10	.0%	10.31	CTA3(2) SM+3(1)
1318	1.3325E-10	.0%	13.48	CYS2(1) CTA3(1) SM+3(1)
1319	6.5503E-11	.0%	10.63	HIS1(1) CTA3(1) SM+3(1)
1339	5.4466E-11	.0%	9.56	CTA3(1) MLA2(1) SM+3(1)
1323	3.4842E-11	.0%	8.56	SO42(1) CTA3(1) SM+3(1)
1263	2.8587E-11	.0%	5.21	OXA2(1) SM+3(1)
1261	2.1326E-11	.0%	4.57	MLA2(1) SM+3(1)
1320	1.7598E-11	.0%	12.76	LYS1(1) CTA3(1) SM+3(1)
1325	1.5673E-11	.0%	10.73	CYS2(1) LTA1(1) SM+3(1)
1258	1.4060E-11	.0%	2.65	LTA1(1) SM+3(1)
1214	1.0458E-11	.0%	5.20	ARG0(1) SM+3(1)
1321	9.8549E-12	.0%	10.95	TRP1(1) CTA3(1) SM+3(1)
1326	7.7048E-12	.0%	7.88	HIS1(1) LTA1(1) SM+3(1)
1233	7.3182E-12	.0%	5.40	LEU1(1) SM+3(1)
1219	6.9256E-12	.0%	7.62	CYS2(1) SM+3(1)
1340	6.4065E-12	.0%	6.80	LTA1(1) MLA2(1) SM+3(1)
1317	6.2608E-12	.0%	11.31	ASP2(1) CTA3(1) SM+3(1)
1225	5.5076E-12	.0%	10.87	GLY1(1) SM+3(1) OH-1(1)
1213	5.2380E-12	.0%	10.82	ALA1(1) SM+3(1) OH-1(1)
1236	5.1357E-12	.0%	5.40	MET1(1) SM+3(1)
1330	4.0982E-12	.0%	5.80	SO42(1) LTA1(1) SM+3(1)
1218	3.6911E-12	.0%	5.21	CIT1(1) SM+3(1)
1259	3.5538E-12	.0%	4.81	LTA1(2) SM+3(1)
1223	3.5191E-12	.0%	5.41	GLU2(1) SM+3(1)
1298	3.3981E-12	.0%	12.80	CYS2(1) HIS1(1) SM+3(1)
1241	3.2135E-12	.0%	16.11	THR1(1) SM+3(1) OH-1(2)
1232	3.1380E-12	.0%	5.40	ILE1(1) SM+3(1)
1228	2.9111E-12	.0%	4.70	HIS1(1) SM+3(1)
1333	2.8255E-12	.0%	11.73	CYS2(1) MLA2(1) SM+3(1)
1226	2.5056E-12	.0%	16.44	GLY1(1) SM+3(1) OH-1(2)
1243	2.4609E-12	.0%	4.17	THR1(1) SM+3(1)
1348	2.3779E-12	.0%	7.72	CTA3(1) PVA1(1) SM+3(1)
1249	2.3168E-12	.0%	2.80	SO42(1) SM+3(1)
1272	2.2553E-12	.0%	5.01	SM+3(1) OH-1(1)
1242	2.1829E-12	.0%	10.03	THR1(1) SM+3(1) OH-1(1)
1221	2.1774E-12	.0%	15.52	GLN1(1) SM+3(1) OH-1(2)
1327	2.0699E-12	.0%	10.01	LYS1(1) LTA1(1) SM+3(1)
1312	1.8075E-12	.0%	10.73	CYS2(1) SO42(1) SM+3(1)
1211	1.5263E-12	.0%	5.40	ABA1(1) SM+3(1)
1334	1.3890E-12	.0%	8.88	HIS1(1) MLA2(1) SM+3(1)
1240	1.3279E-12	.0%	11.30	THR1(1) SM+3(1) H +1(1)
1239	1.2940E-12	.0%	5.40	PRO1(1) SM+3(1)
1224	1.2448E-12	.0%	11.71	GLY1(1) SM+3(1) H +1(1)

MONITOR COMPONENT MDP0 FREE CONC. = 4.6241E-08

SPECIES NO.	SPECIES CONC.		LOG STAB. CONST.	COMPOSITION.
1275	1.7262E-05	20.3%	9.97	MDP0(1) H +1(1)
1290	1.6714E-05	19.7%	13.24	MDP0(1) MG+2(1) H +1(1)
1281	1.4494E-05	17.1%	8.39	MDP0(1) CA+2(2)
1289	1.1509E-05	13.5%	5.68	MDP0(1) MG+2(1)
1282	1.0237E-05	12.0%	12.69	MDP0(1) CA+2(1) H +1(1)
1276	7.0655E-06	8.3%	16.98	MDP0(1) H +1(2)
1280	3.7853E-06	4.5%	4.86	MDP0(1) CA+2(1)
1291	2.8644E-06	3.4%	8.36	MDP0(1) MG+2(2)
1286	9.4411E-07	1.1%	10.31	MDP0(1) ZN+2(1)
1293	6.6429E-08	.1%	18.30	MDP0(1) SM+3(1) H +1(1)
1287	1.0891E-08	.0%	15.77	MDP0(1) ZN+2(1) H +1(1)
1292	1.6607E-09	.0%	9.30	MDP0(1) SM+3(1)
1277	5.1428E-10	.0%	20.24	MDP0(1) H +1(3)
1288	1.1726E-11	.0%	20.20	MDP0(1) ZN+2(1) H +1(2)
1278	3.1136E-15	.0%	22.42	MDP0(1) H +1(4)
1283	8.6104E-19	.0%	7.27	MDP0(1) NI+2(1)
1285	3.2581E-21	.0%	10.76	MDP0(1) NI+2(1) OH-1(1)
1279	6.7202E-25	.0%	27.55	MDP0(1) H +1(6)
1284	5.3091E-33	.0%	11.06	MDP0(1) NI+2(2)

'WELL DONE ECCLES', SAID MORIARTY.

Citrate and Ho(III)

```
*****     ****     ****     *         *****     *****
*         *        *        *         *         *
****      *        *        *         ****      *****
*         *        *        *         *             *
*****     ****     ****     *****     *****     *****
-------------------------------------------------------
```

```
<><><><><><><><><><><><><><><><><><><><><><><><><><><><><><><><><><><><><><><><><><><><><><><><><>
<>
<>                        NORMAL PLASMA WITH ALL THE METALS
<>
<>
<>   INCLUDING HO                                                               100392
<>
<><><><><><><><><><><><><><><><><><><><><><><><><><><><><><><><><><><><><><><><><><><><><><><><><>
```

```
OUTPUT SUPRESSED.
MONITORED COMPONENTS:  HO+3 CTA3
NO SCAN REQUIRED.
ECCLES DATA CHECKING PROCEDURES EMPLOYED.
THERE ARE 20 SPECIES WITH DEFINED CONCENTRATIONS.

DATA INPUT SUCCESSFULLY COMPLETED.
TOTAL NUMBER OF COMPONENTS =  53   (LIMIT = 115 )
NUMBER OF COMPONENTS WITH FIXED FREE CONCENTRATIONS = 13  (LIMIT = 15 )
TOTAL NUMBER OF SPECIES =  4976  (LIMIT =  5000 )
TOTAL NUMBER OF COMPONENTS ENTERED IN KEY ARRAY = 17354  (LIMIT = 18000 )

EXPERIMENTAL PH =       7.398           CALCULATED LOG KW =    -13.3116
```

MONITOR COMPONENT HO+3 FREE CONC. = 2.5000E-11

SPECIES NO.	SPECIES CONC.		LOG STAB. CONST.	COMPOSITION.
1256	1.6349E-07	69.9%	14.31	CTA3(1) HO+3(1) OH-1(1)
1257	4.6284E-08	19.8%	19.67	CTA3(1) HO+3(1) OH-1(2)
1253	9.7623E-09	4.2%	7.17	CTA3(1) HO+3(1)
1268	7.6319E-09	3.3%	13.40	SLA2(1) HO+3(1)
1274	1.4713E-09	.6%	6.26	CO32(1) HO+3(1)
1310	1.3876E-09	.6%	9.08	CTA3(1) LTA1(1) HO+3(1)
1254	1.3218E-09	.6%	10.88	CTA3(2) HO+3(1)
1297	7.6159E-10	.3%	14.10	CYS2(1) CTA3(1) HO+3(1)
1298	3.2608E-10	.1%	11.19	HIS1(1) CTA3(1) HO+3(1)
1318	2.6193E-10	.1%	10.10	CTA3(1) MLA2(1) HO+3(1)
1302	1.6564E-10	.1%	9.09	SO42(1) CTA3(1) HO+3(1)
1263	1.2270E-10	.1%	5.70	OXA2(1) HO+3(1)
1299	9.3871E-11	.0%	13.34	LYS1(1) CTA3(1) HO+3(1)
1261	8.7412E-11	.0%	5.04	MLA2(1) HO+3(1)
1304	7.9950E-11	.0%	11.30	CYS2(1) LTA1(1) HO+3(1)
1258	5.2559E-11	.0%	3.08	LTA1(1) HO+3(1)
1300	4.6851E-11	.0%	11.49	TRP1(1) CTA3(1) HO+3(1)
1214	4.5931E-11	.0%	5.70	ARG0(1) HO+3(1)
1305	3.4231E-11	.0%	8.39	HIS1(1) LTA1(1) HO+3(1)
1296	3.3396E-11	.0%	11.89	ASP2(1) CTA3(1) HO+3(1)
1219	3.2219E-11	.0%	8.14	CYS2(1) HO+3(1)
1233	3.2142E-11	.0%	5.90	LEU1(1) HO+3(1)
1319	2.7497E-11	.0%	7.30	LTA1(1) MLA2(1) HO+3(1)
1236	2.2556E-11	.0%	5.90	MET1(1) HO+3(1)
1277	1.8788E-11	.0%	13.40	CYS2(1) HIS1(1) HO+3(1)
1309	1.7388E-11	.0%	6.29	SO42(1) LTA1(1) HO+3(1)
1225	1.6735E-11	.0%	11.21	GLY1(1) HO+3(1) OH-1(1)
1213	1.5916E-11	.0%	11.16	ALA1(1) HO+3(1) OH-1(1)
1218	1.5482E-11	.0%	5.69	CIT1(1) HO+3(1)
1312	1.5092E-11	.0%	12.31	CYS2(1) MLA2(1) HO+3(1)
1223	1.4863E-11	.0%	5.89	GLU2(1) HO+3(1)
1259	1.4567E-11	.0%	5.28	LTA1(2) HO+3(1)
1232	1.3782E-11	.0%	5.90	ILE1(1) HO+3(1)
1228	1.2785E-11	.0%	5.20	HIS1(1) HO+3(1)
1327	1.0550E-11	.0%	8.23	CTA3(1) PVA1(1) HO+3(1)
1243	9.8573E-12	.0%	4.63	THR1(1) HO+3(1)
1306	9.8543E-12	.0%	10.54	LYS1(1) LTA1(1) HO+3(1)
1291	9.5438E-12	.0%	11.31	CYS2(1) SO42(1) HO+3(1)
1249	8.0826E-12	.0%	3.20	SO42(1) HO+3(1)
1240	7.3420E-12	.0%	11.90	THR1(1) HO+3(1) H +1(1)
1224	6.8826E-12	.0%	12.31	GLY1(1) HO+3(1) H +1(1)
1241	6.7552E-12	.0%	16.29	THR1(1) HO+3(1) OH-1(2)
1211	6.7035E-12	.0%	5.90	ABA1(1) HO+3(1)
1313	6.4617E-12	.0%	9.40	HIS1(1) MLA2(1) HO+3(1)
1242	6.3343E-12	.0%	10.35	THR1(1) HO+3(1) OH-1(1)
1272	6.2500E-12	.0%	5.31	HO+3(1) OH-1(1)
1239	5.6833E-12	.0%	5.90	PRO1(1) HO+3(1)
1279	5.4086E-12	.0%	15.56	CYS2(1) LYS1(1) HO+3(1)
1226	5.3898E-12	.0%	16.63	GLY1(1) HO+3(1) OH-1(2)
1307	4.9183E-12	.0%	8.69	TRP1(1) LTA1(1) HO+3(1)
1221	4.7930E-12	.0%	15.72	GLN1(1) HO+3(1) OH-1(2)
1220	4.3881E-12	.0%	15.31	CYS2(2) HO+3(1)
1215	4.2549E-12	.0%	4.60	ASN1(1) HO+3(1)

MONITOR COMPONENT CTA3 FREE CONC. = 2.6401E-05 23.4%

SPECIES NO.	SPECIES CONC.		LOG STAB. CONST.	COMPOSITION.
1001	5.4287E-05	48.0%	3.26	CTA3(1) CA+2(1)
1042	3.0034E-05	26.6%	3.34	CTA3(1) MG+2(1)
4495	5.2168E-07	.5%	4.00	CTA3(1) LTA1(1) CA+2(1)
998	3.3703E-07	.3%	5.50	CTA3(1) H +1(1)
3993	2.1396E-07	.2%	3.95	CTA3(1) LTA1(1) MG+2(1)
4904	1.7627E-07	.2%	15.65	CTA3(1) PO43(1) CA+2(1) H +1(1
1256	1.6349E-07	.1%	14.31	CTA3(1) HO+3(1) OH-1(1)
4402	9.1012E-08	.1%	15.70	CTA3(1) PO43(1) MG+2(1) H +1(1
1257	4.6284E-08	.0%	19.67	CTA3(1) HO+3(1) OH-1(2)
4635	4.6083E-08	.0%	12.20	CTA3(1) GLN1(1) CA+2(1) H +1(1
4125	4.2312E-08	.0%	12.50	CTA3(1) GLN1(1) MG+2(1) H +1(1
1003	4.0434E-08	.0%	7.53	CTA3(1) CA+2(1) H +1(1)
4537	3.8256E-08	.0%	12.95	CTA3(1) ALA1(1) CA+2(1) H +1(1
4650	3.1952E-08	.0%	12.90	CTA3(1) GLY1(1) CA+2(1) H +1(1
4144	2.9338E-08	.0%	13.20	CTA3(1) GLY1(1) MG+2(1) H +1(1
4031	2.7901E-08	.0%	13.15	CTA3(1) ALA1(1) MG+2(1) H +1(1
4769	2.7128E-08	.0%	13.90	CTA3(1) PRO1(1) CA+2(1) H +1(1
4269	2.2199E-08	.0%	14.15	CTA3(1) PRO1(1) MG+2(1) H +1(1
4951	2.0867E-08	.0%	10.00	LTA1(1) CTA3(1) CA+2(1) H +1(1
4814	1.9614E-08	.0%	12.25	CTA3(1) THR1(1) CA+2(1) H +1(1
4858	1.8200E-08	.0%	12.70	CTA3(1) VAL1(1) CA+2(1) H +1(1
4526	1.6934E-08	.0%	4.15	CTA3(1) SCA2(1) CA+2(1)
1002	7.8760E-09	.0%	4.00	CTA3(2) CA+2(1)
4504	1.5077E-08	.0%	4.20	CTA3(1) MLA2(1) CA+2(1)
4358	1.4894E-08	.0%	12.95	CTA3(1) VAL1(1) MG+2(1) H +1(1
4791	1.3260E-08	.0%	12.30	CTA3(1) SER1(1) CA+2(1) H +1(1
4313	1.2750E-08	.0%	12.40	CTA3(1) THR1(1) MG+2(1) H +1(1
4710	1.2187E-08	.0%	12.80	CTA3(1) LEU1(1) CA+2(1) H +1(1
4012	1.1982E-08	.0%	4.95	CTA3(1) OXA2(1) MG+2(1)
1044	1.1473E-08	.0%	7.32	CTA3(1) MG+2(1) H +1(1)
4206	1.1189E-08	.0%	13.10	CTA3(1) LEU1(1) MG+2(1) H +1(1
4554	1.0988E-08	.0%	12.40	CTA3(1) ARG0(1) CA+2(1) H +1(1
4665	1.0852E-08	.0%	12.45	CTA3(1) HIS1(1) CA+2(1) H +1(1
4612	1.0278E-08	.0%	13.05	CTA3(1) GLU2(1) CA+2(1) H +1(1
1253	9.7623E-09	.0%	7.17	CTA3(1) HO+3(1)
4291	9.6712E-09	.0%	12.50	CTA3(1) SER1(1) MG+2(1) H +1(1
1043	4.5628E-09	.0%	4.10	CTA3(2) MG+2(1)
4161	8.8808E-09	.0%	12.70	CTA3(1) HIS1(1) MG+2(1) H +1(1
4564	8.0854E-09	.0%	12.20	CTA3(1) ASN1(1) CA+2(1) H +1(1
4045	7.1424E-09	.0%	12.55	CTA3(1) ARG0(1) MG+2(1) H +1(1
4976	7.0507E-09	.0%	21.65	PO43(1) CTA3(1) CA+2(1) H +1(2
4020	6.9451E-09	.0%	4.10	CTA3(1) SCA2(1) MG+2(1)
4101	6.6808E-09	.0%	13.20	CTA3(1) GLU2(1) MG+2(1) H +1(1
4749	5.9881E-09	.0%	12.30	CTA3(1) PHE1(1) CA+2(1) H +1(1
4055	5.8970E-09	.0%	12.40	CTA3(1) ASN1(1) MG+2(1) H +1(1
4693	5.2256E-09	.0%	12.80	CTA3(1) ILE1(1) CA+2(1) H +1(1
3996	4.9119E-09	.0%	4.05	CTA3(1) MLA2(1) MG+2(1)
4247	4.9002E-09	.0%	12.55	CTA3(1) PHE1(1) MG+2(1) H +1(1
4189	4.7980E-09	.0%	13.10	CTA3(1) ILE1(1) MG+2(1) H +1(1
3965	4.7251E-09	.0%	4.15	GLN1(1) CTA3(1) MG+2(1)
4514	4.6301E-09	.0%	4.20	CTA3(1) OXA2(1) CA+2(1)
4600	4.1472E-09	.0%	12.75	CTA3(1) CIS2(1) CA+2(1) H +1(1
4090	3.8079E-09	.0%	13.05	CTA3(1) CIS2(1) MG+2(1) H +1(1

'WELL DONE ECCLES', SAID MORIARTY.

APD AND Sr(II)

```
*****      ****     ****     *        *****     *****
*         *        *        *        *         *
****      *        *        *        ****      *****
*         *        *        *        *             *
*****      ****     ****     *****    *****     *****
-------------------------------------------------------
```

```
<><><><><><><><><><><><><><><><><><><><><><><><><><><><><><><><><><><><><><><>
<>
<>                        NORMAL PLASMA WITH ALL THE METALS
<>
<>
<>  INCLUDING SR                                                      100392
<>
<><><><><><><><><><><><><><><><><><><><><><><><><><><><><><><><><><><><><><><>
```

```
UTPUT SUPRESSED.
ONITORED COMPONENTS:  SR+2 APD0
O SCAN REQUIRED.
CCLES DATA CHECKING PROCEDURES EMPLOYED.
HERE ARE 18 SPECIES WITH DEFINED CONCENTRATIONS.

ATA INPUT SUCCESSFULLY COMPLETED.
OTAL NUMBER OF COMPONENTS =  54  (LIMIT = 115 )
UMBER OF COMPONENTS WITH FIXED FREE CONCENTRATIONS = 13  (LIMIT = 15 )
OTAL NUMBER OF SPECIES =  4972  (LIMIT =  5000 )
OTAL NUMBER OF COMPONENTS ENTERED IN KEY ARRAY = 17364  (LIMIT = 18000 )

XPERIMENTAL PH =       7.398            CALCULATED LOG KW =    -13.3116
```

MONITOR COMPONENT SR+2 FREE CONC. = 1.5000E-10

SPECIES NO.	SPECIES CONC.		LOG STAB. CONST.	COMPOSITION.
944	4.8966E-06	98.6%	12.00	PO43(1) SR+2(1)
1020	7.1653E-08	1.4%	10.00	ACA2(1) SR+2(1)
1078	2.5037E-12	.0%	2.80	CTA3(1) SR+2(1)
1103	2.0836E-12	.0%	.90	LTA1(1) SR+2(1)
969	3.0599E-13	.0%	1.00	SO42(1) SR+2(1)
1133	1.9043E-13	.0%	1.60	MLA2(1) SR+2(1)
1252	1.7655E-13	.0%	23.70	APD0(1) SR+2(1) H +1(2)
1250	1.0111E-13	.0%	16.06	APD0(1) SR+2(1) H +1(1)
1238	6.0277E-14	.0%	1.00	SCA2(1) SR+2(1)
1167	5.8480E-14	.0%	1.60	OXA2(1) SR+2(1)
1188	4.4648E-14	.0%	.50	PVA1(1) SR+2(1)
324	2.3061E-14	.0%	.80	GLN1(1) SR+2(1)
756	1.3865E-14	.0%	1.00	THR1(1) SR+2(1)
92	1.3812E-14	.0%	1.40	ARG0(1) SR+2(1)
724	1.0517E-14	.0%	1.10	SER1(1) SR+2(1)
401	7.6713E-15	.0%	1.20	HIS1(1) SR+2(1)
258	5.8492E-15	.0%	1.80	CIS2(1) SR+2(1)
862	4.5647E-15	.0%	1.00	VAL1(1) SR+2(1)
659	2.9966E-15	.0%	.90	PHE1(1) SR+2(1)
291	2.8923E-15	.0%	1.40	GLU2(1) SR+2(1)
361	2.8434E-15	.0%	.75	GLY1(1) SR+2(1)
35	2.8317E-15	.0%	.72	ALA1(1) SR+2(1)
516	1.9285E-15	.0%	.90	LEU1(1) SR+2(1)
185	1.8966E-15	.0%	1.00	CIT1(1) SR+2(1)
591	1.2062E-15	.0%	.85	MET1(1) SR+2(1)
689	6.8039E-16	.0%	1.20	PRO1(1) SR+2(1)
63	5.0636E-16	.0%	1.00	ABA1(1) SR+2(1)
158	2.9528E-16	.0%	1.48	ASP2(1) SR+2(1)
457	3.2317E-17	.0%	.40	HYP1(1) SR+2(1)
959	3.1844E-17	.0%	2.90	SIL2(1) SR+2(1)
629	8.5269E-18	.0%	1.00	ORN1(1) SR+2(1)
562	7.7458E-18	.0%	.90	LYS1(1) SR+2(1)
828	4.1658E-18	.0%	.90	TYR2(1) SR+2(1)
1251	4.4760E-20	.0%	19.53	APD0(1) SR+2(2) H +1(1)
1213	7.2686E-21	.0%	.60	SLA2(1) SR+2(1)
1249	5.4807E-23	.0%	9.22	APD0(1) SR+2(2)

MONITOR COMPONENT APD0 FREE CONC. = 1.4677E-12

SPECIES NO.	SPECIES CONC.		LOG STAB. CONST.	COMPOSITION.
1248	6.8370E-05	80.4%	20.96	APD0(1) CA+2(2) H +1(1)
1268	5.5554E-06	6.5%	17.26	APD0(1) MG+2(1) H +1(1)
1247	5.4051E-06	6.4%	12.46	APD0(1) CA+2(2)
1246	2.9634E-06	3.5%	16.65	APD0(1) CA+2(1) H +1(1)
1243	1.3206E-06	1.6%	20.75	APD0(1) H +1(2)
1269	1.3085E-06	1.5%	24.03	APD0(1) MG+2(1) H +1(2)
1244	5.4054E-08	.1%	26.76	APD0(1) H +1(3)
1261	8.8861E-09	.0%	20.18	APD0(1) ZN+2(1) H +1(1)
1267	8.1781E-09	.0%	7.03	APD0(1) MG+2(1)
1242	5.2325E-09	.0%	10.95	APD0(1) H +1(1)
1262	2.4031E-10	.0%	26.01	APD0(1) ZN+2(1) H +1(2)
1260	2.2215E-10	.0%	11.18	APD0(1) ZN+2(1)
1245	7.8504E-13	.0%	29.32	APD0(1) H +1(4)
1252	1.7655E-13	.0%	23.70	APD0(1) SR+2(1) H +1(2)
1250	1.0111E-13	.0%	16.06	APD0(1) SR+2(1) H +1(1)
1263	9.2170E-14	.0%	13.71	APD0(1) ZN+2(1) OH-1(1)
1265	1.4083E-17	.0%	25.38	APD0(1) FE+3(1) H +1(1)
1264	9.6973E-18	.0%	17.82	APD0(1) FE+3(1)
1257	6.8978E-19	.0%	21.07	APD0(1) CU+2(1) H +1(1)
1256	2.0732E-19	.0%	13.15	APD0(1) CU+2(1)
1254	1.1714E-19	.0%	18.30	APD0(1) NI+2(1) H +1(1)
1251	4.4760E-20	.0%	19.53	APD0(1) SR+2(2) H +1(1)
1253	2.7331E-20	.0%	10.27	APD0(1) NI+2(1)
1255	3.3945E-21	.0%	24.16	APD0(1) NI+2(1) H +1(2)
1258	1.5516E-21	.0%	25.82	APD0(1) CU+2(1) H +1(2)
1266	1.0984E-21	.0%	28.67	APD0(1) FE+3(1) H +1(2)
1249	5.4807E-23	.0%	9.22	APD0(1) SR+2(2)
1259	3.1959E-23	.0%	15.25	APD0(1) CU+2(1) OH-1(1)

APPENDIX G1:

ECCLES modeling input files
See Disk1

The ECCLES input files contaning the concentrations and complexation constants used are presented in the order found in Section 4.4

NorplHoA.MOD (Ho(III) and APD)
NorplSmH.MOD (Sm(III) and HEDP)
NorplSHT.MOD (Sm(III), Transferrin and HEDP)
NorplSmM.MOD (Sm(III) and MDP)
NorplSMT.MOD (Sm(III), Transferrin and MDP)
NorplHoC.MOD (Ho(III) and Citrate)
NorplSrA.MOD (Sr(II) and APD)

APPENDIX H:

Blood and Urine clearance values

The data is included in the following order

Blood clearance values for ^{166}Ho-APD
Blood clearance values for ^{153}Sm-EDTMP and ^{166}Ho-EDTMP
Urine clearance values for ^{166}Ho-APD
Urine clearance values for ^{153}Sm-EDTMP and ^{166}Ho-EDTMP

Blood clearance values for ^{166}Ho-APD

Time (minutes)	Corrected activity (Bq)	Normalized values
0	113000	1
3	95200	0.8424779
6	83640	0.740177
9	66640	0.5897345
14	35320	0.3125664
19	34920	0.3090265
24	34920	0.3090265
34	26040	0.2304425
39	25880	0.2290265
44	20920	0.1851327
49	21680	0.1918584
54	17040	0.1507965
59	15200	0.1345133
120	7040	0.0623009
180	6400	0.0566372

Blood clearance values for ^{153}Sm-EDTMP and ^{166}Ho-EDTMP

Time (minutes)	Normalised values for ^{153}SmEDTMP	Normalised values for ^{166}HoEDTMP
0	1	1
6	0.336	0.621
12	0.259	0.513
18	0.223	0.463
24	0.194	0.428
30	0.169	0.397
36	0.147	0.369
42	0.128	0.343
48	0.111	0.318
54	0.097	0.296
60	0.084	0.275
90	0.042	0.192
120	0.021	0.134
150	0.011	0.095
180	0.006	0.068

Urine clearance values for ^{166}Ho-APD

Time (minutes)	Cumulative activity (Bq)	Normalized values
0		0
5	5	3.562E-08
10	15	1.069E-07
15	30	2.137E-07
20	50	3.562E-07
25	75	5.343E-07
35	110	7.837E-07
55	165	1.176E-06
60	225	1.603E-06
120	345	2.458E-06
180	525	3.74E-06

Urine clearance values for ^{153}Sm-EDTMP and ^{166}Ho-EDTMP

Time (minutes)	Normalised values for ^{153}SmEDTMP	Normalised values for ^{166}HoEDTMP
0	0	0
6	0.024	0.035
12	0.0642	0.055
18	0.105	0.133
24	0.143	0.175
30	0.178	0.212
36	0.211	0.245
42	0.242	0.273
48	0.27	0.298
54	0.297	0.32
60	0.321	0.338
90	0.42	0.402
120	0.489	0.433
150	0.538	0.449
180	0.573	0.457